Supercritical fluid foaming: a novel route to polymeric allografts?

Matthew S. Purcell, MEng.

Thesis submitted to The University of Nottingham
for the degree of Doctor of Philosophy

July 2014

Dedication

I take great pleasure in dedicating this thesis to everyone in my supportive family. In particular my grandfather who never fails to show great interest in my work.

That's the whole problem with science. You've got a bunch of empiricists trying to describe things of unimaginable wonder.

The Days Are Just Packed.

Bill Watterson, 1993.

It's a Magical World.

Bill Watterson, 1995.

Abstract

There is a growing need for synthetic bone graft materials, which is particularly apparent for procedures requiring impaction bone grafting (IBG), such as revision hip arthroplasty. Currently allograft bone is used that has limited supply and associated risks of transmission of infectious agents.

Porous bioresorbable polymeric scaffolds can be created using supercritical carbon dioxide ($scCO_2$). This thesis investigated the use of these scaffolds for impaction bone grafting procedures. Building on previous research within the literature poly(D,L-lactide) ($P_{DL}LA$) and poly(D,L-lactide-*co*-glycolide) ($P_{DL}LGA$) scaffolds of high molecular weight ($\approx$100 kDa) were investigated for this use. Scaffolds were milled using a standard bone mill and impacted to create porous milled chips of bioresorbable scaffolds and impacted for mechanical shear testing and biocompatibilities. The impaction process used forces equivalent to those experienced during IBG.

In vitro cell experiments were used to assess the proliferation and osteoblastic differentiation of mesenchymal stem cells (MSCs) on impacted scaffolds to identify the most promising scaffold compositions. These compositions included pure polymer and polymer:HA microparticle composites. Further experiments using animals (murine and ovine) were then used to investigate the *in vivo* performance of the scaffolds. A critical sized ovine femoral condyle defect established the osteoinductive and osteoconductive potentials of milled $scCO_2$ foamed $P_{DL}LA$ + 10 wt.% hydroxyapatite (HA) microparticle scaffolds *in vivo*.

The scale-up potential of $scCO_2$ foaming of bioresorbable scaffolds was established using a 1 L vessel. Scaffolds $scCO_2$ foamed using either a 60 ml autoclave or a 1 L vessel were characterised using scanning electron microscopy and micro computed tomography. Scaffolds from different batches were characterised and compared to ensure process repeatability was accounted for.

The final chapter investigated differences in the osteoblastic differentiation of MSCs on $P_{DL}LA$ and $P_{DL}LGA$ scaffolds observed in experiments at the start of the study. Spincoated and dipcoated flat films of $P_{DL}LA$, $P_{DL}LGA$, and $P_{DL}LA$:$P_{DL}LGA$ (50:50) were used for *in vitro* cell culture to remove the effect of morphological differences that affected $scCO_2$ foamed scaffold experiments. Additionally, this chapter investigated the effect of the form of

HA using HA nanoparticles and HA microparticles in scCO$_2$ foamed P$_{DL}$LA:HA composites for *in vitro* studies.

Journal Publications

The author's work has contributed to the following publications:

PURCELL, M., M HOWDLE, S., M SHAKESHEFF, K. and J WHITE, L. (2013) Supercritical Fluid Processing of Materials for Regenerative Medicine. *Recent Patents on Regenerative Medicine* 3, 3, 237–248

TANG, M., PURCELL, M., STEELE, J.A., LEE, K.Y., MCCULLEN, S., SHAKESHEFF, K.M., BISMARCK, A., STEVENS, M.M., HOWDLE, S.M. and WILLIAMS, C.K. (2013) Porous Copolymers of ϵ-Caprolactone as Scaffolds for Tissue Engineering. *Macromolecules* 46, 20, 8136–8143

TAYTON, E.R., SMITH, J.O., EVANS, N., DICKINSON, A., AARVOLD, A., KALRA, S., PURCELL, M., HOWDLE, S., DUNLOP, D.G. and OREFFO, R.O. (2013) Effects of Setting Bone Cement on Tissue-Engineered Bone Graft: a Potential Barrier to Clinical Translation? *The Journal of Bone & Joint Surgery* 95, 8, 736–743

TAYTON, E., FAHMY, S., PURCELL, M., AARVOLD, A., SMITH, J.O., KALRA, S., BRISCOE, A., LANHAM, S., HOWDLE, S., SHAKESHEFF, K., DUNLOP, D.G. and OREFFO, R.O.C. (2012) An analysis of polymer type and chain length for use as a biological composite graft extender in impaction bone grafting: A mechanical and biocompatibility study. *Journal of Biomedical Materials Research Part A* 100A, 12, 3211–3219

TAYTON, E., PURCELL, M., AARVOLD, A., SMITH, J., KALRA, S., BRISCOE, A., SHAKESHEFF, K., HOWDLE, S., DUNLOP, D. and OREFFO, R. (2012) Supercritical CO_2 fluid-foaming of polymers to increase porosity: A method to improve the mechanical and biocompatibility characteristics for use as a potential alternative to allografts in impaction bone grafting? *Acta biomaterialia* 8, 5, 1918–1927

Acknowledgements

I would like to express my gratitude to my supervisors Prof. Steve Howdle and Prof. Kevin Shakesheff for their time, help, and guidance throughout my studies. There a number of people that assisted me with practical techniques and I would like to thank each of them: Dr. Lisa White for training on the supercritical foaming rig and μCT scanner; Mr. Edward Tayton for cell culture and assays on my scaffolds at Southampton University; Emily Smith for expertise in XPS analysis; Nicola Weston and Christine Grainger-Boultby for training on SEM and sputter coaters; Dr Glen Kirkham, Dr Hassan Rashidi, and Adam Taylor for expert guidance with tissue culture experiments; Prof. Allen Goodship for execution of the ovine *in vivo* study; Prof. Gordon Blunn for histological staining of ovine samples; Miss Gillian Hughes and other members of the Royal Veterinary College team for help with the ovine study; Mr. James Smith for assistance with surgical procedures; and all the members of Prof. Richard Oreffo's group at Southampton University for help with cell culture and assays.

I would also like to thank all the members of the Howdle group and Tissue Engineering group for their support, guidance, and friendship for the last three years.

Final thanks go to my family and friends for their continued support throughout my studies.

Contents

List of Figures

List of Tables

Abbreviations

Abbreviation	Meaning
α-MEM	*alpha*-Modified Eagle's Medium
μCT	Micro computed tomography
3D	Three-dimensional
ALP	Alkaline phosphatase
ASCs	Adipose derived stem cells
BMD	Bone mineral density
BMP	Bone morphogenic protein
BMP-2	Bone morphogenic protein-2
BPR	Back pressure regulator
BSA	Bovine serum albumin
BSE	Back scattered electrons
BSP	Bone sialoprotein
CAD	Computer aided design
Col-1	Collagen type-1
CTG	Cell Tracker Green
DAPI	4',6-diamidino-2-phenylindole
DMEM	Dulbecco's Modified Eagle's Medium
DMSO	Dimethyl sulfoxide
DNA	Deoxyribonucleic acid
ECM	Extracellular matrix
EDTA	Ethylenediaminetetraacetic acid
EDX	Energy dispersive x-ray spectroscopy
EH-1	Ethidium homodimer-1
FBS	Fetal bovine serum
FDA	Food and Drug Administration
FGF	Fibroblast growth factor
FGF-2	Fibroblast growth factor-2

Abbreviation	Meaning
GFs	Growth factors
GLP	Good laboratory practice
H&E	Hematoxylin and eosin
HA	Hydroxyapatite
IBG	Impaction bone grafting
ILGF	Insulin-like growth factor
M_W	Molecular weight by mass
MSC	Mesenchymal stem cell
NADPH	Reduced nicotinamide adenine dinucleotide phosphate
NPs	Nanoplates
NRs	Nanorods
OC	Osteocalcin
OP	Osteopontin
P_c	Critical pressure
P_DLA	Poly(D-lactide)
P_{DL}LA	Poly(D,L-lactide)
P_{DL}LA	Poly(lactide)
P_{DL}LGA	Poly(D,L-lactide-*co*-glycolide)
P_{DL}LGA	Poly(lactide-*co*-glycolide)
P_LLA	Poly(L-lactide)
P_{tp}	Triple point pressure
PBS	Phosphate buffer solution
PCL	Poly(*epsilon*-caprolactone)
PDGF	Platelet-derived growth factor
PDI	Polydispersity index
PEG	Poly(ethylene glycol)
PFA	Paraformaldehyde
PGSS	Particles from gas-saturated solutions
pNPP	para-Nitrophenyl phosphate
pQCT	Peripheral qunatitative computed tomography

Abbreviation	Meaning
PSEA	Phase-separation enhancing agent
PTFE	Poly(tetrafluorethylene)
PTH	Parathyroid hormone
RESS	Rapid expansion of supercritical solutions
RNA	Ribonucleic acid
SAS	Supercritical antisolvent precipitation
SB	Secondary electron beam
$ScCO_2$	Supercritical carbon dioxide
SCF	Supercritical fluid
SEM	Scanning electron microscopy
T_c	Critical temperature
T_g	Glass transition temperature
T_m	Melting temperature
TCP	Tissue culture plastic
TGF	Transforming growth factor
UHMWPE	Ultrahigh-molecular-weight polyethylene
UV	Ultraviolet
VEGF	Vascular endothelial growth factor
WST-1	Water soluble tetrazolium salt-1
Wt.%	Percentage by weight

CHAPTER 1

Introduction

1.1 Background

1.1.1 Regenerative medicine, tissue engineering, and biomaterials

Mason and Dunhill succinctly described regenerative medicine as replacing or regenerating human cells, tissue or organs, to restore or establish normal function [6]. Longer descriptions of the term preceded Mason and Dunhill's widely cited paper [7–9]. Tissue engineering predates regenerative medicine as a term, having first been used to describe the use of prosthetic devices and surgical manipulation of tissues [10], and defined more recently as "an interdisciplinary field that applies the principles of engineering and the life sciences toward development of biological substitutes that restore, maintain, or improve tissue function" [11]. Prior to Langer and Vacanti's paper defining tissue engineering, [11] they undertook studies to generate functional tissue equivalents utilising biodegradable and biocompatible polymer scaffolds seeded with viable cells [10, 12]. Published reference to tissue engineering, as currently understood, can be dated back to 1991 [13]. In literature today the terms "tissue engineering" and "regenerative medicine" are widely used interchangeably, although typically a fully regenerative medicine solution will leave no residues within the body, while a tissue engineered solution requires no such condition be met.

Tissue engineering and regenerative medicine are fields that are relatively new and growing, and have generated large amounts of research due to high levels of funding in recent years. A report from the U.S. Department of Health and Human Services in 2004 highlighted regenerative medicine as an important interdisciplinary field with huge potential to deliver treatments; bone substitutes along with skin and cartilage substitutes were some of the early regenerative medicine products to reach the market [14].

The high levels of funding for these research fields that have been observed are due to the medical need for solutions. Currently, organ failure or tissue loss is treated through mechanical devices, organ transplantation, or surgical reconstruction and these solutions save many lives. Mechanical devices (e.g. dialysis machines) that fail to perform all functions of the organ they replace merely reduce, rather than halt, patient deterioration. In the case of organ transplantation, the need outweighs demand and many people die awaiting a donor. For example over 16,000 people died of liver disease within the U.K. in 2008 [15], and over 33,000 people died of chronic liver disease within the U.S.A in 2011 [16]; both countries have a rising trend in deaths caused by liver disease, which could be tackled with an abundance

of suitable donor organs.

Various approaches to regenerating tissue have been investigated. They include: the implantation of cells of the required function, which may not be retained following implantation or immunologically rejected; the use of signal molecules such as growth factors, and delivery mechanisms of such factors, to induce tissue growth; and cellular scaffolds to guide and induce tissue growth within the body. Combinations of such techniques are typically used with biodegradable scaffolds seeded with cells prior to implantation and signal molecules embedded or otherwise incorporated within the scaffolds, which act as a targeted delivery device.

Three-dimensional (3D) constructs, or scaffolds, are typically designed to mimic the extracellular matrix (ECM) (connective tissue that supports and surrounds cells) of the tissue to be replaced, either morphologically (form or structure), topographically (surface features), and/or chemically. Ideal tissue engineering scaffolds should be highly porous with interconnected pores; biocompatible and bioresorbable; have suitable surface chemistry to support cell attachment, proliferation, and differentiation; and mechanical properties that match tissues at the implantation site [17]. Interconnected porous networks allow cellular proliferation throughout entire scaffolds, tissue in-growth where appropriate (such as bone repair), and transport of nutrients and waste.

The journal, Biomaterials, defined a biomaterial as "a substance that has been engineered to take a form which, alone or as part of a complex system, is used to direct, by control of interactions with components of living systems, the course of any therapeutic or diagnostic procedure". A more simple and commonly used definition, which is subscribed to within this thesis is "any material that is used to replace or restore function to a body tissue and is continuously or intermittently in contact with body fluids", taken from Biomaterials science and engineering by Park [18]. This definition excludes external prostheses (e.g. artificial limbs, hearing aids) and surgical instruments [19]. Importantly it includes the materials that form cellular scaffolds implanted within the body to promote regeneration of tissue and restore function. The majority of biomaterials in use are either metals, ceramic, polymers, or naturally derived materials. All are required to be biocompatible (should not elicit adverse responses), noncarcinogenic, and nontoxic [19]. Additionally, appropriate mechanical properties are required for the appropriate function (e.g. appropriate strength in a hip prosthesis).

In tissue engineering naturally derived materials are desirable for cellular scaffolds because of their similarity to *in vivo* ECM. For example collagen, which forms a significant component of bone and connective tissues, is the major component of mammalian tissue ECM (25% total protein mass [20]), and has been widely studied for use in various scaffolds [20–24], which include skin replacements [25–27], and bone substitutes [28, 29]. Variation between batches and possible immune responses to naturally derived materials are obstacles to their use in commercially viable products. Despite this collagen is used in Apligraf®, a commercially available and Food and Drug Administration (FDA) approved skin regeneration treatment for diabetic ulcers.

Metals are primarily used for their strength in joint prostheses or screws and supports. Research in coatings for metal prostheses has been reported in the literature with aims to improve integration with the body by reducing wear, promoting bone in-growth into porous coatings, and/or providing osteoinductive surfaces [30–32]. Ceramics, such as β-tricalcium phosphate or hydroxyapatite, are often used for this purpose [30, 31], or to replace bone as extenders of graft material [33]. The properties of polymers can differ greatly with different polymer blends, cross-linking, or variations in molecular weight (M_W), which suits them to a wide range of functions. Some examples of which include the use of: ultrahigh-molecular-weight polyethylene (UHMWPE) as a bearing material in joint prostheses; polylactide and polyglycolide in biodegradable sutures; polytetrafluoroethylene in stents; polydimethyl siloxane and polyurethane in facial prostheses; and polymethylmethacrylate as a bone cement [19].

1.1.2 Hip arthroplasty and revision hip arthroplasty

Sir John Charnley invented the modern hip replacement composing of a metal femoral stem and head and an acetabular cup in the 1960s; it is one of the most cost-effective surgical procedures [34], and one of the most successful orthopaedic procedures. Total hip replacement is predominantly performed in order to treat osteoarthritis, where articular cartilage in the hip joint has worn away resulting in bone rubbing against bone in the joint, causing pain. The main aims of the replacement joint are to eliminate the pain osteoarthritis causes and improve quality of life, function of the joint, and mobility.

The number of hip replacements being performed is increasing annually. In 1996 over 62,000 hip replacements were performed [35] while in 2011 over 88,000 hip procedures were

carried out in England and Wales according to the National Joint Registry [36]. While the number of procedures, which includes both primary and secondary replacements, continues to increase the proportion of revised/secondary replacements is also increasing; from 9% of total procedures in 2007 to 11% of the total in 2011.

1.1.2.1 Primary hip arthroplasty

In total hip arthroplasty (surgical repair of joint) the articular surfaces of the femur and acetabulum are replaced. Figure 1.1 shows a typical hip femoral stem and an acetabular cup prostheses. The socket is replaced with an artificial socket which can either be a polymer cup that is cemented into place, or a metal socket which can be inserted tightly in to the joint with no cement and more firmly attached with screws if required. The head of the femur is replaced with a metal ball attached to a stem either as a complete singular piece or using modular components. The stem is attached to the femur and this can be done with or without the use of bone cement. In 2011 in England and Wales 44% of the total number of primary hip procedures were cementless, 36% were cemented, and 18% were hybrid procedures (the remain 2% were resurfacing procedures) [36].

Unfortunately, a hip replacement does not last for life and revision surgery may have to be performed at a later date. Hip replacements currently last approximately 10–15 years and can fail in a number of ways: loosening of the socket and/or femoral component, infection, bone loss on socket and/or femoral side, unstable or dislocating hips, or subsidence of femoral prosthesis. Aseptic loosening is the primary cause of primary hip replacement failure and of the need for revision surgery. This aseptic loosening is caused by wear particles from the joint inducing osteolysis (bone matrix resorption by osteoclasts - bone resorbing cells) [38, 39]. Osteolysis occurred in the absence of identifiable metallic or polymethylmethacrylate particles and in the presence of polyethylene particles [40] and the mechanism by which polyethylene wear particles induced osteolysis is complex [41, 42]. The size, morphology, and concentration of wear particles was shown to have a significant effect on bone resorbing activity [41, 43]; Green *et al*. [43], for example, demonstrated polyethylene particles <2 μm stimulated bone resorption, while particles >8 μm did not, at a range of different concentrations. Cellular responses to wear particles entail inflammatory and osteoclastogenic cytokine secretion, which exacerbate normal osteoclast activity and enhance osteolysis [42]. Bone resorption by osteoclasts is a normal process in healthy bone as bone is remodelled nat-

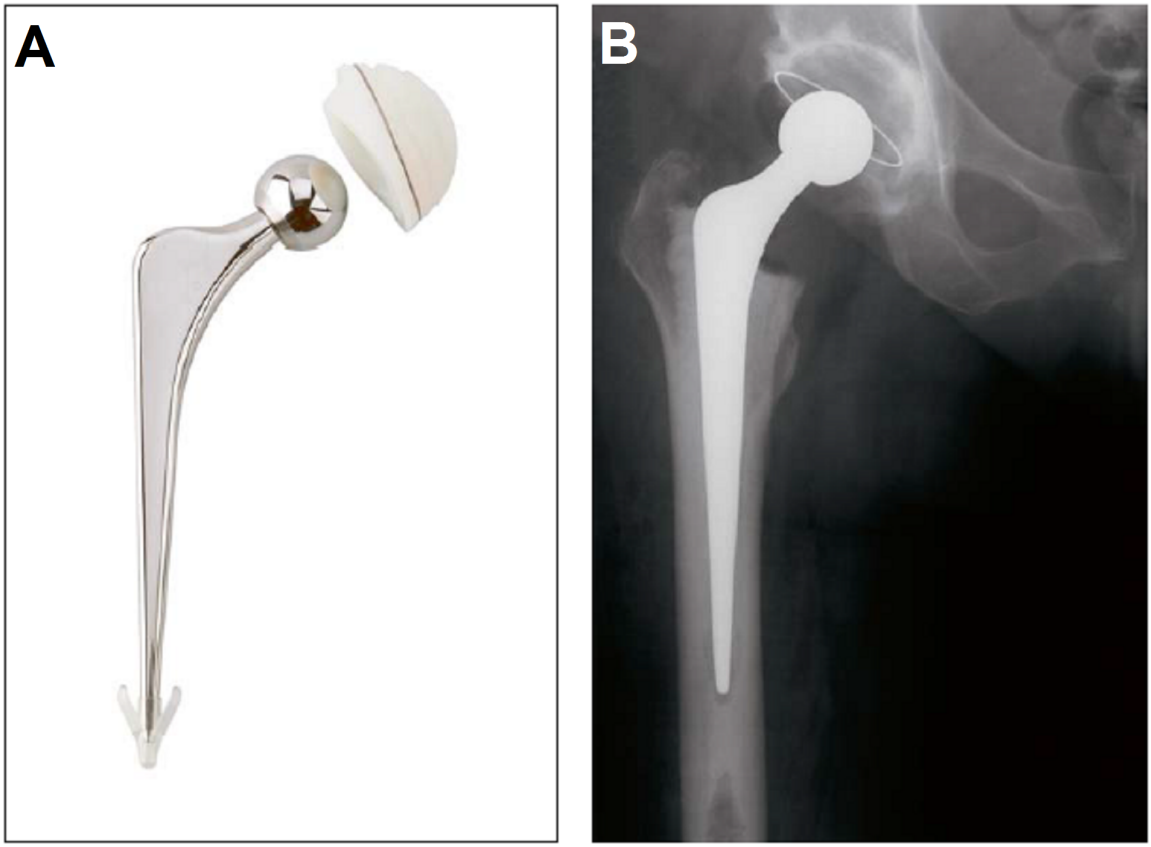

Figure 1.1: The stem, socket and centraliser of an Exeter Universal hip joint prosthesis (A) and an x-ray radiograph of an Exeter prosthesis cemented in place (B) [37].

urally; a balance is maintained between bone formation by osteoblasts and bone resorption by osteoclasts. Enhanced osteoclast activity leads to loss of bone around the implant and subsequent loosening leading to failure of the prosthesis; hip replacement failure results in the need for revision surgery.

1.1.2.2 Revision hip arthroplasty

Revision hip arthroplasty is more complicated than primary total hip arthroplasty because each patient brings individual causes for prosthesis failure. In a retrospective review of reasons for revision hip surgery, Clohisy *et al*. [44] reported that of 439 revision procedures carried out in 1996 55% were for aseptic loosening, 14% were for instability, 13% were for osteolysis, 7% were due to infection, and the remaining were for fractures of the implant or around the prosthesis (periprosthetic), conversion of hemiarthroplasty, and loose implants. Additionally, safe removal of the previous prosthesis and ensuring a stable base for the new prosthesis complicates the procedure. The number of hip revisions performed is growing annually, as is the percentage of these that are revised surgeries; figure 1.2 shows the trend across England and Wales.

In the case of loosening of the socket, shields can be used in the instance of bone loss and a new replacement socket attached in to the shield using bone cement. In the case of femoral components, however, impaction bone grafting (IBG) is used to rebuild damage to the femur before inserting the prosthesis in a similar way to primary surgery. With bone loss in the femur, a stable base needs to be created to support the prosthesis to be inserted. Currently allogeneic cancellous bone graft (i.e. from the same species) is the 'gold standard' material used for this application. A stable outline scaffold is created to ensure a stable rigid base: wires, wire meshes, metal plates or donated bone can be used for this. In the stable femoral tube cancellous bone graft can be inserted and impacted to create a stable base before implantation of the femoral component. The concept of IBG to reconstruct bone stock in the femur with allogeneic bone was introduced by Slooff *et al*. [45] where they also used cement, and the procedure became more common with introduction of instruments specifically for revision operations by Gie *et al*. [46–48]. Various procedures exist for hip revision surgery; a common method, the Exeter X-change bone-impaction technique introduced by Gie *et al*. [46] is shown in Figure 1.3, taken from [37].

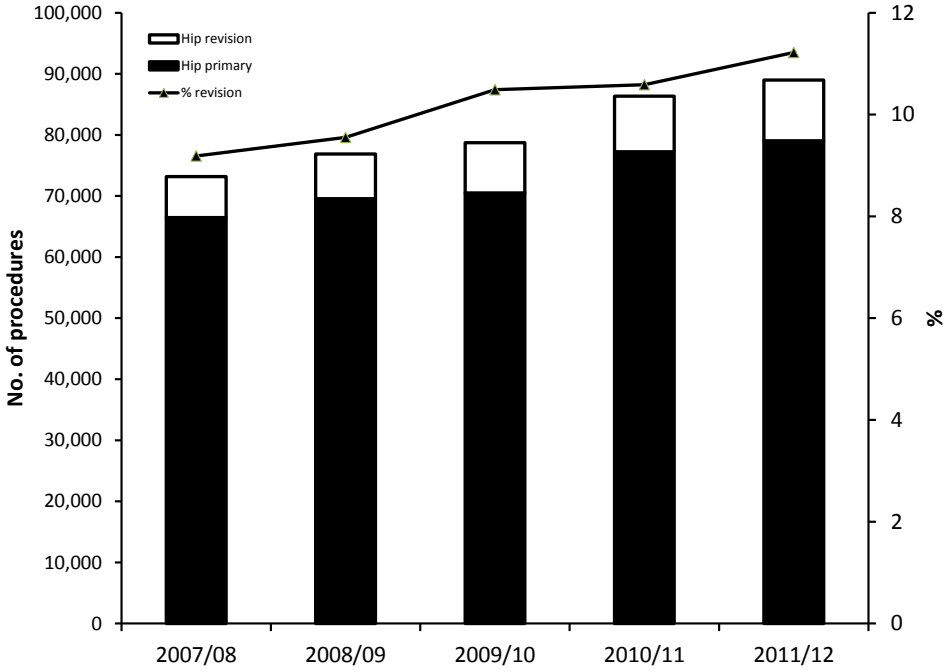

Figure 1.2: Graphical representation of the trend in hip arthroplasty procedures carried out across England and Wales from 2007–2012. Data taken from [36]

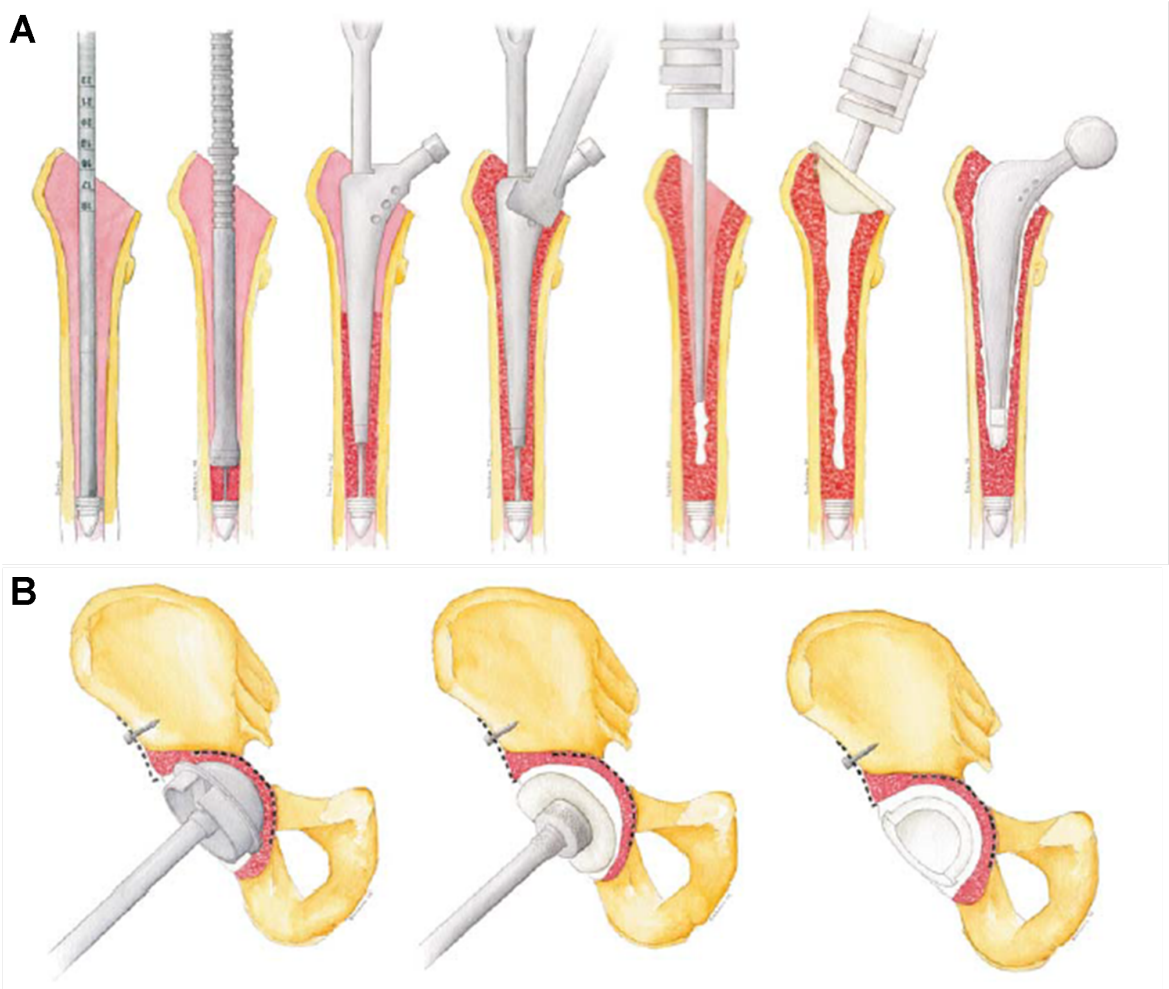

Figure 1.3: Figures of the X-change revision instruments system for A) femoral revision and B) socket revision [37].

1.1.3 Bone grafts

Cortical and cancellous (explained in Section 1.2) bone harvested from the iliac crest forms viable autologous bone graft, autograft (i.e. from the same person), and is the traditional standard for treating conditions requiring bone graft [49–51]. However, its drawbacks include donor site morbidity; increased operative time [49, 50]; and, for application in rebuilding of the femur to provide a stable base for prosthesis, the volume of bone required is too large to be obtained through autograft alone [49, 52].

While blood is the most common transplant tissue, bone graft is the second most common [53]. Allogeneic bone graft, allograft (i.e. from the same species), as mentioned previously, is the clinical 'gold standard' graft material for application in rebuilding bone stock in revision hip surgery [54, 55]. The use of fresh frozen morsellised allograft eliminates donor site morbidity associated with autograft and shortens surgical time [56]. However, it does present the risk of transmission of infectious agents [56–58], including a reported case of transmission of human immunodeficiency virus type 1 (HIV-1) from an organ donor to seven recipients, two of which received femoral head donations [57]. Furthermore, cost and risk of immunological rejection remain disadvantages to allograft use [59, 60]. Tissue processing, and irradiation sterilization much reduce the risk of transmission of infectious agents however the processing steps affect structural strength [58].

Three main characteristics used to describe the capabilities and nature of different bone graft materials and bone graft substitutes are:

- Osteogenesis - which refers to the ability of a graft material to form new bone, a capability present in autograft alone [50].
- Osteoinduction - which leads to osteogenesis through the recruitment of undifferentiated pluripotent cells that are stimulated to differentiate down the osteoblastic lineage into cells capable of forming bone [50, 58, 61].
- Osteoconduction - which refers to the process of providing scaffolding for new bone growth due to the ability of bone to grow on the surface and/or penetrate pores of a material.

  Autograft bone tends to be the benchmark against which bone graft substitutes are compared. Cancellous and, to a lesser extent, cortical autograft contain osteogenic, osteoinductive and osteoconductive properties, hence they are the regular benchmarks

used to compare the in vivo performance of alternative graft materials to [58].

A comparison and qualitative rating of various properties of bone graft materials was reported by Greenwald *et al*. [58] and is shown in Figure 1.4. Allograft, while not osteogenic, is osteoinductive to a lesser degree than autograft [49, 51, 56]. Allograft is still a highly successful viable alternative to autograft in many surgical settings, which extend to impaction bone graft procedures a majority of which constitute revision hip surgery. This is an indicator that, while striving to achieve the ideal substitute bone graft material with osteogenic, osteoinductive, and osteoconductive properties, there is need for a material that improves on these qualities compared to current benchmarks, while simultaneously meeting or improving required mechanical properties, and remaining cost-effective. If improved osteoinduction over allograft and osteogenic properties were displayed in a bone graft substitute while meeting other specifications, this would be sufficient to outperform allograft. Additional specifications an ideal bone graft substitute would be required to meet include: biocompatibility, bioresorbability, and ease-of-use. Bioresorbability of substitute graft material should be matched to the growth rate of new bone for an ideal regenerative medical solution [17]. Hutmacher's review of scaffolds in tissue engineering bone and cartilage [17] is widely cited for the illustration of interdependence of M_W loss, mass loss, and tissue remodelling rate for tissue engineering bone transplants shown in Figure 1.5. The comparability of mechanical properties between allograft and a bone graft substitute is particularly apt in hip revision surgery due to the load bearing nature; mechanical strength required of a substitute bone graft material for non-load bearing applications can be much less [58].

It is important to define the words biodegradable, bioresorbable, bioerodable, and bioabsorbable, which are widely used within literature to describe the properties of bone graft substitutes and tissue engineering scaffolds (and the materials used to form both) to ensure comprehension of differences between the terms. Hutmacher [17] used the definitions of Vert *et al*. [62] and these are the definitions used within this thesis (although not restricted to purely polymeric materials):

- Biodegradable - materials which break down due to degradation and dispersion *in vivo* with no proof of later elimination from the body.
- Bioresorbable - materials which show bulk degradation and elimination from the body due to filtration of degradation by-products through natural pathways with no residual effects. Elimination is assumed to have been shown conclusively.

Bone Graft	*Structural Strength*	*Osteo-Conduction*	*Osteo-Induction*	*Osteogenesis*
Autograft				
Cancellous	No	+++	+++	+++
Cortical	+++	++	++	++
Allograft				
Cancellous				
Frozen	No	++	+	No
Freeze-Dry	No	++	+	No
Cortical				
Frozen	+++	+	No	No
Freeze-Dry	+	+	No	No

Figure 1.4: Comparative properties of various bone grafts [58].

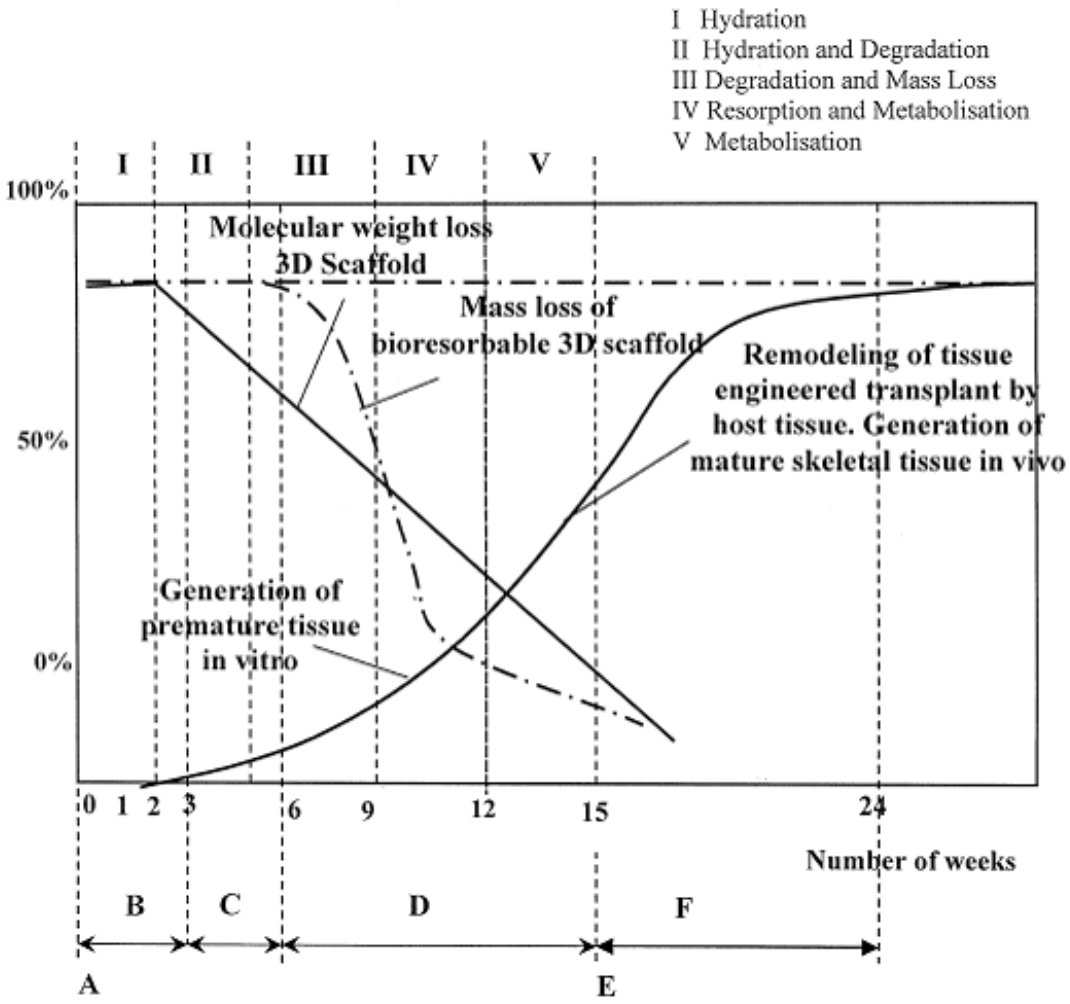

Figure 1.5: Figure demonstrating the complex interdependence of molecular weight loss and mass loss of a 3D scaffold plotted against the time frame for a bone transplant. A) Fabrication of a bioresorbable scaffold, B) seeding of osteoblast populations onto the scaffold *in vitro*, C) growth of premature tissue in a dynamic environment (e.g. spinner flask), D) growth of mature tissue in a physiologic environment (bioreactor), E) surgical transplantation, F) tissue-engineering transplant remodeling [17]

- Bioerodable - materials which show surface degradation, in contrast to bulk degradation of bioresorbable materials, and also show elimination of degradation by-products from the body through natural pathways with no residual effects.
- Bioabsorbable - materials which can dissolve in body fluids without molecular mass decrease or degradation into by-products.

Given the extended surgery time, donor site morbidity, and patient pain associated with autograft, and the impracticality for surgeries requiring large volumes of graft material, allograft is used. However, due to the drawbacks of allograft and the large demand for suitable bone graft materials to meet supply, alternative solutions are sought. The market size for bone graft and substitutes exceeded $250 million in 1999 in the U.S.A alone [58]. Current commercially available products, are osteoconductive and bioresorbable but have limited osteoinductive potential and no osteogenic capabilities; these products include OrthoBlast™, DynaGraft®, ProOsteon®500R, Grafton®, OSTEOSET®, AlloMatrix™, Collagraft™[58]. These commercially available products and other methods of bone repair currently being researched are discussed in Section 1.3.

1.2 Bone physiology

Bones are rigid organs of the body that provide mechanical function in skeletal rigidity, protective roles, sound transduction and transfer forces allowing movement, in addition to providing physiological functions. These functions include: haematopoiesis (formation of blood cellular components), medullary canals in long bones host mesenchymal stem cell populations from which haemopoietic precursors and mature blood cells originate; acid-base balance, bone acts as a reservoir of carbonate and phosphate buffers, particularly calcium carbonate, required when the body has an accumulation of acid (acidosis) causing an imbalance; and acting as a mineral reserve. The majority of the body's phosphorus and calcium is stored within bone, and calcium levels within the body are closely regulated [63].

The long bones of the body, of which the femur is one particularly relevant to hip arthroplasty and impaction bone grafting, have a central long shaft, or diaphysis, which ends with rounded ends, or epiphyses. In a long bone the epiphysis closest to the main body is termed the proximal epiphysis, while the ephysis furthest from the main body is the distal epiphysis.

Bone comprises two types of tissue: cortical or compact bone, and cancellous or trabec-

ular/spongy bone. Both form lamellar bone, where collagen within the architecture forms parallel configurations that give bone strength. Cortical tissue is dense and forms the exterior of bone, while cancellous tissue forms a porous reticular network within the interior of bone [64]. A membrane adheres to the surface of bones, except where cartilage coats extremities, and encloses them; it is through this membrane, the periosteum, that a multitude of small blood vessels permeate into bone tissue.

An osteon is the name of the basic unit of bone, which has a central canal, referred to as Haversian canals, within which mainly blood vessels are contained; they can also contain nerves and lymphatic vessels. These canals run parallel to the longitudinal axis of the bone, while blood vessels running perpendicular to the length of the bone are contained within Volkmann's canals. The Haversian canals are contained within rings of concentrically arranged thin plates of mineralised bone tissue, called lamellae. Also, arranged concentrically around the central Haversian canals are lacunae, which are spaces occupied by star-shaped bone cells named osteocytes. Lacunae are linked by microscopic canals, canaliculi, through which osteocytes form cytoplasmic extensions and form intercellular connections called gap junctions through which nutrients and waste are exchanged. The structure of bone is shown in Figure 1.6, taken from Bayliss *et al*. [63].

Approximately 95% of the organic matrix comprising bone tissue is collagen type-1, which provides (tensile strength) tensional resistance, particularly in lamellar bone where collagen fibres are aligned parallel to each other. No such alignment is observed in woven bone, formed in response to fracture healing and much weaker mechanically. Proteoglycans, osteonectin, osteocalcin, osteopontin, and other non-collagenous proteins form the remainder of the organic matrix, or osteoid [63]. The inorganic/mineral matrix of bone that provides compressive strength constitutes approximately 67% of total bone matrix [63] and is formed from calcium and phosphate ions as hydroxyapatite ($Ca_{10}(PO_4)_6(OH)_2$, not the empirical formula to denote the crystal form).

1.2.1 Bone remodelling

Remodelling of bone is a consistent process that ensures repair of fractures and adaptation to mechanical stimuli, in addition to allowingfor bone growth. Approximately 10% of bone is remodelled annually within the adult skeleton [63]. Three main cell types are involved in bone remodelling - osteoblasts, osteocytes, and osteoclasts. Figure 1.7 depicts the develop-

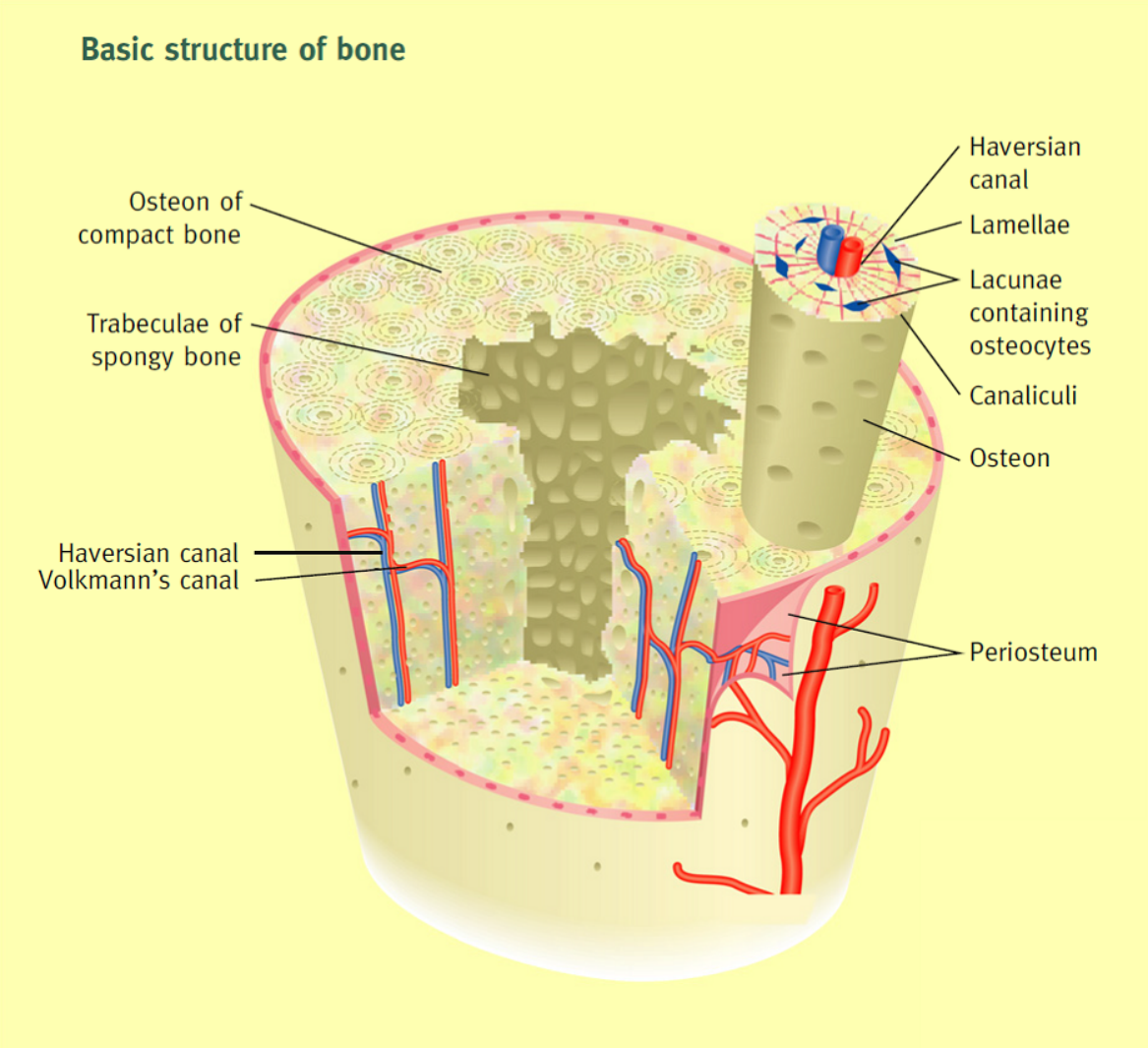

Figure 1.6: The internal structure of bone [63].

ment of these cells and some of their markers and differentiation factors. Figure 1.8A depicts some of the typical characteristics of these cells.

Osteoblasts are cuboid mononuclear cells, which secrete the proteins that form osteoid (primarily collagen-1, osteocalcin, osteopontin, osteonectin, and bone-sialoprotein) [65]. They originate from pluripotent mesenchymal stem cells through a conversion to osteoprogenitor cells, pre-osteoblasts and then mature osteoblasts. This conversion involves interactions between transcriptional regulators, growth factors, hormones, and signalling molecules, which include bone morphogenic protein (BMP), platelet-derived growth factor, and transforming growth factor beta [63]. The majority of osteoblasts become trapped in mineralised bone matrix and further transform to become osteocytes, which make up the majority of bone cells (ten times more numerous than osteoblasts [63]). Also, osteoblasts may undergo apoptosis or become bone-lining cells.

Osteocytes are star-shaped, terminally differentiated osteoblasts entrapped within the mineralised matrix of bone in lacunae, as previously mentioned. Primarily they act as mechano-sensors within the bone and express biochemical signals based on mechanical stimuli [63]. They are recognised as regulating osteoblast:osteoclast activity (bone forming:bone resorbing), and hence bone remodelling rate [63].

Osteoclasts are large multinucleated cells, which stimulate resorption of bone matrix. They derive from the monocyte/macrophage lineage and form a ruffled border that is the active site of bone resorption, underneath which forms a resorptive pit. Their activity is reduced by osteoprotegerin, secreted in the thyroid gland when calcium ion and gastrin levels rise [63]. Osteoblasts also secrete osteoprotegerin which binds to a key differentiator of osteoclast function, RANKL (receptor activator of nuclear factor kappa-B ligand) [63]. Osteoclasts are located in resorption bays called Howship's lacunae. Within resorptive pits evidence has shown areas of low pH form, conducive to resorption of mineralised bone matrix [66]. Cathepsin K, a protease optimal in acidic conditions, is secreted into the resorptive pits and is believed responsible for the degradation of the proteins that form the organic matrix of bone, particularly collagen-1 [67].

Bone not undergoing remodelling (quiescent bone) is activated when lining cells separate, exposing the bone, and osteoclast precursors are recruited. Cytokines and hormones regulate the subsequent osteoclast bone degradation. Osteocytes line the Howship's lacunae that are formed and osteoclasts undergo apoptosis. Formation of osteoid by osteoblasts

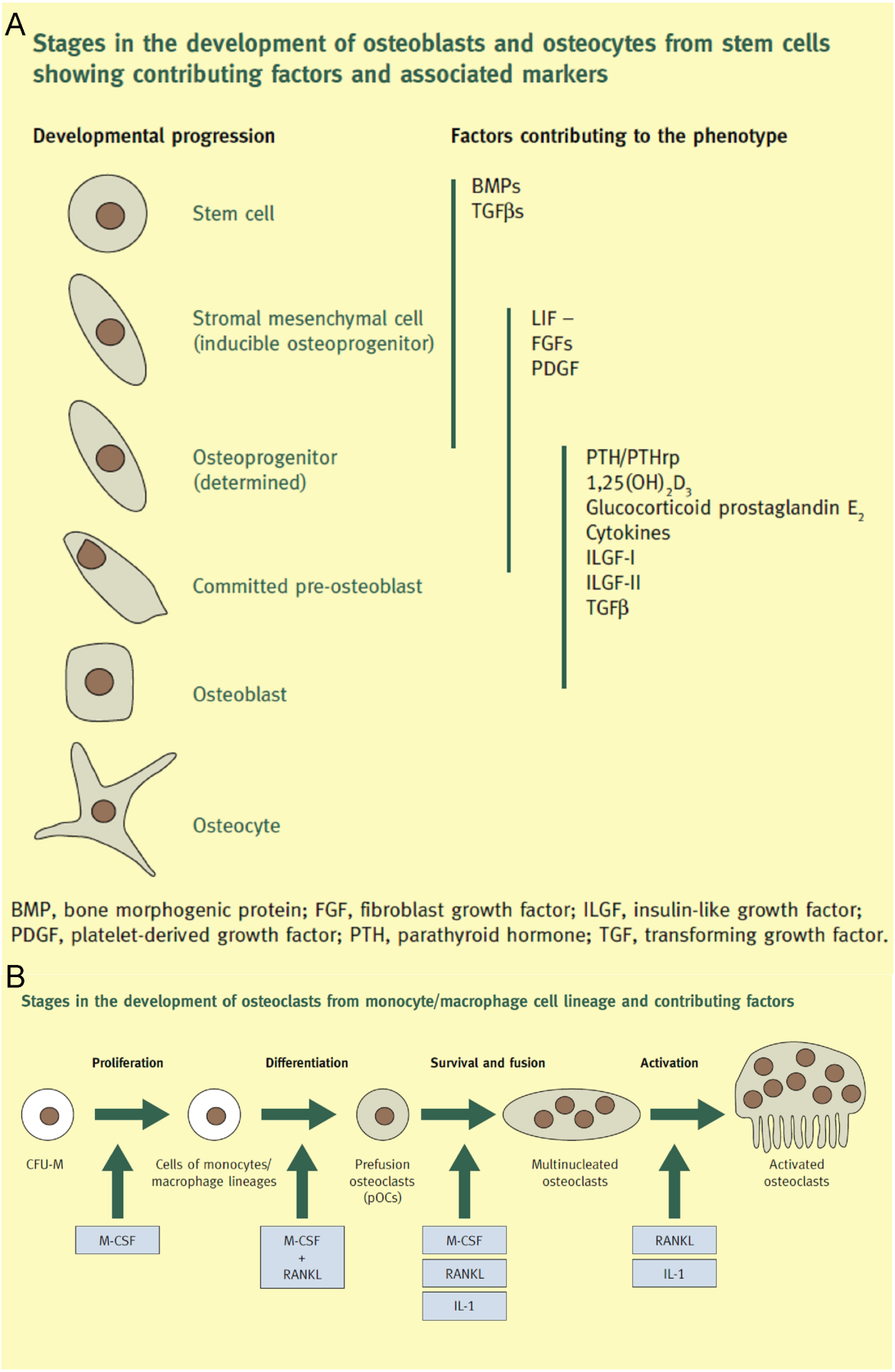

Figure 1.7: The development pathway of A) osteoblasts and osteocytes, and B) osteoclasts with factors affecting their differentiation. [63].

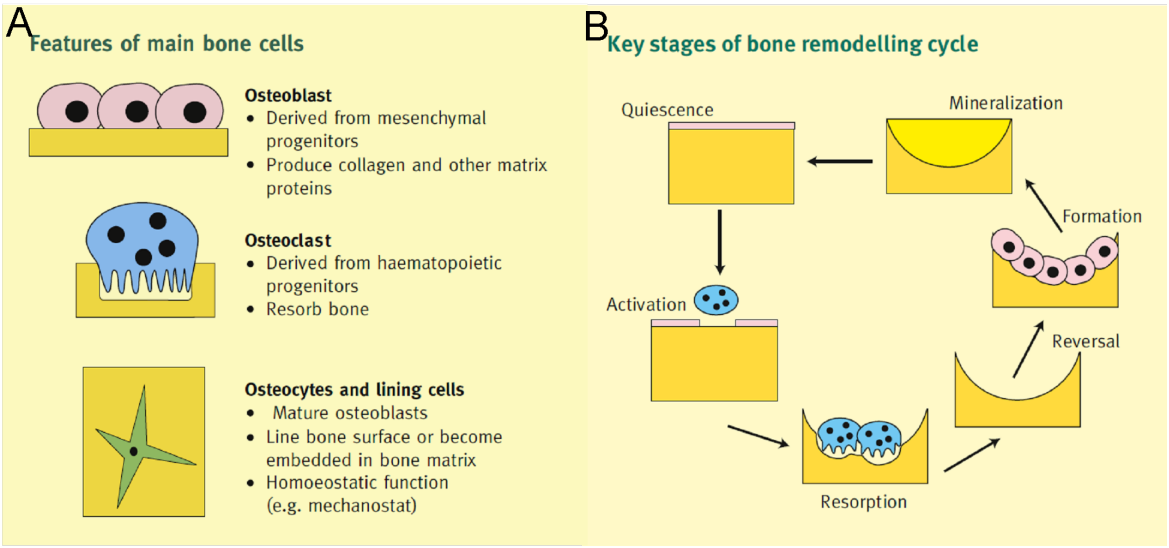

Figure 1.8: A) The typical features of main bones cells. B) The bone remodelling cycle. [63].

follows, which is then mineralised. The whole remodelling cycle ends with the creation of a new osteon. The arrangement of osteoclasts, osteocytes, and osteoblasts that complete the remodelling cycle are called bone remodelling units and are arranged in a conical shape, the front edge of which sees osteoclast bone resorption trailed by osteoblastic secretion of osteoid proteins [63]; the cycle is depicted in Figure 1.8B.

1.3 Approaches to bone repair

A range of different approaches to addressing bone repair are under continuing investigation. Some of these can be categorised into factor, cell, ceramic, or polymer-based approaches. Expander/extender materials for use with autograft or allograft can be used both to improve treatment/bone repair, and to reduce the volume of bone graft required for treatment, but are not discussed here.

1.3.1 Factor-based

Bone repair is controlled by a large number of cytokines, growth factors (GFs), and hormones that provide cellular signals to trigger healing responses and promote both migration of osteoprogenitor cells and specific lineage differentiation [68]. A growing body of research investigates the use of growth factors to promote bone regeneration. Results vary due to differing potency and efficacy of GFs used, physiological system variety, in addition to bone type and function, and bone defect type studied [69].

Bioactive molecules investigated include:

- Bone morphogenetic proteins, BMPs. BMPs are widely used osteoinductive factors in bone tissue engineering for a variety of roles that include acting as an osteoblastic differentiation factor for mesenchymal stem cells, MSCs.
- Insulin-like Growth Factors, IGFs. IGFs are a group of autocrine, endocrine, and paracrine polypeptide growth factors that play a role in bone metabolism and are known to stimulate proliferation and chemotactic migration of cells originating from periodontal ligaments [69, 70].
- Fibroblast growth factor-2, FGF-2. FGF-2 has been shown to have a positive effect on bone healing [71, 72] and to inhibit osteogenesis of stromal cells while maintaining

osteogenic potential state [73].

- Vascular endothelial growth factor, VEGF. VEGF plays an important role in bone angiogenesis (development of new blood vessels) and its administration has been shown to enhance blood vessel formation and ossification in bone damage models [74].

Studies investigating a variety of delivery mechanisms have been carried out and include investigation of a variety of polymer materials acting as carriers to deliver these bioactive molecules in 3D scaffolds, microparticles, or hydrogels. A review by Lee *et al*. [69] provides a more detailed overview of the role of bioactive molecules in bone regeneration.

1.3.2 Cell-based

Preclinical *in vivo* studies have been carried out investigating the use of various cell types as potential methods to improve bone regeneration with generally positive findings. Evidence that showed that MSCs, periosteal cells, and osteoblasts are capable of enhancing bone repair was reported [75, 76]. Osseous tissue reconstruction involves cells undergoing a progression from undifferentiated progenitors to fully differentiated adult cells which explains how a tissue engineering approach for improving osseous healing can be approached through different stages of the bone healing process [77].

MSCs are of particular interest for a cell-based approach to bone healing as they can be harvested easily through the iliac crest and expanded to produce a large enough population for a clinical therapy. Additionally, their ability to differentiate down different cell lineages and the presence of research and evidence demonstrating control of the differentiation paths down which they mature make MSCs particularly relevant in this field [77].

1.3.3 Ceramic-based

The main inorganic component in bone is HA, a calcium apatite with a crystal form and chemical formula $Ca_{10}(PO_4)_6(OH)_2$. Ceramic-based bone graft substitutes are formed from calcium phosphates, calcium sulphates and/or Bioglass®(a range of bioactive glass ceramics, commercially available, with different compositions of SiO_2, Na_2O, CaO, and P_2O_5 [78]) due to the similarity with a large part of the natural components found in bone. These materials are both osteoconductive and biocompatible [79], both of which are important in scaffolds for this application. Similarity to natural hydroxyapatite and their ability to

act as sources of calcium and phosphate ions for bone remodelling and mineralisation are drivers for their use. Additionally researchers have shown bonding of new bone to synthetic hydroxyapatite [80]. A large number of bone graft substitutes are commercially available that are based on calcium sulphates, calcium phosphates and bioactive glasses: Osteograf® (Dentsply Friadent, Germany), Norian SRS® (Synthes, USA), Pro Osteron® 200R and 500R (Biomet, USA), Osteoset® (Wright Medical Technology, USA), Chronos® (Synthes, USA), Actifuse ABX® (Apatech, Germany), Vitoss® (Othovita, USA), Tutoplast® (Tutogen Medical, Germany).

1.3.4 Polymer-based

A range of different polymeric materials have been used in some form for bone repair. A wide array of polymeric materials with many different properties allow for tailoring of scaffolds for different applications. Polymeric materials that have been investigated in this field vary from natural to synthetic. Those of natural origins include collagen, silk fibroin, chitosan, hyaluronic acid, alginates, cellulose, and dextrans. A review of polymers of natural origins and their role as scaffolds in tissue engineering was carried out by Malafaya *et al*. [81]. These roles include commercially available bone graft replacements such as Healos®Bone Graft Replacement (DePuy Orthopaedics, USA). Healos®is a matrix of cross-linked collagen fibres coated with HA and has been approved for clinical use as a bone graft substitute in spinal fusions [81].

Synthetic polymers used in this field include poly (α-hydroxyacids), poly (ϵ-caprolactone), poly (urethane)s, poly (propylene fumarate), poly (phosphazenes), and poly (1,4-butylene succinate). Poly (α-hydroxyacids) include poly (glycolide) (PGA), poly (lactide) (PLA), and poly (ϵ-caprolactone) (PCL), and there is a large body of knowledge about these polymers. These polymers and their copolymers have FDA approval for a variety of clinical applications, and as such are the most commonly used polymers for investigation within the tissue engineering and regenerative medicine field [82]. Various reviews of the many different porous scaffolds under investigation for the application of bone tissue engineering have been reported within the literature [17, 82]. The use of a polymeric based scaffold for bone tissue engineering provides great opportunity to incorporate bioactive molecules, cells, and ceramic materials to form a composite tissue engineering solution that combines benefits of each approach. The innovative combination of the most promising technologies will build

towards optimum solutions for different problems within this field.

1.4 PLA, PGA, and PLGA

Lactide is a dimer of lactic acid. Lactide, the monomer unit for PLA, has three stereoisomers (Figure 1.9A) which lead to three different possible forms of PLA: poly (L-lactide), P_LLA; poly (D-lactide), P_DLA; and poly (D, L-lactide), P_{DL}LA. P_LLA is a semi-crystalline polymer with a melting transition around 180 °C and a glass transition temperature, T_g, at approximately 67 °C [83] that is reported to vary between 63 °C and 71 °C [84]. Crystallinity of P_LLA varies between 10–69% [85, 86]. Amorphous polymers are formed from polymerisation of a racemic mixture of D-lactide and L-lactide and have lower T_gs in comparison to the semicrystalline forms. A value of 62.5 °C was reported for the T_g of P_{DL}LA [84]. P_DLA is used much less than P_LLA and P_{DL}LA for tissue engineering scaffolds.

Glycolide is the dimer of glycolic acid. Glycolide (shown in Figure 1.9B) is the monomer of PGA (shown in Figure 1.9B), a widely used biodegradable polymer. Poly (lactide-co-glycolide), PLGA, is a copolymer formed from glycolide and lactide monomer units. PLGA with different ratios of glycolide:lactide can be produced; the ratios of the different monomer units result in PLGA with different properties; these include a variation in the degradation rate which allows tailoring of the biodegradation rate of scaffolds formed of this polymer based on lactide:glycolide ratios.

A review by Södergård *et al*. [87] was published that provides a comprehensive review of the properties (thermophysical, mechanical, solubility, stability) of a wide number of lactide based polymers and includes a discussion of the preparation of the polymers by polycondensation and ring-opening polymerisation. The ring-opening polymerization is more common for PLA and is also used for PGA; the reaction is commonly catalysed by tin, zinc, or aluminium [85, 88].

L-lactic acid is the enantiomer of lactic acid found in mammalian systems [87]; as such lactic acid is a chemical found within the body for which natural processes for removal already exist (respiratory and renal filtration routes). The polymer eventually degrades to monomeric acids and then to carbon dioxide and water through de-esterification [89]. PLA, PGA, and PLGA degrade within the body through random bulk hydrolysis of ester bonds in the polymer chain; water attacks the polymer chains and through hydrolytic cleavage breaks

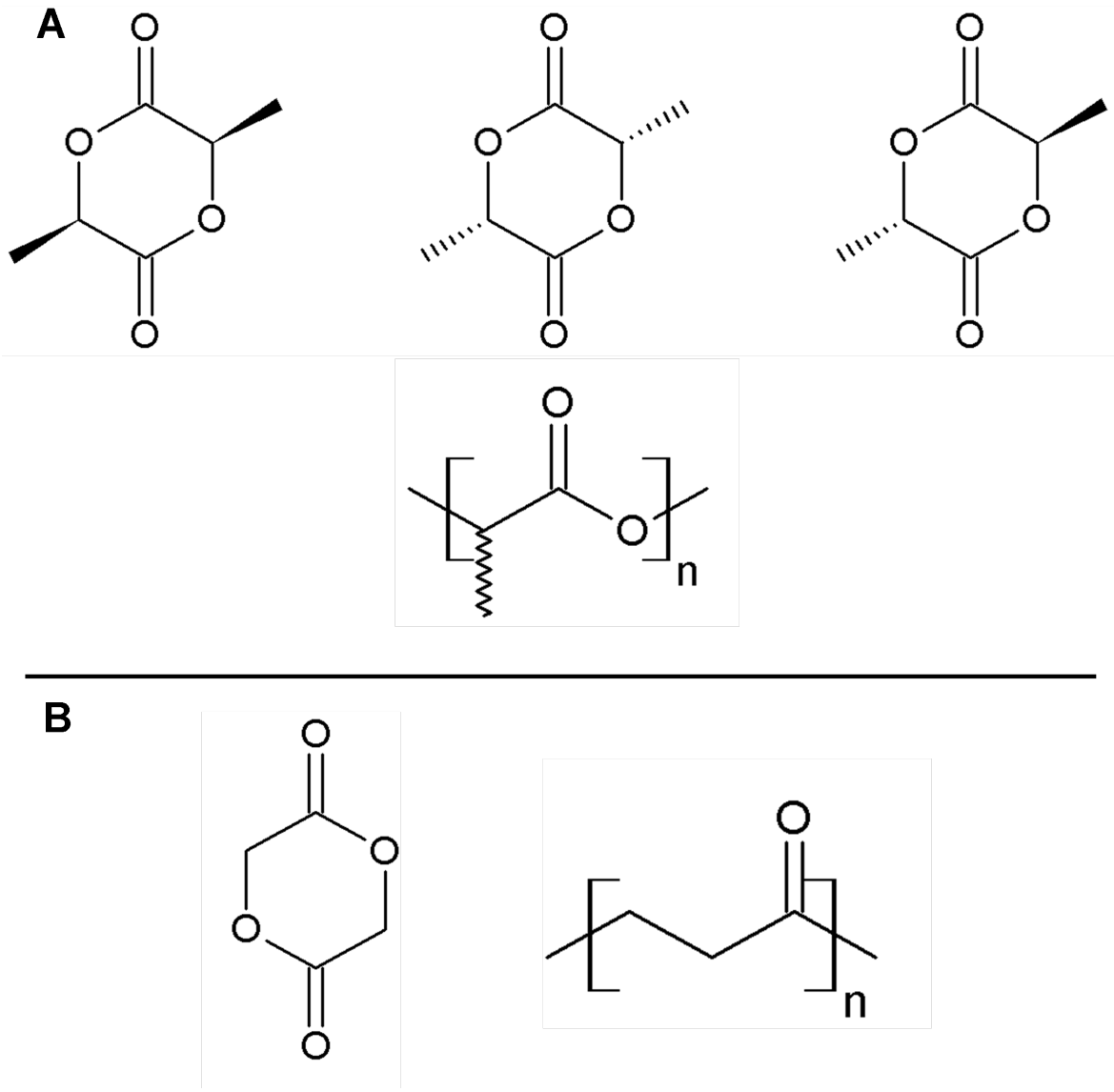

Figure 1.9: A) The chemical structures of lactide stereoisomers, from left to right -D-Lactide, L-Lactide, and *meso*-lactide; and polylactide (below). B) The chemical stuctures of, from left to right, glycolide, and polyglycolide.

them in to oligomers [89]. The degradation rate has been found to be heterogeneous in cases where oligomers within the polymer cannot diffuse away as quickly as oligomers formed at the surface. In these cases the oligomers increase the concentration of carboxylic acid end groups, which results in autocatalytic degradation of the polymer [90, 91]. The acidic degradation products of PLA and PGA can cause inflammation/adverse tissue reactions which can be detrimental to tissue repair. The degradation of the polymers will result in reduced mechanical properties and hence understanding and control of the degradation rates of materials offering structural support *in vivo* is required.

PLA, PGA, and their copolymers are bioresorbable. The degradation rate of these polymers varies with M_W, degree of crystallinity of the polymers, as well as through the previously mentioned copolymer ratios. All of these can be used to target specific degradation rates. The shape of implanted scaffolds formed from these polymers will also affect the degradation rate based on surface area, and diffusion rates of acidic degradation by-products. However, tissue engineering scaffold morphologies are typically optimised for function, hence, the inherent polymer properties such as M_W are preferred for tailoring degradation rates. Blends rather than copolymers can also be utilised to affect the degradation rates of scaffolds formed of these and other polymers.

1.5 Polymer scaffold production methods

There are many methods for producing polymeric scaffolds for tissue engineering with a variety of advantages and disadvantages. Some of the main polymer processing methods are briefly overviewed in this subsection.

Solvent casting/particulate leaching

Solvent casting scaffold production involves the dissolution of a polymer in a solvent to create a solution that is then mixed with water-soluble particles (salt primarily). This mixture is cast in a mould (if a 3D structure is desired) and the solvent removed through vacuum or freeze drying. Water can then be used to leach the particles from the structure creating a porous structure. Porosity and pore size can be controlled through variation of the amount and size of water-soluble particles used.

Downsides to this process include the use of organic solvent and difficulty in removing particles from the internal structure. Thin films (500–2000 μm) which are then layered to

create a laminated structure overcome this difficulty [79, 92].

Emulsion freeze drying

Polymer is dissolved in a solvent and a second immiscible liquid is added to form a stable emulsion using a homogeniser. The emulsion is cast into a mould, frozen in liquid nitrogen, and then freeze dried to remove both liquids. Porous scaffolds (up to 95% porosity) with small pores (13–15 μm) can be formed using this technique [93]. The small pore sizes and use of solvents limit the application of this technique to create scaffolds for tissue engineering applications.

Thermally induced phase separation

Polymer is dissolved completely in solvent with a low boiling point. The solution is then fast cooled moving the solution from a homogeneous single-phase region into its spinodal region (on and beyond the limit of stability of the solution). This leads to a break down in the stability of the solution resulting in liquid-liquid phase separation with polymer rich and polymer poor regions [94]. Liquid nitrogen quenching and subsequent freeze-drying to remove solvent obtains interconnected porous structures. The presence of solvent limits biocompatibility of scaffolds produced by this method.

Solid freeform fabrication

Solid freeform or rapid prototyping technologies build a 3D scaffold up in layers and can use a variety of different processes to achieve this such as: 3D printing, stereolithography, selective laser sintering, and extrusion-based systems [89]. Computer aided design (CAD) software is used to design the 3D model that is produced through the layering process. The advantages of scaffolds produced this way lie in extremely good reproducibility [82, 89] and control of porosity and structure. However, high temperatures and organic solvents may be required in processing and the processes often trap monomer within the scaffolds. The high level of control over structure is such that x-ray or MRI images of defects can be used to allow design of scaffolds to fill the defects using CAD software.

Various forms of 3D printing exist that use a computer controlled head to eject a binder into a bed of powder particles, joining them. In the case of stereolithography a liquid photocurable monomer is polymerised using a laser beam and a scaffold is built up from layers of selective polymerisation. Selective laser sintering utilises a computer controlled infrared

laser to heat a fine polymer powder above its T_g in localised areas allowing particle bonding to occur. In extrusion based systems, or fused deposition modelling, melted polymer fibres are deposited on a stage from a computer controlled nozzle, where they cool and solidify to form a layer; this layer is then deposited on and a 3D scaffold/structure is created from the multiple layers. While computer controlled, rough edges and trailing solidified polymer connections require user removal.

1.6 Supercritical fluids

This section is taken and adapted from a published review on "Supercritical fluid processing of materials for regenerative medicine" [1] authored by the author of this thesis.

Supercritical fluids, SCFs, are substances at or above their critical temperature, T_c, and critical pressure, P_c. On a phase diagram for a substance the point at the T_c and P_c is called the critical point and marks the end of the phase boundary between the gas phase and the liquid phase; the other end of this line marks the triple point, the temperature and pressure at which the substance may exist in all three phases (for water this is 0 °C at atmospheric pressure); both points can be seen in the typical phase diagram shown in Figure 1.10. The critical point for water is 374.2 °C and 2.2 MPa.

Baron Cagniard de La Tour is credited with the discovery of SCFs. His experiments in 1822 involved rolling a steel ball within a sealed gun barrel containing ethanol that was heated [96]. He observed acoustic differences in the sound of the ball rolling within the barrel that appeared to signify the absence of a liquid phase after appropriate heating. The point at which this occurred, the critical point, was previously known as the Baron Cagniard de La Tour point.

Above the critical point the distinction between a gas phase and a liquid phase vanishes and the resultant SCF has properties of both phases - solvating and density properties similar to liquids, and diffusivity and viscosity properties similar to gases. Large density changes can be effected through small changes in temperature and/or pressure at, or around the critical point. The properties of SCFs have been exploited in various processes, such as dry cleaning and decaffeination, in the place of organic solvents. The most commonly used SCF is supercritical carbon dioxide ($scCO_2$), which has a comparatively low critical temperature (31.1 °C), and a critical pressure of 7.38 MPa). Carbon dioxide is readily available, considered

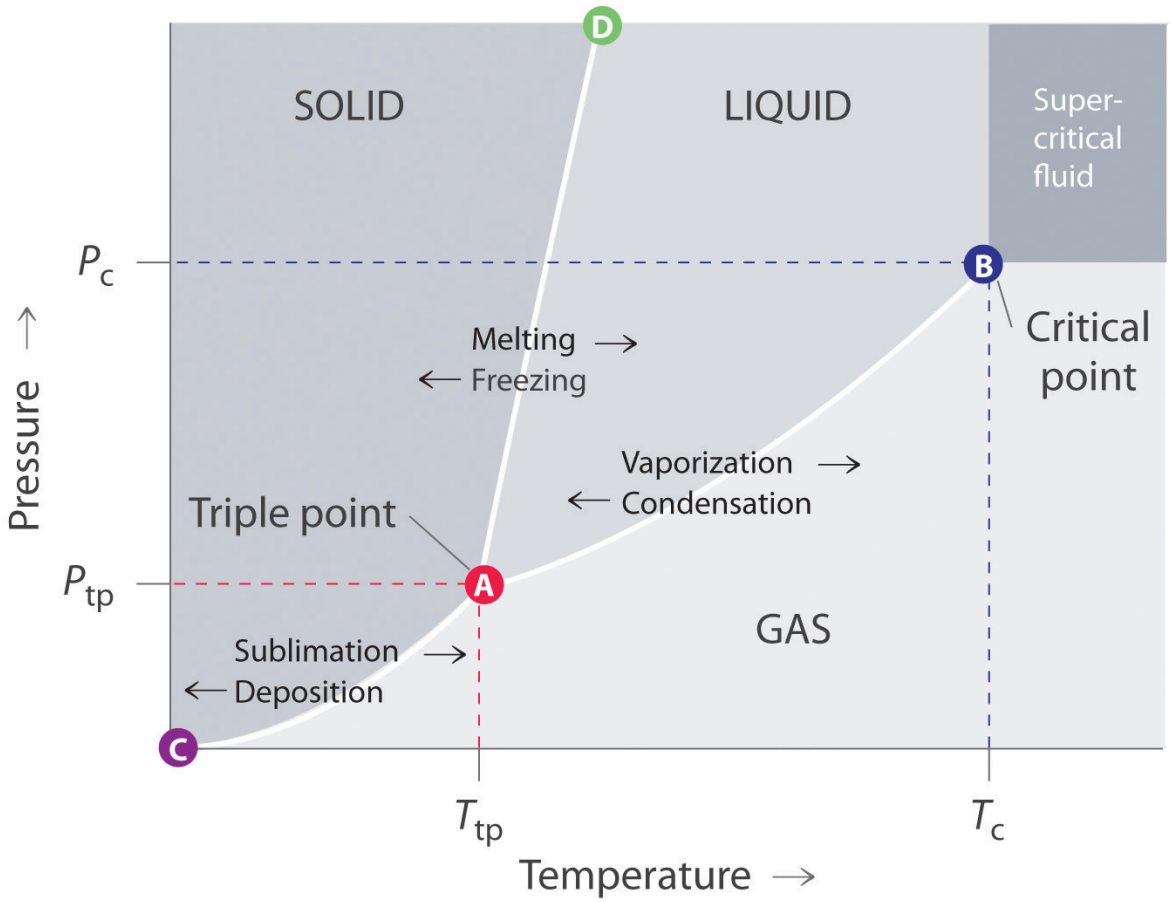

Figure 1.10: A typical substance phase diagram displaying phase boundaries, the triple point, and critical point. [95]

a green solvent due to its reclamation from other processes, where it would otherwise be vented to atmosphere, nonflammable, and has a low toxicity and cost. The value of SCFs, particularly $scCO_2$ has begun to be realised in creation of regenerative medicine scaffolds. Supercritical CO_2 processing of polymers does not require the use of organic solvents, offering advantages over many of the alternative polymer processing methods mentioned due to the final application of the polymer scaffolds: use as a biomedical product.

Polymer exposed to $scCO_2$ for a period of time becomes saturated with the fluid. The SCF plasticises the polymer, reducing the glass transition temperature, T_g. As operating pressure is lowered to below the critical value for CO_2, areas of CO_2 gas nucleate and grow within the polymer forming pores; additionally, as CO_2 diffuses out of the polymer the plasticising effect reduces and the T_g rises. When the T_g of the polymer rises above the processing temperature the porous polymer structure sets [97, 98]. The rate of growth and structure of the pores formed within various polymers can be controlled by varying operating conditions such as temperature, venting time, and operating pressure. Work reported in literature demonstrated the effect of these conditions on the porosity and pore size of resultant $P_{DL}LA$ and $P_{DL}LGA$ foams [97]. The ability of a polymer to be foamed using $scCO_2$ is dependent on the CO_2 absorption. A crystalline polymer or crystalline region requires harsher foaming conditions (higher temperature and/or pressure) in comparison to amorphous polymers to enable $scCO_2$ to penetrate the crystalline regions. The M_W of polymers also affects the foamed structure achieved under identical foaming conditions due to the effect M_W has on inherent polymer viscosity, T_g, and T_m.

Supercritical fluids have been utilised to fabricate regenerative medicine scaffolds since 1990, when De Ponti *et al*. [99] patented the creation of porous sponges of biodegradable polymers such as PLA and PLGA. Although high pressure gases had previously been used to produce bubble nucleation in polymers [100, 101], the foams produced contained closed pores. The advent of the De Ponti patent and a patent by Cha *et al*. [102] in 1991 demonstrated that SCFs could produce open pore foams, suitable for tissue engineering applications. This novel technique removed the need for organic solvents or high operating temperatures in scaffold production through the use of suitable SCFs, such as $scCO_2$.

Figures 1.11 and 1.12 provide a timeline of key patents and papers in the development of SCF formed scaffolds suitable for regenerative medicine applications. Fundamental work published by Goel and Beckman in the 1990s [103–106] demonstrated not only that $scCO_2$

could be used to foam discs of poly(methylmethacrylate) (PMMA) but also that process conditions could significantly affect the pore structure of the foamed construct. Mooney *et al*. [107] published a pivotal paper on the use of a high pressure gas to produce porous sponges and demonstrated that amorphous polymers or copolymers such as P_{DL}LGA foamed more easily than semi-crystalline polymers such as P_LLA. The combination of growth factors (GFs) in foamed constructs was achieved with high pressure gas foaming [108–110] with the addition of salt particle leaching required to achieve internal porosity [109, 110]. Howdle *et al*. [111] demonstrated that $scCO_2$ alone, without the use of *co*-solvents, could be utilised for mixing active molecules with polymers to form composite materials; the low operating temperatures also enabled thermolabile bioactive materials, such as enzymes, to be incorporated into polymer scaffolds. A schematic diagram of $scCO_2$ foaming is provided in Figure 1.13.

In addition to the production of solvent free porous scaffolds, SCFs were also utilised as 'clean' solvents for therapeutic molecules [112, 113], which eliminated the need to remove residual solvents. Sterile filtered SCFs as solvents for pharmaceutical ingredients were patented as early as 1979 [114]. Combining SCFs as solvents with their penetrative ability led to patents for therapeutic or biofunctionally loaded polymer production methods [115–117], where SCFs, active agents, and polymers were contacted or mixed to form composites. These methods were also applied to produce therapeutic loaded coatings for medical devices [118].

Supercritical fluids have also been utilised in the formation of other scaffold types, most notably, electrospun scaffolds. Traditionally, electrospinning has involved the use of a polymer dissolved in an organic solvent pumped through a charged needle to an oppositely charged collection plate. McHugh *et al*. [119] patented a process whereby a high pressure gas (subcritical or supercritical) could replace the organic solvent in electrospinning. Recent developments in $scCO_2$-assisted electrospinning have been reported in scientific literature [120].

Another application of SCFs has been in the field of sterilization, where Dillow *et al*. [121] patented a method using $scCO_2$ above 14 MPa and 30 °C that sterilised materials by altering the internal pH of microorganisms, inactivating them. The attraction over traditional techniques such as steam or ultraviolet sterilization, was that it could be performed at low temperatures and could also clean surfaces [21]. The alteration of internal pH of cells placed time restrictions upon the processing of mammalian cells using $scCO_2$ but a method

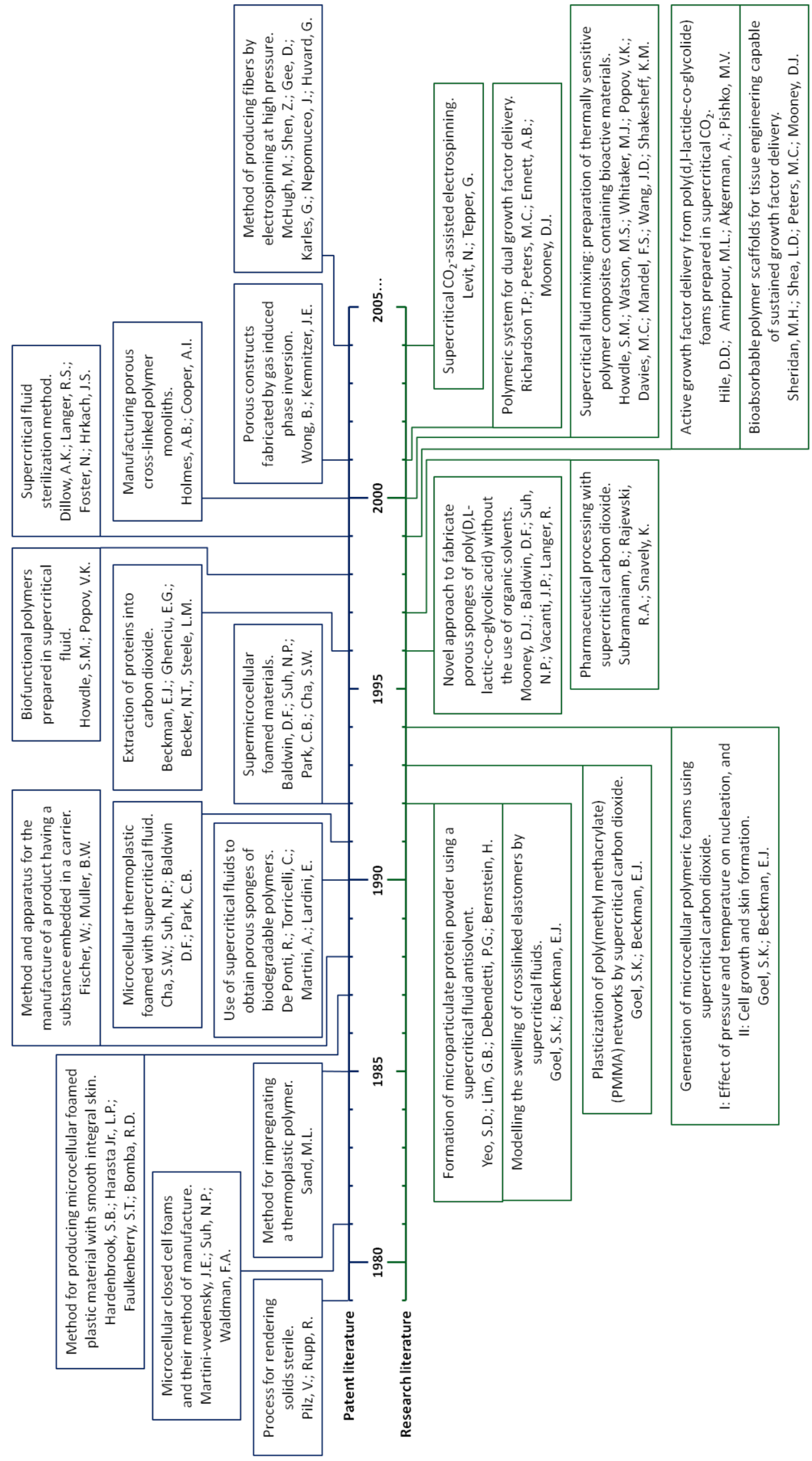

Figure 1.11: Timeline showing the pivotal patent and scientific literature that contributed to the advancement of supercritical fluids for the manufacture of regenerative medicine scaffolds.[1]

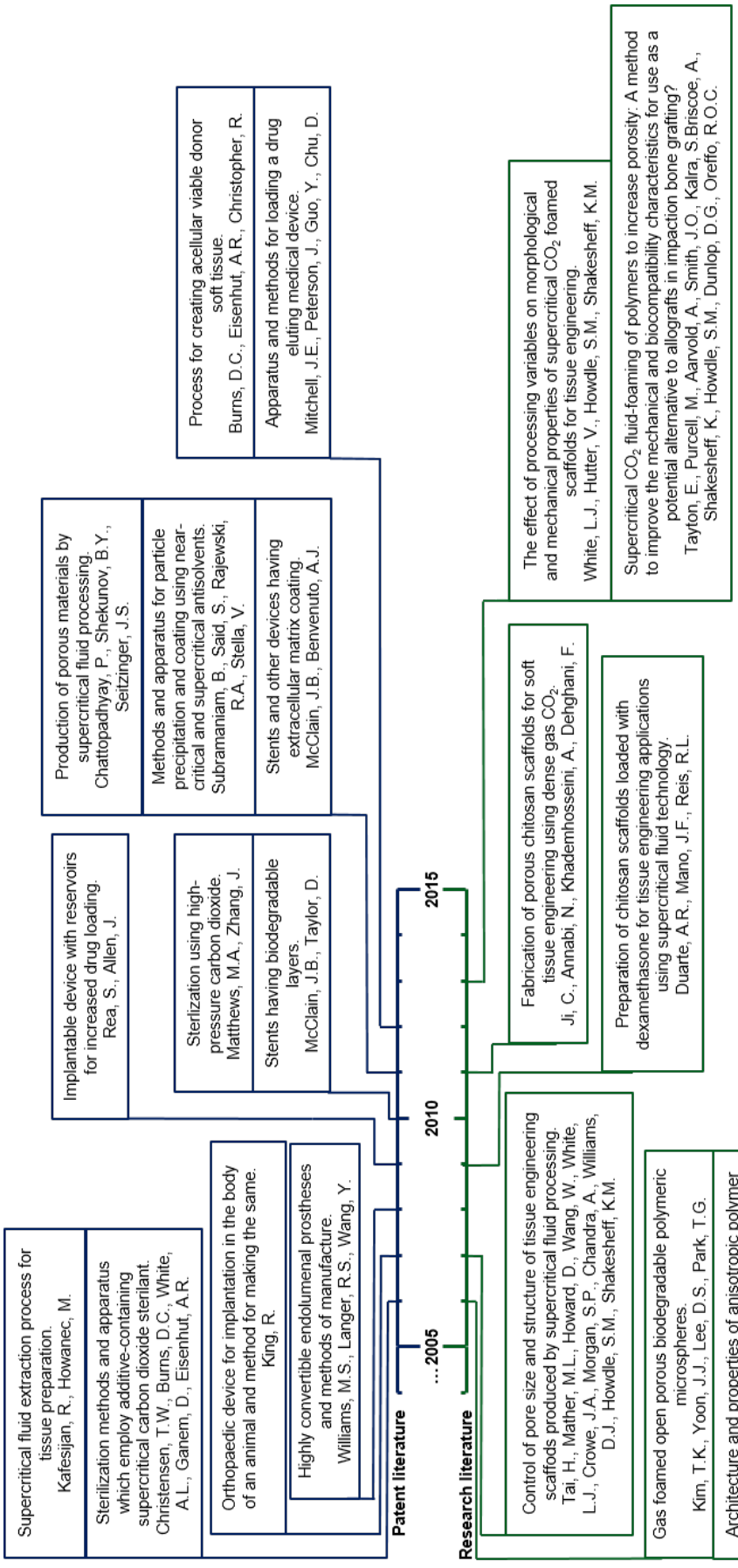

Figure 1.12: Timeline showing the pivotal patent and scientific literature that contributed to the advancement of supercritical fluids for the manufacture of regenerative medicine scaffolds.[1]

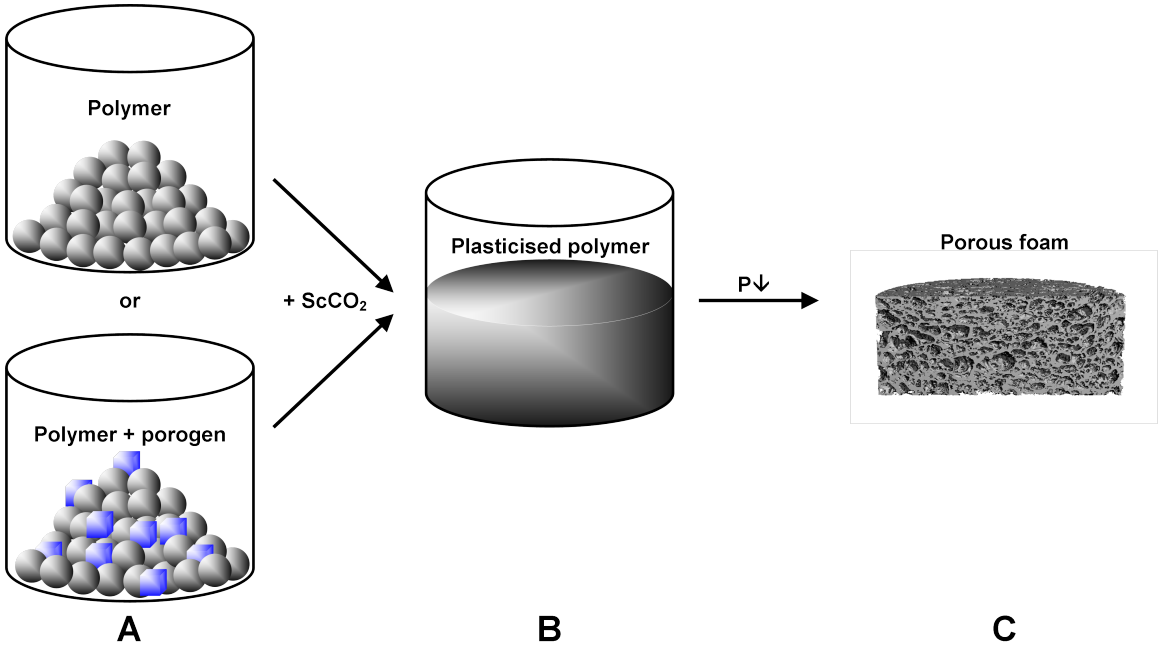

Figure 1.13: Overview of $scCO_2$ foaming whereby A) polymer or polymer and porogen are placed into a foaming vessel, B) $scCO_2$ plasticises the polymer and C) controlled depressurisation produces an interconnected porous foam. The use of a porogen is optional is later leached to improve the interconnectivity of scaffolds produced. Image taken from [1].

to load polymeric tissue engineering scaffolds with cells was patented [122] and studies demonstrated the viability of cells post-processing [123].

1.6.1 Supercritical fluid foaming

Porous matrices require a high degree of interconnectivity for use in regenerative medicine applications; interconnectivity is crucial for cell migration and nutrient transfer within the matrix [124]. To improve interconnectivity, porogens have been included in polymer melts and leached post-foaming [125, 126]. In a recent development, Turng *et al*. [127] patented the novel use of a water-soluble polymer, such as poly(vinyl alcohol), in an extrusion polymer melt and in combination with the use of porogens, to form scaffolds with greater interconnectivity and porosity. This method complemented injection moulding processes and was combined with the use of foaming agents (such as an SCF) to produce foamed complex scaffold shapes. An operator skilled in the art could further adapt this method to include the plasticisation effect of $scCO_2$ to operate at lower temperatures and incorporate thermolabile molecules into the scaffolds.

Chattopadhyay *et al*. [128] developed a method that replaced organic solvents with SCFs for removal of soluble components from traditionally produced (melt extrusion, *co*-precipitation, spray drying, lyophilisation, emulsion formation) composites. This method both reduced residual solvent and impurities which would diminish the need for downstream purification steps and provided a high level of porosity and pore size control.

In addition to porosity requirements, it is important that mechanical strengths (compressive and tensile) of scaffolds are matched to their function [129]. The strength of polymers varies with stereoisomer concentration, e.g., P_LLA or P_DLA contain more crystalline regions and therefore greater strength than amorphous $P_{DL}LA$. Stereocomplexes (where interaction of polymers with different tacticities prevails over those of identical tacticity [130]) of two homopolymers (e.g. P_LLA and P_DLA) formed by solvent casting or melt blending, have different crystalline structures with different mechanical properties than those of the homopolymers alone. Kim *et al*. [131] established the use of $scCO_2$ as a solvent to form stereocomplexes and to produce them in a foamed form.

An alternative method used to increase scaffold mechanical strength has been to utilise reinforcement from nanopowders such as smectite clays or calcium phosphates [132]. Supercritical fluid foaming has been shown to increase the interactions between polymer and clay

to increase bonding strength and this method was patented by Kannan *et al*. [133].

In combination with scaffold porosity and strength requirements, the incorporation of bioactive molecules and materials (e.g. hydroxyapatite and dexamethasone) has improved scaffold function through guided cell differentiation or localised drug delivery [134, 135]. Duarte *et al*. [136] successfully impregnated chitosan scaffolds with dexamethasone using $scCO_2$ for guided osteogenic differentiation of stem cells. Koltzenburg *et al*. [137] recently developed a method with foamed amphiphilic copolymers (such as polyether). These were combined with biodegradable polymers and active ingredients (such as chitin), that are sparingly soluble in water, to produce active ingredient containing polymers. Polymers such as this were extruded in the presence of SCFs to produce foams and the authors claimed improved mechanical properties although this was not shown. Howdle *et al*. [138] had previously demonstrated that biofunctional materials such as hydroxyapatite could be physically mixed with polymers in SCF environments to create composite biofunctional polymers irrespective of material solubility. An alternative method to include bioactive molecules was invented by Chatziniko-laidou *et al*. [139], where dry polymer powders were mixed with aqueous GF solutions to the hygroscopic limit of the powder; this created "slurries" of polymer and GF that were capable of being shaped and utilised in extrusion and foaming processes to create GF containing scaffolds.

Recent patents in the application of polymer foams include their use as hemostatic sponges (used to apply pressure and stop deep bleeding in minimally invasive surgery) and delivery devices [140, 141]. Chang *et al*. formed blends of biodegradable polymer and moisture-absorbent material, such as collagen, that when foamed were suitable to act as degradable hemostatic sponges, eliminating the need for their removal. Sandler *et al*. [140] produced stable nanoporous foams using rapid depressurisation (15,000–2,000,000 MPa s^{-1}) of polymer melts in SCFs; these foams contained a nanoscale open cell network that would not allow cellular ingress but did make them suitable for delivery of incorporated active compounds (e.g. albumin).

1.6.2 Microparticles by supercritical fluid processing

Polymer microparticles can join together to form 3D scaffolds [142], alternatively they can be incorporated as particle components of composite scaffolds - the benefit imparted by the microparticles to the scaffold may be release of bioactive signalling molecules (e.g. BMP-2

[143] or antibiotics to reduce risk of infection post-implantation. There is an abundance of literature surrounding SCF based methods for producing particles (see for example [144–146]). Many papers deal with production of polymer microparticles while others deal with production of active molecule based nanoparticles, with little cross-over between the two. Most recently polymer-based microparticles in regenerative medicine were reviewed by Oliveira and Mano [147], although with limited discussion of SCF based methods. Sheth *et al*. [148] provided a recent and comprehensive review of SCF technologies for nanoparticle production in the pharmaceutical industry.

There are three established techniques for particle production using SCFs. These are:

- Rapid expansion of supercritical solutions (RESS), where an SCF is saturated with a substrate and rapidly depressurised through a heated nozzle to form small particles [146].
- Particles from gas-saturated solutions (PGSS), where a liquid or polymer is saturated with an SCF which is then expanded through a nozzle to produce particles.
- Supercritical antisolvent precipitation (SAS), where a liquid solution is contacted with an SCF in which the solvent is miscible and the solute is insoluble, causing supersaturation and precipitation of the solute [146].

A schematic overview is provided in Figure 1.14

Many innovative adaptations to these techniques have recently been patented. Fulton *et al*. [149] transformed the RESS method of producing nanoparticles into a novel coating process. A stream of charged ions was generated that interacted with the RESS produced nanoparticles, which enabled electrostatic deposition. Previous work from the same group had shown that it was extremely difficult to deposit particles in the range 10–500 nm on to a surface from the RESS technique due to their low mass [150]. This transformed process overcame these coating difficulties, avoided the use of organic solvents, and provided a more uniform coating compared to those prepared by a cloud-point precipitation technique.

Recently patented adaptations to the RESS method tackle the challenge of producing aqueous solutions of insoluble materials [151, 152]. For example, Sun *et al*. [151] patented the use of stabilizing agents (that do not form micelles in aqueous solution), mixed with biologically active material (that has little or no solubility in water) in a solvent such as $scCO_2$ to form a non-aqueous solution. Then, using RESS, an aqueous suspension of particles was

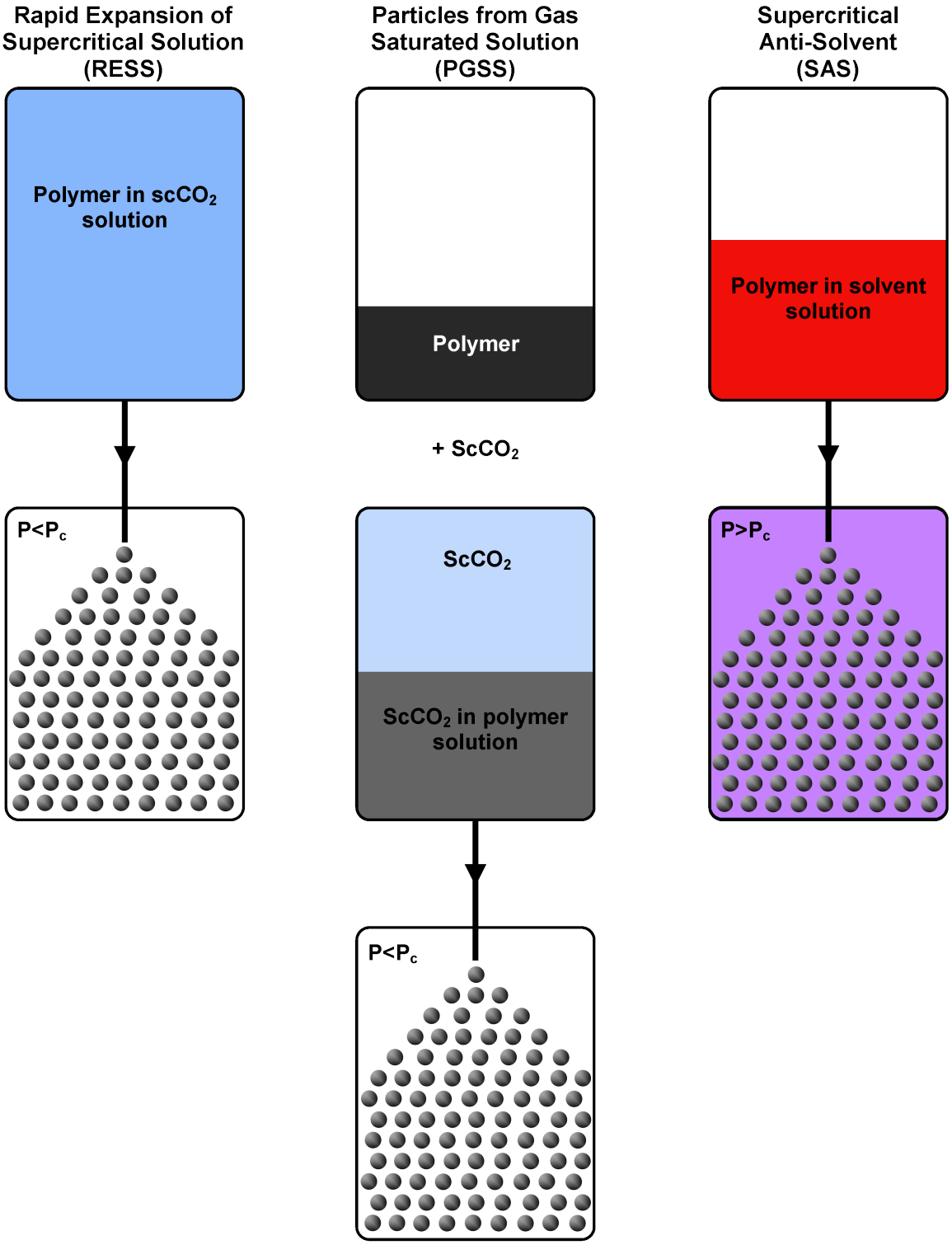

Figure 1.14: Established techniques for SCF particle production utilising $scCO_2$. (P = Vessel pressure and P_c = Critical pressure of CO_2). [1]

achieved where the particles had an average diameter <100 nm. Suspensions of nanoscale materials are treated as equivalent to solutions of the materials when considered for medical applications [153]. Suspensions of nanoparticles were created using established processes such as SCF spray drying, or precipitation by directly collecting the particles created in a media that formed the final formulation [152]. Importantly, this reduced the number of processing steps.

Innovative advances have been made for SAS particle manufacture methods [154–156]. For example, Subramaniam *et al*. [154] adapted the SAS method to produce coated particles. A high energy gas stream was used to break up the fluid dispersion into extremely small droplets which precipitated into small particles (0.1–10 μm) in the SCF anti-solvent. In the precipitation chamber it was possible to coat a counter current flow of "core" particles with the precipitating nanoparticles. Conventional methods for producing nanoparticles such as micronisation are often unsuitable for less brittle materials, like polymers, for which this method is appropriate. An alternative revision of the SAS process, from a different research team, was the use of a modulator (such as a polyethylene oxide), with a solubility inversely proportional to temperature in aqueous solutions [155]. The modulating agent enabled reduction in particle size and agglomeration, and aqueous solutions of a substrate to be used in the SAS process with $scCO_2$. Particle size and agglomeration were reduced by Shekunov *et al*. [156], who developed a method for utilising growth retardant compounds for the SAS technique. Compounds with CO_2-philic and CO_2-phobic groups such as sugar acetates were shown to reduce the particle growth rate and prevent agglomeration.

An adaptation of PGSS was made by Chattopadhyay *et al*. [157] where an emulsion of polymer, wax/lipid, and bioactive compound was created in an SCF environment. The expanded emulsion provided greater control over particle size, morphology, and size distribution than expanded polymer melts have achieved. In contrast, Deschamps *et al*. [158] produced solid micro or nano particles of active substance by expanding $scCO_2$ solutions of the active substance into chambers under conditions where liquid CO_2 was present containing a divided solid. This process produced a solid dry product in a stable form (such as a nifedipine/mannitol formulation), avoiding the use of wet size-reducing steps (e.g. ultrasound) that are common for nanoparticle dispersion production.

The atomisation of substances that are insoluble (or poorly soluble) in $scCO_2$ has previously been limited to methods that avoided the use of $scCO_2$. However, Osada *et al*. [159]

pioneered a method to atomise substances with poor solubility in $scCO_2$ through the combined use of water and $scCO_2$. Compounds or polymers insoluble in scCO2 were reduced to fine particles with an average size up to one hundred times smaller than their starting size. This was achieved by exposure to $scCO_2$ and water in a pressure vessel, followed by reduction of internal pressure. Whilst this method has been proven to be effective, the mechanisms of the atomisation process have not been fully elucidated by the authors.

A one step purification/harvesting method developed by Tsung *et al*. [160] used an SCF, or high pressure gas, to remove a solvent from a microparticle dispersion. This method removed the need for lyophilisation or evaporation steps to dry the microparticles. Castor *et al*. [161] also utilised SCFs as working fluids to purify protein-containing-polymer-microspheres and avoid use of organic solvents. Kaiso *et al*. [162] employed $scCO_2$ as a washing agent in their novel process for forming porous polyamide microparticles. The polyamide was dissolved in a cyclic amide, then heated and cooled to form particles; these contained residual cyclic amide that was recovered using $scCO_2$, allowing recycling of the solvent.

Recent interest has been shown in the use of $scCO_2$ in phase separation processing [163, 164]. Brown *et al*. [164] patented the use of a phase-separation enhancing agent (PSEA) for particle production. The PSEA enhanced or induced liquid-solid phase separation of active ingredients in aqueous solutions to produce spherical particles. Supercritical fluids were then utilised to remove residual PSEA from the particles. Day *et al*. [163] employed thermally induced phase separation to produce polymer microparticles with radial pores. Polymer was dissolved in a solvent, such as an SCF, then homogenised, rapidly frozen, and freeze dried. Microspheres with and without a nonporous skin region were formed by this method.

1.7 Aims of this study

The focus of this thesis is to establish the potential of $scCO_2$ foamed polymeric scaffolds as viable substitutes to allograft for impaction bone grafting (IBG), particularly revision hip arthroplasty. To achieve this $scCO_2$ foamed scaffolds investigated within this thesis were processed as donated femoral heads would be - utilising a bone mill to create chips that retain the porosity imparted through $scCO_2$ foaming.

In the next chapter, Chapter 2, general methods and equipment used for the experimental work of studies within this thesis are described in detail. This chapter is for reference for experimental work carried out and deviations from the general methods are described in the experimental section of the relevant chapter.

In Chapter 3, building on previous work within the literature, melt processed and $scCO_2$ foamed $P_{DL}LA$ and $P_{DL}LGA$ scaffolds were investigated to establish the advantages of porous scaffolds over non-porous. The performance of different $scCO_2$ scaffolds were then assessed in *in vitro* and *in vivo* models of IBG to establish the most promising scaffold formulation to investigate in a large animal *in vivo* model. Hydroxyapatite microparticles were incorporated into some scaffolds and the effect of these particles on scaffold performance was also assessed. The performance of different scaffolds were assessed based on cellular compatibility, cellular differentiation, and resistance to shear forces (a common mechanism of failure for hip prostheses).

In Chapter 4, having determined the most promising scaffold formulation, $scCO_2$ foamed $P_{DL}LA$ + HA microparticles composite scaffolds were studied using an ovine *in vivo* femoral condyle model. The performance of scaffolds *in vivo* were studied both with and without pre-seeded autologous MSCs. In this chapter the potential scale-up of production of $scCO_2$ foamed polymeric scaffolds was also investigated. Establishing this potential is important for determining the viability of $scCO_2$ scaffolds as alternatives to allograft.

The aims of Chapter 5 were to investigate differences in the performances of scaffolds of $P_{DL}LA$ and $P_{DL}LGA$ scaffolds observed in Chapter 3. Given the similarity of the polymers, the large differences observed in the osteoblastic differentiation of MSCs cultured on the scaffolds was unexpected and *in vitro* experiments with MSCs cultured on thin films were carried out to remove morphological difference in the $scCO_2$ foamed scaffolds. Additionally, the incorporation of HA microparticles improved the cellular performance of $scCO_2$ foamed $P_{DL}LA$ and $P_{DL}LGA$ scaffolds in Chapter 3, while having no significant effect on mechanical properties. The effect of incorporation of HA nanoparticles was studied through *in vitro* cell experiments as a promising method to improve formulation performance prior to any further potential large animal studies.

The final chapter, Chapter 6 gives a final discussion of the significance of the results and experimental work presented within this thesis.

CHAPTER 2

Materials and general methods

Table 2.1: Properties of polymers used in the studies contained within this thesis taken from the manufacturers (Surmodics Biomaterials) specification sheets.

Polymer	M_W [kDa]	Polydispersity index (PDI)	Tg	Inherent viscosity [dL g^{-1}]
$P_{DL}LA$	126	1.5	50.3	0.80
$P_{DL}LA$	106	1.9	52.0	0.75
$P_{DL}LGA$	110	1.5	50.0	0.71

2.1 Supercritical CO_2 foaming

Various polymers were purchased from SurModics Biomaterials (Birmingham, U.S.A.) and used to produce $scCO_2$ foamed scaffolds. Table 2.1 displays the properties of the various polymers utilised in the studies within this thesis. Polymers, as purchased from manufacturer, were ground using a blade grinder (Krups, model F203) prior to $scCO_2$ foaming.

Ground polymer powder was weighed into cylindrical wells (11.2 mm $\times$ 10.4 mm) within a custom-made (School of Chemistry, The University of Nottingham) PTFE mould (74.2 mm $\times$ 27 mm $\times$ 12 mm), 300 mg per well, and a stainless-steel lid (with a PTFE insert to aid removal of the scaffolds) was screwed into place above the wells filled with polymer. The mould contained vents at the base and top of each well to enable CO_2 access. For scaffolds containing HA particles, these were weighed into the wells of the mould with the ground polymer powder prior to the lid being screwed into place. Hydroxyapatite microparticles were purchased from Berkeley Advanced Biomaterials and graded to a size range of 100-300 μm.

Hydroxyapatite nanoparticles (both nanorods and nanoplates) were kindly donated by Prof. Edward Lester and Miss Selina Tang (Faculty of Engineering, The University of Nottingham). For supercritical foaming the sealed mould was placed into a custom-made (School of Chemistry, The University of Nottingham) 60 ml stainless-steel autoclave (pressure rated to 35 MPa) and clamp sealed. Swagelok (Ohio, U.S.A.) piping and fittings, and HiP (High Pressure Equipment Company, Pennsylvania, U.S.A.) high pressure valves connected the system. A pressure transducer located on the inlet line between the HiP inlet CO_2 valve and the autoclave inlet enabled internal pressure monitoring. The autoclave was fitted with a heating jacket controlled using a CAL 3000 temperature controller (CAL controls, Brighton

U.K.). A high pressure PM1010 pump (New Ways of Analytics, Lörrach, Germany) was used to pressurise CO_2 from cylinder pressure (≈5 MPa) to 30 MPa. Pressure within the autoclave was controlled using a Bronkhorst (Ruurlo, Netherlands) back pressure regulator, and FLOWDDE version 4.44 and FlowPlot version 3.11 Bronkhorst software.

With the polymer and mould in place the autoclave was jacket heated to 35 °C; then filled with CO_2, the pressure increased to 23 MPa over a period of 20 minutes (fill time); the pressure was held constant for 60 minutes (soak time); the pressure was then reduced over a period of 30 minutes at a constant rate to ambient conditions (the vent time); heating was ceased; the mould was removed from the autoclave, and the foamed polymer scaffolds removed from the mould. Figure 2.1 shows the layout of the $scCO_2$ foaming equipment and an image of the 60 ml autoclave used. Figure 2.2A and B show images of $scCO_2$ foamed polymer scaffolds formed through this process.

The standard operating procedure of the high pressure foaming rig is detailed in Appendix 1.

2.2 Scanning electron microscopy

Scanning electron microscopy (SEM) was carried out on two different machines. Samples for imaging were prepared using a scalpel to create axial slices across the porous scaffolds (in line with the diameter). $scCO_2$ foamed scaffold slices were placed on SEM stubs and sputter coated. Gold sputter coating was performed using a Leica EM SCD005 sputter coater; coating at $\leq$ 4 Pa (in argon) for 180 seconds. A JEOL JSM-6060LV SEM was used for general imaging with an accelerating voltage of 15 keV.

Scanning electron microscopy commonly detects secondary electrons emitted by atoms excited by the electron beam of the microscope. In the micrographs produced from secondary electron detection HA particles were difficult to discern from the background P_{DL}LA. Samples containing HA particles were imaged using both secondary electrons and backscatered electrons (BSEs).

For samples that required imaging using BSE carbon sputter coating was used. Carbon sputter coating was performed using a Polaron SC7640 sputter coater at 4 $\times$ 10-2 mbar (or below) for 40 seconds. A Philips FEI XL30 SEM with an accelerating voltage of 15 keV, and Inca Suite, version 4.14 (Oxford instruments analytical Ltd), were used for imaging.

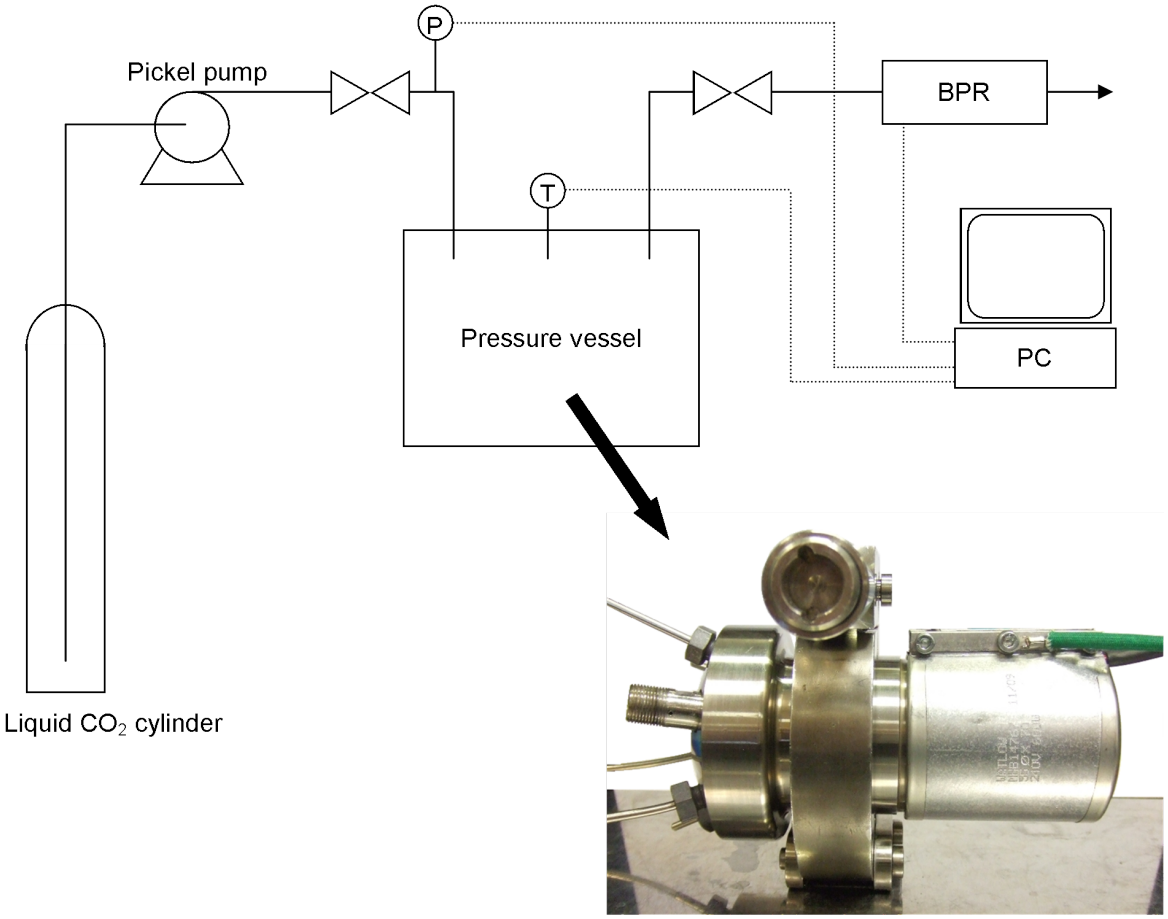

Figure 2.1: The layout of $scCO_2$ foaming equipment and the block arrow indicates an image of the 60 ml autoclave into which PTFE moulds were placed for foaming. A diptube CO_2 cylinder provided a source of CO_2 pressurised in the pickel pump and flowed into the pressure vessel. A back pressure regulator (BPR) controlled the internal pressure. Internal temperature was recorded via a thermocouple (T) linked to a PC.

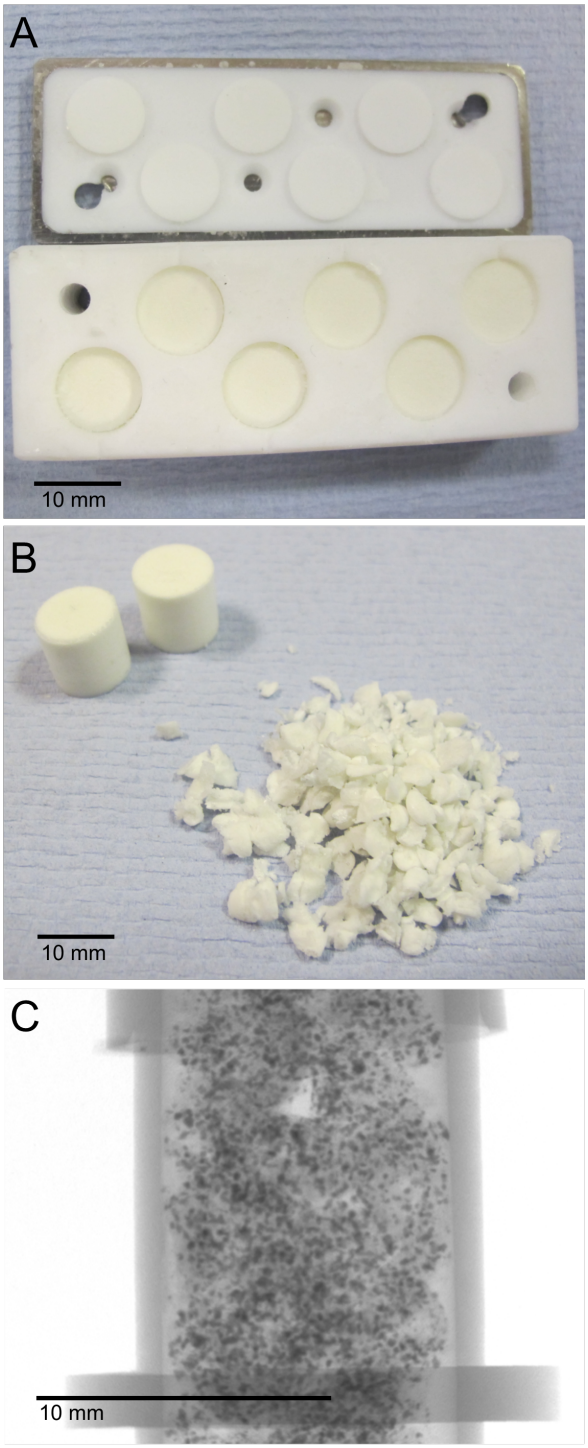

Figure 2.2: Supercritical CO_2 polymer scaffolds are shown in a PTFE mould post-foaming (A) and removed from the mould (B). Image B) also shows chips of $scCO_2$ foamed polymer scaffolds after processing with a standard bone mill. Image C) shows an x-ray image of milled chips of $scCO_2$ foamed $P_{DL}LA$ + 10 wt.% HA microparticles impacted into an impaction chamber, taken using μCT.

Backscattered electrons arise from the electron beam of the microscope (incident beam) scattered back at an angle nearly normal to the incident beam without loss of kinetic energy (elastic scattering). The probability of electrons being elastically scattered increases as the atomic number of elements in the sample increases due to a larger cross-sectional area. A proportional relationship exists between the mean atomic number of a sample and the number of BSEs detected. While $P_{DL}LA$ contains carbon, oxygen, and hydrogen, HA is formed of calcium and phosphorus, which have larger atomic numbers (20 and 15, respectively).

2.2.1 Elemental mapping

Energy dispersive x-ray spectroscopy (EDX) was performed to identify HA particles within the scaffolds. Samples were prepared as for SEM prior to sputter coating. Carbon sputter coating was performed using a Polaron SC7640 sputter coater at $4 \times$ 10-2 mbar (or below) for 40 seconds. A Philips FEI XL30 SEM was used for elemental mapping with an accelerating voltage of 15 keV, and Inca Suite, version 4.14 (Oxford instruments analytical Ltd), was the software used.

X-rays are emitted when a high energy electron in an outer shell of an atom within a sample fills a lower shell from which electrons were ejected due to bombardment by the incident beam in SEM. The emitted x-rays balance the energy difference when the outer electron drops to a lower shell and the intensity of the x-rays emitted are characteristic of the atoms they are emitted from.

2.3 Micro x-ray computed tomography

Micro x-ray computed tomography (μCT) was carried out on two different machines. The details of which machine was used for each study is reported within the individual results chapters, as well as here. The use of μCT enabled non-destructive imaging and quantitative analysis of the 3D microstructure and morphology of $scCO_2$ foamed samples. A Skyscan system was used for all $scCO_2$ foamed scaffolds quantitifed by μCT and for ovine femoral condyle defect samples. An XTEK System μCT scanner was utilised for murine samples post-*in vivo* incubation.

2.3.1 Skyscan

The μCT system utilised for most samples was a Skyscan 1174 μCT scanner (Skyscan, Belgium). Scaffolds were mounted on a holder and placed in the scanner. The stage was set at a height of 6.5 mm and the scaffolds were scanned with the following settings: 40 kV voltage, 800 μm current, and 12.0 voxel resolution. Image reconstruction was performed using NRecon (Skyscan, Belgium) and saved as 8 bit bitmaps (BMP). Analysis of the reconstructed images was performed using CTAn (Skyscan, Belgium) using threshold values of 37 and 255 for $scCO_2$ foamed polymer scaffolds.

2.3.2 XTEK Systems

MicroCT scanning and reconstruction using the XTEK system was carried out at μ-VIS, Southampton University by Dr. Stuart Lanham and Mr. E. Tayton.

Quantitative 3D analysis of implanted impaction chambers was obtained using a Metris Xtek HMX ST 225 kV CT scanning system (X-TEK Systems Ltd, Tring, Hertfordshire, U.K.). Raw data was collected and reconstructed using Next Generation Imaging (NGI) software package (X-TEK Systems Ltd.) with a 10.6 μm voxel resolution. All voxels were automatically assigned Houndsfield units via calibration against a standard water sample. The images were visualised and analysed using Volume Graphics Studio Max software (Volume Graphics, Heidelberg, Germany). The regions of interest (contents of the impaction chambers), thresholds for new bone, polymer, and HA microparticles were selected manually, and the volumes of new bone calculated via the software. From this data, the mean and standard deviations for bone volume were calculated for each experimental group. Both 2D and 3D images (saved as TIFFS) were created, with different colour assignments to certain greyscale value ranges in order to highlight areas of interest.

2.4 Mechanical characterisation

2.4.1 Shear testing

Shear testing was carried out at Southampton University by Mr. E. Tayton.

Shear testing was carried out on milled $scCO_2$ foamed scaffolds. The scaffolds were processed using a standard bone mill (Tessier Osseous Microtome, Stryker Leibinger, Freiberg,

Germany) and impacted into custom-made acrylic rings (School of Engineering Sciences, University of Southampton) with an internal diameter of 65 mm and 10 mm high. The acrylic rings had removable perforated lids and bases. A custom-made impactor (School of Engineering Sciences, University of Southampton) was used for the impaction process. This was designed to mimic the forces of impaction bone grafting, which has been shown to be the equivalent of a 1.98 kg mass dropping 65 mm onto a 60 mm diameter circular base [165]. The impactor was scaled to exert an identical pressure, this was achieved by dropping a 344 g mass a distance of 65 mm onto a 25 mm diameter base. The impaction process involved filling the rings with milled polymer scaffold and impacting twenty-four times, and this process was repeated twice more to fill the centre of the rings with impacted, milled, $scCO_2$ foamed polymer scaffolds. The perforated lid and base were applied and the impacted polymer discs were incubated at standard physiological conditions (37 °C, 5% CO_2) in PBS for 1 week to replicate *in vivo* conditions. Figure 2.3A shows the impactor and a prepared sample impacted into an acrylic ring.

After 1 week incubation the impacted polymer discs (65 mm × 10 mm) were removed whole from the acrylic rings and placed into a custom-made Cam shear tester (School of Engineering Sciences, University of Southampton) that consisted of two stainless-steel rings, each 5 mm in height with 65 mm internal diameters. The rings were vertically stacked and the upper ring was fixed in position, while the lower ring could be moved horizontally. Impacted polymer discs, positioned in the centre of the stainless-steel rings, were placed under a normal/compressive load; this was achieved through placing weights onto a plunger running on a linear bearing and resting on the polymer disc. A time of 5 minutes was allowed for the sample to settle after applying the normal load. The lower ring was then driven by a hydraulic actuator (Instron Ltd., Bucks, U.K.) at a constant rate of 1.2 mm min^{-1} .This movement forced the impacted polymer disc to shear and the force required to move the lower ring and the distance travelled were recorded using load and displacement sensors within the actuator. For each polymer scaffold type three compressive loads (50, 150, and 250 N), which gave compressive stresses of 102, 306, and 509 kPa to simulate physiological stresses [54], were used on different samples (n=4). This method has been used previously within the literature by Bolland *et al*. [54].

The resultant stress-strain curves were used to plot the Mohr-Coulomb failure envelope curves for each scaffold type and shear strength and interlocking particle cohesion were derived for each. The mean shear strength at 10% strain (standard engineering practice) was

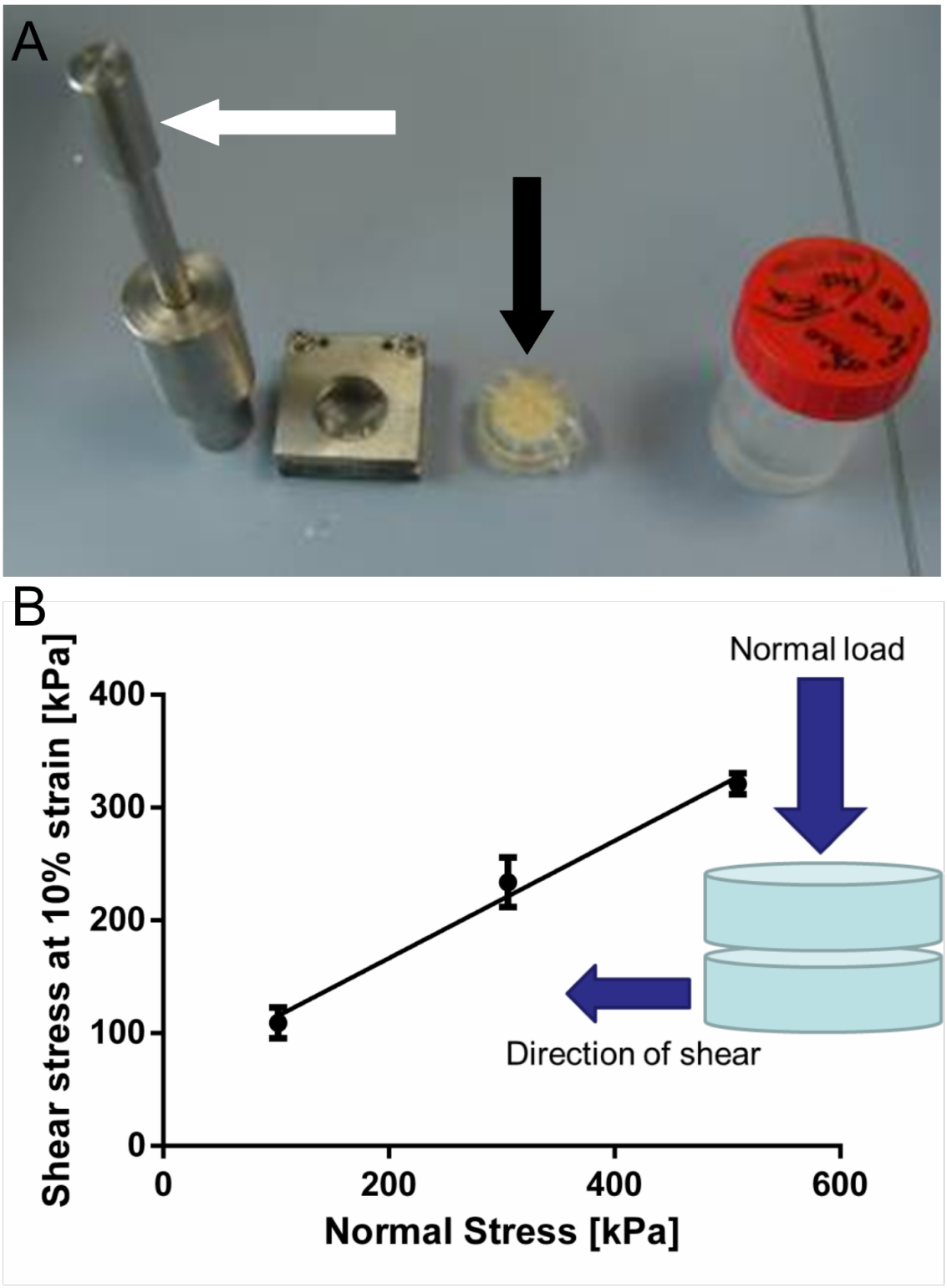

Figure 2.3: A. Impactor for preparing samples for mechanical shear testing. White arrow indicates the impactor device and the black arrow indicates an impacted sample of milled $scCO_2$ foamed polymer in an acrylic ring. B. Example Mohr-Coulomb failure curve for impacted allograft morsels. The inset diagram shows the direction of the forces applied to impacted rings under test.

plotted against the normal load and grouped linear regression analysis carried out (GraphPad Prism 6, GraphPad Software Inc., CA, U.S.A.). The Mohr-Coulomb failure criterion is expressed as $\tau = \sigma tan(\phi) + c$, where τ is the shear strength, σ is the normal stress, ϕ is the angle of internal friction, and c, the intercept is the interparticulate cohesion. An example Mohr-Coulomb failure curve is shown in Figure 2.3B.

2.5 General cell culture

Cell culture was performed using aseptic technique in a class II microbiological safety cabinet (Envair, Haslington, U.K.). *In vitro* incubation of cells was in a Sanyo MCO-17AIC incubator (Sanyo Electric, Biomedical, IL, U.S.A) at 37 °C and 5% CO_2.

Primary human mesenchymal stem cells were used for the majority of the cell culture studies within this thesis. Ovine mesenchymal stem cells were utilised for the parallel *in vitro* studies that accompanied the ovine femoral condyle defect study in Chapter 4. Immortalised human mesenchymal stem cells were used for the polymer film experiments in Chapter 5. Protocols for these studies are included in the materials and methods sections of the appropriate chapters.

For cell expansion and cell seeding basal medium was used which was α-Modified Eagle's Medium (α-MEM) supplemented with 10 vol.% fetal bovine serum (FBS), and 100 μg ml^{-1} penicillin and 100 μg ml^{-1} streptomycin (Pen-Strep, Invitrogen).

Osteogenic differentiation of MSCs was stimulated utilising osteogenic medium which was basal medium supplemented with 100 μM ascorbate-2-phosphate and 10 nM dexamethasone.

2.5.1 Primary human mesenchymal stem cells

All culture of primary MSCs was performed at Southampton University by Mr. E. Tayton.

2.5.1.1 Isolation of cells

Mesenchymal stem cells were harvested from the bone marrow of a 66 year-old male undergoing routine hip replacement surgery with the approval of the local hospital ethics committee (LREC 194/99/w, 21/10/10). They were then expanded *in vitro* in T150 flasks in

basal medium (α-MEM with 10% FBS and 1% penicillin and streptomycin) at 37 °C and 5% CO_2 until confluent. Media changes were performed every 3 days during culture. At confluence the cells were washed in phosphate buffered saline (PBS) and treated with trypsin in ethylenediaminetetraacteic acid (EDTA) for 2 minutes to detach cells from tissue culture plastic (TCP). An equal volume of serum-containing medium was used to deactivate the trypsin and the cell suspension transferred to a universal tube and centrifuged for 5 minutes at 180 g. Supernatant was aspirated and cells resuspended in FBS + 10% dimethyl sulfoxide (DMSO) to a concentration of 1 million cells ml^{-1}. Cells were stored in 1 ml cryo-vials at -80 °C for one week and then transferred to liquid N_2 storage.

2.5.1.2 Cell culture

For each study an appropriate number of cryo-vials of cells (passage 1, P1) were reanimated by thawing and suspension in 10 ml of basal medium. Then they were centrifuged for 5 minutes at 180 g. The supernatant was aspirated and the cells re-suspended in basal medium. Cell concentration was determined using a haemocytometer and appropriate dilution with basal medium to reach a final concentration of 5×10^5 cells ml^{-1}.

2.5.1.3 Preparation of scaffolds

Polymer scaffolds were milled in a standard bone mill (Tessier Osseous Microtome, Stryker Leibinger, Freiberg, Germany) to produce small chips of porous scaffold. These chips were sterilised in 5% antibiotic/antimycotic solution (Sigma-Aldrich, U.K.), placed under ultraviolet (UV) light for 24 hours and submerged in basal medium for a further 24 hours prior to cell seeding. Figure 2.2B shows an image of milled chips of polymer scaffolds.

2.5.1.4 Cell seeding

Sterilised milled chips of polymer scaffolds were placed in sterile universal tubes and 20 ml of cell suspension (5×10^5 cells ml^{-1} in basal medium) was added to each. The universal tubes were placed in an incubator under standard conditions (35 °C, 5% CO_2) for 2 hour with gentle agitation every 30 minutes.

2.5.1.5 Impaction of seeded scaffolds

A smaller scale impaction device to the one described in Section 2.4.1 was sterilised in an autoclave. The design of the device was such that it applies equal pressure upon impaction to the larger device to simulate the forces experienced during IBG. Approximately 1 ml of milled polymer chips seeded with cells was loaded into an open ended plastic impaction chamber in three equal portions and the impaction device was used to give 24 impactions between each addition. The open ended impaction chambers were placed in non-TCP six well plates (1 sample per well) and cultured in osteogenic conditions (basal medium + 100 μM ascorbate-2-phosphate and 10 nM dexamethasone) at 37 °C and in 5% CO_2. Cell culture medium was changed every 3 days. Figure 2.2C shows an x-ray image of chips of polymer scaffold impacted into an impaction chamber.

2.6 Cellular assays

2.6.1 WST-1 proliferation assay

The WST-1 (Water soluble tetrazolium salt-1 (2-(4-Iodophenyl)-3-(4-nitrophenyl)-5-(2,4-disulfophenyl)-2H-tetrazolium)) metabolic assay (Roche Ltd, Welwyn Garden City, U.K.) was used to assess cell viability and proliferation. WST-1 is reduced by metabolically active cells to a water-soluble formazan dye that then allows a colorimetric measurement of metabolic activity that can be correlated to number of viable cells. This reduction is dependent on reduced pyridine nucleotides NADH (reduced nicotinamide adenine dinucleotide) and NADPH (reduced nicotinamide adenine dinucleotide phosphate) and occures primarily at the extracellular surface of the plasma membrane [166].

The protocol varied for each study and deviations are detailed in individual chapters. An example protocol follows for milled, seeded, and impacted polymer scaffolds in impaction chambers. For each scaffold type three samples (and one control without cells) were submerged in 2.5 ml of 1:10 dilution WST-1 substrate. At 2 and 4 hr, 400 μl of substrate was removed and read in triplicate via a Bio-Tek KC4 microplate fluorescent reader (Bio-Tek, USA) at 450 nm. Mean and standard deviation values for each sample at both time points were calculated and mean control values subtracted.

2.6.2 Alkaline phosphatase activity assay

Alkaline phosphatase (ALP) is a membrane bound enzyme utilised as an early indicator for osteoblastic differentiation [167, 168]. Its expression is not entirely specific to osteoblastic cells and other indicators are required to confirm osteoblastic differentiation [169]. The levels of alkaline phosphatase expression were determined through a colorimetric assay. para-Nitrophenylphosphate and water react in the presence of alkaline phosphatase to phosphate and para-nitrophenol; para-nitrophenol has a yellow appearance and the concentration can be determined through optical absorbance reading at 405 nm. The concentration of para-nitrophenol is proportional to the concentration of alkaline phosphatase in each sample if read at the same time point, under the same conditions, and if the same starting concentration of para-nitrophenylphosphate is used.

The protocol varied for each study and deviations are detailed in individual chapters. An example protocol follows for milled, seeded, and impacted polymer scaffolds in impaction chambers. The contents of three impaction chambers and one control from each group were washed in PBS and fixed in 90% ethanol prior to air drying; then rewashed with PBS and suspended in 2 ml of 0.5% Triton X-100. Three freeze thaw cycles were carried out with vigorous agitation between cycles. p-Nitrophenyl phosphate (1 mg ml^{-1}) was used as substrate in 2-amine-2-methyl-1-propanol alkaline buffer solution (Sigma-Aldrich, U.K.) for lysate measurements for ALP activity. Cell lysate samples has ALP substrate solution added and were incubated at room temperature for 30 minutes. Cell lysate (10 μl) was run in triplicate for three impacted cell seeded samples and a single control sample of each scaffold type on a plate against $\times 2$ standards, read on a Bio-Tek KC4 and FLX-800 microplate fluorescent reader (Bio-Tek, USA) at 405 nm and the mean and standard deviations were calculated. The standards were used to calculate a standard curve from which ALP concentration within cell lysate samples could be calculated. Mean ALP activity was calculated for each polymer scaffold type by dividing the mean ALP concentration by the mean DNA concentration for each group, which gave the specific ALP activity in units of nanomoles of para-nitrophenyl phosphate per hour per nanograms of DNA [nmols pNPP h^{-1} ng DNA^{-1}].

2.6.3 DNA assay

The protocol varied for each study and deviations are detailed in individual chapters. The cell lysate used for ALP assays was also used for DNA assays. An example protocol fol-

lows for milled, seeded, and impacted polymer scaffolds in impaction chambers. PicoGreen (Molecular Probes, U.K.) was used to quantify deoxyribonucleic acid (DNA) concentration as per manufacturer protocol. Triplicate measurements of 10 μl of lysate for each sample were measured against $\times 2$ standards on a Bio-Tek KC4 and FLX-800 microplate fluorescent reader. Calf thalmus DNA was used for the standards. Means for each group were calculated and the means of controls subtracted (for the appropriate group). The standards were used to calculate a standard curve from which DNA concentration within cell lysate samples could be calculated.

The PicoGreen assay uses a fluorescent nucleic acid stain that has a linear detection range over three orders of magnitude (500 pg ml^{-1} - 500 ng ml^{-1}. The dye bonds to double-stranded DNA, although it will also bond to RNA and single-stranded DNA. When bonded to double-stranded DNA it excites at a wavelength of 480 nm and fluoresces at 520 nm with minimal interference from single-stranded DNA and RNA bound dye.

2.7 Immunohistochemical staining

Immunostaining of primary MSCs and ovine MSCs was performed at Southampton University by Mr. E Tayton. Confocal microscopy of these samples was performed at Southampton University by Dr. David Johnston. Immunostaining and fluorescent microscopy of immortalised human MSCs (Chapter 5) was performed at The University of Nottingham by the author.

The protocol varied for each study and deviations are detailed in individual chapters. An example protocol follows for milled, seeded, and impacted polymer scaffolds in impaction chambers. The contents of an impaction chamber for each scaffold type was washed in PBS and fixed for 24 hours in 4% paraformaldehyde. Samples were kept in PBS until immunohistochemically stained, which involved 10 min incubation in 1% bovine serum albumin (BSA) followed by incubation overnight in 1 ml primary antibodies for collagen-1 (LF68, whole rabbit serum; 1:3000 diultion), osteocalcin (OC; monoclonal antibody OS 35; 1:100 dilution), and bone sialoprotein (BSP; anti-human BSP; 1:100 dilution). Then three washes with 0.1% PBS Tween were carried out. The appropriate secondary antibody was added for an hour at ambient conditions followed by three 0.1% PBS Tween washes. DAPI (1:100) was added as a nuclear counter stain via 10 min incubation. Specificity was confirmed by treating a portion of each sample with secondary antibody only. Samples were stored in PBS and kept

away from light until imaged via confocal microscopy (Leica SP5 Laser Scanning Confocal Microscope and software, Leica, Germany).

2.8 Statistical analysis

GraphPad Prism 6 software (GraphPad Software Inc., CA, U.S.A.) was used to carry out statistical analysis on quantitative results. One way analysis of variance with Tukey's multiple comparison test was carried out to assess statistical significance of results.

CHAPTER 3

Supercritical CO_2 foamed polymeric scaffolds for impaction bone grafting applications

In this chapter the difference between non-porous and porous polymer scaffolds produced through $scCO_2$ is highlighted. Both $P_{DL}LA$ and $P_{DL}LGA$ scaffolds are used to demonstrate improved cell compatibility and shear resistance of foamed scaffolds over nonfoamed scaffolds. Given that both $P_{DL}LA$ and $P_{DL}LGA$ compare favourably against allograft in mechanical shear tests polymer choice was left to cellular responses. MSCs were shown to proliferate well on both types of polymer but osteoblastic differentiation was demonstrably greater in the time period on $P_{DL}LA$ scaffolds. This was shown to be improved with the inclusion of hyrdoxyapatite and mechanical strength remained unaffected by the composite scaffold. A small scale *in vivo* model demonstrated the same results and additionally demonstrated vascularisation of the scaffolds and cell staining was used to confirm cells seeded on the scaffolds remained.

3.1 Introduction

In Chapter 1 the increasing need for bone graft materials was established, particularly for impaction bone grafting (IBG). Various biomaterials used to produce bone tissue engineering scaffolds including bioresorbable polymers were described. Methods of producing porous bioresorbable polymeric scaffolds were also described. Supercritical CO_2 foaming is one such method that holds particular promise due to the low operating temperature and no requirement to utilise organic solvents. High operating temperatures limit the use of thermolabile, bioactive molecules that can enhance scaffold performance such as BMP-2. Organic solvents leave residues that are harmful to cells and limit the cellular compatibility of scaffolds, or add the need for a solvent extraction step which can decrease the economic viability of a process.

A large volume of scientific research has been generated on the subject of bone tissue engineering/regeneration. Bone properties (modulus, porosity, tensile strength, and compressive strength) vary widely with function which has led to a diverse range of studies for different application of scaffolds in bone tissue engineering. Where a scaffold may be perfect for maxillofacial [170] or dental applications, a different scaffold may perform better in load bearing applications such as spinal [171] or long bone repair. Targeted scaffold application and well-designed studies demonstrate the capabilities of this field more strongly.

The studies described in this chapter were undertaken to determine the most favourable polymeric scaffolds to use, in conjunction with MSCs, as osteogenic alternatives to allograft bone in IBG procedures. The scaffolds tested with the most promising results were then used in a large animal model as detailed in Chapter 4. The number of scaffolds that could be investigated in the large animal model were severely restricted because of the associated costs and time investment. Therefore, the studies within this chapter were required to identify the most promising scaffolds worthy of this investment.

Previous work demonstrated enhanced MSC survival and proliferation on high molecular weight, M_W (>80 kDa) $P_{DL}LA$, $P_{DL}LGA$, and PCL over low M_W (<35 kDa) forms of the same polymers [4]. Tayton *et al*. [4] studied the proliferation of MSCs on melt processed polymer scaffolds. These melt processed scaffolds were milled using a standard bone mill, sterilised, and seeded with MSCs. After seeding, the milled chips were aseptically impacted in a process to mimic the forces of an IBG procedure and cultured for 8 days. A metabolic assay (WST-1) and live/dead fluorescent staining revealed significantly greater proliferation

(P<0.05) on high M_W (126 kDa) P_{DL}LA and high M_W (110 kDa) P_{DL}LGA scaffolds, than low M_W (26 kDa for P_{DL}LA and 36 kDa for P_{DL}LGA) scaffolds of the same polymers; the same trend was observed for MSCs cultured on high M_W (85 kDa) PCL scaffolds to those on low M_W (14 kDa) PCL, although this was not significant at the P<0.05 level. In the same study the authors investigated the resistance to mechanical shear of impacted, milled chips of the polymers. They reported that both high and low M_W P_{DL}LA and P_{DL}LGA outperformed milled and impacted chips of allograft bone; high and low M_W PCL samples did not. These results provided a basis for the further study of high M_W P_{DL}LA and P_{DL}LGA scaffolds.

The importance of porosity in bone regeneration targeted scaffolds has been strongly established [172]. Kuboki *et al*. [173] established BMP-induced osteogenesis occurred *in vivo* (inside a living organism) (rat ectopic model) on porous HA and not on solid HA. Fujibayashi *et al*. [174] were the first to report bone induction in a non-osseous site by titanium metal (a material accepted as being bioinert) attributed purely to the macrostructures (>100 μm) and microstructures ($\leq$100 μm) of the implants. In contrast to the findings of Fujibayashi *et al*., Yuan *et al*. [175] reported osteoinductive properties of HA (a material generally accepted as having osteoinductive properties) varied with the microstructure of implants to such an extent that while *in vivo* (3 and 6 months in canines) bone formation was found with macroporous HA implants (average pore size 400 μm, porosity 60–70%) with rough irregular pore walls (observed by SEM), no bone formation was detected in the same model in macroporous HA implants (average pore size 200 μm, porosity 70%) with smooth pore walls. With the importance of porosity established, many investigations in the literature are published on novel porous scaffolds targeted for bone tissue engineering with the absence of non-porous controls for comparison [176–178].

In addition to the body of evidence supporting osteoinductive properties of micro porosity within bone tissue engineering scaffolds, the presence of porosity, particularly interconnected porosity, is required for cell migration, cell proliferation, vascularisation, nutrient transfer, and bony in-growth. Work in 1970 by Hulbert *et al*. [179] recommended minimum pore sizes of 100 μm for improved osteogenesis in porous implants. Subsequent work has demonstrated improved osteogenesis in comparative studies where porous implants with pores >300 μm were utilised [180, 181].

The consensus on optimal pore size for bone regeneration scaffolds is not definitive, particularly given the wide range in bone properties such as porosity and mechanical strength.

A porosity greater than 100 μm is widely regarded as optimal but ranges from 100–400 μm are cited [182–184], while other published studies demonstrate no significant difference in bone growth on scaffolds with different pore sizes [129]. Additionally, it is inappropriate to use optimal properties for animal *in vivo* models and regard the results as definitive for human application. Karageorgiou *et al*. [172], in a review of porosity in osteogenic scaffolds, identified that there are no reports indicating beneficial effects for implants with low porosity in terms of cell behaviour. For scaffolds formed of the same material, mechanical strength typically decreases as porosity increases.

Additionally optimal porosity is also dependent on the scaffold materials. Degradation rates and mechanical properties vary between materials and an optimal balance between the required properties of a bone tissue engineering scaffold is required [17]. Where biodegradable polymers are utilised as scaffold materials degradation rates and mechanical strength will vary based on M_W even for identical polymers e.g. P_{DL}LA $M_W \approx 20$ kDa will undergo hydrolytic degradation more quickly than P_{DL}LA $M_W \approx 100$ kDa.

In IBG a bone mill is utilised to process allograft into mm sized particles for impaction into the cavity created through loss of bone stock. The milling process imparts additional macro porosity into the allograft, whereby the milled and impacted particles form a scaffold to support bone regeneration and the impacted particles do not fit perfectly together when impacted, that results in macro porosity between particles [185]. Whether this level of porosity is sufficient, or whether greater osteogenic performance can be imparted into polymer scaffolds undergoing milling and impaction is important. This study provided a comparison between milled and impacted polymer versus porous milled and impacted polymer.

Previously, supercritical CO_2 foaming was utilised to create porous polymeric foams using biodegradable polymers such as PLA and PLGA [108, 186, 187]. The process is free from the use of organic solvents which appeals for tissue engineering applications by removing the need for drying steps and residual entrapped organic solvents within the polymeric scaffolds as with other processes e.g. solvent casting/particulate leaching. The supercritical CO_2 foaming process was performed at low temperatures (35 °C) which favourably compares to melt extrusion processing or solvent casting/particulate leaching by allowing incorporation of thermolabile or chemically sensitive bioactive molecules such as BMP-2 that would lose activity under the more harsh conditions of the alternative processes. Howdle *et al*. [188] demonstrated the incorporation of thermolabile molecules into polymers utilising supercrit-

ical CO_2 technology and BMP-2 is a potential molecule of interest that may further enhance osteogenic performance of these scaffolds [189].

While allograft is the current clinical gold standard for IBG procedures it lacks the osteogenic (ability to form new bone) properties of autograft. Allograft is osteoinductive (stimulates pluripotent cells to differentiate down the osteoblastic lineage) and osteoconductive (provides scaffolding for new bone). A synthetic alternative to allograft would demonstrate clear advantages by providing osteogenic properties in addition to osteoinductive and osteoconductive properties. Cells (osteoblastic or osteoprogenitor) must be incorporated into a scaffold to impart osteogenic properties. For cells to be incorporated into scaffolds for IBG applications the cells must be capable of surviving the impaction process.

A study by Bolland *et al*. [54] established osteogenic potential in allograft when seeded with MSCs. The work utilised an impaction process to mimic IBG that had previously been used by Dunlop *et al*. and Brewster *et al*. [165, 190]. This experimental model demonstrated cell survival on allograft through an impaction process. Bolland *et al*. also demonstrated improved shear strength in allograft seeded with hBMSCs in comparison to allograft alone. While this study established improved performance of allograft with hBMSCs the issues associated with allograft use such as availability and risk of infection transmission remain.

The studies detailed in this chapter demonstrate cell survival on $scCO_2$ foamed scaffolds through an impaction process that mimics forces used in IBG for the first time. This is an important initial step in demonstrating the potential of supercritical foamed polymer scaffolds and MSCs as composite alternatives to bone allograft in IBG. Initial *in vitro* (outside of a living organism) experiments are described that were used to determine the most promising scaffold formulations for a 5 week murine *in vivo* model. These were carried out using proliferation assays and osteogenic differentiation assays. The *in vitro* experiments were carried out to reduce the number of animals required for *in vivo* study. The murine *in vivo* model was undertaken to establish the *in vivo* performance of the most promising formulations to distinguish the most promising to be taken forward in to an ovine *in vivo* model that is detailed in Chapter 4.

3.2 Materials and methods

3.2.1 Reagents

All reagents were obtained from Sigma-Aldrich (U.K.) unless otherwise stated. This includes α-MEM, FCS, ascorbate-2-phosphate, and dexamethasone. Fluorescent dyes including Cell Tracker Green (CMFDA, 5-chloromethylfluorescein diacetate), Vybrant Alexafluor, and Ethidium Homo-dimer-1 were purchased from Invitrogen (U.K.). Collagen-1 polyclonal antibodies were obtained as a gift from Dr. Larry Fisher (NIH, MD, U.S.A.).

3.2.2 Importance of supercritical foaming

3.2.2.1 Preparation of polymer scaffolds

Supercritical CO_2 foamed P_{DL}LA and P_{DL}LGA scaffolds and melt processed P_{DL}LA and P_{DL}LGA scaffolds were used for this study. The processes for producing these scaffolds are detailed below. Once the scaffolds were formed they were milled in a standard bone mill (Tessier Osseous Microtome, Stryker Leibinger, Freiberf, Germany), sterilised, seeded with primary human MSCs, and impacted into open ended impaction chambers. The milling and sterilisation process is detailed in Section 2.5.1.3.

Supercritical carbon dioxide foaming

Supercritical CO_2 foamed polymer scaffolds were prepared as detailed in Section 2.1 using P_{DL}LA and P_{DL}LGA. Briefly, 300 mg of ground polymer powder was loaded into cylindrical wells of a PTFE mould and foamed in $scCO_2$ at 35 °C and 23 MPa for 1 hour with a 30 minute constant rate vent back to atmospheric pressure.

Melt processing of polymer

Melt processed scaffolds were made in the same PTFE moulds used for $scCO_2$ foamed scaffolds. Polymer powder was heated to 150 °C on a PTFE sheet on a hot plate and the softened polymer transferred into cylindrical wells of the PTFE mould and subsequently cooled. The polymer scaffolds were then removed from the moulds.

3.2.2.2 Scanning electron microscopy

Scanning electron microscopy was used on scaffolds prior to the milling process to characterise the internal porous structure. Obtaining SEM images was a destructive process. The protocol used for SEM is detailed in Section 2.2 .

3.2.2.3 Micro x-ray computed tomography

Like SEM, μCT was used to characterise scaffolds prior to the milling process. Unlike SEM however, μCT was non-destructive. The protocol used for characterising scaffolds using μCT is detailed in Section 2.3.1.

3.2.2.4 Mechanical shear testing

Mechanical shear testing was carried out using the protocol detailed in Section 2.4.1. Samples of allograft were also characterised using this method. Donated fresh femoral heads were stored at -80 °C prior to use. They were retrieved with consent of patients undergoing hip surgery with approval of the local ethics committee (LREC 194/99/w, 27/10/10). Under sterile conditions femoral heads were defrosted, had the cartilage and cortical bone removed, and were then milled using a standard bone mill (Tessier Osseous Microtome, Stryker Leibinger, Freiberf, Germany). Milled bone graft was soaked in 6% hydrogen peroxide for 30 min, to remove fat and marrow. The fat and hydrogen peroxide were removed and allograft was then saline washed $\times 3$, soaked in antibiotic/antimycotic solution and subjected to UV light for 24 hours. It was then washed in PBS and submerged in basal media for 24 hours prior to use. It was impacted as polymer scaffolds were impacted, using the protocol detailed in Section 2.4.1.

3.2.2.5 Cell culture

The isolation of primary human MSCs and their expansion and storage prior to use is detailed in Section 2.5.1.1. The subsequent seeding and impaction of seeded scaffolds is detailed in Sections 2.5.1.4 and 2.5.1.5, respectively. Cells were incubated *in vitro* for 2 weeks under standard cell culture conditions (37 °C and 5% CO_2).

Live/dead immunocytochemical stain

Cell Tracker Green is a widely used marker used to label viable cells. Ethidium homodimer-1 is a widely used marker for nectrotic cells. Together the two stains are used for live/dead staining and imaging of cellular samples. Following 2 weeks of *in vitro* incubation the contents of two impaction chambers from each group (melt processed $P_{DL}LA$, melt processed $P_{DL}LGA$, $scCO_2$ foamed $P_{DL}LA$, and $scCO_2$ foamed $P_{DL}LGA$) were removed and placed in six well plates. They were incubated for 90 minutes in 5 ml of standard CTG/EH-1 solution (10 μg ml^{-1} CTG, 5 μg ml^{-1} EH-1). Samples were then fixed in ethanol and stored in PBS prior to imaging under confocal microscopy (Leica SP5 and software, Leica Microsystens, Germany).

WST-1 assay

The WST-1 assays were carried out for samples following the protocol described in Section 2.6.1.

ALP/DNA assay

The ALP and DNA assays were carried out using the protocols described in Sections 2.6.2 and 2.6.3, respectively.

3.2.3 Assessing formulation performance

3.2.3.1 Preparation of polymer scaffolds

Supercritical CO_2 foamed $P_{DL}LA$ and $P_{DL}LGA$ scaffolds as pure polymer and with 10 wt.% HA microparticles were used for this study. Supercritical CO_2 foamed polymer scaffolds were prepared as detailed in Section 2.1 using $P_{DL}LA$ and $P_{DL}LGA$. Briefly, 300 mg of ground polymer powder (or 270 mg ground polymer and 30 mg HA microparticles) was loaded into cylindrical wells of a PTFE mould and foamed in $scCO_2$ at 35 °C and 23 MPa for 1 hour with a 30 minute constant rate vent back to atmospheric pressure. Once the scaffolds were formed, they were milled in a standard bone mill (Tessier Osseous Microtome, Stryker Leibinger, Freiberf, Germany), sterilised, seeded with primary human MSCs, and impacted into open ended impaction chambers. The milling and sterilisation process is detailed in Section 2.5.1.3.

3.2.3.2 Mechanical shear testing

Mechanical shear testing was carried out using the protocol detailed in Section 2.4.1.

3.2.3.3 Cell culture

The isolation of primary human MSCs and their expansion and storage prior to use is detailed in Section 2.5.1.1. The subsequent seeding and impaction of seeded scaffolds is detailed in Sections 2.5.1.4 and 2.5.1.5, respectively. Cells were incubated *in vitro* for 2 weeks under standard cell culture conditions (37 °C and 5% CO_2).

Live/dead immunostain

Live/dead immunocytocehmical staining was carried out using the protocol described in Section 3.2.2.5.

WST-1 assay

The WST-1 assays were carried out for samples following the protocol described in Section 2.6.1.

ALP/DNA assay

The ALP and DNA assays were carried out using the protocols described in Sections 2.6.2 and 2.6.3, respectively.

Collagen-1 immunohistochemical stain

Collagen-1 immunostaining was carried out utilising the protocol described in Section 2.7.

3.2.3.4 Murine *in vivo* model

The osteogenic capacity of the $scCO_2$ foamed $P_{DL}LA$ scaffolds with and without 10 wt.% HA microparticles was assessed utilising an *in vivo* murine subcutaneous model. The $P_{DL}LA$ scaffolds were chosen over $P_{DL}LGA$ scaffolds due to better performance in *in vitro* studies (greater observed osteoblastic differentiation after 2 weeks). It was desirable to reduce the scaffolds tested *in vivo* to conform to Good Laboratory Practices (GLP) for animal studies and reduce the animals required for testing.

Primary human MSCs were used as described Sections 2.5.1.1 and 2.5.1.4. The polymer scaffolds used were $scCO_2$ foamed and prepared as described in Sections 2.1 and 2.5.1.3. The milled polymer scaffolds were then impacted into open ended impaction chambers as described in Section 2.5.1.5. These scaffolds were then incubated *in vitro* for 1 week in osteogenic medium under standard cell culture conditions (35 °C and 5% CO_2). Impacted scaffolds with no cells were cultured under the same conditions for 1 week and used *in vivo* as controls. On day six the cells in two impaction chambers of both groups ($scCO_2$ foamed $P_{DL}LA$ and $scCO_2$ foamed $P_{DL}LA$ + 10 wt.% HA microparticles) were immunostained for long-term tracking by submersion in 8 ml of 1:800 dilution Vybrant:PBS for 15 minutes. This was followed with a PBS wash and 24 hour incubation in osteogenic medium under standard culture conditions (35 °C and 5% CO_2).

After 1 week of *in vitro* incubation, pre-acclimatised male *foxn1nu* mice (Harlan, Loughborough, U.K.) were anaesthetised intraperitoneally using fentanyl fluanisone (Janssen-Cilag Ltd., Bucks, U.K.) and midazolam (Roche Ltd., Welwyn Garden City, U.K.). Small (1 cm) incisions were made into the subcuticular tissue over the loin area, bilaterally, and pockets created into which the open ended impaction chambers containing the impacted polymeric scaffolds were placed. The incisions were closed under aseptic conditions, the mice allowed to recover, and were subsequently allowed ad libitum access to standard mouse chow and water.

After 5 weeks the mice were euthanized, and half were perfused with radio-opaque contrast (a mixture of barium sulfate and 2% laponite solution) via the left ventricle as detailed in Bolland [191], in order to display the neo-vasculature around and throughout the open ended impaction chambers.

Micro x-ray computed tomography

The protocol used for characterising scaffolds using μCT is detailed in Section 2.3.2.

Histological analysis

Following μCT analysis, the samples were removed from the impaction chambers and was used for histological analysis. They were washed and decalcified as detailed by Miao and Scutt [192], followed by dehydration in a graded series of alcohols, low melting point paraffin wax embedding, and cut into 7 μm sections. Staining included an Alcian Blue (for proteoglycan rich ECM) and Sirius Red stain (for collagen), and Goldner's Trichrome stain for bone

and osteoid. Alcian blue staining required deparaffinizing the samples and hydration with distilled water; then coating in alcian blue solution (pH2.5, alcian blue 10 mg ml^{-1}, acetic acid 3%) for 30 minutes; and washing in distilled water. Sirius red staining followed with submersion in sirius red solution (sirius red 1 mg ml^{-1}, 1.3 % picric acid in water) for 1 hour and $\times 3$ washes in acidified water (acetic acid 5 ml L^{-1}). Goldner's trichrome staining required staining in poncea acid fuchsin solution (ponceau 2R 750 μg ml^{-1}, acid fuchsin 250 μg ml^{-1}, azophloxine 100 μg ml^{-1}, acetic acid 0.2%) for 5 minutes, washing in 1% acetic acid, submersion in phosphomolybdic acid-orange G solution (orange G 20 mg ml^{-1}, phosphomolybdic acid 40 mg ml^{-1}) to decolourise collagen, washing in 1% acetic acid, staining in light green stock solution (light green 2 mg ml^{-1}, acetic acid 0.2%), and final washing in 1% acetic acid.

Immunohistochemical staining

Sections of impacted scaffolds removed from the impaction chambers post-*in vivo* incubation underwent immunohistochemical staining for collagen-1, bone sialo protein, osteocalcin, and von Willebrand factor following the protocol detailed in Section 2.7.

3.3 Results and discussion

3.3.1 Importance of supercritical foaming

The aim of this study was to determine the most favourable polymeric scaffolds for use with MSCs as an osteogenic alternative to allograft. Previous work demonstrated high M_W $P_{DL}LA$ and $P_{DL}LGA$ as promising scaffold materials over PCL, an alternative widely used biodegradable polymer [4]. The importance of porosity in bone tissue engineering scaffolds is widely established [173, 174, 180, 181, 193] and various methods for porous scaffold formation exist which were discussed in chapter 1. To establish the need for microporosity in scaffolds that are milled using a bone mill, which incorporates macroporosity, $scCO_2$ foamed scaffolds were compared to non-foamed polymer scaffolds produced through melt processing. These scaffolds were initially characterised by SEM and μCT was used to characterise the internal structure of porous scaffolds.

3.3.1.1 Structure characterisation

Scanning electron microscopy

Representative SEM images of milled polymer scaffolds are displayed in Figure 3.1 at x50 and x200 magnification. Figures 3.1A and B demonstrate the lack of porosity throughout the non-foamed scaffolds for both $P_{DL}LA$ and $P_{DL}LGA$, respectively, in comparison to the $scCO_2$ foamed scaffolds (Figures 3.1C and D for $P_{DL}LA$ and $P_{DL}LGA$, respectively). The differences in porosity and pore size were expected due to the use of identical $scCO_2$ foaming protocols for both polymers, which interact differently with the $scCO_2$.

Micro x-ray computed tomography

Representative axial μCT slices of $scCO_2$ foamed $P_{DL}LA$ and $P_{DL}LGA$ are shown in Figure 3.2. These images give an indication of the porosity of the foamed polymer scaffolds prior to milling. μCT analysis of the scaffolds calculated the mean porosity of the scaffolds as: 58.7 $\pm$ 0.6% and 45.5 $\pm$ 0.6% for $scCO_2$ foamed $P_{DL}LA$ and $scCO_2$ foamed $P_{DL}LGA$, respectively. The average pore size of the scaffolds was also calculated using micro CT analysis as: 118 $\pm$ 3 μm and 85 $\pm$ 11 μm for $scCO_2$ foamed $P_{DL}LA$ and $scCO_2$ foamed $P_{DL}LGA$, respectively.

3.3.1.2 Mechanical characterisation

Scaffolds were then milled using a standard bone mill and impacted in a process that mimicked the forces of a surgical IBG process. Milled and impacted polymer scaffolds were tested for shear resistance under different normal loads and compared to milled and impacted allograft as a control. The mean of the shear resistance for samples under each normal loading are displayed in Figure 3.3. Linear regression analysis was used to analyse these results and calculate interparticulate cohesion values for each sample from plotted Mohr-Coulomb failure curves (example curve shown in Figure 2.3B). The interparticulate cohesion values for the milled polymer scaffolds were compared to allograft controls for statistical significance and both the interparticulate cohesion and statistical significance are shown in Table 3.1.

Revision hip allografts are common surgical procedures that utilise allograft for IBG into the femur and acetabulum. Shear failure has been identified as a common cause of failure of revision hip allografts through stem subsidence. The mechanical shear tests carried out were consistent tests reported within the literature [54, 190, 194], and established that $P_{DL}LA$ and $P_{DL}LGA$ (both $scCO_2$ foamed and non-foamed) had significantly higher interparticulate

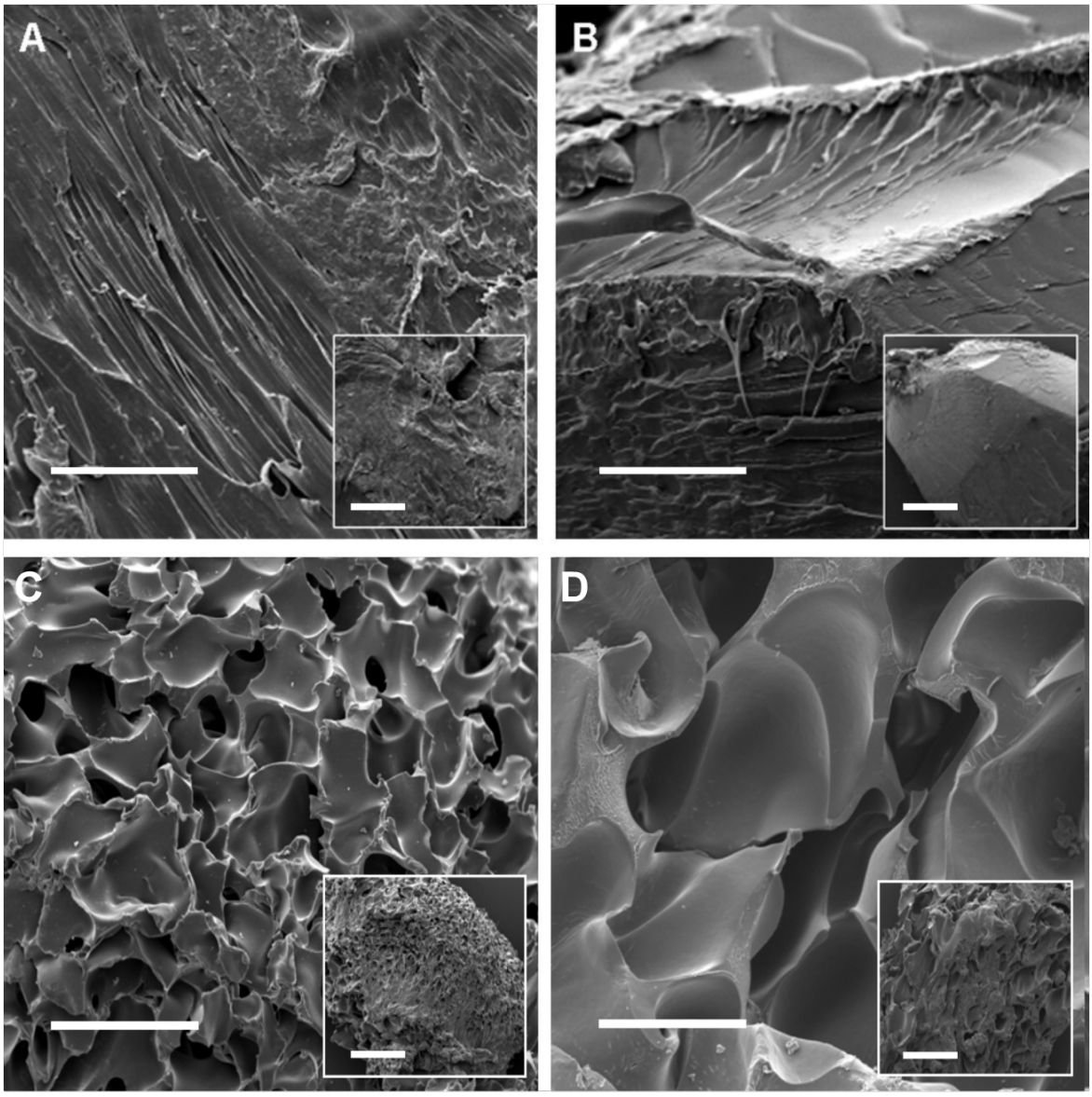

Figure 3.1: Representative SEM images of polymeric scaffolds post-milling (bone mill) to demonstrate microscale morphological differences between (A) non-foamed $P_{DL}LA$, (B) non-foamed $P_{DL}LGA$, (C) $scCO_2$ foamed $P_{DL}LA$, and (D) $scCO_2$ foamed $P_{DL}LGA$. Main images at x200 magnification and inset images at x50 magnification. Scale bars equal 300 μm.

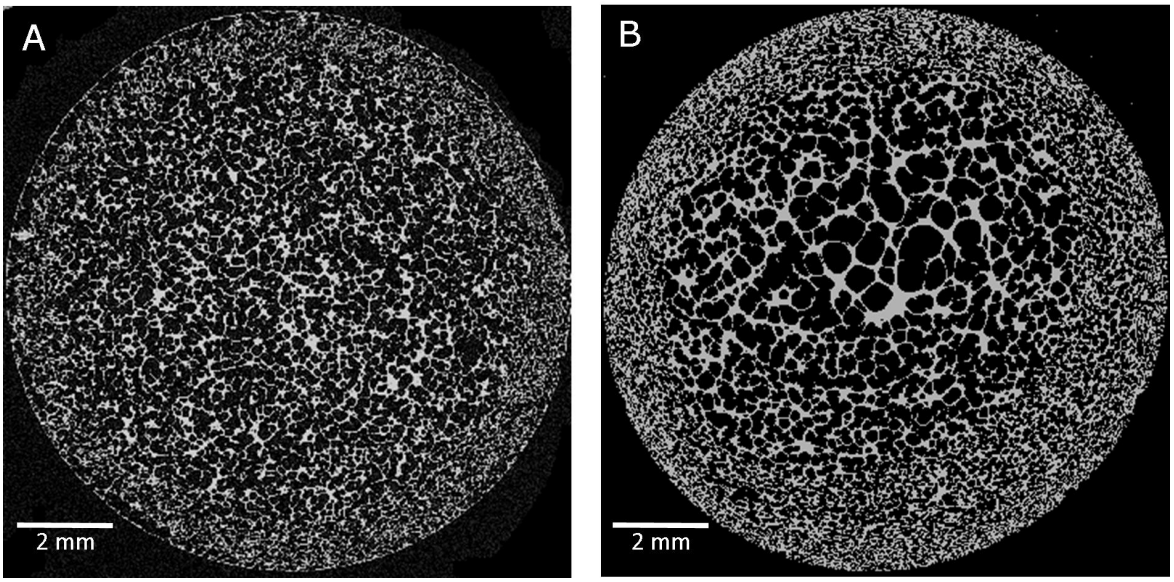

Figure 3.2: Axial micro CT images of $scCO_2$ foamed scaffolds prior to milling for: (A) $scCO_2$ foamed $P_{DL}LGA$ and (B) $scCO_2$ foamed $P_{DL}LA$.

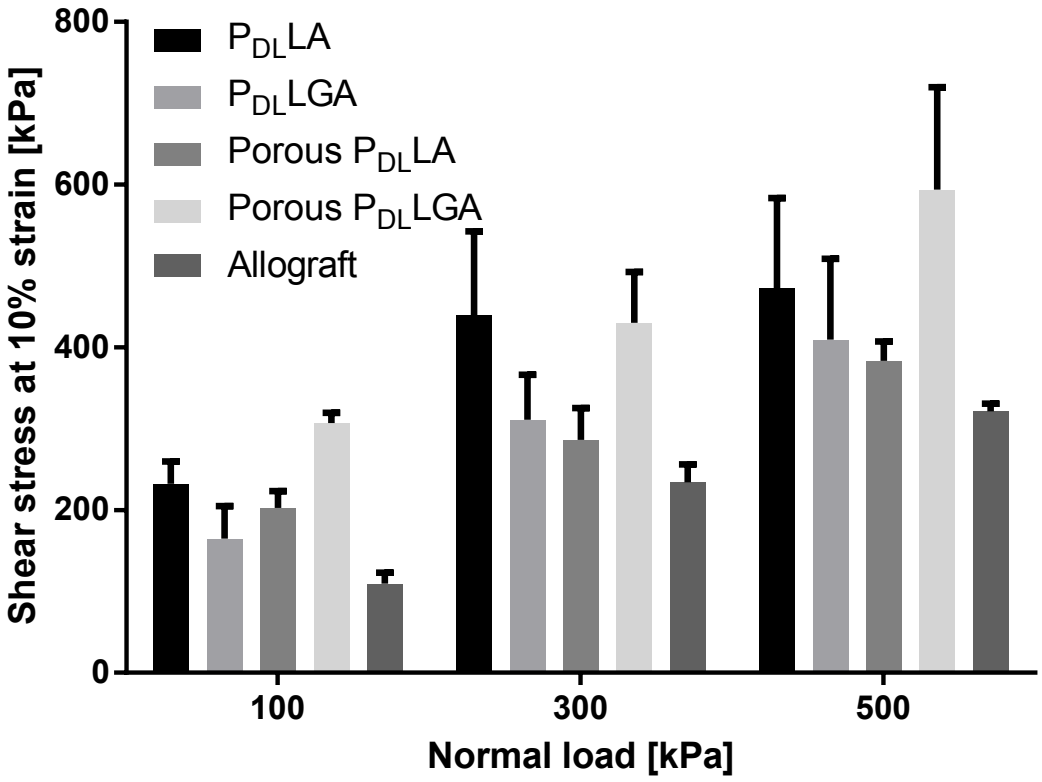

Figure 3.3: Mean shear stress at 10% strain (n=4) for milled and impacted samples at different normal loads. Porous refers to $scCO_2$ foamed scaffolds. Both PLA and PLGA are amorphous. Error bars represent standard deviation.

Table 3.1: Mohr Coulomb failure curve interparticulate cohesion and R^2 values calculated from Figure 3.3 results (n=4). Statistical significance from linear regression analysis of test materials compared to allograft controls also shown.

Test material	Interparticulate cohesion	Statistical significance	Linear regression R^2 value
Allograft	62.5	N/A	0.990
$P_{DL}LA$	201.3	P<0.0001	0.852
$ScCO_2$ foamed $P_{DL}LA$	155.1	P<0.0001	0.998
$P_{DL}LGA$	111.6	P<0.001	0.987
$ScCO_2$ foamed $P_{DL}LGA$	228.5	P<0.0001	0.994

cohesion values than allograft controls. Results between foamed and non-foamed polymer scaffolds were inconclusive limiting further conclusions.

3.3.1.3 *In vitro* assessment of biocompatibility

Cellular compatibility

Representative live/dead confocal images of hMSCs seeded onto milled polymer scaffolds and subsequently impacted and cultured for two weeks in osteogenic medium are shown in Figure 3.4. Cells (green) are shown to have survived on all samples with few dead cells (red) showing and a higher rate of proliferation evident on the $scCO_2$ foamed scaffolds. Visual observation showed a higher density of cells on $scCO_2$ foamed scaffolds compared to non-foamed scaffolds (Figures 3.4 B & D shows $scCO_2$ foamed scaffolds versus non-foamed counterparts in Figures 3.4 A & C).

Results from WST-1 assays demonstrated quantitative evidence of increased metabolic activity, and hence survivability and proliferation, of cells on $scCO_2$ foamed scaffolds in comparison to non-foamed scaffolds as can be seen in Figure 3.5. The mean metabolic activity (n=3) of cells cultured on $scCO_2$ foamed $P_{DL}LA$ is significantly greater than on non-foamed $P_{DL}LA$ ($P<0.01$) and similarly the mean metabolic activity of cells cultured on $scCO_2$ foamed $P_{DL}LGA$ is significantly greater than on non-foamed $P_{DL}LGA$ ($P<0.01$). WST-1 assays provide a quantitative measure of cell metabolic activity that can be correlated to total cell number, but does not provide exact information. There is significant evidence from the results of these assays, in conjunction with confocal images, that $scCO_2$ foamed scaffolds support a greater population of cells to corresponding non-foamed scaffolds. This is likely due to the greater specific surface area of the porous scaffolds.

Figure 3.6 shows live/dead confocal images taken of MSCs cultured in osteogenic media for 2 weeks on non-milled $scCO_2$ foamed $P_{DL}LA$ (Figure 3.6 A and C) scaffolds and non-milled $scCO_2$ foamed $P_{DL}LGA$ Figure 3.6 B & D). Figures 3.6 A & B show cells growing on the outer surface of the porous scaffolds while Figures 3.6 C & D show cells growing in the pores of the scaffold which demonstrates cell migration into the scaffolds. This evidence that cells are able to penetrate into non-milled $scCO_2$ scaffolds is also evidence that this would be possible in milled impacted $scCO_2$ scaffolds.

O'Brien *et al.* [195] found strong correlation between scaffold specific surface area and cell attachment for MC3T3 cells (murine osteoblast precursors) over 48 hours. Greater cell

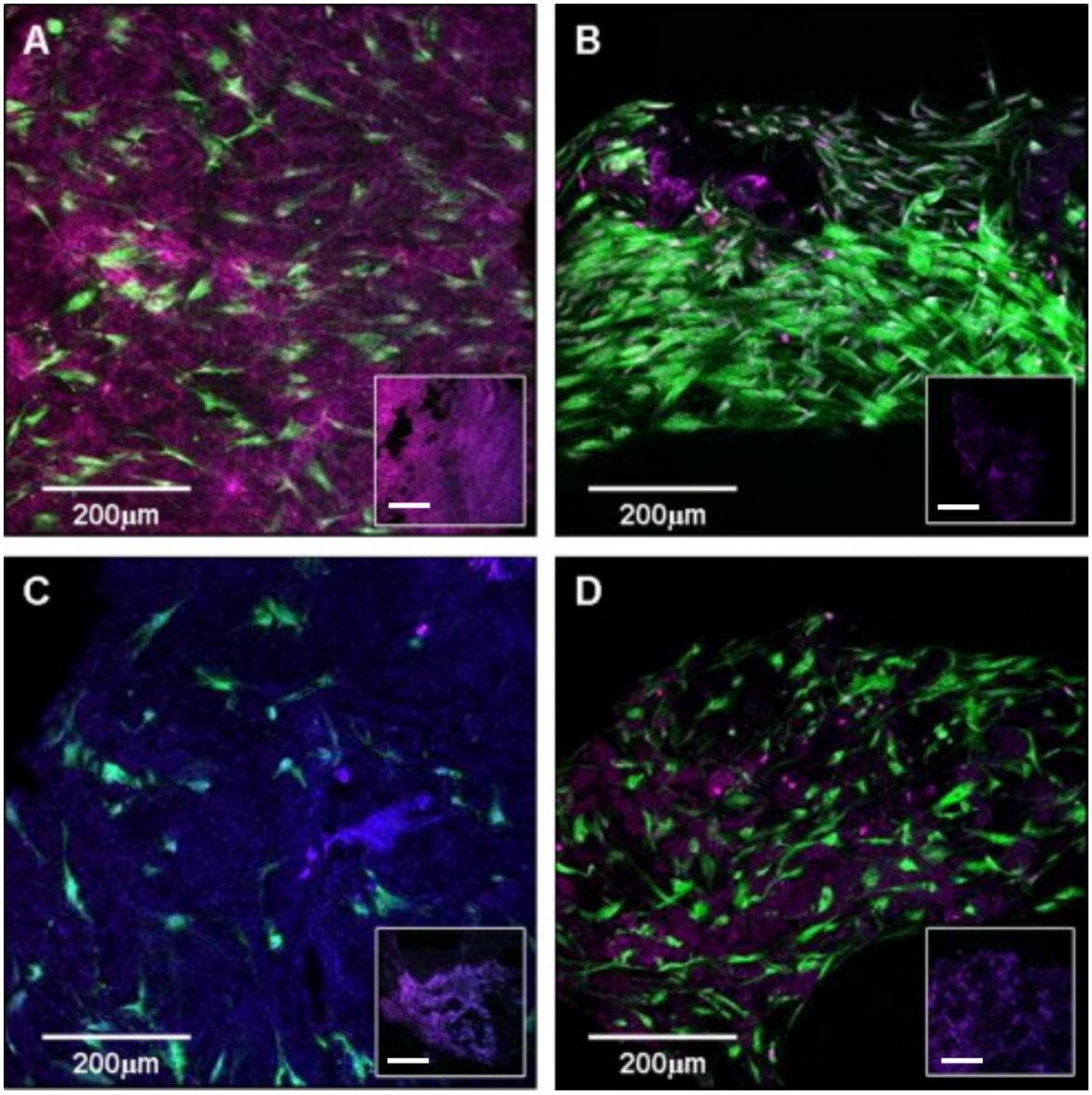

Figure 3.4: Confocal images of live/dead stained hMSCs cultured on milled polymer scaffolds of (A) $P_{DL}LA$, (B) $scCO_2$ foamed $P_{DL}LA$, (C) $P_{DL}LGA$, and (D) $scCO_2$ foamed $P_{DL}LGA$ at x40 magnification. Cells were cultured for two weeks prior to immunostaining. Inset images are control samples containing no cells. Inset scale bars equal 200 μm.

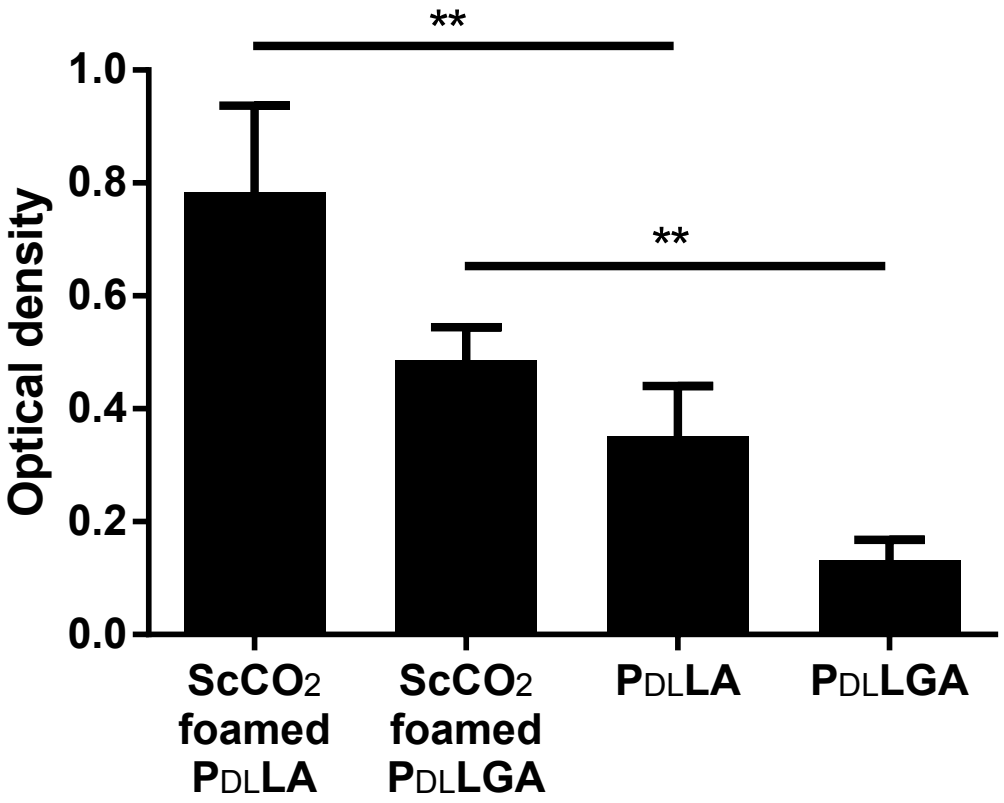

Figure 3.5: WST-1 assay readings showing optical density readings at 450 nm for hMSCs cultured on milled and impacted polymer scaffolds for two weeks in osteogenic medium (n=3). Assay readings were taken in triplicate after 2 hour incubation and statistical significance between $scCO_2$ foamed and non-foamed $P_{DL}LA$ and $P_{DL}LGA$ is shown (**P<0.01). Other results not significant at p<0.05 level).

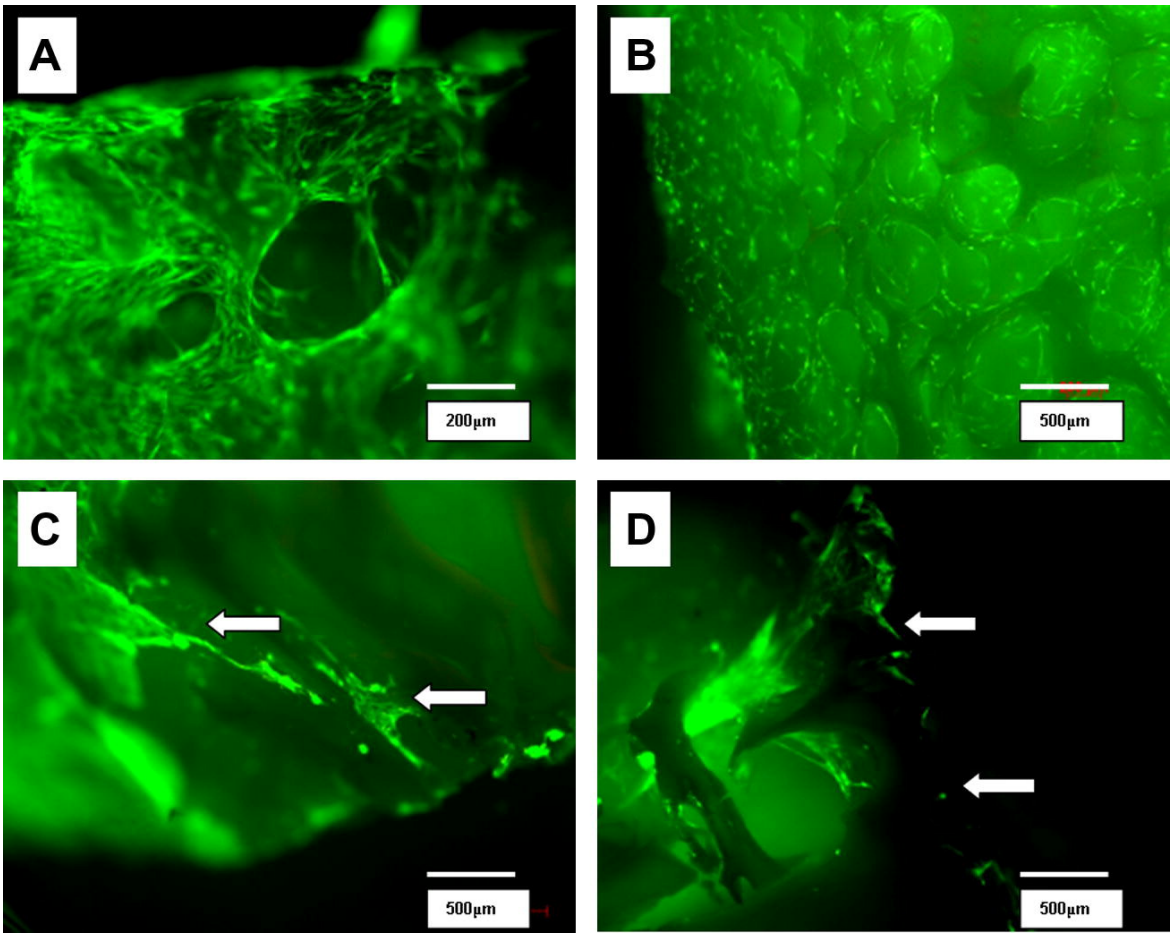

Figure 3.6: Confocal images of live/dead stained hMSCs (bright green) cultured on: (A) outer surface of scCO$_2$ foamed P$_{DL}$LA, (B) outer surface of scCO$_2$ foamed P$_{DL}$LGA, (C) inner sectioned surface of scCO$_2$ foamed P$_{DL}$LA, and (D) inner sectioned surface of scCO$_2$ foamed PLGA. Cells were cultured for two weeks in osteogenic media. Arrows highlight cells that demonstrate cell growth within the scaffolds.

attachment on porous scaffolds and similar population doubling times between porous and non-porous scaffolds would lead to a larger cell population on porous scaffolds, as observed, until confluent. With a greater specific surface area, and cells able to penetrate the porous scaffolds, porous scaffolds would allow a larger cell population. There were significant ($P<0.05$) differences in WST-1 assay readings between cells cultured on $scCO_2$ foamed $P_{DL}LA$ and $scCO_2$ foamed $P_{DL}LGA$ which would imply greater proliferation of cells on $scCO_2$ foamed $P_{DL}LA$ scaffolds. However, given the $scCO_2$ foamed $P_{DL}LA$ scaffolds were more porous (58.7%) than the $scCO_2$ foamed $P_{DL}LGA$ scaffolds (45.5%), this is likely due to the difference in specific surface area between the two scaffold types. This porosity difference is due to the different polymers undergoing an identical supercritical foaming process and behaving slightly differently under identical conditions.

The porosity in $scCO_2$ foamed scaffolds may provide protective cavities for cells to reside in during impaction; this could also be attributed to the larger stem cell population observed on the porous scaffolds. If cells are damaged through the impaction process when seeded onto non-foamed scaffolds and cells seeded on $scCO_2$ foamed scaffolds are protected from the impaction forces we would expect a greater cell population on the $scCO_2$ foamed scaffolds, as observed. Korda *et al.* [196, 197] previously demonstrated that hMSCs could survive typically impaction forces when seeded on allograft. Allograft itself is porous and may provide cavities for cells to reside in during impaction. This makes it difficult to confirm whether cells are withstanding the force of the impaction or are shielded from the full force of the impaction through scaffold/allograft porosity.

Osteoblastic differentiation

Specific activity of ALP was measured in triplicate for cells cultured on each of the milled and impacted polymer scaffolds as an early indicator of osteoblastic differentiation. The results presented in Figure 3.7 show negligible ALP specific activity for cells cultured on non-foamed polymer scaffolds and $scCO_2$ foamed $P_{DL}LGA$. A significantly greater ($P<0.001$) ALP specific activity was observed from cells cultured on $scCO_2$ foamed $P_{DL}LA$ scaffolds. As an additional indicator of osteoblastic differentiation collagen-1 (red) immunostaining was carried out with DAPI nuclear stains (green) and representative images are shown in Figure 3.8. Figure 3.8 B shows strong positive staining for collagen-1 for cells cultures on $scCO_2$ foamed $P_{DL}LA$ while Figure 3.8 A shows some positive collagen-1 staining for cells cultured on $P_{DL}LA$ and Figures 3.8 C and D show presence of cells but a lack of collagen-1

for cells cultured on P_{DL}LGA scaffolds, both $scCO_2$ foamed and non-foamed.

Total specific activity of ALP was utilised as an early indicator for osteoblastic differentiation of MSCs on the different scaffolds. Alkaline phosphatase is used as an indicator for osteoblastic differentiation [167, 168], and while its expression is not entirely specific to osteoblastic cells, collagen type-1 (col-1) immunohistochemical stains were used to confirm evidence of osteoblastic differentiation of MSCs in these experiments [169]. From specific ALP activity there is significant evidence ($P<0.001$) that MSCs cultured on $scCO_2$ foamed P_{DL}LA scaffolds differentiated more quickly down the osteoblastic lineage than MSCs cultured on non-foamed P_{DL}LA and both $scCO_2$ foamed and non-foamed P_{DL}LGA (Figure 3.7). This was supported by confocal imaging showing greater levels of col-1 surrounding cells on $scCO_2$ foamed P_{DL}LA scaffolds.

3.3.2 Assessing formulation performance

Having established the improved biocompatibility and osteoinductive properties of $scCO_2$ foamed scaffolds over non-foamed scaffolds, further improvements in osteoinductive properties were investigated through the use of HA microparticles. Polymer:HA composites were formed using $scCO_2$ foaming and compared to pure polymer scaffolds formed through $scCO_2$ foaming.

3.3.2.1 Mechanical characterisation

Milled and impacted $scCO_2$ foamed polymer samples (P_{DL}LA and P_{DL}LGA) were prepared with and without 10% HA microparticles added prior to foaming. These samples were tested for shear resistance under different normal loads and compared to allograft as a control. The mean shear resistance for samples under each normal loading are displayed in Figure 3.9. Linear regression analysis was used to analyse these results and calculate interparticulate cohesion values for each sample from Mohr-Coulomb failure curves. The interparticulate cohesion values for the milled polymer scaffolds were compared to allograft controls for statistical significance and both the interparticulate cohesion and statistical significance are shown in Table 3.2.

In this chapter shear testing was performed without cells; similar experiments with impaction and shear testing of allograft demonstrated that allograft seeded with MSCs in-

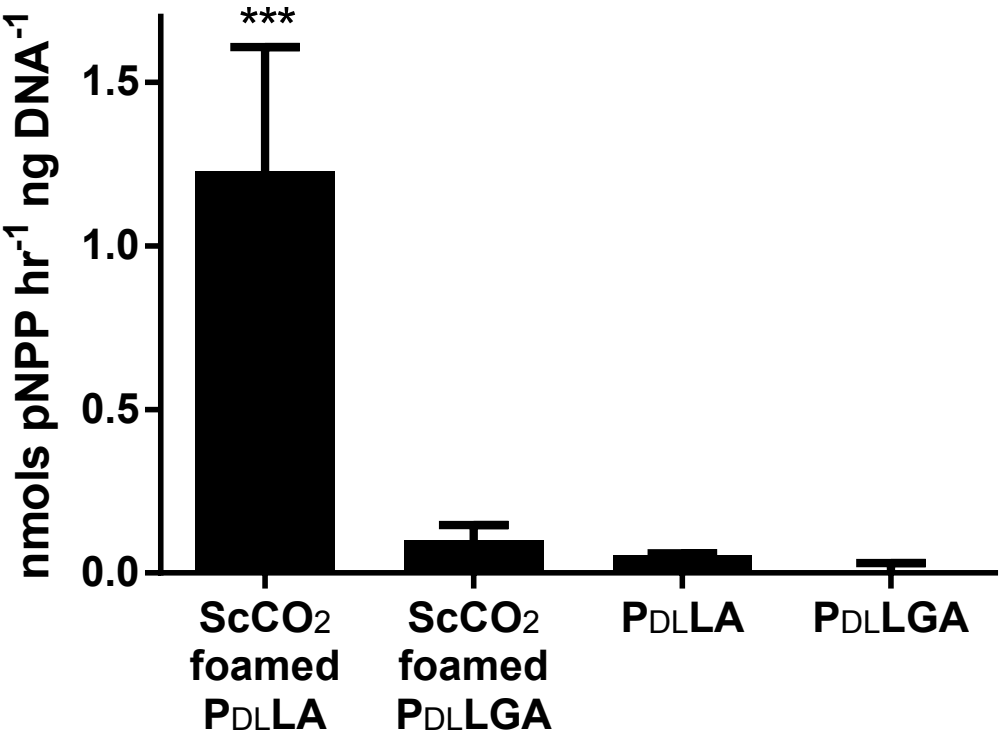

Figure 3.7: Mean ALP specific activity for hMSCs cultured *in vitro* on both $scCO_2$ foamed and non-foamed $P_{DL}LA$ and $P_{DL}LGA$ scaffolds for 2 weeks (n=3) (***P<0.001). Scaffolds were milled and impacted and cultured in osteogenic medium. Error bars show standard deviation.

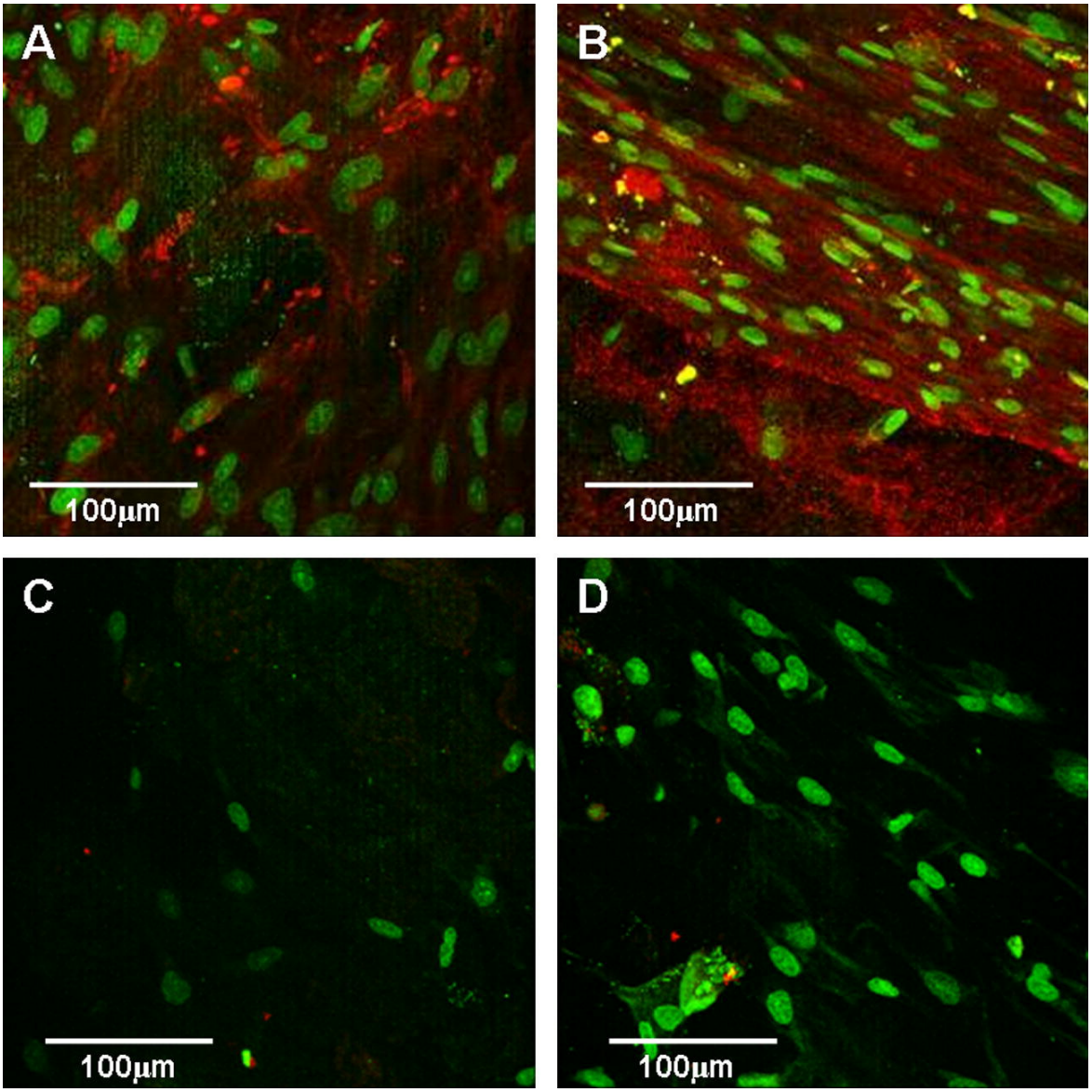

Figure 3.8: Confocal images at x80 magnification of collagen-1 immunostained (AlexaFluor 594, red) with DAPI nuclear counterstain (green) of hMSCs cultured on: (A)P_{DL}LA, (B) $scCO_2$ P_{DL}LA, (C) P_{DL}LGA, and (D) $scCO_2$ P_{DL}LGA. Cells were cultured for two weeks in osteogenic medium.

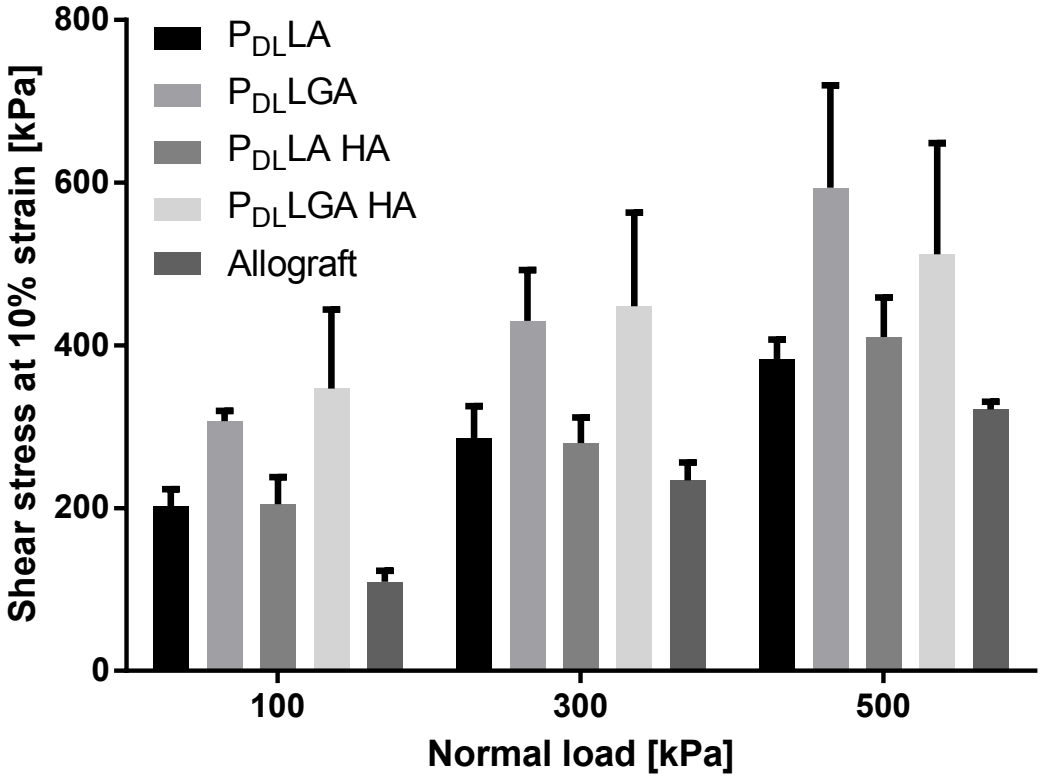

Figure 3.9: Mean shear stress at 10% strain (n=4) for milled and impacted $scCO_2$ foamed samples at different normal loads. PLA and PLGA are amorphous and samples containing HA are polymer:HA 90:10 weight loading. Error bars represent standard deviation.

Table 3.2: Mohr Coulomb failure curve interparticulate cohesion and R^2 values calculated from Figure 3.9 results (n=4). Statistical significance from linear regression analysis of $scCO_2$ foamed polymer scaffolds and HA composites compared to allograft controls also shown.

Test material	Interparticulate cohesion	Statistical significance	Linear regression R^2 value
Allograft	62.5	N/A	0.990
$P_{DL}LA$	155.1	P<0.0001	0.998
$P_{DL}LA$+ HA	144.2	P<0.0001	0.977
$P_{DL}LGA$	228.5	P<0.0001	0.994
$P_{DL}LA$+ HA	311.7	P<0.0001	0.983

creases the shear strength of the impacted construct [54]. Further published work went on to demonstrate an enhancement of this effect through functionalising allograft/cell constructs with HA and collagen [55]. In contrast to this finding, impaction shear testing of milled $scCO_2$ foamed scaffolds of $P_{DL}LA$ and $P_{DL}LGA$ found no significant difference between samples with 10% HA and samples without. The enhancement in shear resistance Jones *et al.* reported may be due to the enhanced differentiation of MSCs coated in HA nanoparticles; the ECM the cells produced may have added structural integrity that increased the shear resistance of the scaffold.

3.3.2.2 *In vitro* assessment of biocompatibility

Cellular compatibility

Representative live/dead confocal images of MSCs seeded onto milled polymer scaffolds and subsequently impacted and cultured for 2 weeks in osteogenic medium are shown in Figure 3.10. Viable cells (green) are shown to have survived on all samples with few dead cells (red) apparent. Cells were observed to have proliferated to near 100% confluence on all samples with little observable difference of cell proliferation and viability between cells cultured on HA containing samples (Figures 3.10 B & D) or polymer type ($P_{DL}LA$ samples in Figures 3.10 A & B; $P_{DL}LGA$ samples in Figures 3.10 C & D). Figures 3.10 E–H display control samples with no cells stained and imaged for the corresponding scaffold compositions in the images above (3.10 A–D), confirming specificity of the stains. Polymer autofluorescence shows as purple in all images.

Results from WST-1 assays, shown in Figure 3.11, provide quantitative data to substantiate the live/dead images. Cells cultured on non-foamed $P_{DL}LA$ were used as controls and significantly greater cell viability was observed on $scCO_2$ foamed $P_{DL}LA$ scaffolds ($P<0.01$ on $scCO_2$ foamed $P_{DL}LA$ and $P<0.05$ on $scCO_2$ foamed $P_{DL}LA$ + 10% HA). Greater cell viability was observed on $scCO_2$ foamed $P_{DL}LA$ scaffolds than $scCO_2$ foamed $P_{DL}LGA$ scaffolds ($P<0.05$) but for all other comparisons between samples there was no significant difference in cell viability following two weeks cell culture in osteogenic medium. The incorporation of 10 wt.% HA microparticles appeared to have no noticeable effect on the cell population density on either of the scaffold compositions.

Bolland *et al.* [194] previously established the survival of hMSCs on milled $scCO_2$ foamed $P_{DL}LA$ utilised as a bone graft extender. Osteoprogenitor cells seeded on polymer scaffolds

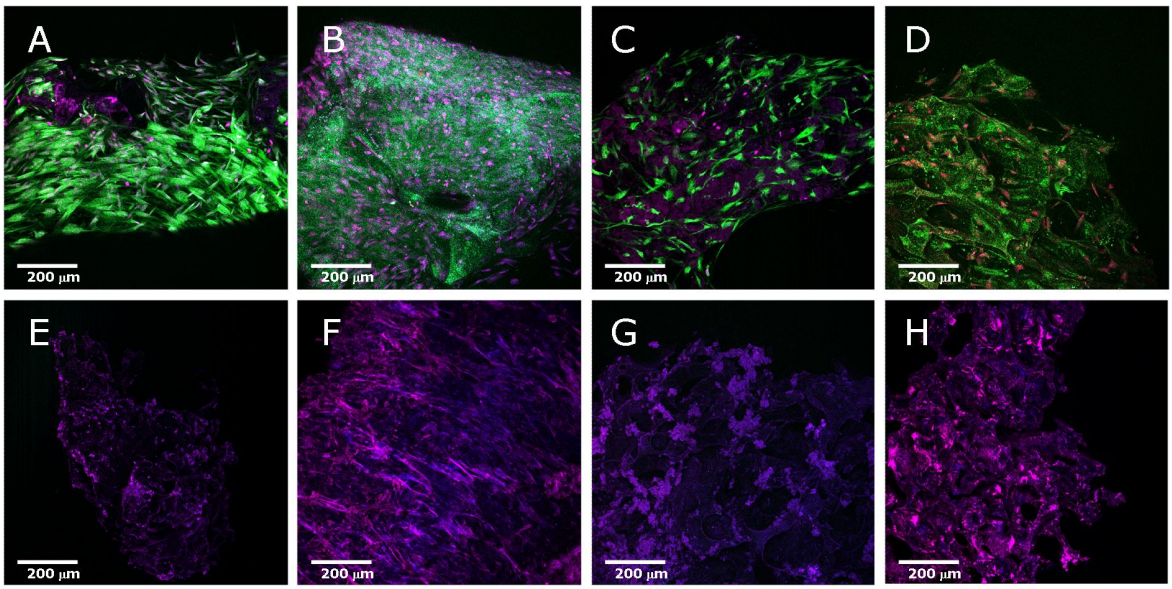

Figure 3.10: Confocal images of live (green)/dead (red) hMSCs cultured on milled polymer scaffolds of (A) scCO$_2$ foamed P$_{DL}$LA (control image E), (B) scCO$_2$ foamed P$_{DL}$LA + 10 wt.% HA (control image F), (C) scCO$_2$ foamed P$_{DL}$LGA (control image G), and (D) scCO$_2$ foamed P$_{DL}$LGA + 10 wt.% HA (control image G) at x20 magnification. Cells were cultured for two weeks in osteogenic medium prior to immunostaining. Control samples contained no cells.

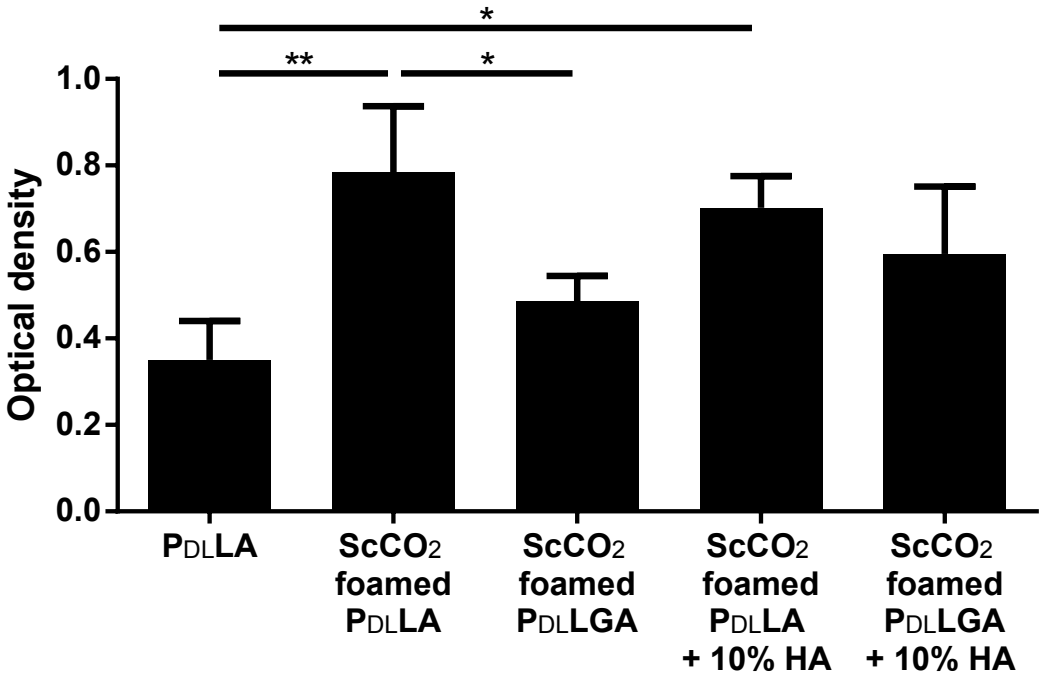

Figure 3.11: WST-1 assay readings showing optical density readings at 450 nm for hMSCs cultured on milled and impacted polymer scaffolds for two weeks in osteogenic medium (n=3). Assay readings were taken in triplicate after 2 hour incubation and statistical significance between: non-foamed $P_{DL}LA$ and $scCO_2$ foamed $P_{DL}LA \pm 10\%$ H, and $scCO_2$ foamed $P_{DL}LA$ and $scCO_2$ foamed $P_{DL}LGA$ (**P<0.01, *P<0.05).

were shown to survive an impaction process that mimicked IBG which matches our findings. Live/dead staining, confocal imaging, and tetrazolium salt colorimetric assays (WST-1) (Figures 3.4, 3.5, 3.10 & 3.11) provide evidence of cell proliferation on such scaffolds post impaction for both P_{DL}LA and P_{DL}LGA scaffolds. Bone graft extenders reduce, but do not eliminate the downsides of allograft (cost, risk of infection, and limited availability).

Osteoblastic differentiation

Specific activity of ALP was measured in triplicate for cells cultured for 2 weeks in osteogenic medium on each of the milled and impacted polymer scaffolds as an early indicator of osteoblastic differentiation. The results presented in Figure 3.12 show significantly greater ALP specific activity for cells cultured on $scCO_2$ foamed P_{DL}LA + 10 wt.% HA than on all the other scaffold types. There was no significant difference between P_{DL}LGA samples, although greater specific ALP activity was measured for cells cultured on P_{DL}LGA + 10% HA scaffolds than scaffolds without HA. Cells cultured on P_{DL}LA + 10% HA scaffolds had significantly higher specific activity than cells cultured on P_{DL}LA scaffolds ($P<0.01$). Cells cultured on all P_{DL}LA scaffolds (both with and without HA) expressed significantly higher ALP specific activity than cells cultured on P_{DL}LGA scaffolds (both with and without HA).

The osteoblastic differentiation of MSCs appeared to have progressed for cells cultured on $scCO_2$ foamed P_{DL}LA compared to $scCO_2$ foamed P_{DL}LGA again when 10 wt.% HA microparticles were incorporated. The presence of HA microparticles appeared to further accelerate the differentiation; significantly higher ALP expression was observed in MSCs cultured on P_{DL}LA scaffolds with HA than without HA ($P<0.01$). This trend appeared to repeat in MSCs cultured on $scCO_2$ foamed P_{DL}LGA with HA than without, although the results were not significant at the 5% level (Figure 3.12). Hydroxyapatite was incorporated into the scaffolds to improve the osteoblastic differentiation and these results confirm HA presence in the scaffolds improved the scaffolds osteoinductive properties as has been found previously in the literature [131, 198, 199].

3.3.2.3 *In vivo* assessment of biocompatibility

The performance of P_{DL}LA scaffolds in *in vitro* experiments was greater than that of P_{DL}LGA scaffolds in terms of osteoinductive properties. While P_{DL}LGA scaffolds demonstrated greater resistance to shear both P_{DL}LA and P_{DL}LGA scaffolds showed greater resistance

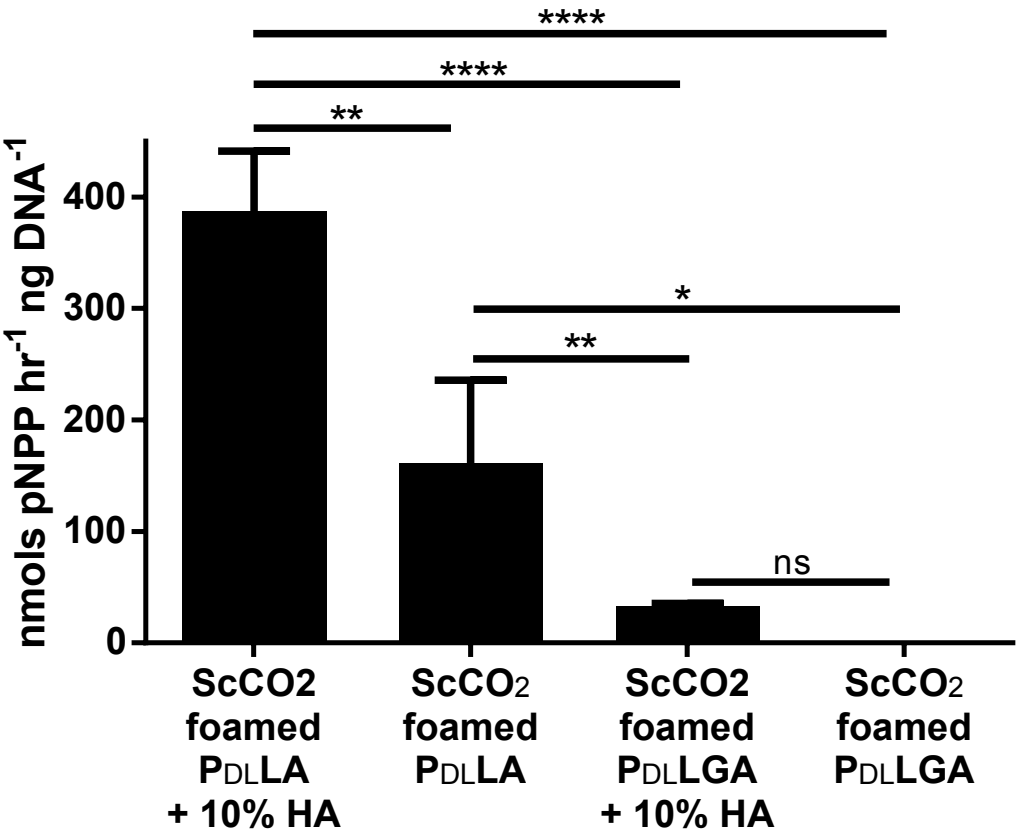

Figure 3.12: Mean ALP specific activity for hMSCs cultured on milled and impacted scaffolds in osteogenic medium for two weeks (n=3) (****P<0.0001, **P<0.01, *P<0.05, ns = not significant). Error bars show standard deviation.

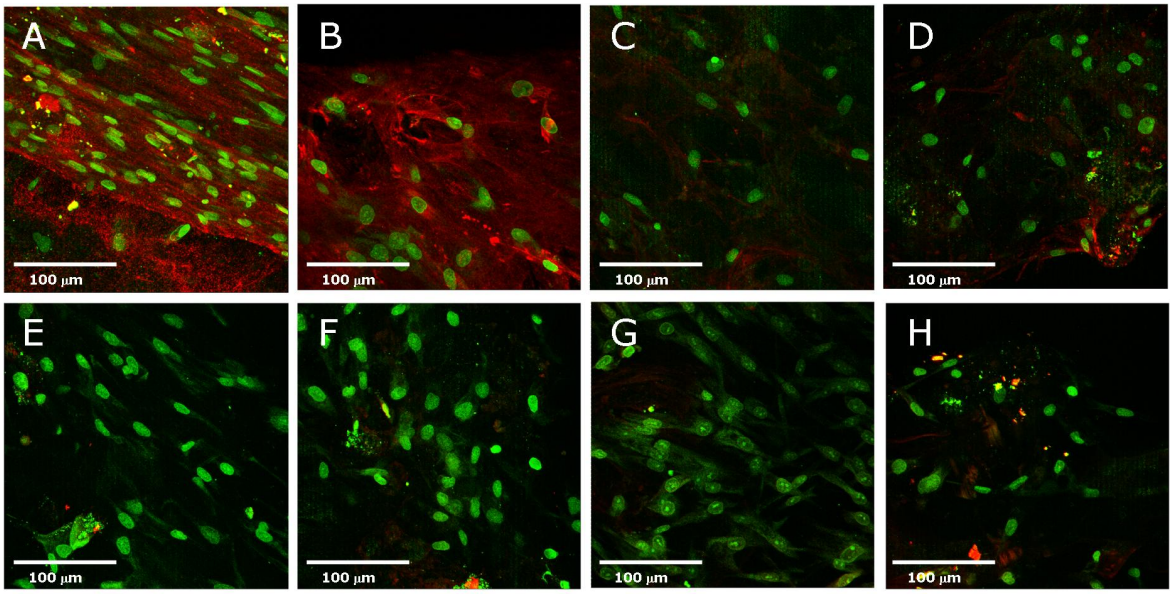

Figure 3.13: Confocal images of collagen-1 immunostained (AlexaFluor 594, red) with DAPI nuclear counterstains (green) of hMSCs cultured in osteogenic medium for two weeks on (A) $scCO_2$ foamed $P_{DL}LA$ (control image E), (B) $scCO_2$ foamed $P_{DL}LA$ + 10 wt.% HA (control image F), (C) $scCO_2$ foamed $P_{DL}LGA$ (control image G), and (D) $scCO_2$ foamed $P_{DL}LGA$ + 10 wt.% HA (control image H) at x40 magnification. Negative controls with no primary antibody were used.

to shear than allograft bone. In line with animal testing principles to reduce the number of animals tested it was possible to rule out P_{DL}LGA scaffolds; of the $scCO_2$ foamed scaffolds the P_{DL}LA scaffolds with and without HA demonstrated greater potential based on the increased osteoblastic differentiation observed *in vitro*. For these reasons $scCO_2$ foamed P_{DL}LA with and without 10 wt.% HA microparticles were taken forward to *in vivo* testing. The scaffolds were foamed, milled, sterilised, seeded with MSCs, aseptically impacted, and then implanted subcutaneously into mice and incubated *in vivo* for 5 weeks.

Micro x-ray computed tomography

μCT analysis was carried out on samples post murine incubation and quantitative analysis of bone-like matrix formation revealed the values presented in Table 3.3. There was a significant increase in mineralised matrix formation between P_{DL}LA scaffolds implanted with MSCs and P_{DL}LA scaffold control ($P<0.01$). An increase in bone formation was observed between P_{DL}LA + HA scaffolds implanted with MSCs and the control scaffolds but this did not reach significance. There was a highly significant increase in bone-like matrix formation between P_{DL}LA + HA scaffolds and 100% P_{DL}LA scaffolds for both samples implanted with MSCs and controls ($P<0.001$).

A representative 3D reconstruction of a P_{DL}LA scaffold (implanted with hMSCs) post murine incubation is shown in Figure 3.14. Figure 3.14 A shows the entire implanted scaffold contained within a cylindrical pot, open at both ends, and Figure 3.14 B is the same image with the low density plastic pot and scaffold removed, leaving the higher density bone like matrix formed visible.

Figure 3.15 shows post murine incubation (five weeks) representative axial and longitudinal μCT slices of P_{DL}LA + 10 wt.% HA scaffolds implanted with (Figures 3.15 A–C) and without MSCs (Figures 3.15 D–F). Hydroxyapatite particles, as the most dense material within the samples, are visible as white circular shapes across the slices. Bone like matrix formed has a lower density than HA and has been coloured red in the images to improve visible contrast. The newly formed mineralised matrices have a range of densities that approach that of HA and reduce the overall reliability in absolute values of matrix volumes formed within the HA containing samples. Comparison of the μCT slices show that for the scaffolds implanted with hMSCs (Figures 3.15 A–C) bone like matrix has formed across the scaffold around HA particles and in areas removed from HA particles. For samples implanted without hMSCs (Figures 3.15 D–F) the formation of bone like matrix appears more

focused around HA particles.

Four groups were tested *in vivo*: P_{DL}LA with MSCs, and without MSCs; P_{DL}LA + 10 wt.% HA microparticles with MSCs, and without MSCs. Utilisation of μCT gave quantitative values for mean volumes of mineralised matrix within the scaffolds following *in vivo* incubation (five weeks). A 10 μm resolution was possible which allowed visualisation of HA particles and, through contrast agent injection, imaging of vessel formation within and around the scaffolds. Thresholding is a requirement in μCT analysis and is subjective. Thresholding values have a major impact on the quantitative results produced through μCT [200–202]. Due to the density difference between P_{DL}LA and mineralised ECM effective threshold ranges were assigned for each to ensure accurate volume calculations. Mineralised matrix deposited in scaffolds during *in vivo* culture has a similar density to HA, a main constituent of bone. Due to the defined shape of HA particles incorporated in the scaffolds it was possible to threshold using mineralised matrix formed away from any particles as a guide to minimise the unavoidable crossover. Exposure of HA to physiological conditions may lead to degradation of the particles and hence reduction of HA density at the particle periphery. This would lead to HA volume inclusion with new mineralised matrix volume in μCT analysis. However HA, as a crystallised form of calcium phosphate, has a low bioresorbability and remains within the body for some time following implantation [203]. One study demonstrated HA implants unaffected by biodegradation processes following 22 weeks implantation texitin vivo[204]. This adds confidence to the μCT image analysis that demonstrated much of the mineralised matrix formed within the scaffolds surrounding the HA particles and that the P_{DL}LA + 10% HA scaffolds implanted without MSCs also show mineralised matrix to have been deposited within the scaffolds, primarily around HA particles, during *in vivo* incubation (Figure 3.15). Visualisation of vasculature formed within the scaffolds during five week murine implantation was possible utilising radiocontrast agent barium sulfate injection and μCT imaging. Resulting images are shown in Figure 3.16 and provide evidence of neo-vessel formation in P_{DL}LA (Figure 3.16 B) and P_{DL}LA + 10% HA (Figure 3.16 B) scaffolds.

Implanted cell survival

In two samples per group ($scCO_2$ foamed P_{DL}LA and $scCO_2$ foamed P_{DL}LA + 10 wt.% HA) MSCs were labelled with fluoromarkers (Vybrant) pre *in vivo* incubation. Samples recovered post five week *in vivo* incubation were imaged using confocal microscopy and images are shown in Figure 3.17. This provides evidence of sustained implanted cell survival in both

$P_{DL}LA$ (Figure 3.17 A) and $P_{DL}LA$ + 10 wt.% HA (Figure 3.17 B) scaffolds.

Immunohistochemical staining

In addition to μCT analysis, immunohistochemical stains and histological stains gave comparative qualitative results. Immunohistochemical staining was carried out on all samples post 5 week murine incubation and representative confocal images are shown in Figure 3.18. Stains for early osteoblastic differentiation markers collagen-1 and bone sialoprotein stained positive for both $P_{DL}LA$ and $P_{DL}LA$ + 10% HA samples implanted with MSCs, while $P_{DL}LA$ + 10% HA control samples also stained positive. $P_{DL}LA$ control samples did not show positive staining. Osteocalcin immunostains were carried out as late markers of osteoblastic differentiation but no positive staining was observed on any samples. Von Willebrand factor immunostains were carried out as a vascularisation indicator and limited positive stains are shown for samples $P_{DL}LA$ and $P_{DL}LA$ + 10% HA samples implanted with cells and $P_{DL}LA$ + 10% HA control samples.

Histological analysis

Post murine implantation samples were stained with Sirius Red and Alcian Blue for collagen and proteoglycan deposition which was evident in both $P_{DL}LA$ and $P_{DL}LA$ + 10% HA samples implanted with hMSCs as shown in Figures 3.19 A and D, respectively. Some positive indicators were evident in the $P_{DL}LA$ + 10% HA control samples implanted without cells (Figure 3.19 C) while none were observed on $P_{DL}LA$ control samples (Figure 3.19 A). Goldner's Trichrome staining of samples for osteoid was also used and showed positive staining on samples that also stained positive for collagen: $P_{DL}LA$ + hMSCs, $P_{DL}LA$ + 10% HA, and $P_{DL}LA$ + 10% HA + hMSCs (Figures 3.19 F-H, respectively). Control $P_{DL}LA$ samples implanted without cells showed no positive staining for osteoid (Figure 3.19 E).

The presence of mineralised matrix observed in $P_{DL}LA$ + 10% HA scaffolds implanted *in vivo* without MSCs imaged through μCT is substantiated by: the positive staining for collagen-1 and BSP, which did not stain positively on $P_{DL}LA$ scaffolds implanted without MSCs; and positive histological staining for osteoid (Goldner's trichrome in Figure 3.19. The combined results provide evidence of HA particles improving the performance of the $scCO_2$ foamed $P_{DL}LA$ scaffolds *in vivo* by providing osteoinductive properties to host cells in addition to implanted cells. The osteoinductive properties of HA were expected given previous published results [205, 206]. Previously, hMSCs cultured on $scCO_2$ foamed $P_{DL}LA$

Table 3.3: Mean bone volume (n=4) formed during five week *in vivo* murine study for $scCO_2$ foamed $P_{DL}LA$ with and without 10% HA implanted with and without hMSCs

Scaffold material	Mean bone volume $[mm^3]$	SD
$P_{DL}LA$ + MSCs	0.6575	0.312
$P_{DL}LA$ control	0.0825	0.025
$P_{DL}LA$+ HA + MSCs	24.6175	3.976
$P_{DL}LA$ + HA control	18.1800	4.627

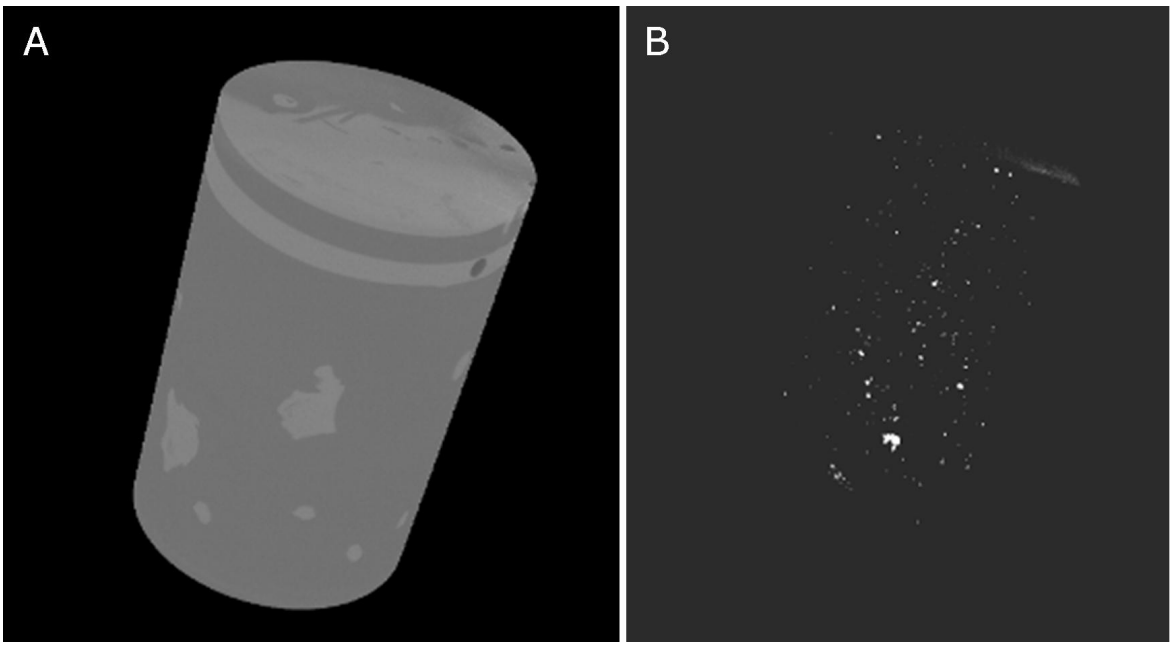

Figure 3.14: Reconstructed post murine implantation μCT scan into 3D model of milled $scCO_2$ foamed $P_{DL}LA$, seeded with hMSCs, impacted into cylindrical pot (A); and the same image with the low density pot and $P_{DL}LA$ removed to show higher density bone like matrix.

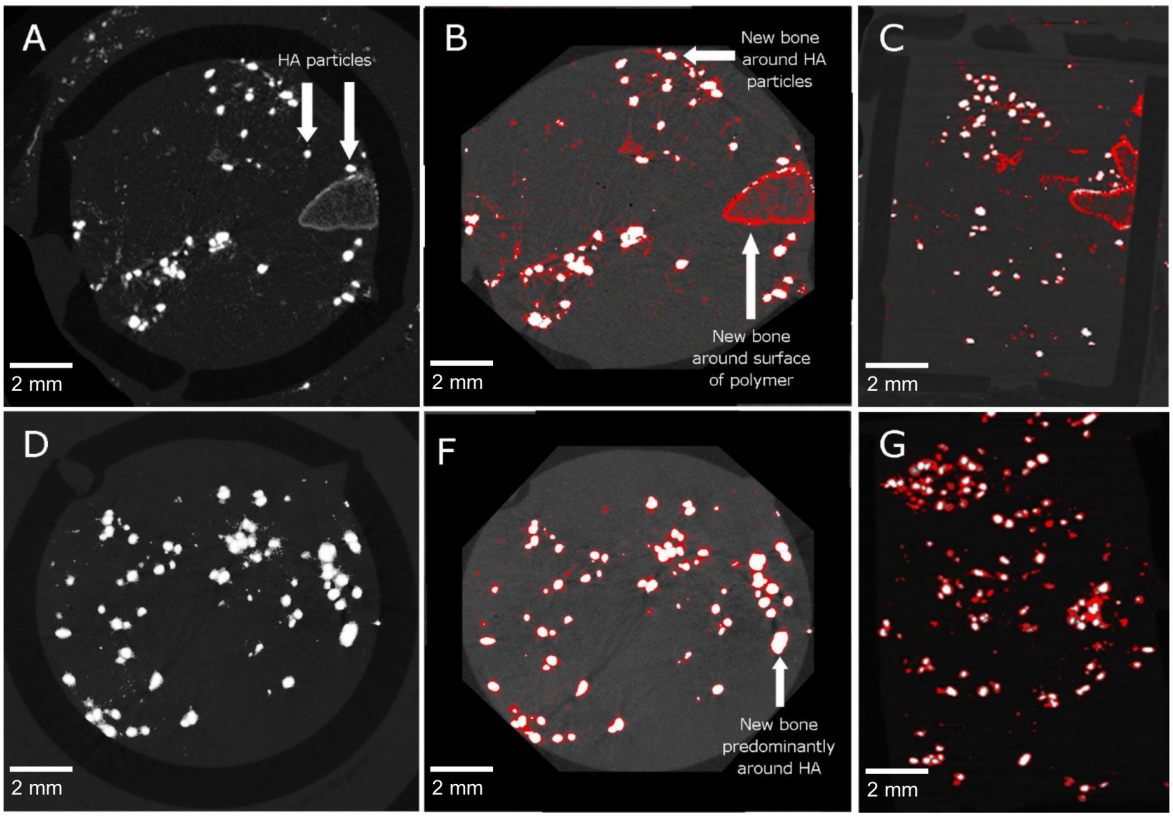

Figure 3.15: Representative micro CT slices of milled $scCO_2$ foamed $P_{DL}LA$ + 10 wt.% HA scaffolds implanted in *Foxn1nu* mice both with (A-C) and without (D-F) hMSCs and recovered post five week *in vivo* incubation. White circular shapes show HA particles while bone like matrix has been coloured red to improve visual contrast in images B-C and E-F.

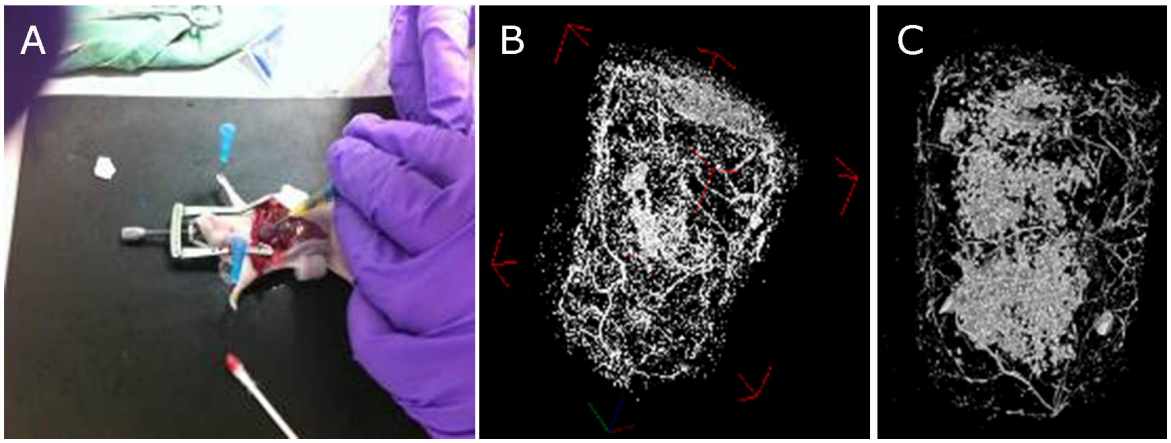

Figure 3.16: Injection of barium sulfate radiocontrast agent (A) enabled visualisation of neo vessel formation in μCT reconstructed models of post five week *in vivo* incubation $P_{DL}LA$ scaffold (B) and $P_{DL}LA$ + 10% HA scaffold (C).

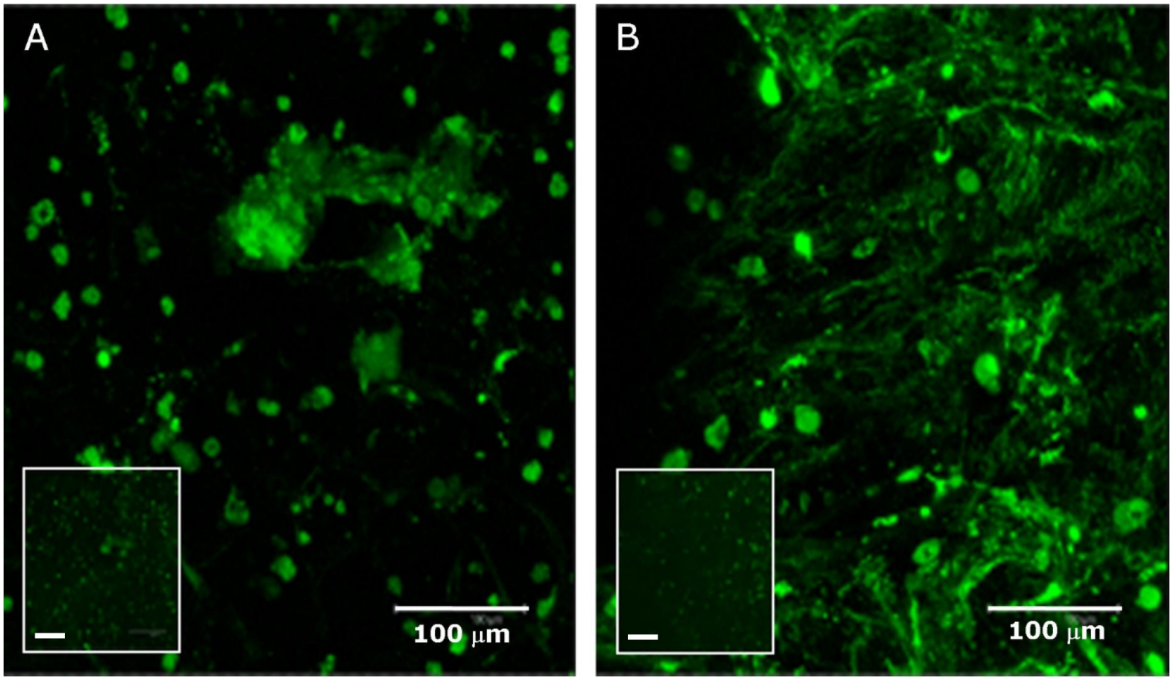

Figure 3.17: Confocal images of hMSCs stained with Vybrant, incubated subcutaneously in *Foxn1nu* mice for five weeks on P_{DL}LA scaffolds and recovered post implantation. (A) shows cells survived on P_{DL}LA scaffolds and (B) shows cells survived on P_{DL}LA + 10% HA scaffolds. Main images at x40 magnification, inset images at x10 magnification.

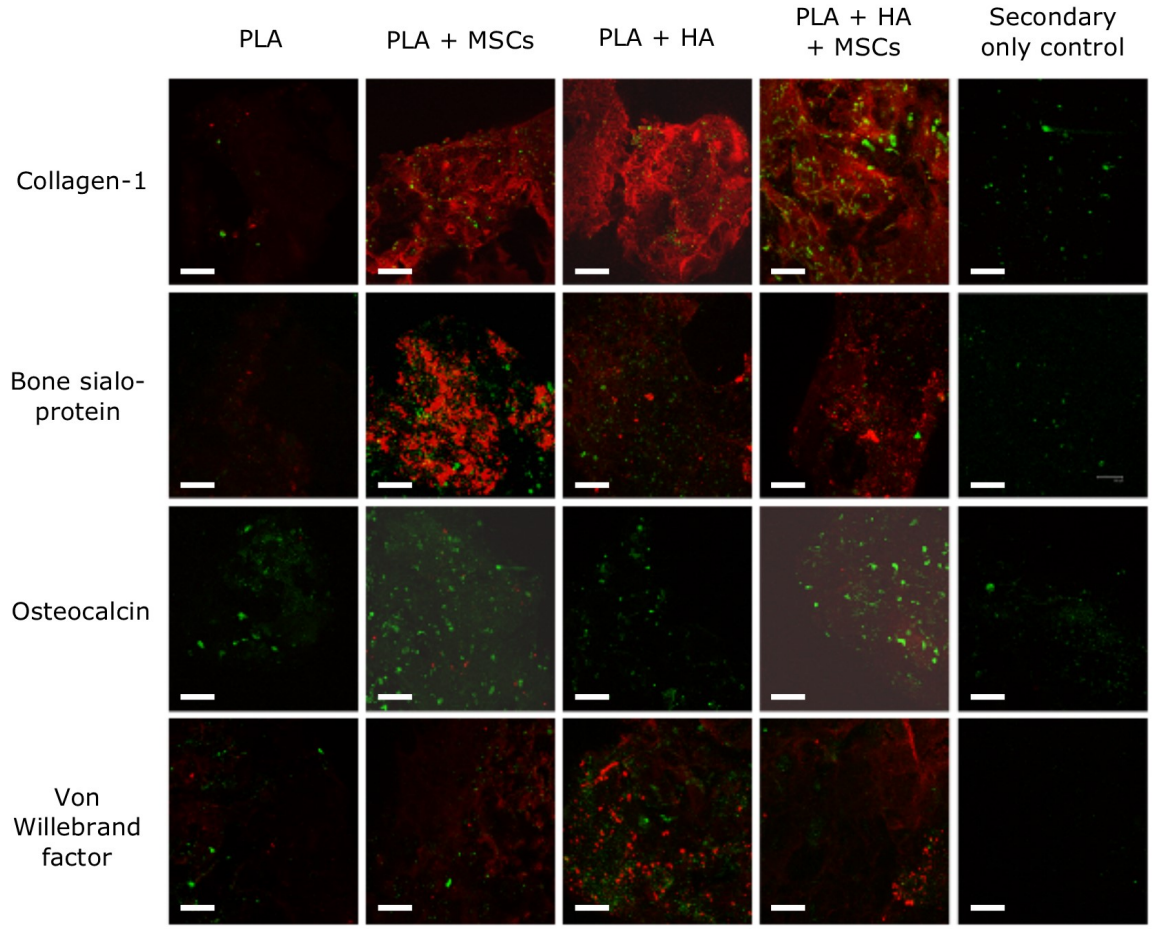

Figure 3.18: Confocal images of samples post five week murine implantation at x20 magnification showing immunostains (red) for: osteoblastic differentiation markers collagen-1, bone sialoprotein, and osteocalcin; and vascularisation marker von Willebrand's factor. DAPI nuclear counterstains (green) are also shown. Negative controls were stained without the use of primary antibody. Scale bars equal 200 μm.

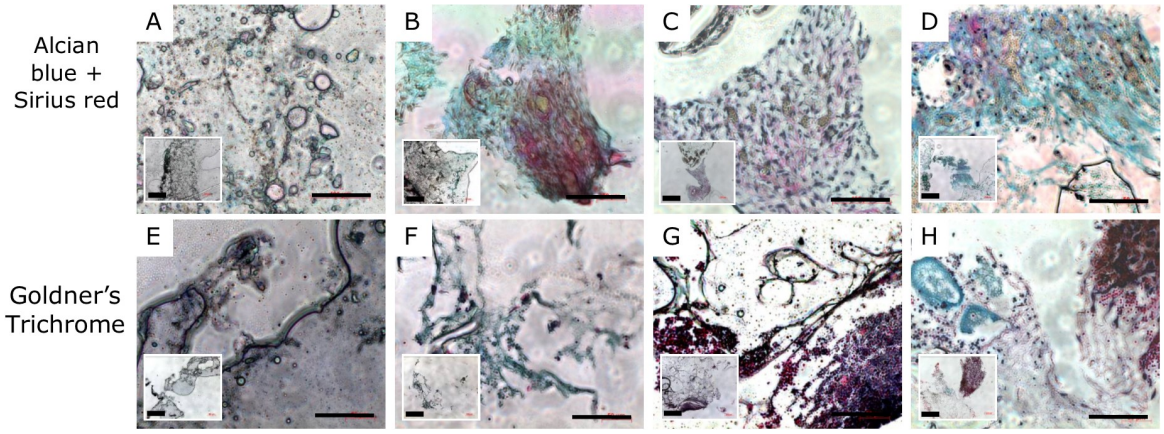

Figure 3.19: Histological samples imaged utilising optical microscopy at x20 magnification (inset images at x5 magnification) post five week murine incubation. Scale bars = 100 μm. Alcian blue and Sirius red stained for proteoglycan and collagen, respectively. Goldner's trichrome stained for osteoid. Control $P_{DL}LA$ samples implanted without cells stain show no positive staining (A & E) while all other samples show positive staining.

(12 kDa) were implanted in mice for 11 weeks and bone formation was observed [207], although in these experiments the $P_{DL}LA$ was a much lower (≈90%) M_W and the cells were not impacted as they were for the experiments detailed in this chapter. Similarly, Wang *et al.* [208] prepared composite polyamide/HA scaffolds and implanted them into rabbits with and without MSCs. Through quantification of histological slides they provide evidence that MSC/scaffold implants had significantly greater new bone volume than pure scaffold implants ($P<0.05$). These findings are in agreement with our μCT analysis which show significantly greater mineralised matrix formed on scaffolds implanted with cells than those implanted without.

Hollister [129] points out, answering the question "is there an optimal material for regeneration of specific tissues?" requires textitin vivo experiments using scaffolds made with controlled characteristics. While Hollister is referring to carefully controlled porosity, among other properties scaffold milling imparts macro porosity into the final impacted scaffold. For IBG providing a viable alternative to the current clinical 'gold standard' material will likely require compatibility with current clinical procedures, which include scaffolds being easy to handle and that can be processed as allograft is now i.e. milled and chips impacted into defect. In this study $scCO_2$ foamed polymers with similarly high M_W (≈100 kDa) were foamed to produce scaffolds with porosities ≈50%. These scaffolds were found by clinicians (Southampton collaborators) to be easy to handle and possibly to mill utilising a bone mill, found in theatres for IBG.

To answer the question "is there an optimal material for IBG?" the scaffolds with the most potential were studied *in vivo*. Subcutaneous implantation in a murine model provided initial promising results. While this model is on a small scale in a non-load bearing application the study did provide an assessment of both osteoinductive and osteogenic capacity and vascularisation potential of the scaffolds and scaffold/cell composites. The *in vivo* study also provided evidence that inflammation and toxicity of the scaffolds is minimal. Degradation time in physiological conditions for these scaffolds will be measured in months not days with no significant degradation observed after five week *in vivo* incubation. It is important that scaffolds do not degrade faster than new bone can be formed, and additionally that acidic degradation products should have time to diffuse and be removed from the site to prevent both build of acidic products which may cause detrimental inflammation levels, and autocatalyse the hydrolytic degradation of the polymer. Further study in a larger animal model (ovine) using a condyle defect followed and the results are presented in the

next chapter. From these results HA inclusion and MSC/scaffold composites both demonstrated improved performance. Therefore $scCO_2$ foamed $P_{DL}LA$ with 10% HA and MSCs was taken forward into the large animal model and controls without cells were also used as a comparison.

3.4 Conclusion

The work described in this chapter has demonstrated that $scCO_2$ foamed biodegradable polymer scaffolds can withstand shear forces to the same or to a greater extent than allograft bone chips when both are milled and impacted to simulate IBG. High M_W $scCO_2$ foamed $P_{DL}LA$ and $P_{DL}LGA$ were shown to support greater numbers of MSCs, which differentiated toward the osteoblastic lineage more quickly than cells cultured on non-foamed scaffolds of the same polymers.

Comparison of $scCO_2$ foamed $P_{DL}LA$ and $scCO_2$ foamed $P_{DL}LGA$ scaffolds showed variation in pore size and porosity under identical foaming conditions (118 μm mean pore size and 59% porosity for $P_{DL}LA$, 85 μm mean pore size and 46% porosity for $P_{DL}LGA$). Both scaffolds were easily milled and impacted, and while both scaffolds resisted shear $P_{DL}LGA$ scaffolds were able to resist to a greater extent. Cellular assays demonstrated that, while cell proliferation was closely matched on both scaffolds, MSCs were capable of osteoblastic differentiation (observed through ALP assays and collagen-1 immunostaining) on $P_{DL}LA$ scaffolds over 14 days to a significantly greater extent than was observed for MSCs cultured on $P_{DL}LGA$ scaffolds. This result was repeatable and observed in the initial study comparing $scCO_2$ foamed scaffolds to non-foamed scaffolds, and the second study comparing scaffolds with and without HA.

Hydroxyapatite was utilised to improve scaffold osteoinductive properties and mechanical strength. Shear resistance of milled and impacted scaffolds was not significantly different with or without HA microparticles at 10 wt.% concentration. The presence of HA did appear to improve the osteoinductive properties of the scaffolds. The $scCO_2$ foamed $P_{DL}LA$ scaffolds with HA recruited host cells which formed osteoid and mineralised matrix textitin vivo, observed through histological staining and μCT. Supercritical CO_2 foamed $P_{DL}LA$ scaffolds without HA did not show evidence of recruiting host cells over five weeks with subcutaneous murine incubation.

Production of mineralised matrix to form new bone appeared to centre around HA particles. While mineralised matrix was formed within $scCO_2$ foamed $P_{DL}LA$ scaffolds without HA, more was formed in the scaffolds with HA particles, demonstrated through quantitative analysis of μCT scans. Where mineralised matrix had been formed, it was possible to highlight in μCT reconstructed images newly formed mineralised matrix and HA microparticles. In these images mineralised matrix predominantly surrounded HA particles. By providing further sites for mineralised matrix to form around, it may be possible to improve the rate at which new bone might be formed. This could be achieved by using smaller particles (such as nanoparticles) and increasing the specific surface area available to MSCs.

The significant difference in osteoblastic differentiation between cells cultured on $P_{DL}LGA$ scaffolds and $P_{DL}LA$ scaffolds was not anticipated. Both polymers used to form scaffolds had M_Ws $\approx$100 kDa and the lactide:glycolide ratio in $P_{DL}LGA$ was 85:15. After two weeks *in vitro* culture, the significant amounts of ALP and collagen-1 expressed by cells cultured on $P_{DL}LA$ scaffolds was a large contrast to the almost negligible amounts expressed by cells cultured on $P_{DL}LGA$ scaffolds. The morphology of the scaffolds was slightly different, as observed through μCT and SEM, which may contribute to the difference in cell differentiation between the scaffolds. Further work will be required to investigate this.

The murine model used within this study has provided confirmation that $scCO_2$ foamed $P_{DL}LA$ scaffolds with HA and MSCs are suitable for impaction and implantation without observable toxic or detrimental effects in the time frame. The short time frame, non-load bearing site (subcutaneous implantation), and small scale are limits to the study. Further investigation of the performance of these scaffolds in a critical sized bone defect in a larger animal (ovine condyle defect) is detailed in the following chapter. Additionally, scale-up of scaffold production is also considered within the following chapter.

CHAPTER 4

Investigation of the scalability of manufacturing $scCO_2$ foamed scaffolds and their utilisation *in vivo*

This chapter investigates *in vivo* bone regeneration of critical sized condyle defects within ovine femoral condyles filled with $scCO_2$ foamed scaffolds. Additionally investigation of the scale-up of production of porous $scCO_2$ foamed scaffolds is performed.

4.1 Introduction

In Chapter 3, high M_W (106 kDa) $scCO_2$ foamed $P_{DL}LA$ scaffolds with 10% HA were identified as the most promising scaffolds, of those tested, for use in impaction bone grafting procedures. This was determined by mechanical shear testing of milled and impacted scaffolds: a common mechanism of failure in revision hip replacements, which constitute a large proportion of IBG procedures. Additionally, *in vitro* cellular compatibility and differentiation, and an *in vivo* small animal model identified these $P_{DL}LA$ scaffolds as those with the most potential for this application. Scaffolds were implanted with and without hMSCs in immunodeficient mice and the presence of implanted MSCs appeared to improve the bone formation observed.

This chapter describes the *in vivo* performance of $scCO_2$ foamed $P_{DL}LA$ scaffolds with 10% HA in an ovine model. An ovine hemiarthroplasty (hip replacement) model was initially planned to provide a clinically relevant loaded model for later application to human clinical trials following strong indications of good bone repair. An ovine model appealed for several reasons: adult sheep have a similar bodyweight (70-90 kg) to adult humans [209], sheep long bones are large enough to accept human-scale implants [209], and the joint forces in sheep have been characterized [210–212]. Additionally, in large animals the bone biology, mineral composition, turnover, and loading environments are similar to human conditions [211]. The use of large animal models for bone regeneration scaffolds provides high value data relating to scaffold degradation, resorption, and biomechanical properties [211].

A comparison of key attributes of human and ovine bone that included macrostructure, microstructure, and remodelling was made by Pearce *et al*. [213] from a review of literature. The overall hierarchical structure of bone was described in Chapter 1. Here macrostructure refers to the overall geometry (e.g. cross sectional area) and properties of bone, such as bone mineral density and mechanical strength [214], while Pearce *et al*. separate bone mineral density and strength into a separate category, bone composition. Microstructure refers to the structure and shape of bone concentric layers formed around blood vessels (Haversian systems, osteons, or bone structural units). Bone remodelling refers to the process of co-ordinated osteoclast mediated bone resorption, osteoblast mediated bone matrix formation, and matrix mineralisation [215]. As previously mentioned, dimensionally the macrostructure of ovine long bones is similar to that of human long bones. However, ovine bones demonstrate greater apparent density and strength, in comparison to human bones

[213, 216, 217], but do not show significant differences in mineral composition [218].

Microstructurally, sheep are reported as having predominantly primary bone (woven or immature bone), which is more irregular than secondary bone and contains osteons with diameters <100 μm, and lack a cement line. Human bone is predominantly secondary bone (lamellar/mature bone), which is more organised, contains larger osteons (100 - 300 μm diameter) with larger vascular channels within the centre than primary osteons. Martin *et al*. [219] hypothesized that the smaller vascular channel size in primary bone may result in greater mechanical strength compared to secondary bone, which may explain the greater mechanical strength reported between ovine and human bone [216, 217]. Secondary bone remodelling in sheep does become more prevalent with age and is reported in 7-9 year old sheep by Newman *et al*. [209].

While differences between ovine and human bone structures exist, ovine models remain valuable for remodelling and bony in-growth into porous implants [211, 213, 220, 221]. In a weight-bearing ovine model for bone in-growth there was no significant difference reported between the amount of cancellous bone in-growth over time in the ovine model and from human total bilateral knee replacement data [221]. Additionally, ovine bone metabolic and remodelling rates are similar to human rates [222, 223], supporting the value of ovine models for human bone remodelling [220].

Due to insufficient funding for an ovine hemiarthroplasty model a femoral condyle critical sized defect model was substituted. Critical sized defects have been defined as "the smallest size intraosseous wound in a particular bone and species of animal that will not heal spontaneously during the lifetime of the animal" [224, 225]. Ovine femoral condyle models have previously been used to study the osteoconductivity and bone in-growth of other scaffold types targeted as either bone graft extenders (scaffolds to be used in conjunction with allograft to reduce the required volume of allograft) or scaffolds to augment bone healing [226–230]. This chapter describes the bony in-growth observed within an ovine femoral condyle model filled with $scCO_2$ foamed $P_{DL}LA$ with 10% HA scaffolds and the effect MSCs implanted with scaffolds had on the bony in-growth observed. Similar ovine condyle studies utilising different scaffolds are reported in the literature and extended the scope of the conclusions that could be drawn from this study. Empty defects were not used as negative controls to confirm the defects were critically sized, but the limited regenerative potential of such defects is reported within the literature [230, 231]. Van der Pol *et al*. [230]

reported a bone density within the empty defects of 28.4 ± 15.3% after 12 months. This was an increase of 1.5% from the bone density reported at 4 months; additionally, the bone formed within the defect was concentrated around the edge. Flautre *et al*. [231] reported 5.9% and 11.0% new bone formed within empty cavities after 12 and 24 weeks, respectively.

Alternative critical sized defect animal models of bone repair could have been substituted. Particularly, canine models are reportedly more suitable models of human bone biologically [213, 232]. However, the use of companion animals (e.g. dogs and cats) for medical research is less desirable from ethical and public perception viewpoints [213]. A canine hemiarthroplasty model would be unsuitable in terms of loading environment, animal weight, and implant design. Clinical translation of $scCO_2$ foamed biodegradable polymer scaffolds into viable alternatives to allograft will require regulatory approval. For this to occur, comprehensive *in vitro* and *in vivo* studies need to be performed, which should include a clinically relevant hemiarthroplasty model [211]. Reichert *et al*. state this strongly: "To establish a tissue engineering concept in a clinical setting, a rigorous demonstration of the level of therapeutic benefit in clinically relevant animal models is a *conditio sine qua non* [a condition without which it could not be]" [211]. In this case a clinically relevant animal model is most likely to take the form of an ovine hemiarthroplasty model; hence, an ovine condyle defect model was preferred to viable alternatives (e.g. canine) because it would provide more relevant data to support the success of a later loaded ovine model.

The manufacturing process of tissue engineering scaffolds must be scalable and commercially viable to be successful. A gap exists whereby the discovery phase of tissue engineering research receives the majority of funding, while the products resulting from the research remain few [211, 233]. Hollister *et al*. [233] claim two reasons for tissue engineering technology failure: lack of design for specific application, and inability to be scaled to clinical level production. The $scCO_2$ foamed scaffolds studied within this thesis have been specifically targeted at impaction bone grafting as potential replacement to allograft bone. The supercritical fluid foaming process is scalable and within this chapter scaffolds produced on the small scale (60 ml autoclave, 1.8 g/six scaffolds per batch) were characterised alongside scaffolds produced within a larger vessel (1 L autoclave, 54 g/one hundred and eighty scaffolds per batch). For consistency, scaffolds produced within the larger vessel were not used in the ovine study.

4.2 Materials and methods

4.2.1 *In vivo* ovine study

Supercritical CO_2 foamed scaffolds with 10 wt.% HA microparticles performed the most favourably in previous studies and were investigated in an ovine femoral condyle model.

The *in vivo* ovine study was carried out at the Royal Veterinary College, Potters Bar, by Prof. A. Goodship, Mr. E. Tayton, Miss G. Hughes, and Mr J. Smith.

4.2.1.1 Sheep selection

Six healthy skeletally mature (>2 years old) welsh mule ewes weighing between 60 and 90 kg were obtained, vetted, and acclimatised in a barn for 4 weeks prior to the start of the study, which was initiated with harvesting of ovine MSCs.

4.2.1.2 General anaesthesia

General anaesthesia following a standard protocol was carried out prior to interventional procedures. Premedication consisted of 0.1 mg kg^{-1} intramuscular xylazine (Rompun, Bayer PLC., U.K.) injection and 5 mg of the prophylactic antibiotic sodium cefalexin (Ceporx, Schering-Plough, U.K.). Anaesthesia was induced using 2.5 mg intravenous midazolam (Hypnovel, Roche, U.K.) and 2 mg $^{-1}$kg intravenous ketamine hydrochloride (Ketaset, Fort Dodge Animal Health Ltd., U.K.). The sheep were then intubated and general anaesthesia was maintained using inhaled isofluran, oxygen, and nitrous oxide.

4.2.1.3 Harvest and expansion of mesenchymal stem cells

Once fully anaesthetised sheep were placed in the left lateral position (i.e. lying on their left side) and an area shaved over the iliac crest. This was cleaned using 10% povidine-iodine (betadine) solution followed by 2% chlorhexidine gluconate solution. A trochar was then inserted through the cortical bone, and approximately 5-10 ml aspirated. The aspirate from each sheep was then placed into a separate universal container and into a cool box for transportation to the laboratory. The sheep were then recovered, and given analgesia as required. They were housed in the barn, penned, and fed standard food until further use.

The universal tubes containing the ovine aspirates had 10 ml of basal medium (α-MEM, 10% FBS, 1% penicillin and streptomycin) added and the solutions were then filtered (70 μm filter) into separate universal tubes and centrifuged at 180 g for 4 minutes. The supernatants were aspirated and cell pellets resuspended in 40 ml basal medium. These solutions were split equally into four T75 tissue culture flasks and incubated under standard culture conditions (37 °C and 5% CO_2) until confluent. Cell media was changed every three days. When required for scaffold seeding the cell monolayers were released using 10% trypsin in EDTA for 2 minutes. The trypsin was neutralised with the addition of equal volume of basal media, and cell pellets obtained via centrifugation (180 g for 4 minutes). The supernatants were aspirated and the cell pellets resuspended in basal media. Total cell number was approximated using a haemocytometer. Appropriate dilution with basal media was used to achieve a concentration of 5×10^5 cells ml^{-1}.

4.2.1.4 Scaffold seeding

Supercritical CO_2 foamed $P_{DL}LA$ scaffolds + 10 wt.% HA microparticles were produced as described in Section 2.1 (270 mg ground $P_{DL}LA$, 30 mg HA microparticles). They were then milled and sterilised as detailed in Section 2.5.1.3. The sterilised milled polymer scaffolds were placed in universal tubes and 20 ml of the solutions of ovine MSCs were added to each and incubated for 2 hours with gentle agitation every 30 minutes. The medium was then aspirated from each universal tube and the seeded scaffolds were placed into individual wells of six well plates and cultured in osteogenic medium (basal media + 100 μM ascorbate-2-phosphate, and 10 nM dexamethasone) for 2 weeks. Media was changed every 3 days.

4.2.1.5 Operative procedure

The sheep were given two fentanyl patches (75 mcg hr^{-1}) 12 hours prior to surgery and were randomised to receive scaffold + MSCs or scaffold alone to either the right or left side. The sheep again underwent full general anaesthesia as described in Section 4.2.1.2. They were placed in the supine position (lying flat face up), with surgical gloves placed over their hooves. The hind legs were both secured to the operating table with rope, shaved, and cleaned thoroughly using 10 % povidone-iodine (betadine) solution followed by 2% chlorhexidine gluconate solution. Each sheep was then covered with sterile drapes such that only the surgical sites were exposed. Longitudinal incisions (10 cm in length) were

made centred over the palpable bony protuberances located on the medial sides of the medial femoral condyles of each leg (Figure 4.1A shows the location the condyle defect was drilled), with careful dissection through subcutaneous tissue, fascia, muscle, and periosteum to expose the underlying bone. A customised 8 mm drill bit was then used to create a hole with a consistent depth of 15 mm into the underlying cancellous bone (Figure 4.1B). After the hole was drilled a reamer was used to give the hole a flat bottom. Scaffold was packed into the holes on either side, one with scaffold only (control), one with scaffold + MSCs, as per the randomisation for each sheep. Scaffolds were packed into each hole such that they were filled (Figure 4.1 D&E). Two guide wires were placed superior and inferior to the holes for radiographic location purposes at a later stage. The periosteum and other layers were then closed over the filled holes using 2/0 Vicryl in order to contain the scaffold, and the skin was closed with interrupted sutures using 2/0 Ethilon and op-site spray. The wounds were subsequently covered with betadine soaked gauze, wool, and crepe bandage. The sheep received a five day post-operative antibiotic regime (Ceporex 5 ml OD) with fentanyl patches and buprenorphine (0.6 mg) for 72 hours after application of the patches (for analgesia) and regular wound checks. After surgery the sheep were housed individually in pens for 5 days, followed by group housing in pens for the remainder of the study. The sheep were fed according to standard practice, with free access to water from troughs.

4.2.1.6 Radiographic analysis

Miss G. Hughes collected the x-ray radiographs at both timepoints.

Craniocaudal radiographs were taken using a portable x-ray unit (PLH Medical Ltd, U.K.). Radiographs were taken directly after the surgical procedure, after 6 weeks, and after 13 weeks. Under general anaesthesia, the sheep were placed in appropriate positions for antero-posterior (AP) and lateral radiographs with the hip and knee fully extended. The radiographic plate was positioned dorsal with the x-ray source ventral and then the radiographic plate was placed lateral with source medial using standardised distances (80 cm) and exposure times.

4.2.1.7 Retrieval of specimens

The sheep were euthanased with barbiturate overdose (0.7 mg kg^{-1}) 13 weeks post implantation of the specimens. The femoral condyles were harvested along with the popliteal lymph

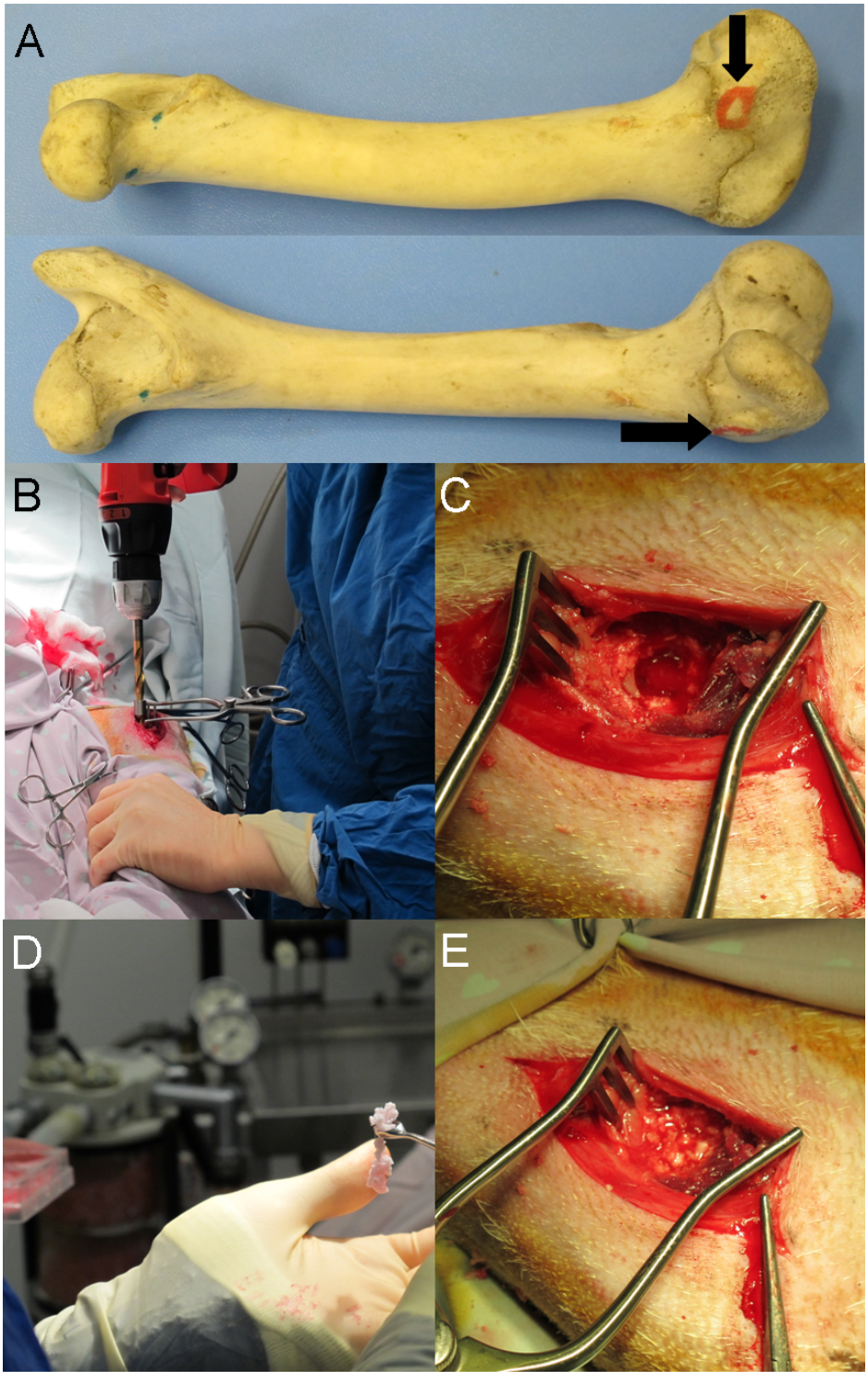

Figure 4.1: Images of steps of the femoral condyle defect implantation. The arrows in image (A) show the location the femoral defect was drilled in the femur. B) shows drilling into the condyle; C) shows the drilled, reamed, defect; D) shows milled chips of scCO_2 seeded with ovine MSCs; E) shows the condyle defect filled with implanted polymer scaffold.

nodes.

4.2.1.8 Peripheral quantitative computed tomography (pQCT)

Retrieved femoral condyles were scanned using a pQCT scanner (XCT 2000, Stratec Biomedical, U.K.) by Miss G. Hughes. The bone mineral density within the condyle defect sites was calculated by manufacturer's software.

4.2.1.9 Preparation of condyles

Post pQCT scan the femoral condyles were were prepared and mechanically tested within 6 hours of harvest. The condyles were placed in a jig and carefully orientated via the use of the radiographs and marker wires, such that when cut with a diamond-edged EXAKT band saw (EXAKT, Hamburg, Germany), the polymer scaffold filled cylindrical defect drill holes were transected longitudinally in the coronal plane at the midpoints. One half of each specimen was subsequently taken for immediate mechanical testing and μCT evaluation, and the other half was prepared for histological staining.

4.2.1.10 Mechanical testing

One half of each of the femoral condyles was used for mechanical indentation testing. The specimens were position onto the stage of a Z005 static materials testing machine (Zwick/Roell, Leominster, Herefordshire, U.K.), and the metal indentation rod (diameter 4 mm) was placed in opposition to the desired test area, and a preload of 10 N applied with a speed of 5 mm min^{-1}. The test areas are shown in Figure4.6, where areas 1 and 2 correspond to the superficial and deep areas of the scaffold within the drill hole, and areas A and B correspond to proximal and distal areas of normal cancellous bone. The test was started and the indentation rod was advanced at a rate of 10 mm min^{-1}, and the force measured at each time point recorded via a load cell.

The data was transferred to a spreadsheet (Microsoft Excel 2007) and graphs of force against strain plotted (load deformation curve). From these graphs a peak was visible, which corresponded to the failure of the test area. The force required at this peak was recorded for each area under test. Mean stress values (along with standard deviations) were calculated for each area of the femoral defects filled with the scaffold alone, and those implanted with

the scaffold + MSCs, and they were compared using Student's unpaired t test.

4.2.1.11 Micro x-ray computed tomography

After indentation testing the specimens were frozen until μCT scanning and analysis could be performed. They were individually defrosted and scanned using a SkyScan 1176 μCT. Samples were focused, calibrated, and adjusted to prevent x-ray saturation. The scans were at an 18 μm voxel resolution. Data reconstruction was performed using NRecon (Skyscan, Belgium) and saved as 8 bit bitmaps (BMP). Analysis of the reconstructed images was performed using CTAn (Skyscan, Belgium). The region of interest (corresponding to the volume within the original drill hole) was extracted manually using the software, and via comparison with standard phantoms, new bone was deemed to correspond to all density values over 0.25 g cm^{-3}. Mean volume of new bone within the region of interest was calculated for the femoral condyle defects implanted with the scaffold alone, and those implanted with the scaffold + MSCs, and they were compared using Student's unpaired t test.

4.2.1.12 Histological examination

The half of each the femoral condyles not used for indentation testing was used for histological analysis. The samples were fixed in buffered formal saline for one week followed by dehydration through an ascending alcohol series over a three week period. The samples were then de-fatted in chloroform for one further week, followed by infiltration and embedding in LR White methacrylate resin (London Resin Co Ltd, Berks, U.K.). Using the band saw, longitudinal slices measuring 5 mm thick were taken through specimens, and from these slices thinner sections measuring between 50 and 80 μm thick were made. The sections were attached to an acrylic slide using U.V. curable cyano-acrylate glue, before being grinded and polished on an EXACT grinding machine. Sections were stained with toluidine blue to stain the soft tissue followed by hematoxylin and eosin (H&E) to stain the bone, before being viewed by light microscopy.

Histological staining of femoral condyle defects was performed by Prof. G. Blunn at Stanmore. Imaging of histologically stained samples was performed by the author and by Mr. E. Tayton at Stanmore.

Histological staining of femoral condyle defects was performed by Prof. Gordon Blunn at Stanmore. Imaging of histologically stained samples was performed by Mr. Matthew Purcell

and Mr. E. Tayton at Stanmore.

The lymph nodes were fixed in formaldehyde, and dehydrated in graded ethanol solutions prior to wax embedding on a mounting plate. Sections were cut (7 μm thick), transferred to a water bath, and mounted on slides, prior to transfer to an oven set to 37 °C for 4 hours. They were subsequently stained using a standard Haematoxylin and Eosin (H + E) stain, and assessed by a consultant pathologist for the presence of abnormal inflammatory cells.

Histological staining of lymph nodes was performed at Southampton University by Mr. E. Tayton.

Histological staining of lymph nodes was performed at Southampton University by Mr. E. Tayton and thanks go to Dr. Darren Fowler, a consultant pathologist, for help with analysis of stained samples.

4.2.2 Parallel *in vitro* study

Polymer scaffold seeded with ovine MSCs and unused to fill the femoral condyle defects was kept for a parallel *in vitro* study. Approximately 1 g of seeded scaffold was placed into individual wells of 24 well plates and incubated under standard cell culture conditions (37 °C and 5% CO_2) in osteogenic media.

4.2.2.1 WST-1 assay

Three samples for each sheep were assessed for cell viability after 2 week *in vitro* incubation (first day of ovine *in vivo* incubation) and 8 week *in vitro* incubation (6 week of ovine *in vivo* incubation/mid-point of *in vivo* study). Each sample was submerged in 1 ml 1:10 dilution WST-1 substrate (Roche Ltd., U.K.). Polymer scaffolds not seeded with MSCs were used as negative controls. After 4 hours, $\times 3$ 100 μl of substrate solution were taken from each sample well and analysed via a Bio-Tek KC4 microplate fluorescent reader (Bio-Tek, U.S.A) at 410 nm. Section 2.6.1 contains details of the WST-1 assay used.

4.2.2.2 ALP/DNA assay

Similarly to the WST-1 assays, ovine MSCs were assessed in triplicate for each sheep at 2 week and 8 week *in vitro* incubation time-points, which corresponded to the first day of

ovine incubation and to the mid-point of ovine incubation, respectively. Identical protocols to those detailed in Sections 2.6.2 and 2.6.3 were used; the only difference is that, rather than referring to the contents of an impaction chamber, portions of seeded scaffold cultured in individual wells of 24 well plates were used.

4.2.2.3 Immunohistochemical staining

Two samples of milled polymeric scaffolds seeded individually with MSCs collected and expanded from the bone marrow aspirate different sheep were immunohistochemically stained for collagen-1 and imaged as described in the procedure detailed in Section 2.7.

4.2.3 Production scale-up

The production of scCO_2 foamed scaffolds was scaled up through the utilisation of a custom-made (School of Chemistry, The University of Nottingham, U.K.) 1 L vessel. The 1 L vessel is shown in Figure 4.2A while the smaller scale 60 ml autoclave used to produce the scaffolds for the cell studies within the thesis is shown in Figure 4.2B. While the vessel is scaled up, the piping, control valves, and back-pressure regulator used to control the pressure within the vessel, were identical to those used for the 60 ml autoclave as described in Section 2.1.

Custom-made (School of Chemistry, The University of Nottingham, U.K.) PTFE moulds with a diameter smaller than the internal diameter of the 1 L vessel were used. Each mould was circular and contained 36 cylindrical wells of identical dimensions to those in the moulds used in the 60 ml autoclave (11.2 mm $\times$ 10.4 mm). Stainless steel base plates and lids were also made for the moulds, with PTFE sheets to fit between the base plates and the mould and the lid and the mould. This was to prevent polymer scaffolds bonding to the stainless-steel and to aid removal of the scaffolds post-scCO_2 foaming. Moulds for the 1 L vessel are shown in Figures 4.2 C, E, & F; and a mould for the 60 ml autoclave is shown in Figure 4.2D. Figure 4.2 C shows the gas inlet ports for the large rig mould. In Figure 4.2D the arrow points to a gas inlet port in a mould for the 60 ml autoclave. Small channels act as gas inlet ports in the top and bottom of the mould for each individual well.

The protocol used for scCO_2 foaming of P_{DL}LA scaffolds in the 1 L vessel is identical to that used in the 60 ml autoclave as detailed in Section 2.1. When foaming using one mould, for practical and safety reasons, PTFE spacers were used to fill the volume of the 1

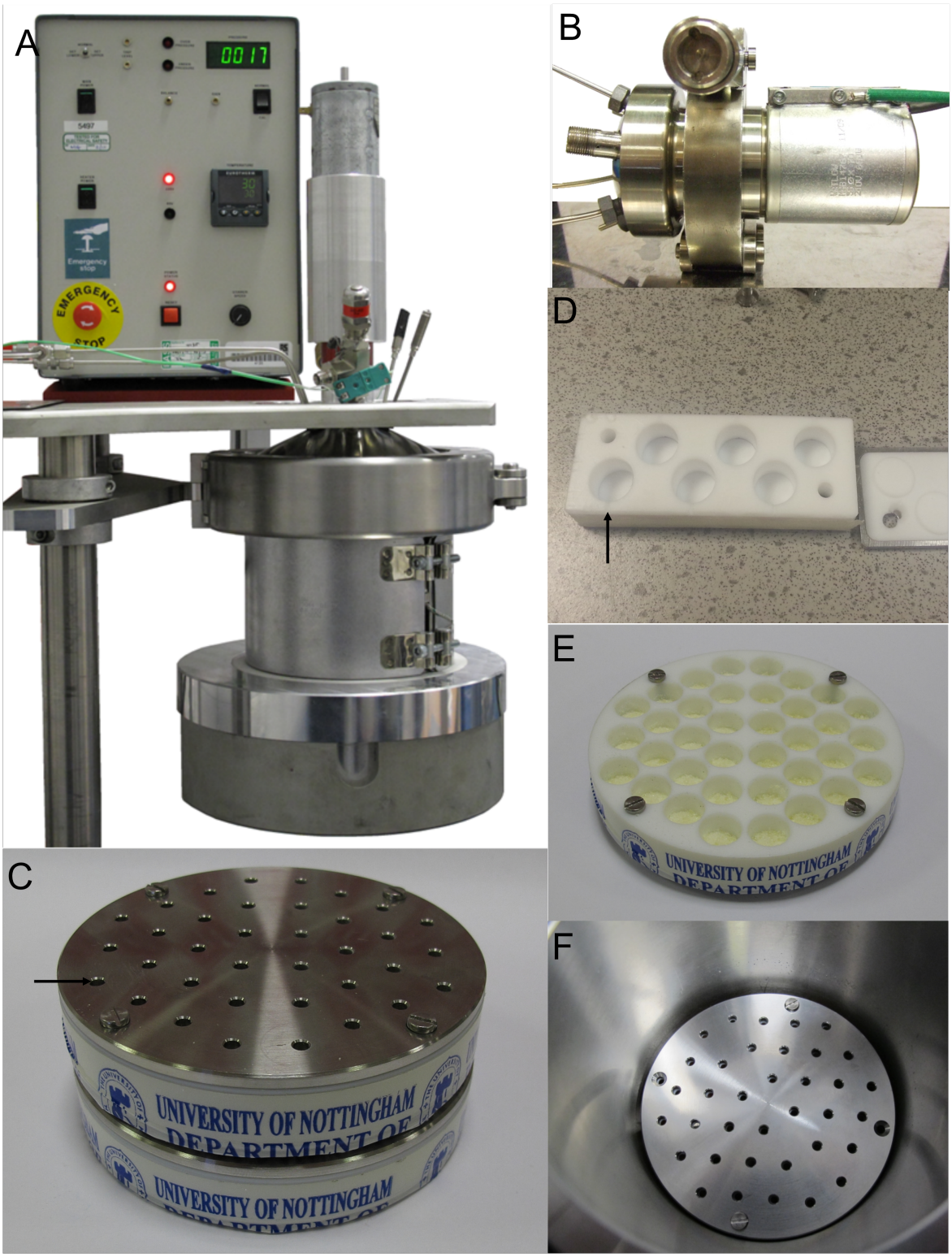

Figure 4.2: Images of the 1 L vessel (A) and 60 ml autoclave (B) used for $scCO_2$ foaming. Moulds for the 1 L vessel (C, E, & F) and 60 ml autoclave (D) are also shown. Arrows indicate gas inlet port locations in moulds.

L vessel to lower the volume of stored energy in the form of pressurised fluid within the vessel. Both the orientation of the moulds and the position within the moulds were tracked to provide a spectrum of scaffolds from different locations within the vessel. Additionally, the PTFE spacers were used to vary the height of the moulds within the 1 L vessel in different batches. Scaffolds from different batches and different locations within the vessel during scCO_2 foaming were used for comparison with scaffolds produced in the 60 ml autoclave, and to determine the variation in scaffold properties produced using the 1 L vessel.

4.2.3.1 Supercritical CO_2 foaming in large vessel

The protocol for scCO_2 foaming in the 60 ml autoclave is detailed in Section 2.1. Scaffolds from different batches were used for comparison with those produced in the 1 L vessel.

4.2.3.2 Supercritical CO_2 foaming in small vessel

The protocol for scCO_2 foaming in the 60 ml autoclave is detailed in Section 2.1. Scaffolds from different batches were used for comparison with those produced in the 1 L vessel.

4.2.3.3 Structure characterisation

Scanning electron microscopy

The protocol used for SEM is detailed in Section 2.2.

Micro x-ray computed tomography

The protocol used for characterising scaffolds using μCT is detailed in Section 2.3.1.

4.3 Results and discussion

4.3.1 *In vivo* ovine study

The aim of the ovine critical sized condyle defect study was to establish the bone regeneration potential of scCO_2 foamed P_{DL}LA + HA scaffolds in a larger, more clinically relevant (similar body weight, long bone size suitable for human protheses [209]) animal model than the previous murine studies. Additionally, the bone regenerative potential of scaffold and

MSCs composites was compared to scaffold only controls. This was to determine the importance of implanting MSCs, which were hypothesised to provide osteogenic properties in scaffold + MSCs composites over the scaffold only controls.

The ovine *in vivo* incubation was initially due to end after 6 weeks. X-ray radiographs taken at this point showed limited radiopacity (radiation opacity) within the defect sites (Figure 4.3) which indicated limited new bone formation and repair. The *in vivo* incubation time was therefore extended to 13 weeks. Radiographs taken after 13 weeks (Figure 4.4) demonstrate less radiopacity in the defect volumes filled with milled $scCO_2$ foamed $P_{DL}LA$ + HA + MSCs than the defects filled without cells. This implied defects filled without cells formed more dense new bone or a greater quantity of new bone.

Following removal, the ovine femoral condyles were analysed on-site using peripheral quantitative computed tomography (pQCT). This technique measures bone mineral density (BMD) and was utilised for comparison of BMD within the defects to surrounding cancellous bone within the same condyles. Comparison of BMD between defects filled with milled $scCO_2$ foamed $P_{DL}LA$ + HA (10 wt.%) + MSCs and controls without MSCs was also performed (Figure 4.5). A difference in mean bone density, between defects filled with milled $scCO_2$ foamed $P_{DL}LA$ + HA (10 wt.%) + MSCs and controls with no cells, of 29% was observed, but was not statistically significant at the $P<0.05$ level.

Two surrounding areas of cancellous bone were used as controls for BMD measured by pQCT. There was a significant difference in BMD between cancellous bone area one and defects filled with $P_{DL}LA$ scaffold + MSCs of 58% ($P<0.01$) and a smaller significant difference in BMD between bone area one and defects filled with $P_{DL}LA$ scaffold alone of 38% ($P<0.01$). The BMD in bone area two was $\approx$ 24% less than that of bone area one ($P<0.05$). Comparison of BMD between the defect sites and bone area two was therefore more favourable with a significant difference of 44% ($P<0.01$) between bone area two and defect filled with $P_{DL}LA$ scaffold + MSCs, and 20% ($P<0.01$) between bone area two and defect filled with $P_{DL}LA$ scaffold alone.

Bone strength and BMD vary significantly within the knee. Behrens *et al*. [234] reported values of bone strength in rheumatoid or osteoarthritic knees varying from 2.9 - 29.4 MPa and BMD varying from 0.3 - 1.0 g cm^{-3}. This variation was found across ten different (human) autopsy patients, with eleven sampling sites across the femoral and tibial condyles for each patient. Given the reported 3-fold variation in human condyle BMD, the variation ($\approx$ 24%)

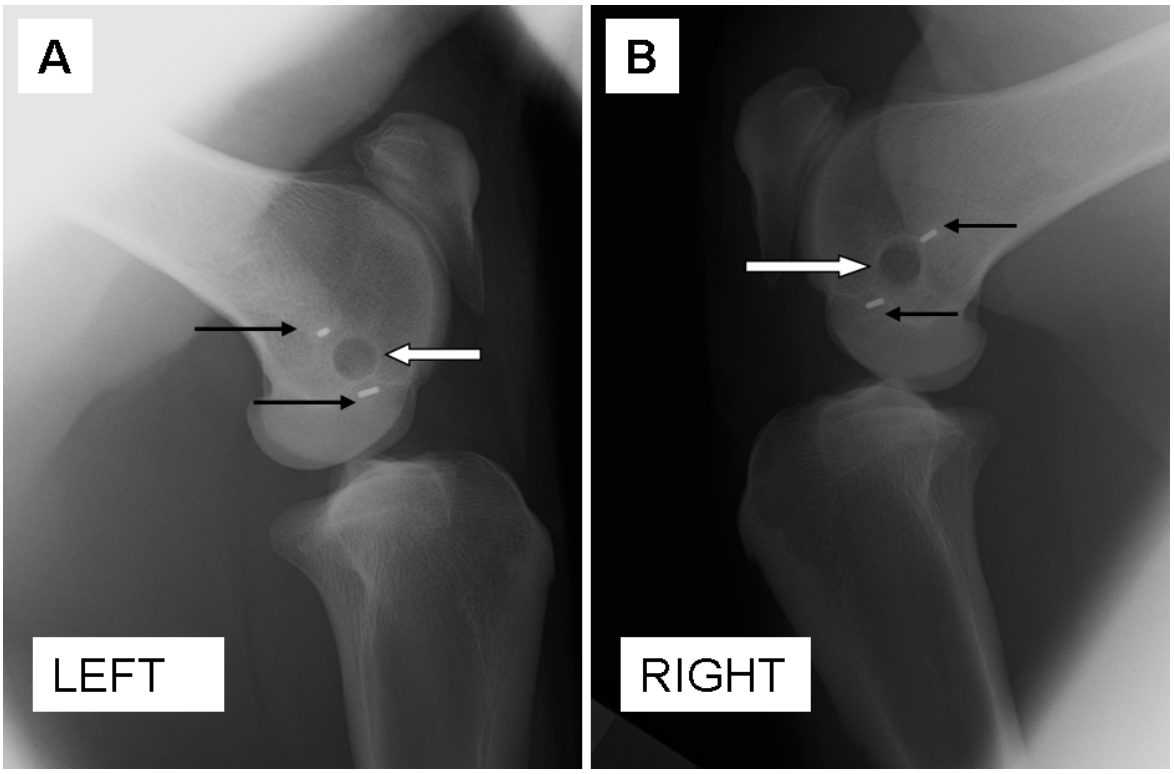

Figure 4.3: Representative lateral x-ray radiographs of femoral ovine condyles thirteen weeks post implantation of: (A) milled scCO_2 foamed scaffold and (B) milled scCO_2 foamed scaffold. Black arrows indicate implanted metallic guides for locating defect. White arrows indicate defects.

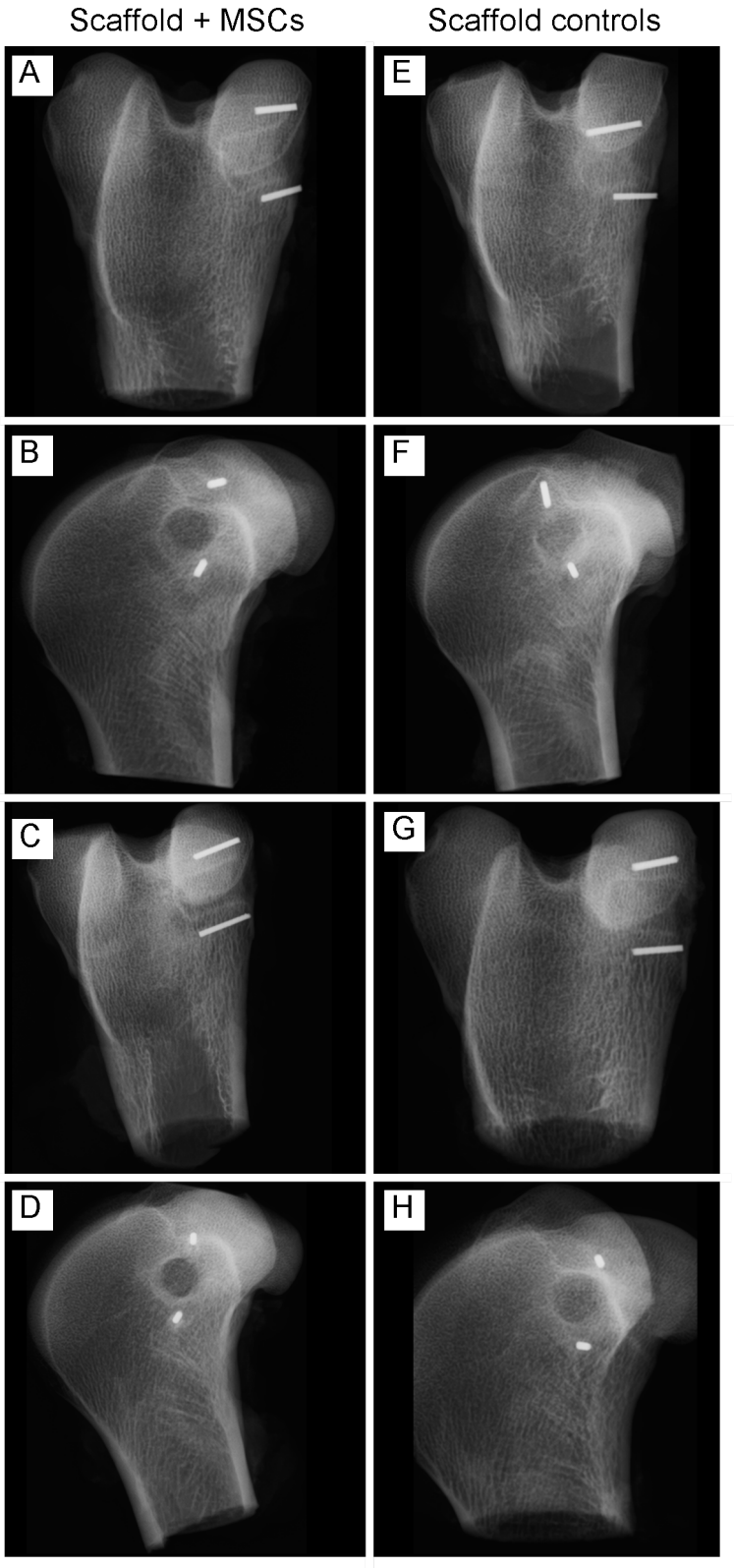

Figure 4.4: Representative medial (A, C, E, & G) and lateral (B, D, F, & H) x-ray radiographs of a sheep's knees six weeks post implantation of: (A) milled scCO_2 foamed scaffold + MSCs and (B) milled scCO_2 foamed scaffold.

in BMD between ovine control areas of bone (bone area one and two) for pQCT analysis was anticipated. The ovine BMD values are low compared to reported ovine values [235] but within the lower range of human BMD reported by Behrens *et al*. [234]. Armstrong *et al*. measured BMD values from volumes that included cortical and cancellous bone. Cortical bone is more dense than cancellous bone [236] and this may account for the lower values of BMD recorded here in control regions.

The ovine femoral condyles were halved vertically down the centre of the cylindrical defect using a diamond bandsaw as detailed in Section 4.2.1.9. Indentation tests were performed on one half of the condyles for each sheep leg on two areas within each defect and two areas in the surrounding cancellous bone as shown in Figure 4.6. The stress at failure was recorded for each area and the mean of these values is displayed in Figure 4.6. The mean strength at failure of defects filled with milled $scCO_2$ foamed $P_{DL}LA$ + HA + MSCs was measurably less than that of defects filled with milled $scCO_2$ foamed $P_{DL}LA$ + HA controls. In position one the difference was 41% while in position two the difference was 72%; however, these differences were not statistically significant.

Indentation testing results have been found to correlate well (correlation values of 0.823 - 0.952) with compressive tests [232, 237]. Eitel *et al*. [232] reviewed recorded literature values of the ultimate strength of cancellous bones and reported a range of 38 - 71 MPa (or N mm^2). The ultimate strength reported here for ovine cancellous bone remains within this range with 40 - 70 MPa (Figure 4.6). This range of values within the same region of bone is not unusual [232]. It is clear the strength of $P_{DL}LA$ scaffold and new bone within the defect volumes is less than surrounding bone and less than the minimum strength we would expect for cancellous bone (38 MPa).

When implanted the milled $P_{DL}LA$ was pushed into the defect and not impacted. The degree of compaction of loose chips of material affects the ultimate strength due to the innate weaknesses built in by lack of bonding. More compact chips of material will display a higher ultimate strength, up to the ultimate strength of the material itself, compared to less compact chips of the same material (assuming identical properties of the chips, such as roughness, size distribution, and porosity). Had the chips of $scCO_2$ foamed $P_{DL}LA$ been more forcefully impacted into the defects a higher ultimate strength may have been observed. The indentation test results showed some strength in the defect volumes (>10 MPa), but this had yet to reach that of cancellous bone.

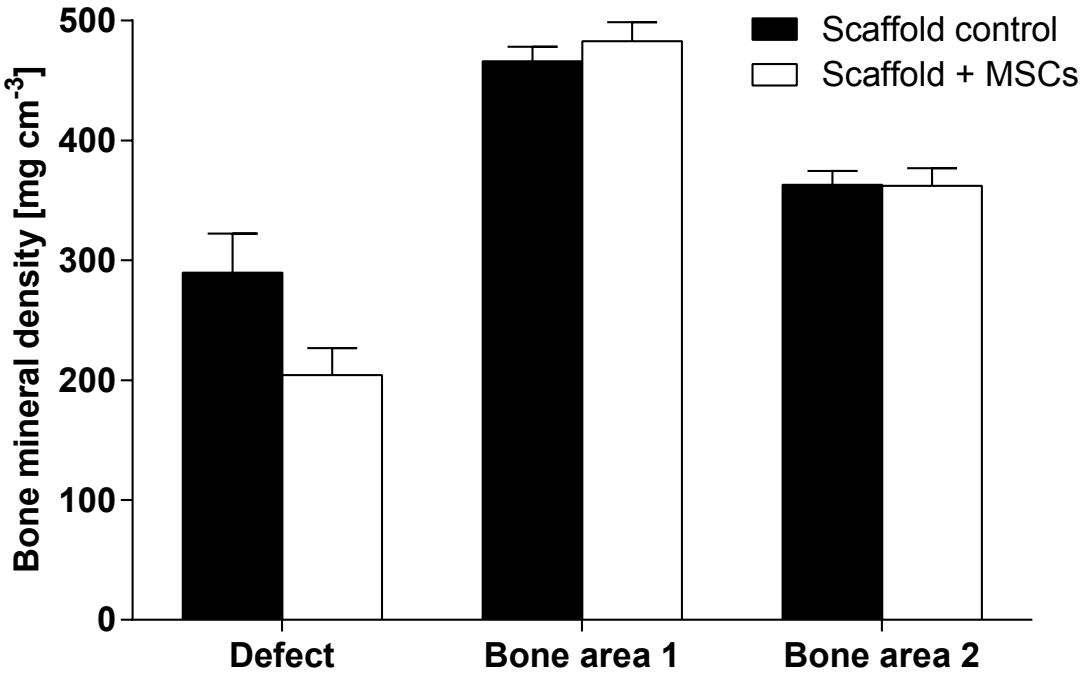

Figure 4.5: Bone mineral densities measured by pQCT post 13 week *in vivo* incubation of defect areas and surrounding bone. No statistical significance at P<0.05 level.

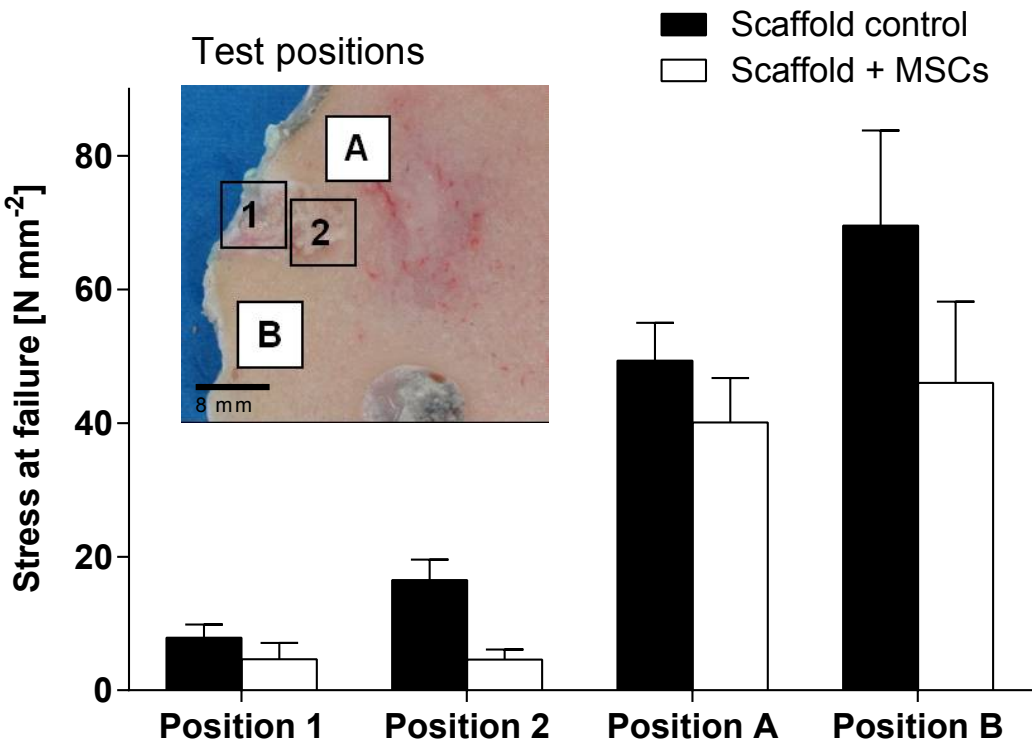

Figure 4.6: Indentation test mechanical stress at failure for test areas (n=6). Positions 1 and 2 on defect and positions A and B surrounding cancellous bone. No statistical significance at $P<0.05$ level.

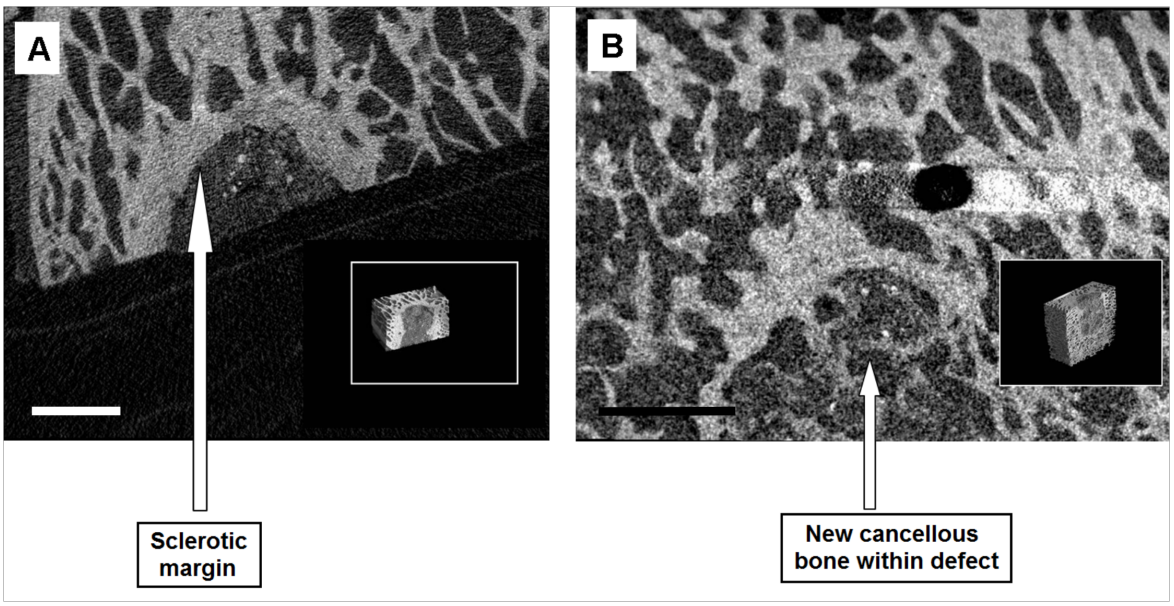

Figure 4.7: Post ovine implantation (13 week) axial μCT slices of defect sites and surrounding bone structure of: (A) milled scCO$_2$ foamed scaffold + MSCs and (B) milled scCO$_2$ foamed scaffold. Inset images show 3D reconstructions from which displayed slices were taken. Scale bars = 4 mm.

The femoral condyle halves that underwent indentation testing post ovine incubation were further analysed with μCT. Scans of the defects were reconstructed and representative axial slices of the 3D reconstructions are displayed in Figure 4.7. In the reconstructions the defect sites remained discernible from surrounding cancellous bone following 13 week ovine incubation. Due to *in vivo* degradation times of P_{DL}LA and P_{DL}LGA of high M_W reported as >13 weeks [238] this was anticipated. Defects filled with milled scCO_2 foamed P_{DL}LA + HA + MSCs were observed to have a sclerotic margin (bony rim) around the outer surface of the defect volume, with little in-growing bone. Defects filled with milled scCO_2 foamed P_{DL}LA + HA alone (no implanted MSCs) appeared to have a sclerotic margin around the outer surface of the defect volume, with evidence of bony in-growth/new cancellous bone within the defect volume (Figure 4.7).

A sclerotic margin refers to a complete or incomplete rim of bone at the interface of, in this work, defect site and cancellous bone interface. The presence of a sclerotic margin and little in-growing bone for defects filled with polymer and MSCs implies the bone repair process sealed off the wound. In turn this implies polymer and MSCs composites were less osteoconductive than polymer alone: defects filled with polymer alone demonstrated increased bony in-growth.

The mean percentage bone volume within the defects was calculated from the μCT scan data for defects filled with milled scCO_2 foamed P_{DL}LA + HA + MSCs and the controls without cells (Figure 4.8). A higher mean percentage of bone formation within defects filled with milled scCO_2 foamed P_{DL}LA + HA (no MSCs) was calculated than defects filled with the same + MSCs. These results were not significant at the $P<0.05$ level. The porous nature of normal cancellous bone would result in a bone volume of $\approx$40% following μCT scan and analysis.

The calculation of mean percentage bone volume within defects by μCT includes the volume taken up by HA incorporated within the P_{DL}LA through scCO_2 foaming. The HA loadings should not be significantly different for defects filled with polymer scaffold and cells or scaffold alone. The scaffolds were produced following the same protocol and milled and sterilised as a batch. The volume of MSCs was significantly less than the volume of the polymer scaffolds at implantation and did not noticeably impact the implanted scaffold volumes. Due to the presence of HA within the scaffolds the absolute value of bone volume within defects calculated from μCT scans is not accurate. However, the method is suitable

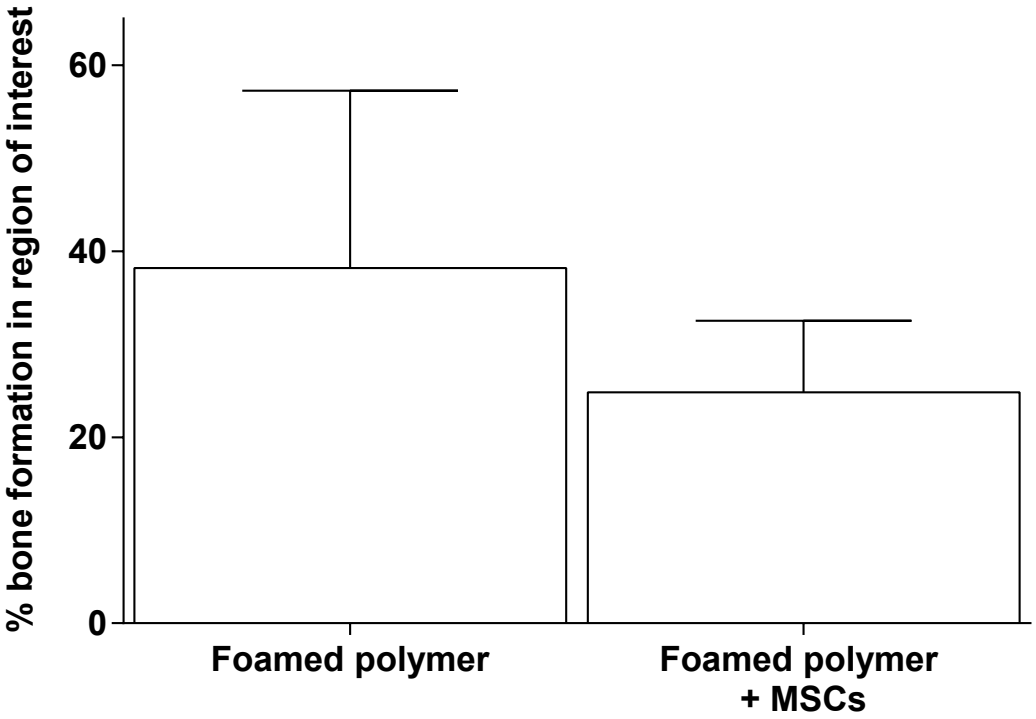

Figure 4.8: Mean percentage bone (density $\geq$0.25 g cm^{-3}) formation within condyle defects post 13 week ovine implantation. No statistical significance at P<0.05 level.

to provide a comparison of the bone growth in the defects with and without the presence of MSCs. Histological analysis was used to assess the regeneration of normal bone within the defect site.

Each femoral condyle was halved and one half from each was used for indentation testing and μCT analysis; the second half from each condyle was histologically stained. Histological staining showed similar results to μCT analysis with visible sclerotic margins around the outer edge of the defects, limited bony in-growth evident in defects filled with polymer and MSCs, and evidence of bony in-growth into defects filled with polymer scaffolds alone (no MSCs) (Figures 4.9 and 4.10).

The popliteal lymph nodes receive the lymphatic vessels from the knee joint and were removed with the femoral condyles. Hematoxylin and eosin (H&E) histological stains were used on each lymph node and examined for evidence of inflammatory reaction (Figure 4.11). Evidence of inflammatory response would be important to note prior to further *in vivo* studies or clinical trials. Some small circular spaces were revealed from examination of the stained lymph nodes with no observable inflammatory response. These spaces likely represent scaffold material lost as polymer was implanted. In the fat adjacent to one lymph node a larger number of roughly circular spaces surrounded by fibrous tissue were observed. This resembled histology previously seen around biodegradable implants and is of limited concern [239–241].

4.3.2 Parallel *in vitro* study

In parallel to the *in vivo* study MSCs were also cultured *in vitro*. *In vivo* implantation and 6 weeks *in vivo* correspond to the *in vitro* time points of 2 weeks and 8 weeks, respectively. The cells in the *in vivo* study were cultured *in vitro* for 2 weeks prior to implantation. Cell viability on milled scCO$_2$ foamed P$_{DL}$LA + HA (10 wt.%) *in vitro* was assessed using WST-1 assays carried out after incubation for 2 weeks and 8 weeks (Figure 4.12). A large change in optical density over the assay period indicated good cell viability at both time points. A significant ($P<0.05$) drop from 2 weeks to 8 weeks suggests either a drop in total viable cell number, or reduced cell metabolic activity by week eight.

In the previous murine study, cells implanted *in vivo* were labelled with Vybrant (a fluorescent dye) prior to implantation and were imaged post 5 week *in vivo* incubation. This confirmed the presence of cells implanted with the scaffolds at the end of the study period.

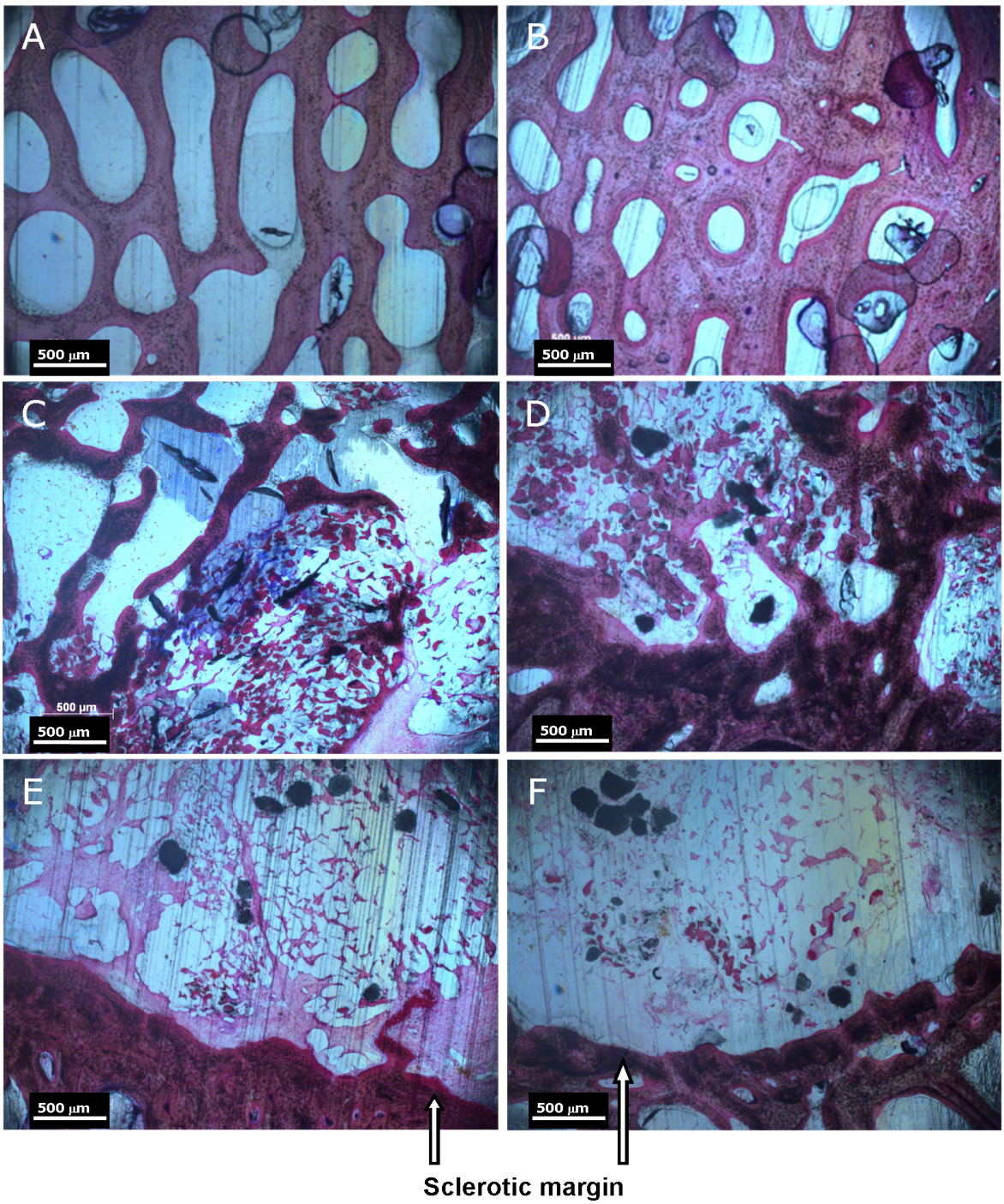

Figure 4.9: Histological staining (H&E) at x2.5 magnification post ovine implantation of: (A) and (B) normal bone, (C) and (D) defect filled with scaffold control, (E) and (F) defect filled with scaffold + MSCs.

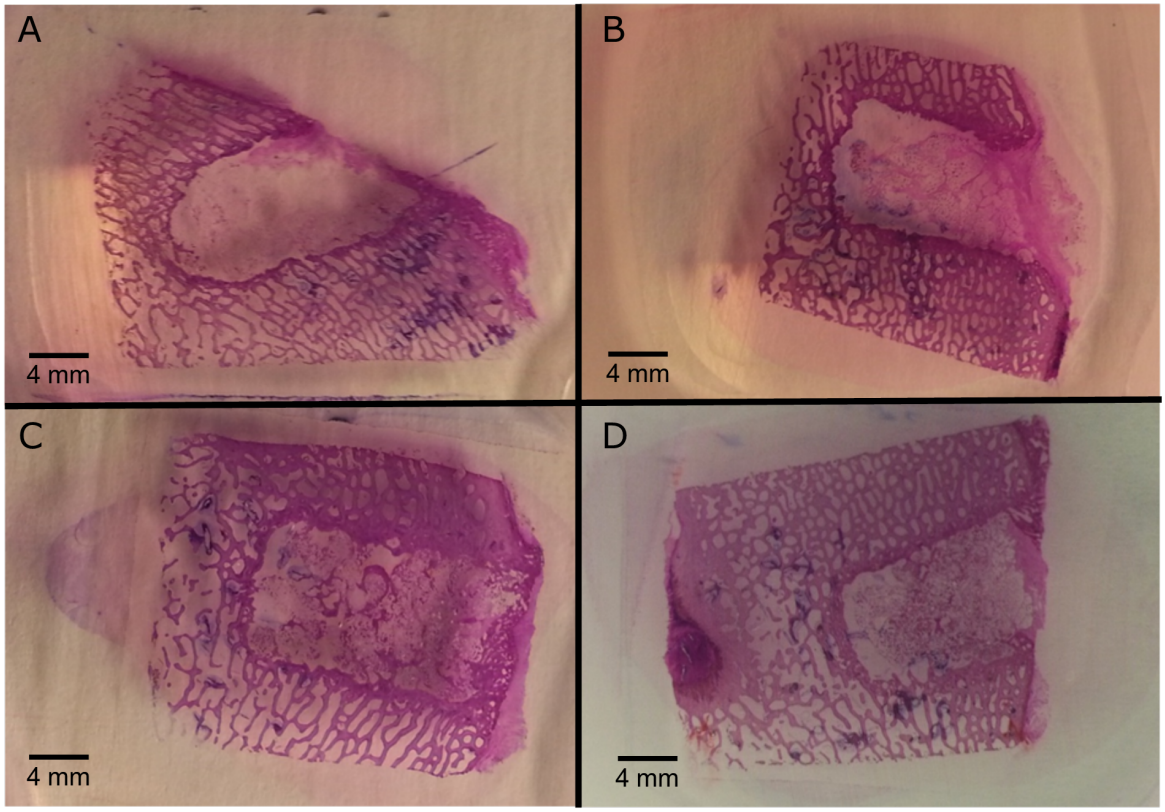

Figure 4.10: Histological staining (H&E) post ovine implantation of: (A) and (B) defect filled with milled scCO$_2$ foamed P$_{DL}$LA + HA (10 wt.%) + MSCs, (C) and (D) defect filled with milled scCO$_2$ foamed P$_{DL}$LA + HA (10 wt.%.

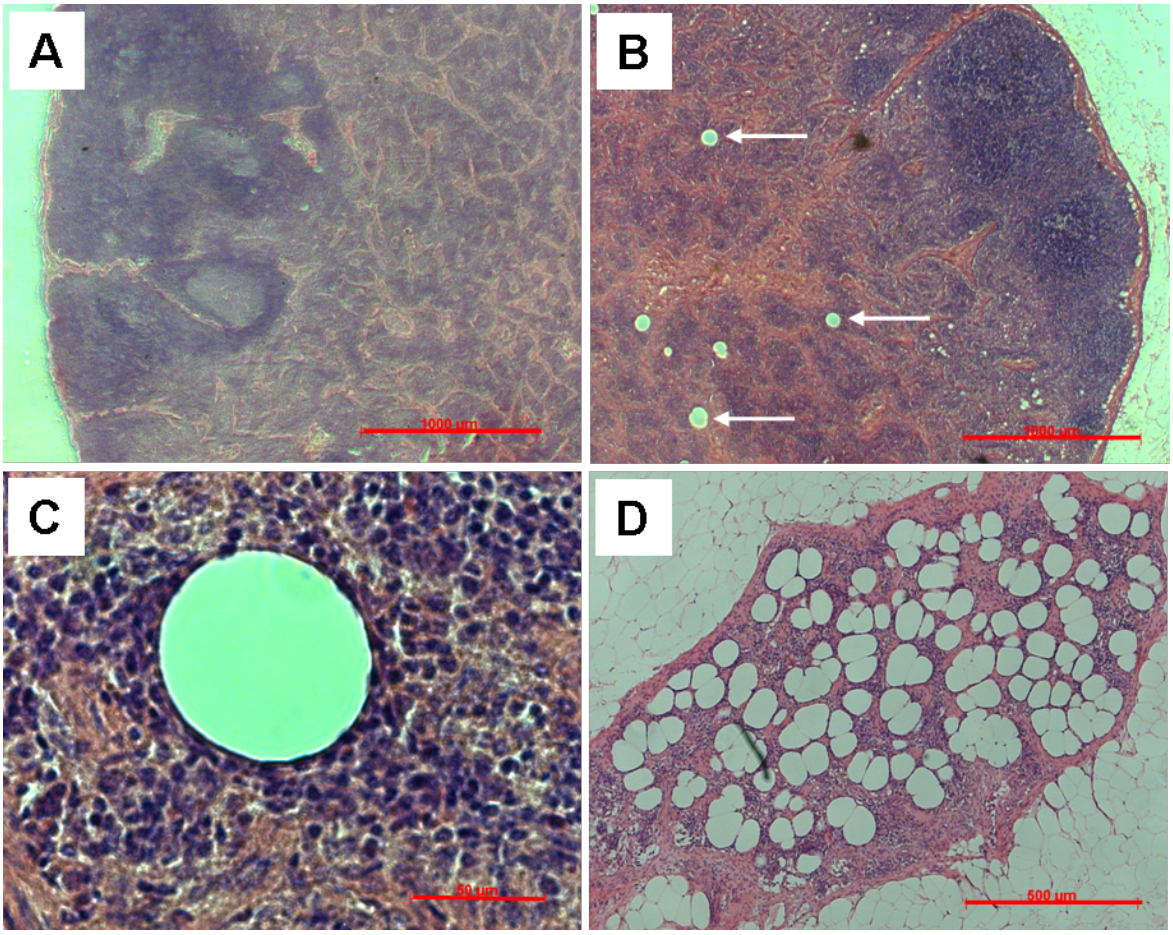

Figure 4.11: Ovine popliteal lymph nodes collected post study and H&E stained. (A) shows normal lymph node appearance (x25 magnification). (B) (x25 magnification) and (C) (x400 magnification) show circular spaces with no surrounding inflammation. (D) shows fibrous tissue containing macrophages, lymphocytes, and plasma cells, within the peri-lymphatic fat (x50 magnification). A + B scale bars = 1000 μm. C+ D scale bars = 500 μm.

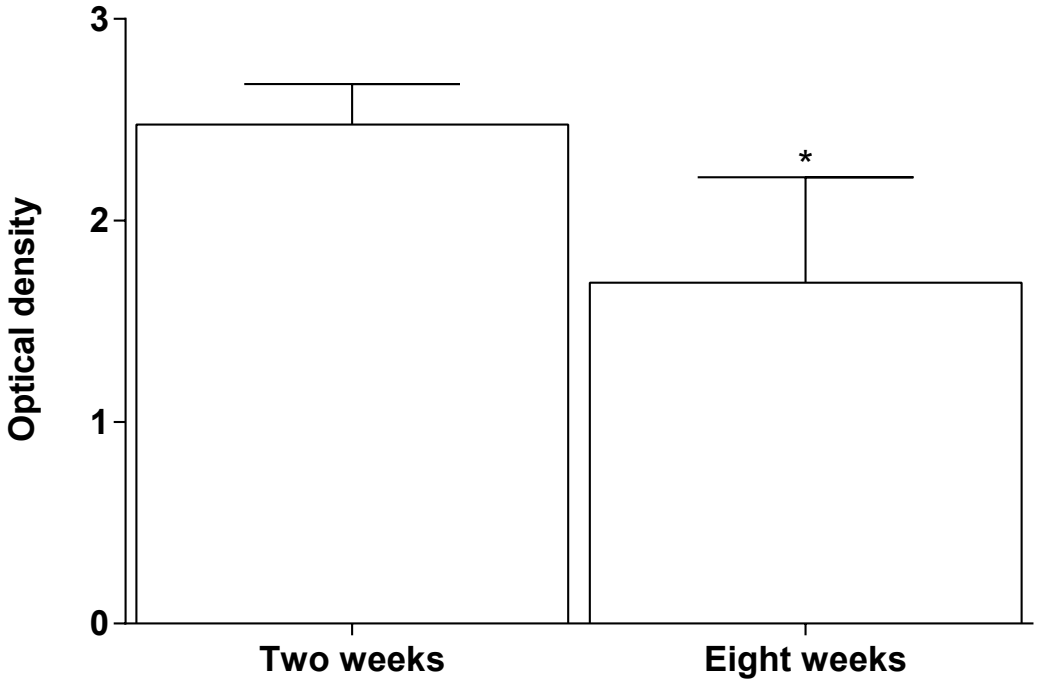

Figure 4.12: WST-1 assay readings showing optical density at 450 nm for ovine MSCs cultured on milled scCO$_2$ foamed P$_{DL}$LA + HA (10 wt.%) scaffolds for two (day 1 *in vivo*) and eight weeks (textitin vivo midpoint) in osteogenic medium (n=6, *P<0.05).

This staining was not carried out for implanted cells in the ovine model. Hence, we are unable to confirm that cells implanted on scaffolds in the ovine model survived the length of the study within the defect site. Cell apoptosis or migration away from the defect site may have occurred. This may limit the conclusions that can be drawn from the *in vitro* study that ran in parallel to the ovine *in vivo* study. Despite this limitation the cells for both studies (ovine *in vivo* and *in vitro*) came from identical sources and *in vitro* behaviour may shed light on *in vivo* results.

Osteoblastic differentiation assays were carried out in addition to cell viability assays *in vitro*. Alkaline phosphatase assays were used to assess osteoblastic differentiation following 2 weeks and 8 weeks *in vitro* culture in osteogenic medium on milled scCO_2 foamed P_{DL}LA + HA (10 wt.%) (Figure 4.13). A significant increase ($P<0.05$) was detected in ALP specific activity after 8 weeks compared to 2 weeks. However the mean ALP specific activities measured at both time points are very low and suggest low levels of osteoblastic differentiation.

Following 8 weeks *in vitro* incubation in osteogenic medium, samples were immunohistochemically stained for osteoblastic differentiation markers (collagen-1, osteocalcin, and bone sialoprotein). The confocal microscopy images (Figure 4.14) indicated the presence of bone sialoprotein (BSP), but limited levels of collagen-1 and osteocalcin expression. Differentiated osteoblasts express high levels of collagen-1, which forms 90% of total protein by weight in osteoblastic ECM [242]. While BSP is used as a marker of osteoblast differentiation its role in function is unclear [242] although it has been implicated as a nucleator of HA crystal formation [243]. Additionally BSP is expressed by osteoclasts, chondrocytes [244, 245], and tumor cells [246], as well as, osteoblast and osteoblast progenitors. Osteocalcin is considered a specific marker for osteoblasts and is not expressed in other ECM-producing cell types [247, 248].

The limited levels of collagen-1 and osteocalcin expression indicated in Figure 4.14 imply limited osteoblastic differentiation of MSCs over 8 weeks of *in vitro* incubation. This is despite some BSP expression. Human and ovine bone marrow derived MSCs are known to undergo osteoblastic differentiation under osteogenic conditions [249] and [250]). McCarty *et al*. [250] established osteoblastic differentiation of ovine MSCs using a procedure for human MSC differentiation reported earlier by Gronthos *et al*. [249]. This protocol used a 100 nM concentration of dexamethasone, compared to the protocol employed here, which required

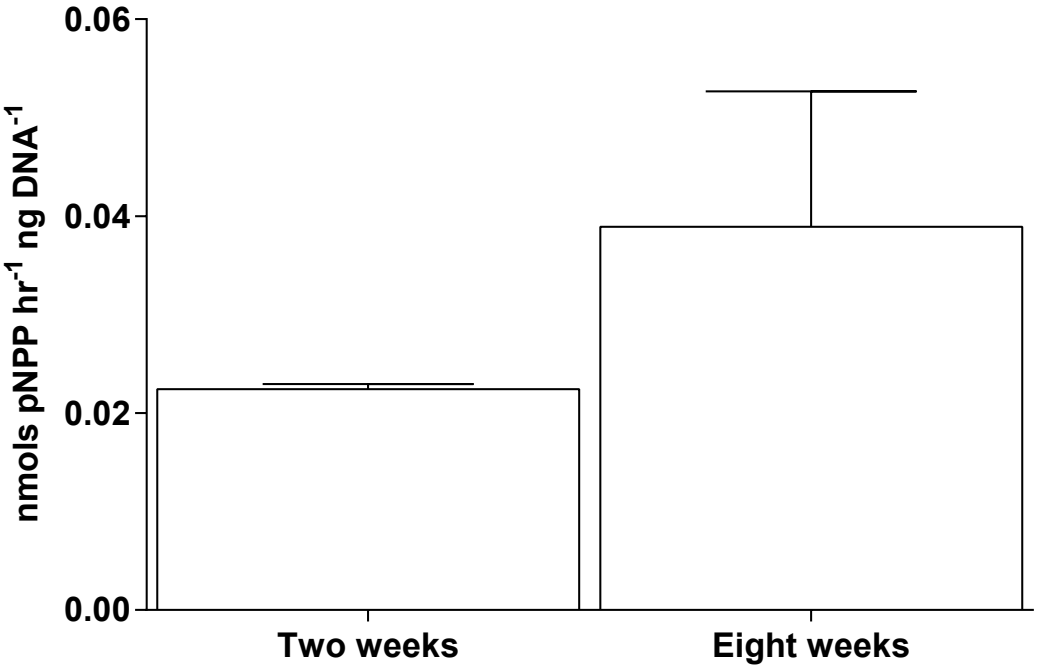

Figure 4.13: Mean ALP specific activity for ovine MSCs cultured on milled scCO$_2$ foamed P_{DL}LA + HA (10 wt.%) scaffolds in osteogenic medium two (day 1 *in vivo*) and eight weeks (textitin vivo midpoint) in osteogenic medium (n=3). No statistical significance at P<0.05 level.

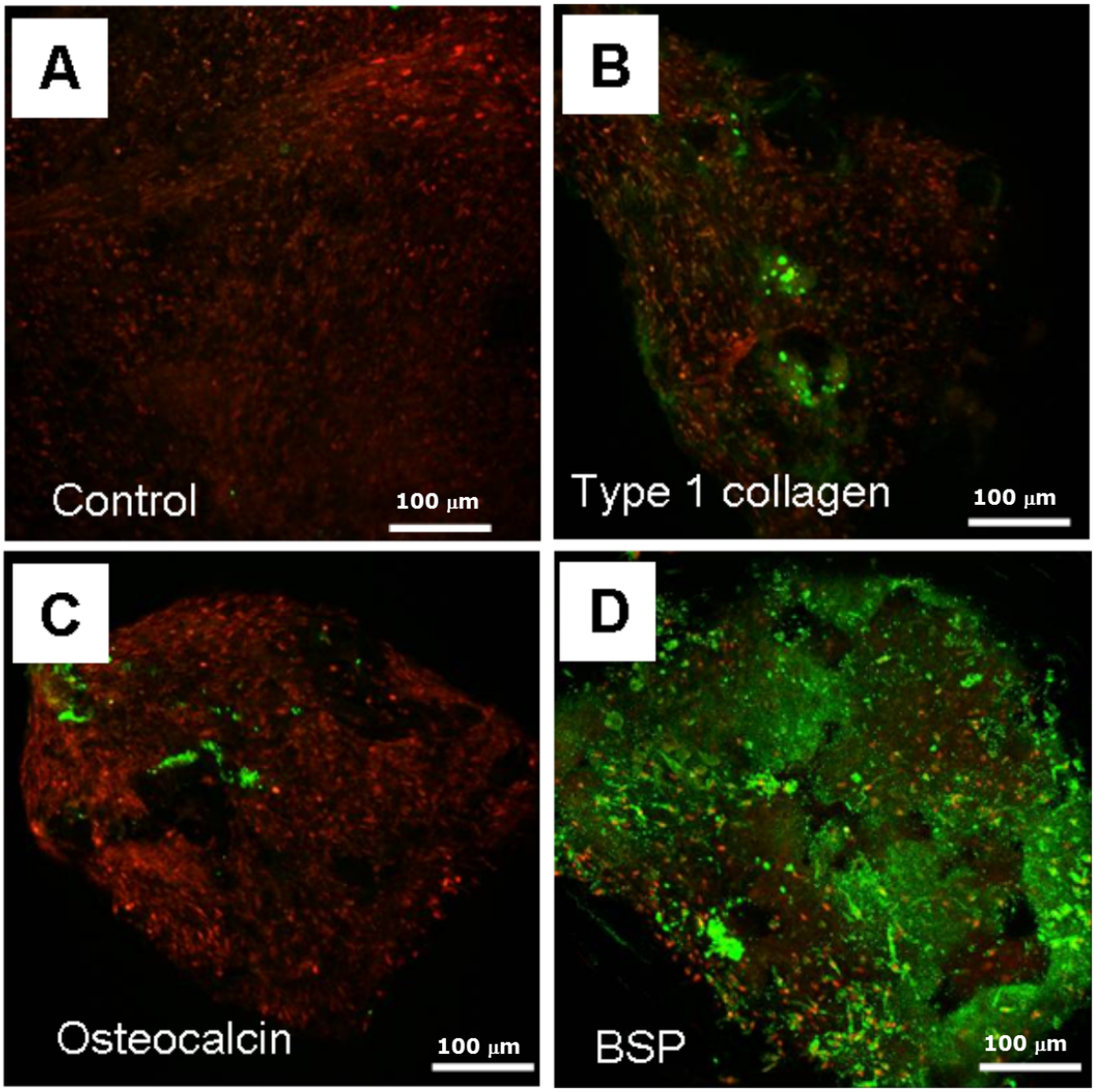

Figure 4.14: Confocal images of immunostained (AlexaFluor 594, green) ovine MSCs post 8 week *in vitro* culture on milled polymer scaffolds of: (A) secondary antibody only control, (B) collagen-1, (C) osteocalcin, and (D) bone sialoprotein. Nuclear counterstains (DAPI) in red.

10 nM concentration of dexamethasone. The protocol utilised here to stimulate osteoblastic differentiation had been optimised for human bone marrow derived MSCs and was not optimised for ovine bone marrow derived MSCs. This may have resulted in limited osteoblastic differentiation of ovine MSCs prior to implantation for the *in vivo* study. Implantation of cells other than osteoblasts/osteoblast progenitors could account for the reduced levels of new bone observed through x-ray radiograph, μCT analysis, and histological staining in the *in vivo* study. If the implanted MSCs had differentiated along a different lineage then they may have impeded bony in-growth from the host. Interestingly however, van der Pol *et al*. [230] observed fibrous tissue formation at 2 and 4 months in ovine femoral and tibial defects did not preclude long-term application of a scCO_2 foamed P_LLA + βTCP scaffold, demonstrated by osteointegration after 12 months. If the study had been extended, osteointegration of scaffolds implanted with MSCs may have been observed at a later time point.

A variety of studies similar to the ovine *in vivo* model established that greater levels of new bone formed in bone repair studies with the use of MSCs compared to implanted scaffolds without cells. Korda *et al*. [196] performed ovine hip replacements and implanted femoral stems with grooves on the stem that were filled with allograft + MSCs or allograft alone as a control. Niemeyer *et al*. [251] implanted mineralized collagen sponges unseeded, seeded with ovine MSCs, and seeded with ovine adipose-tissue derived stem cells (ASCs) into critical sized ovine tibia defects. After 12 weeks both of these studies demonstrated increased new bone formation when comparing implants seeded with MSCs compared to unseeded implants. Similarly, Cao *et al*. [252] reported autologous MSCs seeded on β-TCP and implanted into a femoral condyle defect formed more new bone and demonstrated greater repair of the defect compared to implanted β-TCP after 16 weeks in a goat osteoporotic model.

4.3.3 Supercritical CO_2 foaming scale up study.

Commercially viable tissue engineering scaffolds typically require the ability to be produced on a clinical scale. To demonstrate scale-up of scCO_2 foaming of P_{DL}LA a 1000 ml vessel was utilised and moulds produced in house as detailed in Section 4.2.3. The 12 mm x 11.2 mm cylindrical foams produced in the 60 ml autoclave were easy to handle and suitable for milling using a standard bone-mill as would typically be found within hospitals that perform surgeries requiring impaction bone grafting. Rather than produce larger foams,

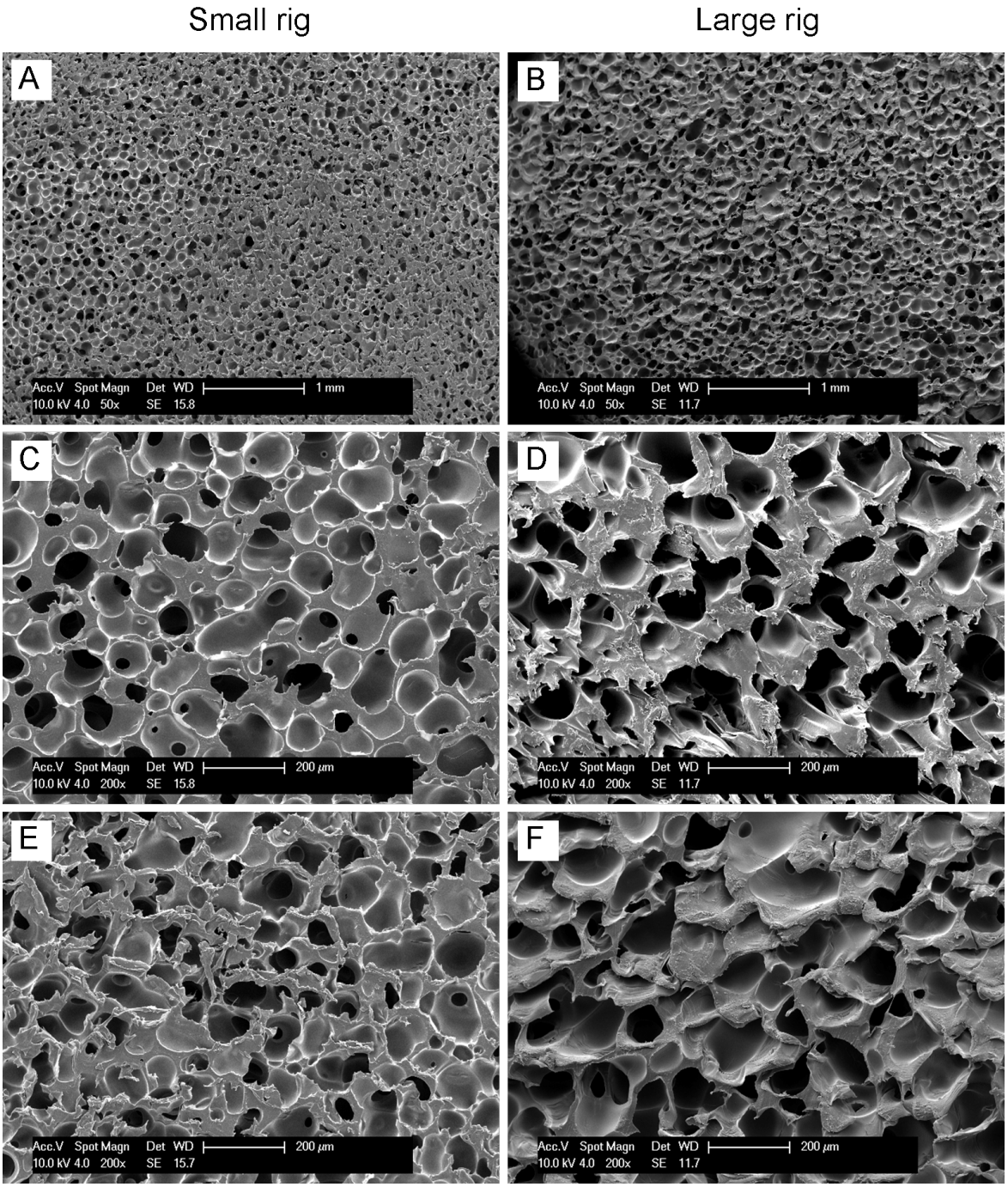

Figure 4.15: Representative SEM images of $P_{DL}LA$ scaffolds $scCO_2$ foamed in a 60 ml autoclave (small rig, images: (A), (C), and (E)) and a 1000 ml vessel (large rig, images: (B), (D), (F)). Images (A) and (B) at x50 magnification and images (C), (D), (E), and (F) at x200 magnification.

which would change the diffusion times of CO_2 out of the polymer upon depressurisation of the vessel, more P_{DL}LA foam scaffolds of an identical size to those produced in the 60 ml autoclave were produced in the 1000 ml vessel. This enabled direct comparison of the foams produced in each vessel. Representative micrographs displayed in Figure 4.15 showed that there is an extremely similar pore size and distribution between scaffolds produced in the different vessels. The degree of pore anisotropy was not analysed quantitatively, but qualitatively through observation of the micrographs the pores in foams manufactured in the large rig appear slightly more irregular.

The quantitative differences between foams produced in each vessel were assessed through μCT. Representative images and reconstructed axial slices (400 slices) are displayed in Figure 4.16. Analysis of the μCT scans calculated the mean porosity of scCO_2 foamed P_{DL}LA produced in the 60 ml autoclave as 51.9 $\pm$ 0.9 % (n=4), and produced in the 1000 ml vessel as 50.0 $\pm$ 1.4% (n=13), with a significant difference between the two ($P<0.05$). Each foam produced in the 60 ml autoclave and analysed was produced in a separate batch. The foams produced in the 1000 ml vessel and analysed were taken from three separate batches and from different locations within the mould; the moulds were placed at different heights within the vessel for each batch. The standard deviation in the porosity of scaffolds produced in the 1000 ml vessel is < 3% and even less for those produced in the 60 ml autoclave, which indicated limited variance between batches. The mean pore size calculated was 79.3 $\pm$ 5.2 μm for foams produced in the 60 ml autoclave, and 59.2 $\pm$ 5.2 μm for foams produced in the 1000 ml autoclave, which represented a significant difference ($P<0.01$). The variance in mean pore size was <10% for scaffolds produced in both vessels.

The importance of a uniform pore size in scCO_2 foamed scaffolds for bone tissue engineering and impaction bone grafting has not been established and was not the purpose of this study. The difference in pore size observed through μCT analysis demonstrated that despite identical polymer sources and foaming conditions some differences were noted in the scaffolds produced from the different vessels. Heating in the 1000 ml vessel may result in the observed difference, or differences in the moulds used in each vessel may significantly affect how the scaffolds foam. Many factors that affect how polymers foam in scCO_2 have been studied [97]. These factors represent control of the scCO_2 foaming process enabling a wide variety of porosity, pore sizes, and interconnectivity to be achieved.

Scale-up of porous scaffold production by scCO_2 foaming has received very limited

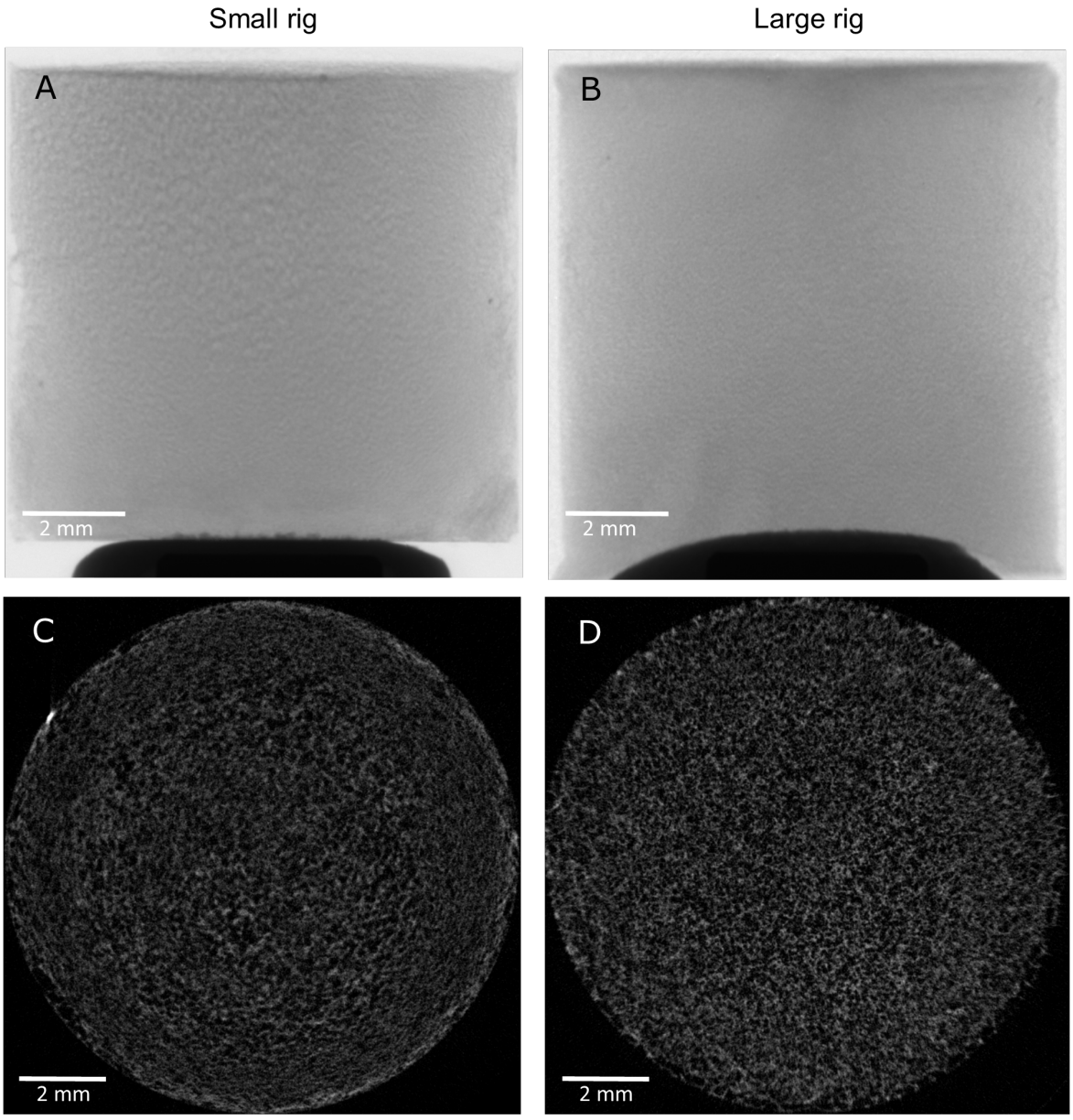

Figure 4.16: Representative μCT images ((A) and (B)) and reconstructed axial μCT slices ((C) and (D)) of $P_{DL}LA$ scaffolds scCO_2 foamed in a 60 ml autoclave (small rig, images: (A) and (C)) and a 1000 ml vessel (large rig, images: (B) and (D)).

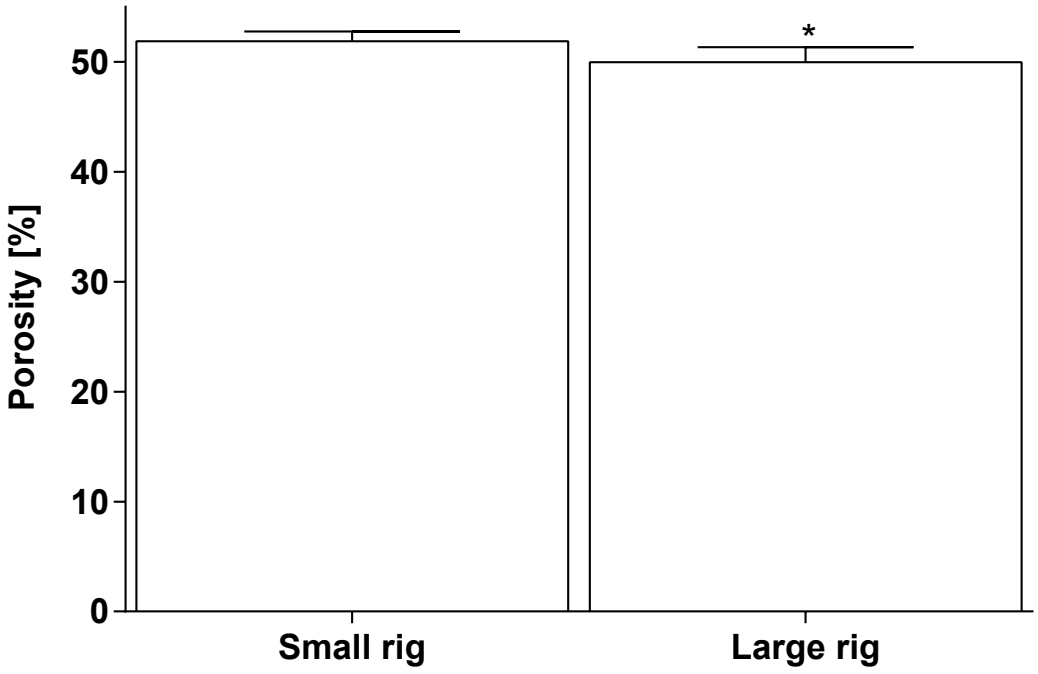

Figure 4.17: Mean porosity values calculated from μCT data of scCO$_2$ foamed P$_{DL}$LA scaffolds foamed in a 60 ml autoclave (small rig, n=4) and a 1000 ml vessel (large rig, n=13) (* P<0.05). Error bars show standard deviation.

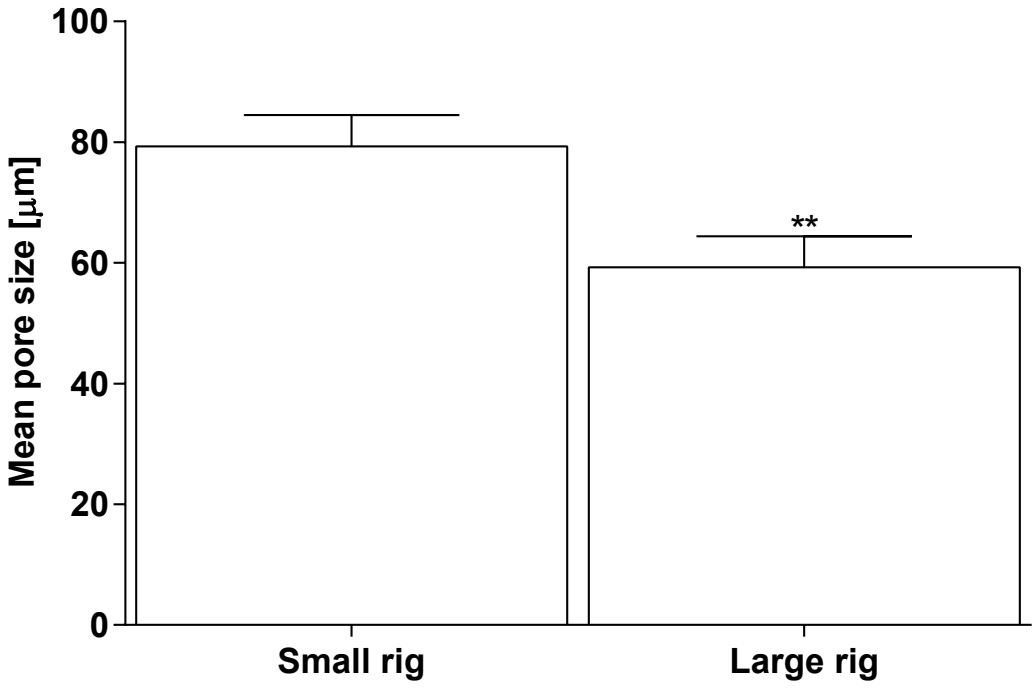

Figure 4.18: Mean pore diameters calculated from μCT data of scCO$_2$ foamed P$_{DL}$LA scaffolds foamed in a 60 ml autoclave (small rig, n=4) and a 1000 ml vessel (large rig, n=13) (** P<0.01). Error bars show standard deviation.

discussion within the literature [253]. Here we have demonstrated the scCO_2 foaming of thirty six scaffolds per mould in a 1000 ml vessel that holds five moulds; one hundred and eighty scaffolds can be foamed in one batch. The scaffolds produced had a similar porosity (within 1%) to scaffolds foamed in a 60 ml autoclave, but had a different mean pore size. While it is possible to scCO_2 foam many more scaffolds in the large vessel compared to the small vessel further study is required to match the two processes.

The moulds for the large vessel required small holes in the lid and base of each well within the moulds to allow CO_2 to reach the polymer. The location of these holes differed in the moulds for the large vessel compared to the moulds for the small vessel. For the small vessel moulds these holes were in the side of each, at the top and the bottom; they were located in the centre of each well in the large vessel moulds. New lids and bases with CO_2 access holes in the centre of each well could be produced for the small vessel, which may reduce the differences observed in the scaffolds foamed in each vessel. However, it is still likely that some optimisation will be required through variation of temperature, pressure, or vent time to more closely match scaffolds produced in the 1000 ml vessel to those produced in the 60 ml autoclave.

4.4 Conclusion

The work presented in this chapter demonstrated new bone formation within an ovine femoral condyle defect filled with scCO_2 foamed P_{DL}LA + HA 10% (wt%). Limited new bone formation was demonstrated in defects filled with the same seeded with ovine MSCs. The apparent detrimental effect of seeding scaffolds with MSCs before implantation contradicts findings reported in the literature and parallel *in vitro* work indicated MSCs had not differentiated along the osteolastic lineage. Future work with ovine MSCs should confirm a working osteoblastic differentiation protocol. Defects filled with scaffolds without MSCs for 12 weeks *in vivo* incubation showed good osteoconductive and osteoinductive properties, and while not fully healed, the new bone formed gave good indication that the defect would heal over time.

Proof-of-concept of the scale-up of scCO_2 foaming process has been demonstrated with the production of 10.8 g of foamed scaffolds in a 1000 ml vessel in a single batch compared to 1.8 g in a batch foamed in a 60 ml autoclave. Furthermore, the 1000 ml vessel has a volume that allows for scCO_2 foaming 54 g of P_{DL}LA per batch. The scaffolds produced in each

vessel were foamed using an identical protocol and significant differences in the porosity and pore size of the resulting scaffolds were observed. While significantly different, the porosities were similar for scaffolds produced in different vessels. Further work is required to scCO_2 foam scaffolds with matching characteristics in each vessel. P_{DL}LA was scCO_2 foamed in different locations within the 1000 ml vessel and at different heights, and the standard deviation in porosity values was <3%. While the standard deviation in mean pore size matched that for P_{DL}LA scaffolds foamed within the 60 ml autoclave. This is evidence that scCO_2 foaming porous biodegradable scaffolds is possible on a large scale.

CHAPTER 5

Investigation of factors affecting scaffold performance

This chapter investigates the reason behind differing performance of P_{DL}LA and P_{DL}LGA scaffolds that, due to their similarity, was unanticipated. This chapter also investigates HA particle size and concentration for improving mechanical strength, important in load bearing applications, and osteoblastic differentiation of MSCs following observation of new bone growth concentrated around HA microparticles in the earlier murine model.

5.1 Introduction

Results presented in Chapter 3 demonstrated that the osteogenic differentiation of MSCs differed between cells cultured on $P_{DL}LA$ and $P_{DL}LGA$ scaffolds, both $scCO_2$ foamed and non-foamed. This was observed through ALP assays and collagen-1 immunohistochemical stains after 2 weeks *in vitro* culture in osteogenic medium. A significantly higher ALP specific activity was observed for MSCs cultured *in vitro* on $scCO_2$ foamed $P_{DL}LA$ compared to MSCs cultured on $scCO_2$ foamed $P_{DL}LGA$ scaffolds. The same result was observed in the study that incorporated 10% HA microparticles; significantly higher ALP specific activity was reported for MSCs cultured on $P_{DL}LA$ scaffolds (with and without 10 wt.%HA microparticles) than MSCs cultured on $P_{DL}LGA$ scaffolds (with and without 10 wt.% HA microparticles) (Figure 3.12). The differences in MSC osteoblastic differentiation observed were unexpected because the polymers had extremely similar properties (high M_W, amorphous, random chirality), the lactide:glycolide ratio was high (85:15) for $P_{DL}LGA$, and both had been used in scaffolds promoted for bone tissue engineering [254–257]. Additionally on $P_{DL}LGA$ matrices, osteoblasts had been reported to produce significantly higher levels of ECM proteins than on $P_{DL}LA$ matrices [258].

This chapter investigates the differentiation of MSCs *in vitro* on $P_{DL}LA$, $P_{DL}LGA$, and $P_{DL}LA$:$P_{DL}LGA$ (50:50) films produced by spin-coating and dip coating. Establishing differences in the differentiation of MSCs on these films was required to elucidate the results reported in chapter 3; specifically, to establish that the differences in MSC osteoblastic differentiation observed on $scCO_2$ foamed scaffolds were primarily due to morphological differences in the foamed structures. The use of flat films removed micro-scale morphological variation between the polymers. Films of a 50:50 blend of $P_{DL}LA$ and $P_{DL}LGA$ were used in addition to 100% $P_{DL}LA$ and 100% $P_{DL}LGA$ films to provide a midpoint, and establish if any trends observed were linear.

There are many variables that may have affected the MSC osteoblastic differentiation in the earlier experiments reported in Chapter 3 , such as: scaffold pore size, scaffold porosity, polymer degradation rate, polymer wettability, polymer stiffness, surface (any surface cells adhered to including inner pore walls) topography, and surface roughness. The differences in MSC osteoblastic differentiation on different polymer scaffolds ($P_{DL}LA$ and $P_{DL}LGA$) observed may not be limited to a single cause, but could arise due to a combined effect of several variables. However, studies have reported that substrate nano-scale and micro-scale

structures have a significant effect on the osteogenic differentiation of MSCs [168, 259–270]. Both Oh *et al*. [271] and Dalby *et al*. [259] demonstrated that nanotopographical cues can guide MSC osteogenic differentiation in the absence of chemical cues commonly used (such as dexamethasone or BMP2). In a 1:1 adipogenic induction:osteogenic induction medium different microtopographical cues induced MSC differentiation towards different lineages [262]. Additionally, MSCs cultured on 10 μm deep squares and 30 μm deep grooves demonstrated enhanced osteocalcin (a specific osteoblast marker [247]) expression, establishing that microtopographical cues enhance osteoblastic differentiation. The strong effects on MSC differentiation of topographical cues reported in the literature ensured that establishing if scaffold morphological features affected the osteogenic differentiation of MSCs in the studies reported in Chapter 3 was a priority over other possible variables to investigate.

In the murine study reported in Chapter 3, μCT analysis revealed the formation of bone-like matrix in $P_{DL}LA$:HA composite scaffolds ($scCO_2$ foamed, then milled and impacted, $P_{DL}LA$ + 10 wt.% HA microparticles) was focused primarily around the HA microparticles. Increasing the specific surface area of HA particles within the scaffolds may provide more sites for osteogenesis to occur and improve the bone regeneration rate *in vivo*. Many bone tissue engineering scaffolds reported in the literature comprise composite materials that incorporate HA nanoparticles [186, 198, 208, 254, 272–283]. Nanoparticles are defined as particles where at least one dimension is on the nanoscale, i.e. <1 μm.

Various authors have demonstrated the efficacy of nanocomposite scaffolds for bone repair, both *in vitro* [198, 208, 273, 277, 279, 281] and *in vivo*. [186, 198, 254, 275, 280]. Nejati *et al*. [278] and Eslaminejad *et al*. [281] compared $P_L LA$ + nanorods (NRs) composite scaffolds to $P_L LA$ and $P_L LA$ + HA microparticle composite scaffolds; bone related gene expression (collagen-1, osteocalcin, and RunX2 (Runt-related transcription factor 2)) in MSCs cultured on the scaffolds was significantly higher ($P<0.05$) than in MSCs cultured on the microcomposite or pure $P_L LA$ scaffolds. Additionally, the nanocomposite scaffolds demonstrated increased compressive strength (8.46 MPa) compared to plain $P_L LA$ (1.79 MPa) and microcomposite (4.61 MPa) scaffolds [281]. Mechanical properties of nanocomposite scaffolds are reportedly greater than pure scaffolds. Kothapalli *et al*. demonstrated a linear increase in compression modulus (from 5 MPa, 0wt.% HA, to 10 MPa, 50% HA) and yield strength (from 0.3 MPa, 0 wt.% HA, to 0.4 MPa, 50 wt.% HA) with increasing HA content (10 wt.% increments) in PLA porous scaffolds (chirality not reported). Similarly, Wei *et al*. reported an increase in compression modulus from 4.3 MPa (0 wt.% HA) to 8.3 MPa (50 wt.% HA)

in P_LLA scaffolds. Further increases in the strength of PLA:HA nanocomposite scaffolds were demonstrated through modification of surface grafting of the HA particles. Hong *et al*. reported higher bending strengths, impact energies, and moduli for 4% and 20% P_LLA: surface grafted nano HA to P_LLA:nano HA scaffolds.

The reported improvements in nanocomposite scaffolds within the literature provided motivation to investigate the effect of HA nanoparticles compared to HA microparticles on $scCO_2$ foamed P_{DL}LA scaffolds. In this chapter milled $scCO_2$ foamed P_{DL}LA scaffolds containing nanorods (NRs) and nanoplates (NPs) are investigated *in vitro* with $scCO_2$ foamed pure P_{DL}LA and P_{DL}LA + 10 wt.% HA microparticles controls for comparison. Two concentrations of nanoparticles were used, 1 wt.% and 10 wt.%, corresponding to the weight and volume (of powder) of microparticles used in the control scaffolds containing 10 wt.% microparticles. Cellular compatibility and differentiation experiments were carried out *in vitro* with human MSCs. Scaffolds were characterised with mechanical compression and SEM.

5.2 Materials and methods

5.2.1 Cell differentiation studies on P_{DL}LA and P_{DL}LGA films

5.2.1.1 Spin coated polymer films

Polymer films were spin coated onto 22 mm $\times$ 22 mm glass coverslips for cell differentiation studies on different polymers: P_{DL}LA, and P_{DL}LGA. P_{DL}LA with a M_W of 108 kDa, inherent viscosity of 0.71 dL g^{-1}, polydispersity index of 1.6, and T_g of 49.1 °C was used. P_{DL}LGA (85:15 lactide:glycolide) with a M_W of 110 kDa, inherent viscosity of 0.71 dL g^{-1}, polydispersity index of 1.5, and T_g of 50 °C was used. Glass coverslips were washed in acetone and air dried prior to spin coating. Solutions of P_{DL}LA, P_{DL}LGA and 50:50 P_{DL}LA:P_{DL}LGA were made at a concentration of 5% polymer in acetone by dissolving 50 mg ml^{-1}. Solutions were agitated to ensure that the high M_W polymers fully dissolved to create homogeneous solutions. A 5 ml syringe was used to collect the polymer solution and a coverslip placed in the spin coater (400 Lite Spinner, model WS-650SX, Laurell Technologies Corporation, PA, U.S.A.). Under vacuum, 800 μl of polymer solution were dispensed onto the surface of the coverslip which was then spun at 1000 rpm for 1 minute. Coated coverslips were then stored in individual wells of six well plates.

5.2.1.2 Film washes

Two methods were used for washing of spin coated polymer films: washing with hexane, and washing with $scCO_2$.

Hexane washing

Hexane (1 ml) was pipetted onto each film $\times 3$. This was repeated in triplicate with fresh hexane and the samples were vented in an extraction hood.

$scCO_2$ washing

For washing with $scCO_2$, glass coverslips were carefully positioned within a 60 ml autoclave which was heated to 35 °C and filled with pressurised CO_2 to a pressure of 23 MPa. The autoclave was held under these conditions for 1 hour and then vented at a constant rate over 30 minutes back to atmospheric pressure. The thin films allowed rapid diffusion of absorbed $scCO_2$ which prevented $scCO_2$ foaming of the films from occurring.

5.2.1.3 Water contact angle measurement

Statis water contact angle measurements were taken for unwashed films and films washed using both hexane and $scCO_2$. Ultrapure water droplets were dispensed onto the surface of each film and images were recorded at 1 s intervals using a CAM 200 Optical Contact Angle Meter (KSV Instruments Ltd., KSV NIMA, Finland). Manufacturer's software was used to calculate the contact angle for each image after the initial image using a Young Laplace fit. The water contact angle for each film at time = 0 was determined using linear regression analysis of the angles calculated. The measurements were taken in triplicate for each film and the mean water contact angles of each film at time = 0 recorded.

5.2.1.4 X-ray photoelectron spectroscopy

X-ray photoelectron spectroscopy was performed by Emily Smith (School of Chemistry, The University of Nottingham).

Polymer films both unwashed and hexane washed were analysed using x-ray photoelectron spectroscopy (XPS). In XPS the surface of a substrate is irradiated with x-rays which transfers energy to electrons in the surface (0-10 nm) elements of the substrate. Excited

electrons are ejected via photoemission. An ultrahigh vacuum is used to prevent ejected electron scattering via collision with gas molecules. A spectrometer is used to detect the kinetic energies of ejected electrons and electron binding energy is calculated using the Einstein equation (E_B = hν - E_K - W, where E_B is binding energy, hν is photon energy, E_K is kinetic energy, and W is the spectrometer work function). The spectra output can be used to identify elements present and are usually reported as signal intensity plotted against binding energy.

Polymer films were fractured and mounted on a sample bar. A Kratos AXIS ULTRA instrument (Kratos Analytical Ltd., U.K.) configured with a monochromated Al Kα (1486.6 eV) was used to collect XPS data for the films. CASAXPS (Casa Software Ltd.) was used to analyse the XPS data.

5.2.1.5 Dipcoated polymer films

Dipcoated polymer films of P_{DL}LA, P_{DL}LGA, and P_{DL}LA:P_{DL}LGA (50:50) were produced. Polymer solutions using the same polymers for spin coated films (described in Section 5.2.1.1) were made at a 10% concentration in acetone. Solutions were agitated to ensure the polymers were fully dissolved. Glass coverslips 22 mm $\times$ 22 mm were washed in acetone and air dried prior to dip coating. The dipcoating procedure for a single coverslip is detailed as follows. Tweezers were used to hold the coverslip by an edge and to dip the coverslip into the polymer solution. After dipping, excess solution was allowed to drain from the coverslip by contacting one corner of the coverslip with the container of the polymer solution. The coverslip was then held and allowed to air dry prior to being placed into an individual well of a six well plate.

5.2.1.6 Cell culture

Immortalised human MSCs expressing green fluorescent protein (GFP) were gifted by Dr Hassan Rashidi (School of Pharmacy, The University of Nottingham). These cells were expanded in T175 flasks until confluent and stored in cryo-vials in a liquid nitrogen storage tank until required for *in vitro* cell experiments.

For cell expansion and cell seeding, basal medium was used, which was Dulbecco's Modified Eagle's Medium (DMEM) supplemented with 10 vol.% fetal bovine serum (FBS), 2mM L-glutamin, 100 μg ml^{-1} penicillin and 100 μg ml^{-1} streptomycin (Pen-Strep, Invitrogen).

For expansion, cells were cultured in T175 flasks and at 80-90% confluence the cells were washed in phosphate buffered saline (PBS) and treated with trypsin in EDTA for 2 minutes to detach cells from tissue culture plastic (TCP). An equal volume of serum-containing medium was used to deactivate the trypsin and the cell suspension transferred to a universal tube and centrifuged for 5 minutes at 180 g. Supernatant was aspirated and cells resuspended in FBS + 10% DMSO to a concentration of 1 million cells ml^{-1}. Cells were stored in 1 ml cryo-vials at -80 °C for one week and then transferred to liquid N_2 storage.

Polymer films were sterilised under U.V. light for 1 hour prior to cell seeding. For each study a cryo-vial of cells was reanimated by thawing and suspension in 20 ml of basal medium. Then they were seeded in a T175 flask and grown until 90% confluent. Media changes were performed every 3 days. At 90% confluence cells were released with trypsin in EDTA for 2 minutes and an equal volume of basal medium was added. The cell suspension was centrifuged for 5 minutes at 180 g. The supernatant was aspirated and the cells re-suspended in basal medium. Cell concentration was determined using a haemocytometer and appropriate dilution with basal medium to reach a final concentration of 1×10^6 cells ml^{-1}. Cells were seeded onto polymer films in non-TCP six well plates at a concentration of 10,000 cells cm^2 (i.e. ≈48,000 cells per film). Cells were cultured on polymer films in basal medium for 24 hours prior to media change. The cell media was changed from basal medium to osteogenic medium after 24 hours. Osteogenic medium for these experiments was basal medium + dexamethasone 0.1 μM, L-ascorbic acid 50 μM, and β-glycerophosphate 10 mM. Cells were cultured on polymer films in osteogenic medium for 2 weeks and incubated under standard cell culture conditions (37°C and 5% CO_2).

5.2.1.7 WST-1 assay

A WST-1 assay was carried out at 1 week and 2 week time points of *in vitro* culture. Background information of the WST-1 assay is included in Section 2.6.1. The cells cultured on three of each group of polymer films (P_{DL}LA, P_{DL}LGA, and P_{DL}LA:P_{DL}LGA (50:50)) were assayed at each time point. Media was aspirated from each well and films were washed with PBS and aspirated ×2. Basal medium was then added to each well (1 ml) and 100 μl of WST-1 reagent (Roche Ltd. U.K.). Basal medium (1 ml) was added to an empty well of a six well plate ×2 and used as a negative controls. After 30 minutes of incubation (37°C and 5% CO_2) 100 μl was taken from each well and transferred to a 96 well plate; this was performed

in triplicate for each individual sample. Optical absorbance values were quantified at 450 nm using a μQuant 96 well plate reader (Bio-Tek Instruments, U.K.).

5.2.1.8 ALP assay

An ALP assay was carried out at 1 week and 2 week time points of *in vitro* culture. Background information of the ALP assay is included in Section 2.6.2. The cells cultured on three of each group of polymer films (P_{DL}LA, P_{DL}LGA, and P_{DL}LA:P_{DL}LGA (50:50)) were assayed at each time point. Media was aspirated from each well and the films washed in 0.2 M tris buffer. A solution of pNPP 1 mg ml^{-1} (Sigma-Aldrich, U.K.) in 0.2 M tris buffer was prepared through dissolution and vortexing. Within 1 hour of preparation 1 ml of pNPP solution was added to each film and incubated (37°C and 5% CO_2) for 1 hour. Then 200 μl was taken in triplicate from each well and transferred into a 96 well plate; optical absorbance values were quantified for each sample at 405 nm using a μQuant 96 well plate reader (Bio-Tek Instruments, U.K.). ALP standards were used to derive a standard curve and determine ALP concentration in the cellular samples.

5.2.1.9 Collagen-1 immunohistochemical stains

After 2 weeks of *in vitro* incubation the cells cultured on two of each group of polymer films (P_{DL}LA, P_{DL}LGA, and P_{DL}LA:P_{DL}LGA (50:50)) were immunohistochemically stained for the presence of collagen-1. The media in each well was aspirated and cells on each film were fixed in 4% paraformaldehyde for 5 minutes. After fixing samples were stored under PBS at 3°C until immunohistochemical staining was performed. Immunohistochemical staining involved permeabilisation of samples using 400 μl of 0.1% TYriton X-100 in PBS for 30 minutes followed by $\times$ washes in PBS. Blocking of non-specific proteins was performed using 400 μl per film of 3% donkey serum in 1% BSA in PBS. Overnight incubation of samples was performed in a primary antibody solution (1:200 dilution in 1% BAS in PBS); 400 μl per film. The primary antibody solution was then removed and samples washed $\times$3 using PBS. Samples were then incubated at room temperature under secondary antibody solution (1:200 in 1% BSA in PBS) for 2 hours. Subsequently, the secondary antibody solution was removed and samples washed $\times$3 using PBS. Hoechst nuclear counterstaining was used with incubation for 20 minutes under 500 μl per film of Hoechst solution (1:1000 dilution in 1% BSA in PBS) followed by further washing in PBS ($\times$ 3). Samples were mounted under Pro-fade and stored

at 3°C until imaged using fluorescent microscopy. An inverted-microscope (Leica DM-IRB, Leica, Germany), a Hamamatsu digital camera, and Volocity imaging software (Improvision, U.K.) was used for imaging of immunohistochemically stained films. The primary antibody used was collagen-1 (rabbit host, Millipore, MA, U.S.A.). The secondary antibody used was anti-rabbit IgG (AlexaFluor546, Life technologies, U.K.).

5.2.2 Studies of HA particle size and morphology effect on cell differentiation

5.2.2.1 Supercritical carbon dioxide foaming

Supercritical CO_2 foamed polymer scaffolds were prepared as detailed in Section 2.1 using $P_{DL}LA$. Briefly, 300 mg of ground polymer powder was loaded into cylindrical wells of a PTFE mould and foamed in $scCO_2$ at 35 °C and 23 MPa for 1 hour with a 30 minute constant rate vent back to atmospheric pressure. For scaffolds containing HA, 270 mg of polymer and 30 mg of HA (either microparticles, nanorods, or nanoplates) were used for 10 wt.% HA containing scaffolds. For scaffolds containing 1 wt.% HA, 297 mg of polymer and 3 mg of HA (either nanorods or nanoplates) were used.

5.2.2.2 Preparation of polymer:HA composite scaffolds

Once the scaffolds were formed they were milled in a standard bone mill (Tessier Osseous Microtome, Stryker Leibinger, Freiberf, Germany), sterilised, seeded with primary human MSCs, and impacted into open ended impaction chambers. The milling and sterilisation process is detailed in Section 2.5.1.3.

5.2.2.3 Scanning electron microscopy

Scanning electron microscopy was used on scaffolds prior to the milling process to characterise the internal porous structure. Obtaining SEM images was a destructive process. The protocols used for SEM are detailed in Sections 2.2; SEM was used both for imaging and elemental mapping.

5.2.2.4 Mechanical compression testing

A TA.HD plus texture analyser (Stable Micro Systems Ltd., Surrey, U.K.) was used for compression testing of whole $scCO_2$ foamed scaffolds (not milled). A 20 mm aluminium head and a 50 kg load cell was used to apply a compressive load at a rate of 0.02 mm s^{-1} to $scCO_2$ foamed scaffolds in a chamber at 37 °C. Stress strain curves were recorded for each scaffold and average compressive failure points for each scaffold type were calculated. The yield stress was determined by the initial peak of the stress-strain plot. The compressive mechanical strength of the scaffolds was utilised as an additional indicator to compare the scaffolds with different HA contents to identify those with the most potential for use. The targetted application of scaffolds (impaction into the femur) is a loaded environment, and hence compressive strength is relevant. Compression testing should not replace shear testing, which is required because it is a common mode of failure for implanted femoral stems.

5.2.2.5 Cell culture

The isolation of primary human MSCs and their expansion and storage prior to use is detailed in Section 2.5.1.1. The subsequent seeding and impaction of seeded scaffolds is detailed in Sections 2.5.1.4 and 2.5.1.5, respectively. Cells were incubated *in vitro* for 2 weeks under standard cell culture conditions (37 °C and 5% CO_2).

WST-1 assay

The WST-1 assays were carried out for samples following the protocol described in Section 2.6.1.

ALP/DNA assay

The ALP and DNA assays were carried out using the protocols described in Sections 2.6.2 and 2.6.3, respectively.

Immunohistochemical staining

Collagen-1, osteocalcin and bone sialoprotein immunostaining was carried out utilising the protocol described in Section 2.7.

5.3 Results and discussion

5.3.1 Cell differentiation studies on P_{DL}LA and P_{DL}LGA films

The aim of the studies investigating osteogenic differentiation of immortalised human MSCs on P_{DL}LA and P_{DL}LGA films was to establish whether the difference in osteogenic differentiation observed in Chapter 3 was intrinsic to the properties of the polymers by removing morphological differences. The results from the studies in Chapter 3 demonstrated greater specific ALP activity ($P<0.001$) and collagen-1 expression after 2 weeks *in vitro* culture in osteogenic medium for MSCs cultured on P_{DL}LA scaffolds, compared to MSCs cultured on P_{DL}LGA scaffolds. The characterisation of the scaffolds used in those studies demonstrated a difference in porosity and pore size between the $scCO_2$ foamed P_{DL}LA and P_{DL}LGA scaffolds. Scaffold porosity and pore size are both known to influence osteogenesis (the formation of bone) [180, 181]. Removing differences in scaffold morphology by utilising flat films allowed any osteogenic differentiation differences observed to be attributed to differences between the polymers (P_{DL}LA and P_{DL}LGA). Polymer films formed from a 50:50 (wt./wt.) blend of P_{DL}LA and P_{DL}LGA were also utilised as midpoints, and glass coverslips as controls.

Initially, spincoated polymer films were utilised. These were characterised by initial water contact angle and XPS analysis as shown in Figure 5.1 and Table 5.1, respectively. Measurement of water contact angles on different polymeric films indicated surface wettability, which is known to affect cellular behaviour (e.g. cell adhesion, spreading, and migration) [284–286], was not significantly different between P_{DL}LA and P_{DL}LGA polymer films. The behaviour of MSCs cultured on P_{DL}LA and P_{DL}LGA films may have been affected by differences in surface wettability between the films. These studies were carried out to remove morphological differences, which were present in the investigations presented in Chapter 3. These studies were not carried out to investigate the effect of differences in surface wettability on osteoblastic differentiation of MSCs. Water contact angle characterisation for P_{DL}LA and P_{DL}LGA films confirmed that surface wettability was not significantly different between the films, and hence that it had a limited effect on the osteoblastic differentiation of MSCs cultured on different polymer films.

Surface characterisation of polymer films by XPS analysis was carried out to identify surface contamination and to confirm coverage of the glass substrate upon which the films

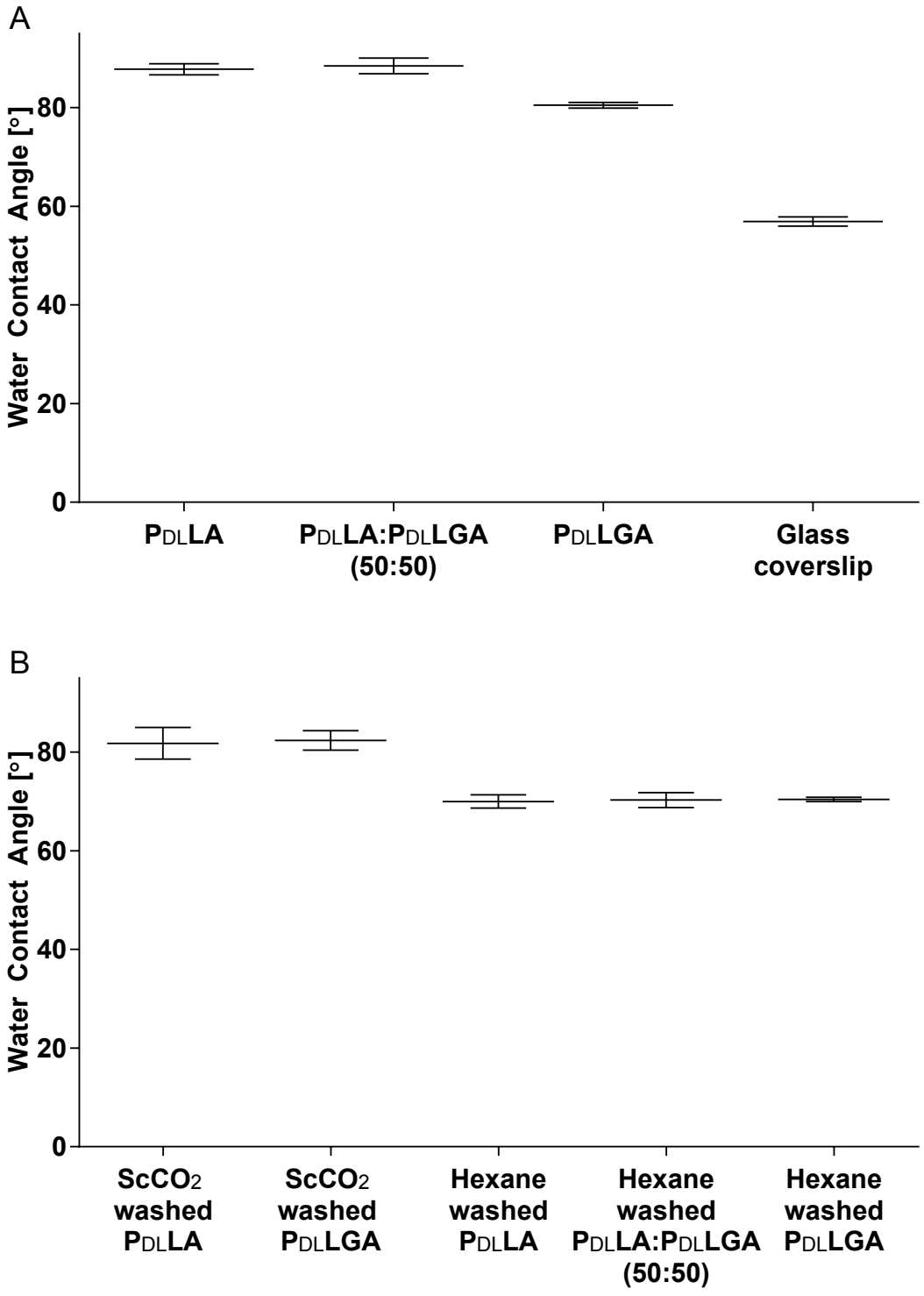

Figure 5.1: Initial water contact angle results for polymer films spincoated onto glass coverslips (n=3). (A) Shows results for unwashed films. (B) Shows results for films washed with supercritical CO_2 or hexane.

Table 5.1: XPS results for polymer films spincoated onto glass coverslips, shown as percentages of total elemental signal.

Sample	C 1s%	O 1s%	Si 2p%	Ti 2p%	Zn 2p%	B 1s%	K 2p%	Na 1s%
Glass	15.19	59.13	15.37	0.84	1.48	2.01	2.23	3.75
$P_{DL}LA$	60.73	36.02	3.25					
$P_{DL}LA$:$P_{DL}LGA$ (50:50)	59.94	37.26	2.81					
$P_{DL}LGA$	59.79	37.98	2.23					
Hexane washed $P_{DL}LGA$	61.45	38.49	0.05					

were spincoated or dipcoated. This increased confidence that osteogenic differentiation differences observed in MSCs cultured on the films were due tothe properties of the polymers being studied.

In Figure 5.1A the initial water contact angles are shown for spincoated films with no washing steps prior to production. These were measured in triplicate for three different samples of each polymer film type and the means plotted as shown. Similarly, in Table 5.1 the percentage of total elemental signal for carbon, oxygen, and silicon peaks are shown for spincoated films of each polymer film type with no washing steps. The carbon:oxygen ratio was similar for each polymer film type (P_{DL}LA 1.69, P_{DL}LA:P_{DL}LGA 1.61, P_{DL}LGA 1.57) as expected due to the similarity between the polymers; while lactide has a C:O ratio 3:2 and glycolide a ratio 1:1 the P_{DL}LGA used was 85:15 lactide:glycolide.

The presence of silicon peaks in the XPS analysis of the polymer films (Table 5.1) indicated a contaminant source. The absence of titanium, zinc, boron, potassium, and sodium peaks in the polymer films indicated the silicon contamination was not from the glass substrate. The equipment used to spincoat films was previously used to produce poly (dimethylsiloxane) (PDMS) films and this was identified as a likely source of contamination. In Figure 5.1B the initial water contact angle is shown for spincoated polymer films washed either with $scCO_2$ or with hexane. The initial water contact angles were unchanged for films washed with $scCO_2$: with 87.8±1.9° unwashed and 81.8±5.5° washed for P_{DL}LA, and 80.5±1.0° unwashed and 82.4±3.4° washed for P_{DL}LGA. The films washed with hexane however, had lower initial water contact angles than the unwashed films with reductions to 70.0±2.3° for P_{DL}LA, to 70.3±2.6° for P_{DL}LA:P_{DL}LGA (50:50) (from 88.5±2.8°), and to 70.4±0.7° for P_{DL}LGA. Cai *et al*. [287] reported similar values for P_{DL}LA films of 69±3°. XPS analysis of hexane washed P_{DL}LGA films confirmed a 98% reduction in the percentage total elemental signal for silicon compared to unwashed P_{DL}LGA films. This confirmed hexane washing as an effective method of removing the suspected PDMS contaminant from the polymeric films.

As in Chapter 3, WST-1 assays were used to assess cell viability and ALP assays were used to assess osteogenic differentiation. Immortalised human MSCs were cultured *in vitro* on hexane washed, spincoated polymer films for 4 weeks in osteogenic medium. An increase in measured optical density over the WST-1 assay period indicated good cell viability on all films after 1 week and 2 weeks *in vitro* culture (Figure 5.2. The assay results indicated

significantly greater metabolic activity for cells cultured on P_{DL}LGA films compared to cells cultured on P_{DL}LA:P_{DL}LGA (50:50) films after 1 week. ($P<0.05$). After culture for 2 weeks there were indications of significantly greater metabolic activity in MSCs cultured on P_{DL}LA:P_{DL}LGA (50:50) films compared to cells cultured on P_{DL}LA films ($P<0.01$) and P_{DL}LGA films ($P<0.05$) (Figure 5.2B).

The osteogenic differentiation assays indicated an increase in ALP expression from 1 week to 2 weeks culture for MSCs on all films. Osteogenic differentiation after 1 week culture was significantly less for MSCs on polymer films compared to tissue culture plastic (TCP) controls ($P<0.01$) (Figure 5.3A. However, after 2 weeks there was no significant difference in ALP expression between cells cultured on TCP, or on P_{DL}LA and PLGA films. There was significantly greater ALP expression in cells cultured on P_{DL}LA:P_{DL}LGA (50:50) films compared to on P_{DL}LA films and TCP ($P<0.05$) (Figure 5.3B. Due to failure of the DNA assay the ALP assay results do not refer to specific activity as in Chapters 3 and 4. Therefore the higher ALP expression evident in P_{DL}LA:P_{DL}LGA films may be due to increased cell number indicated by higher metabolic activity measured by the WST-1 assays (Figure 5.2B).

Some spincoated polymer films changed shape during cell culture; film edges pulled away from the glass coverslips and stretched towards the centre of the film. This reduced the surface area of the films and resulted in samples that could not be used for analysis. Even though spare samples were created, too many of each polymer type were lost, which prevented assays being taken at 4 weeks and samples being immunohistochemically stained and imaged. When the films are created through spincoating the forces acting on the polymer molecules due to the high rotation speed likely orientates the molecules to stretch out towards the film edges. When the rotation halts and the films are placed in cell culture medium the stretched polymer molecules will return to a lower energy shape rather than remain stretched out, which may cause the shrinkage of the spin coated films and formation of the creases.

Various solutions were considered to prevent films pulling away from the edges of the glass coverslips. Fixing the edges of the films to the coverslips with a cyanoacrylate was considered but proved toxic to the cells. An alternative method for creating polymer films was utilised, which involved dipping the glass coverslips in an acetone:polymer solution, hence referred to as dipcoating. Dipcoating was theorised to cover the entire coverslip in a polymer film rather than the upper surface only, as with spincoating. The advantage in this

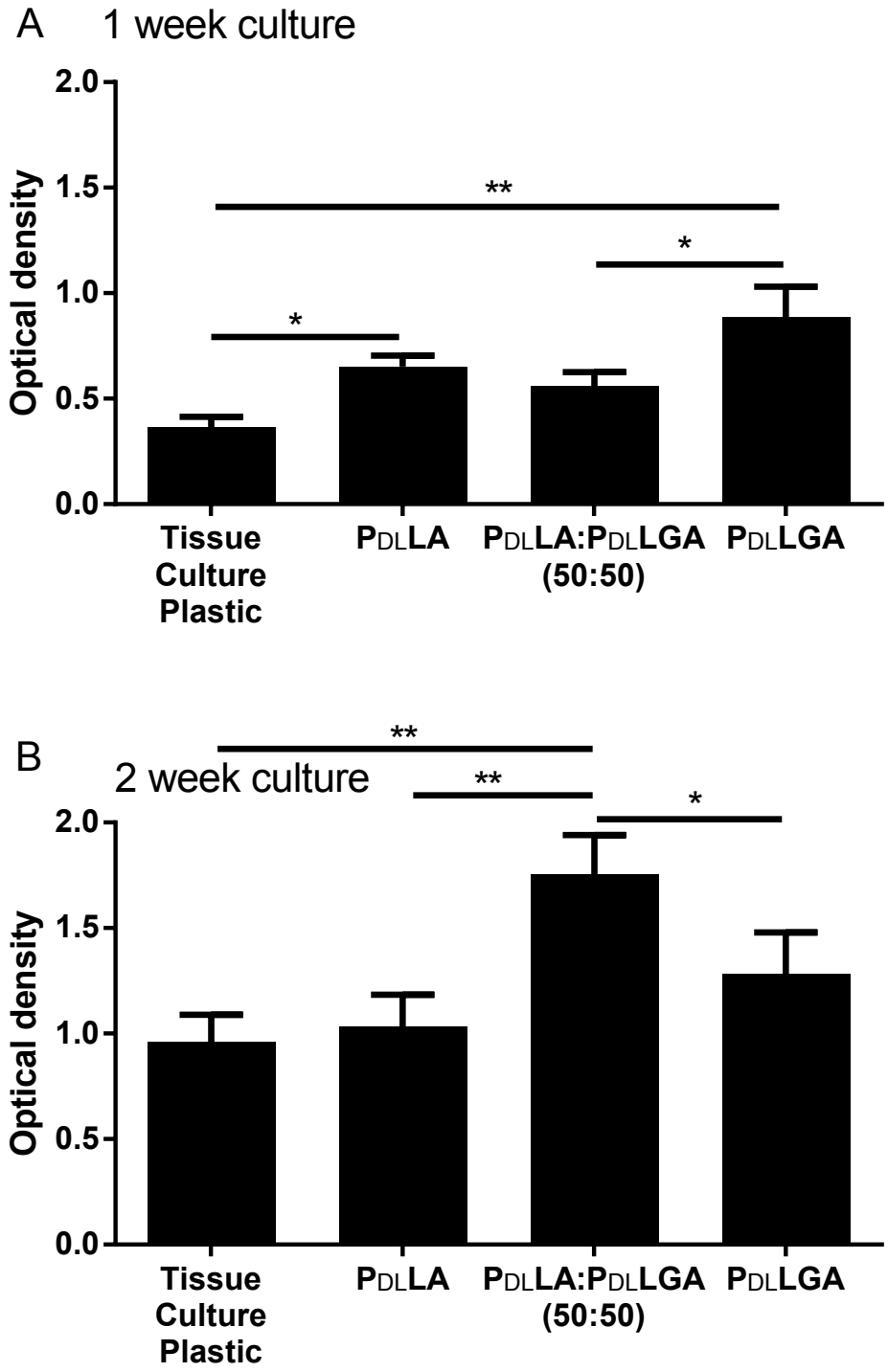

Figure 5.2: Mean WST-1 assay readings showing optical density at 450 nm for immortalised human MSCs cultured *in vitro* on hexane washed spincoated polymer films for (A) one week, and (B) two weeks in osteogenic medium (n=3). Statistically significant differences shown (* $P<0.05$, ** $P<0.01$). Error bars show standard deviation.

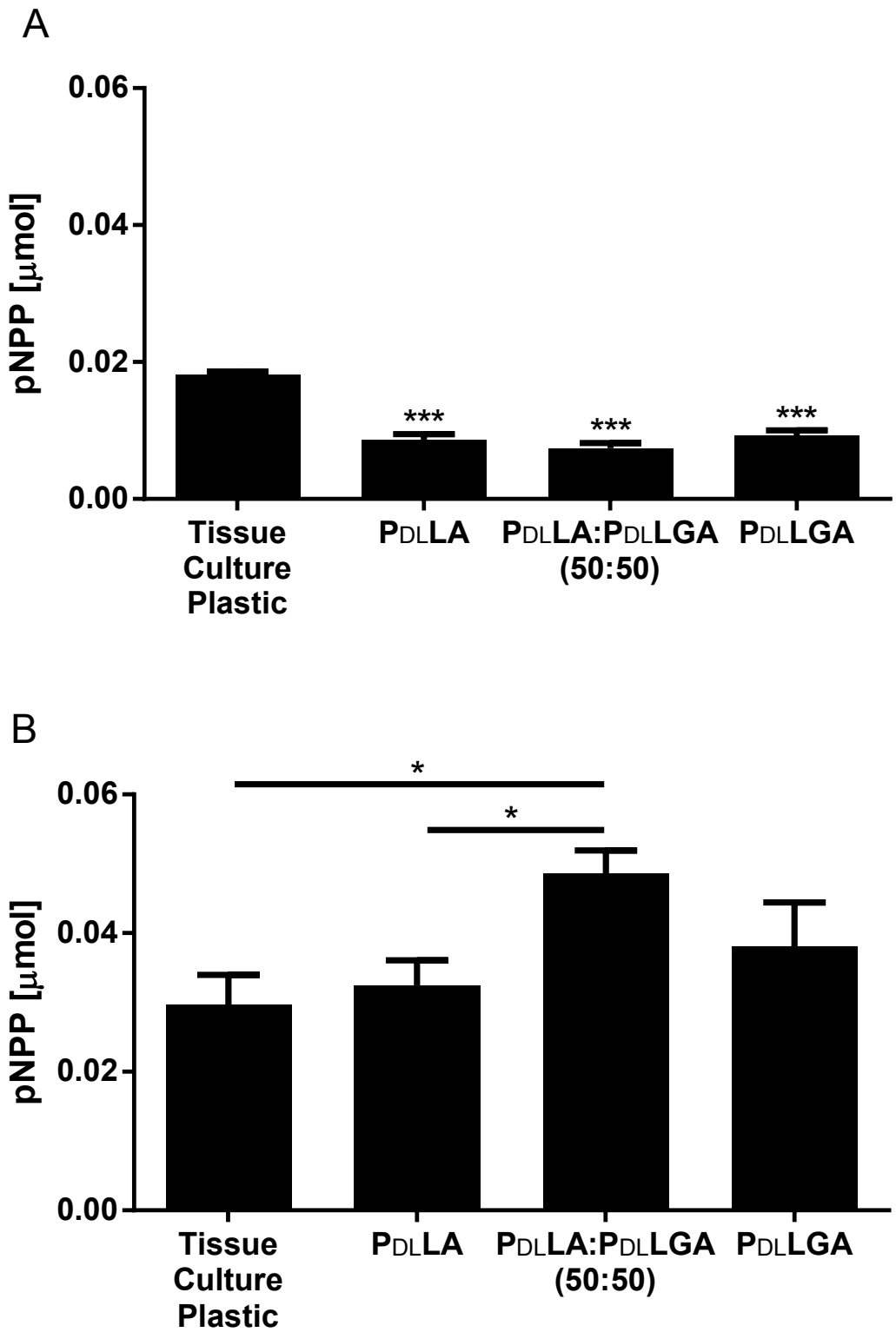

Figure 5.3: Mean ALP activity for immortalised human MSCs cultured *in vitro* on hexane washed spincoated polymer films for (A) one week, and (B) two weeks in osteogenic medium (n=3). Statistically significant differences shown (* $P<0.05$, *** $P<0.001$). Error bars show standard deviation.

was to prevent water ingress between the underside of the polymer films and the surface of the glass coverslips, and prevent the film edges detaching from the glass. Unfortunately some of the polymer films produced using the dipcoating method still pulled away from the coverslips and crumpled inwards, which reduced the surface area and prevented the use of the samples. This stopped assay results being collected after 4 weeks *in vitro* culture. Repeats of WST-1 metabolic assays at 1 week and 2 weeks, and ALP osteogenic differentiation assays at 2 weeks were collected for MSCs cultured on dipcoated P_{DL}LA, P_{DL}LA:P_{DL}LGA (50:50) and P_{DL}LGA films. The results are presented in Figures 5.4 and 5.5, respectively. Highest results for cell metabolic activity and ALP expression at 2 weeks were for cells cultured on P_{DL}LA:P_{DL}LGA (50:50) films, although there were no statistically significant differences in WST-1 and ALP assay results between cells cultured on the different polymer films in the study.

Additionally, MSCs cultured on dipcoated polymer films for 2 weeks were immunohistochemically stained for collagen-1 and imaged using fluorescence microscopy, as shown in Figures 5.6 and 5.7. In Figure 5.6 cells cultured on areas of the polymer films that were flat against the glass substrate (not raised away from the glass substrate/ridged) are shown. Cells appeared to be confluent demonstrated by GFP expression (green) and DAPI nuclear counterstains (blue). Presence of collagen-1 (red) was indicated on glass coverslip controls, P_{DL}LA, and P_{DL}LA:P_{DL}LGA (50:50) films while negligible collagen-1 was observed on P_{DL}LGA films. The secondary-only control samples confirmed specificity of the fluorescent secondary antibody. The polymer films did not remain flat and formed creases/ridges. Cells grew to confluency over the entire film exposed surface area, which included these creases and raised regions. The films for the samples imaged and displayed in Figure 5.6 were not uniformly flat and cells growing on polymer film ridges in the samples are shown in Figure 5.7. In these raised areas there was positive staining for collagen-1 on all polymer films, including P_{DL}LGA. This confirmed evidence of osteogenic differentiation indicated by cellular expression of ALP.

The fluorescent images shown in Figures 5.6 and 5.7 gave qualitative results of a limited number of samples with varying surface morphology. They appeared to indicate that osteogenic differentiation of MSCs cultured *in vitro* in osteogenic medium on flat areas of P_{DL}LA films expressed higher levels of collagen-1 than MSCs cultured on P_{DL}LGA films, under the same conditions after 2 weeks. They also indicated that MSCs that grew on ridged areas of P_{DL}LA films and P_{DL}LGA films both express collagen-1 after 2 weeks. Lack of a

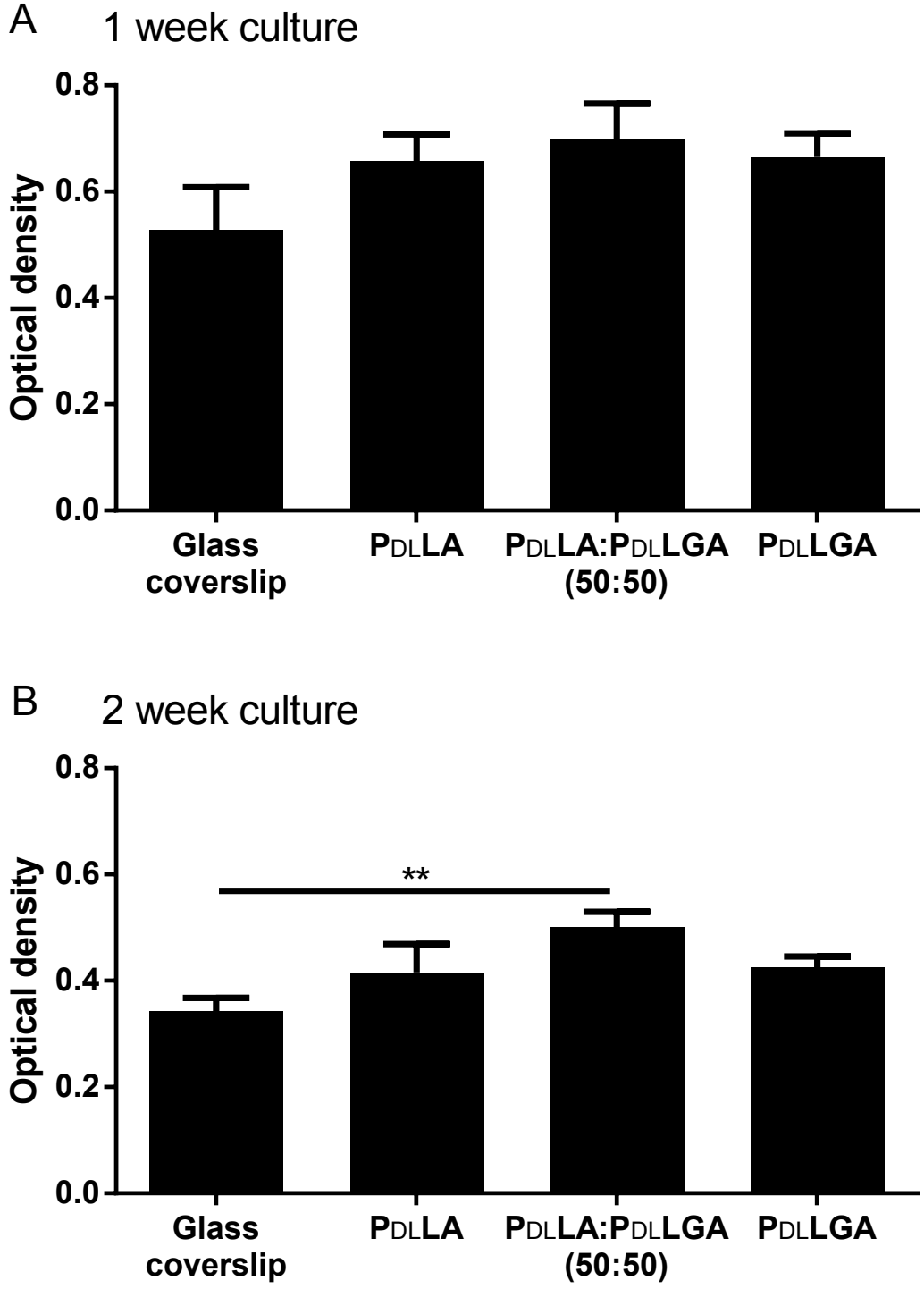

Figure 5.4: Mean WST-1 assay readings showing optical density readings at 450 nm for immortalised human MSCs cultured *in vitro* on dipcoated polymer films for (A) one week, and (B) two weeks in osteogenic medium (n=3). Statistically significant differences shown (** P<0.01). Error bars show standard deviation.

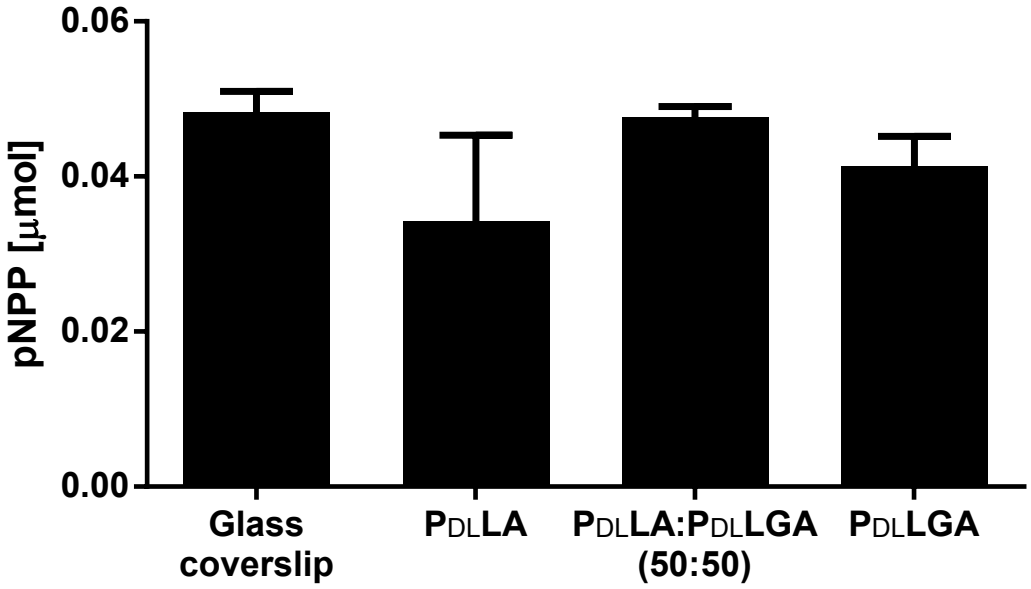

Figure 5.5: Mean ALP activity for immortalised human MSCs cultured *in vitro* on dipcoated polymer films for two weeks in osteogenic medium (n=3). No statistically significant differences (one-way ANOVA , Tukey's multiple comparisons). Error bars show standard deviation.

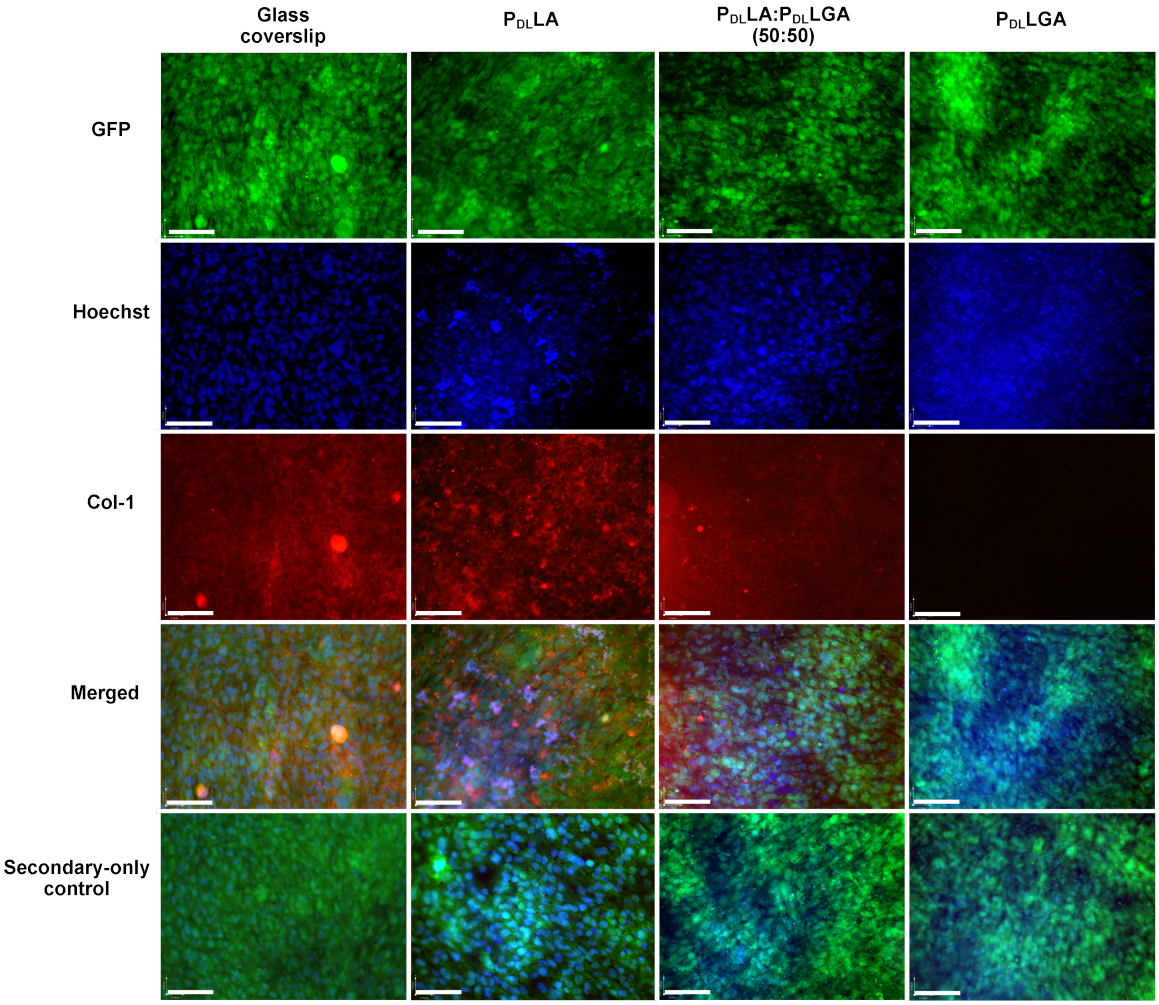

Figure 5.6: Fluorescent microscope images of immortalised human MSCs cultured *in vitro* on dipcoated polymer films for two weeks at $\times 20$ magnification. Collagen-1 (red) immunostaining and Hoechst nuclear counterstains (blue) were used. Scale bars signify 100 μm. Collagen-1 was positively stained on all films other than P_{DL}LGA films. Secondary antibody only controls demonstrate the specificity of the stain.

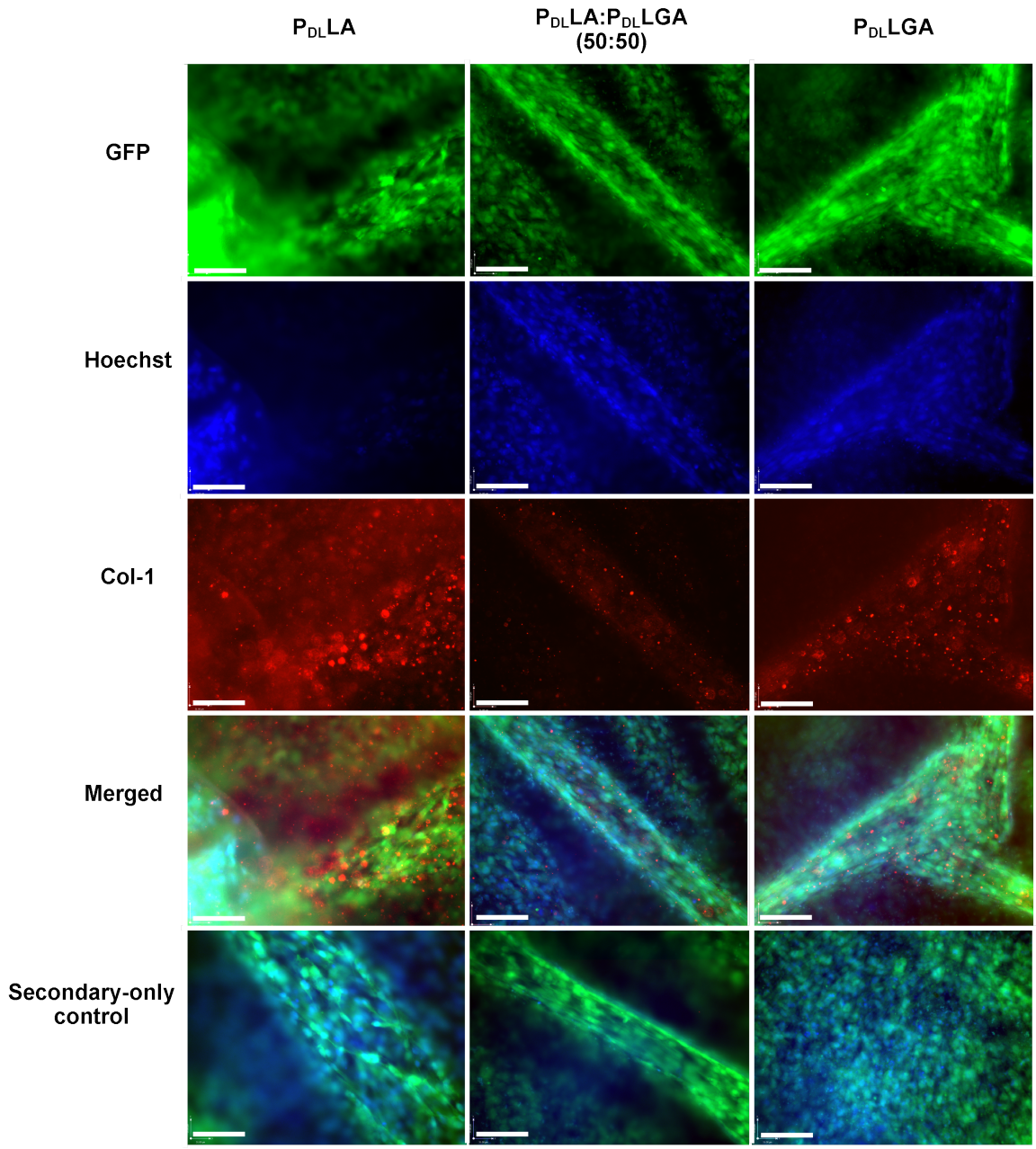

Figure 5.7: Fluorescent microscope images of immortalised human MSCs cultured *in vitro* on dipcoated polymer films for two weeks at ×20 magnification. Images show MSCs on raised/ridged areas where films pulled away from the glass substrate. Collagen-1 (red) immunostaining and Hoechst nuclear counterstains (blue) were used. Scale bars signify 100 μm. Collagen-1 was positively stained on all films. Secondary antibody only controls demonstrate the specificity of the stain.

statistically significant difference in ALP expression between cells cultured on P_{DL}LA films to cells cultured on P_{DL}LGA films may have resulted from osteogenic differentiation of MSCs on ridged areas of P_{DL}LGA films. This differentiation may have masked differences in differentiation on flat areas of the P_{DL}LGA films compared to MSCs cultured on P_{DL}LA films, which expressed collagen-1 in both flat areas and creased areas of the films. These results are not conclusive evidence that there are no differences in osteogenic differentiation of MSCs cultured on P_{DL}LA and P_{DL}LGA flat films. The experiment should be repeated in the future with films clamped with sterilised clips to limit changes in morphology and prevent the raised ridges from forming. Additionally, the study would ideally be extended to 28 days for full osteogenic differentiation and further differentiation markers stained for, such as osteocalcin and/or osteopontin.

5.3.2 Studies of HA particle size and morphology effect on cell differentiation

The incorporation of HA particles in $scCO_2$ foamed polymer scaffolds described within this thesis was initially limited to microparticles at 10 wt.(%) concentration. In Chapter 3 MSCs cultured on $scCO_2$ foamed P_{DL}LA and P_{DL}LGA scaffolds with 10% HA expressed higher levels of ALP in comparison to cells cultured on respective $scCO_2$ foamed 100% polymer controls. Additionally, the formation of bony matrix within milled $scCO_2$ foamed P_{DL}LA + 10% HA scaffolds cultured *in vivo* (murine) for 5 weeks appeared to be concentrated around HA microparticles within the scaffolds. The action by which bony matrix formed around the HA microparticles *in vivo* was not elucidated in Chapter 3; HA may be a nucleation site for mineralisation to occur and/or osteoinductive properties of the HA microparticles may prompt osteogenesis. Bony matrix within the scaffolds was desirable and it would be regarded as an improvement to increase the rate at which it forms. To achieve this, an increased specific surface area of HA within the scaffolds was investigated; a larger specific surface area would provide a greater number of sites around which bony matrix may form. Smaller HA particles at the same weight concentration increased the specific surface area. Nanoparticles of HA with two different morphologies were used: nanorods (NRs) and nanoplates (NPs). Loosely packed HA nanoparticles occupy a larger volume than the same weight of HA microparticles. While scaffolds containing 10% HA nanoparticles were investigated, concentrations of 1 wt.% HA NRs and NPs were also investigated that occupied similar volumes to 10 wt.% HA microparticles within the PTFE $scCO_2$ foaming moulds.

Representative micrographs displayed in Figure 5.9 demonstrate the pore size and distribution of $scCO_2$ foamed $P_{DL}LA$ scaffolds with 10% HA (microparticles, NRs, and NPs), with 1% HA (NRs and NPs), and without HA. Scanning electron microscopy commonly detects secondary electrons emitted by atoms excited by the electron beam of the microscope. In the micrographs produced from secondary electron detection HA particles were difficult to discern from the background $P_{DL}LA$.

In Figure 5.9 BSE micrographs are displayed of the same areas shown in the secondary electron beam (SB) micrographs for samples containing HA particles. Bright spots can be seen in the BSE images that are absent in the SB images, these represent the HA particles. This was confirmed with energy dispersive x-ray spectroscopy (EDX) as shown in Figure 5.10. Calcium and phosphorus peaks were detected when EDX was used on bright spots identified by BSEs; these peaks were absent in areas of the images corresponding to areas of $P_{DL}LA$. Carbon was used to coat the samples imaged in Figures 5.9 and 5.10 to prevent interference with BSE and EDX that platinum or gold (high atomic numbers: 78 and 79, respectively) coatings may have introduced.

The micrographs in Figure 5.9 show a similar porous structure in $scCO_2$ foamed $P_{DL}LA$, $P_{DL}LA$ + 10% HA microparticles, $P_{DL}LA$ + 1% NRs, $P_{DL}LA$ + 1% NPs scaffolds. The internal structure of $scCO_2$ foamed $P_{DL}LA$ + 10% NRs and $P_{DL}LA$ + 10% NPs contained smaller pores, thicker interporous walls, and a more closed internal structure. The scaffolds that contained nanoparticles had aggregated clumps of particles rather than a dispersed homogeneous mix throughout.

The compressive yield stresses of $scCO_2$ foamed $P_{DL}LA$ + 10% HA microparticles, $P_{DL}LA$ + 1% NRs, $P_{DL}LA$ + 1% NPs, $P_{DL}LA$ + 10% NRs, and $P_{DL}LA$ + 10% NPs scaffolds were recorded (Figure 5.11). One-way analysis of variance and Tukey's multiple comparisons revealed no significant differences between the compressive yield stresses of any of the scaffolds. This contrasts to literature where composite scaffolds of HA nanoparticles and poly(α-hydroxyacids), such as PLA have demonstrated improved mechanical strength over poly(α-hydroxyacid) scaffolds alone [186, 198, 208, 254, 272–283].

The aggregation of nanoparticles prevented a homogeneous distribution throughout the scaffolds which could have limited the strengthening of the polymer by HA particles. Methods utilised within the literature to mix HA nanoparticles used solutions of polymer in chloroform or 1,4-dioxane; HA nanoparticles were added to these solutions and then sonicated

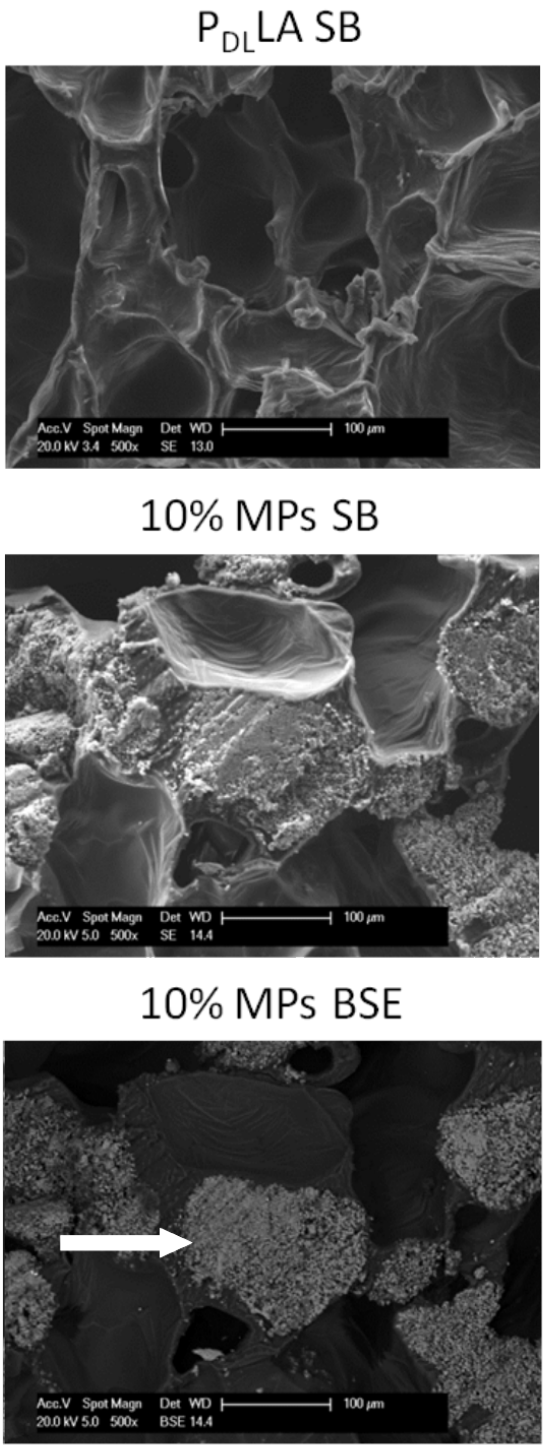

Figure 5.8: SEM images of $scCO_2$ foamed $P_{DL}LA$ scaffolds at $\times 500$ magnification. Scaffolds containing HA particles (indicated by arrow) (microparticles, MPs) are imaged with both secondary beam (SB) and back scattered electrons (BSE) to highlight the HA content.

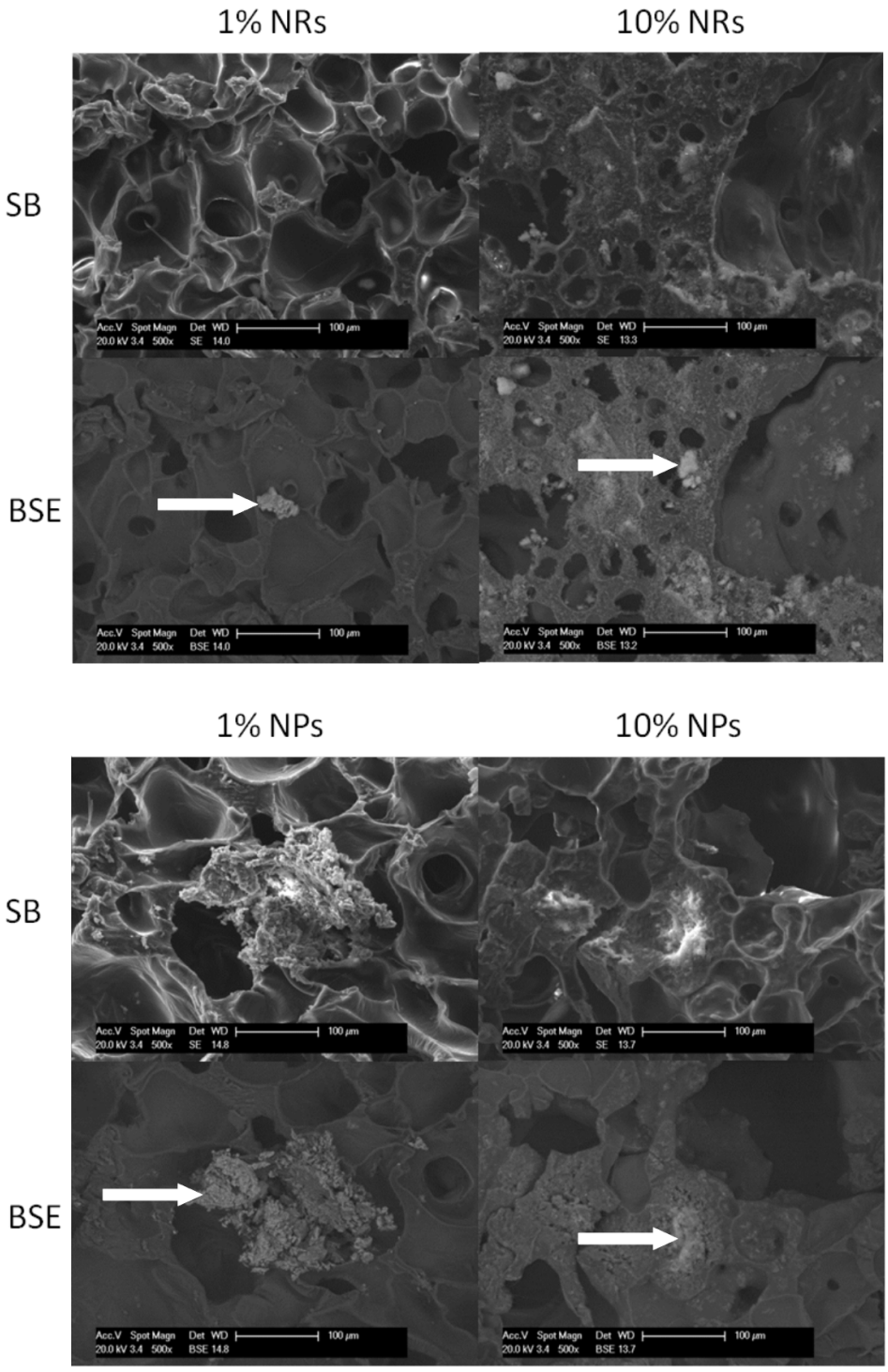

Figure 5.9: SEM images of $scCO_2$ foamed $P_{DL}LA$ scaffolds at $\times 500$ magnification. Scaffolds containing HA particles (indicated by arrows) (nanorods, NRs; and nanoplates, NPs) are imaged with both secondary beam (SB) and back scattered electrons (BSE) to highlight the HA content.

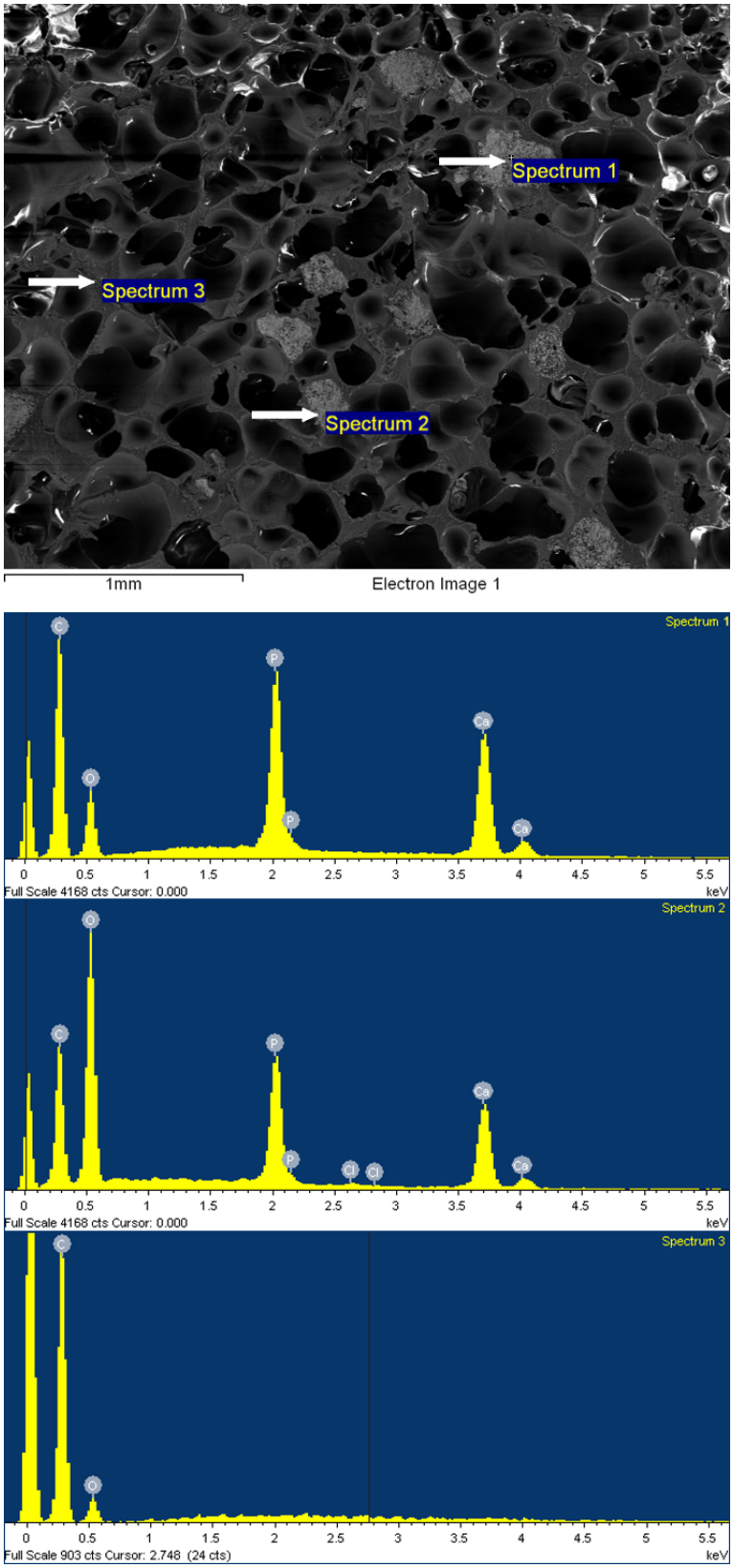

Figure 5.10: SEM BSE image (top) and energy dispersive x-ray (EDX) analysis spectra (bottom) of $scCO_2$ foamed $P_{DL}LA$ scaffolds + 10% HA microparticles at $\times 50$ magnification. Spectra taken from top left hand points (arrows) of spectrum boxes marked on SEM image.

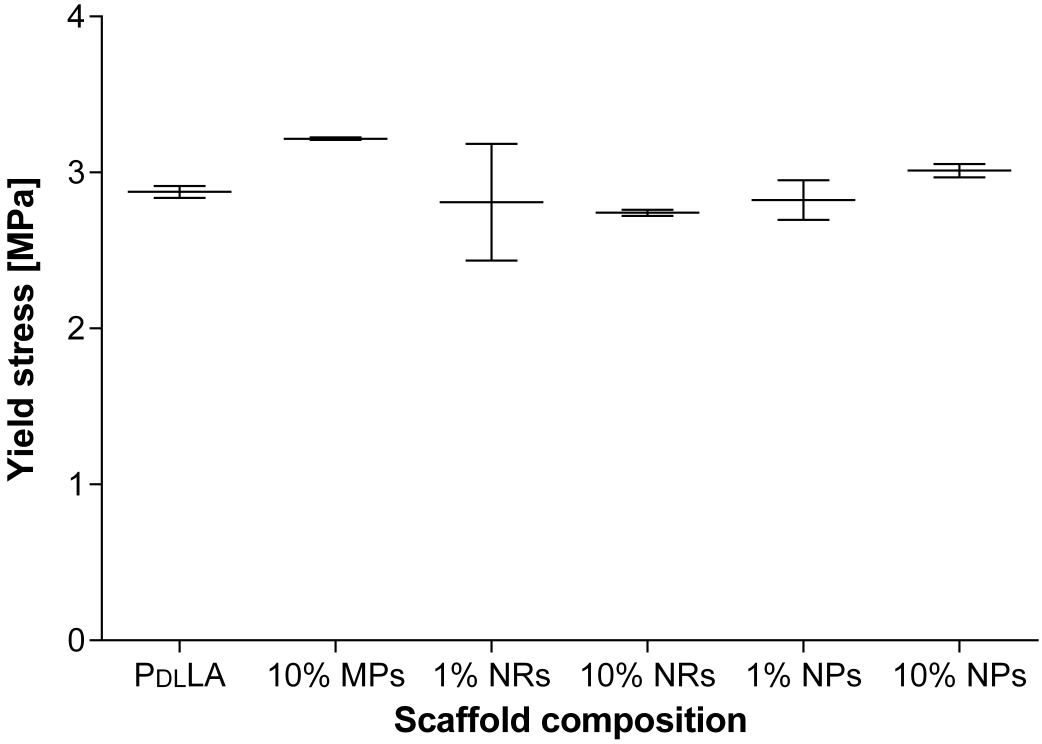

Figure 5.11: Mean compression yield points for different $scCO_2$ foamed $P_{DL}LA$:HA scaffold compositions with SD error bars (n=3). No statistical significance at $P<0.05$ level.

and mixed to create particle dispersions [276, 277]. Quantitative assessment of the degree of particle dispersion within the scaffolds produced was not used. Particle dispersions were frozen and lyophilized, or polymer and HA were precipitated in excess of ethanol [277]. The use of either method could be utilised in the future to create more dispersed $P_{DL}LA$ + HA nanoparticles scaffolds. The utilisation of solvents is not desirable but may be unavoidable for desired dispersion and the benefits of nanoparticles may overcome detrimental solvent residue effects. Additionally, the $scCO_2$ foaming step can double as a solvent extraction step. A comparison was made between solvent cast and particle leached scaffolds (an alternative method to $scCO_2$ foaming for producing porous polymeric scaffolds described in Section 1.5) to gas foamed and particle leached scaffolds within the literature [198]. They reported gas foamed and particle leached scaffolds were more desirable than solvent cast and particle leached scaffolds as they: exposed HA nanoparticles to a greater extent, exhibited higher compressive moduli (4.5 MPa compared to 2.3 MPa), and demonstrated higher cell growth rates, ALP activity, and mineralization [198]. Enhanced bone formation following *in vivo* culture was also reported for gas foamed and particle leached scaffolds [198].

The integration of HA particles with PLGA scaffolds was improved within the literature through surface grafting L-lactide to the particles which resulted in improved strength compared to the incorporation of ungrafted HA particles [273, 288]. Kutikov *et al*. [283] investigated utilising polyethylene glycol (PEG) to improve structural homogeneity and mechanical integrity in $P_{DL}LA$:HA composites; a PEG containing triblock copolymer (a copolymer comprising three distinct homopolymer subunits linked covalently) comprising $P_{DL}LA$-PEG-$P_{DL}LA$ was synthesised and mixed with HA particles (particle size not commented on). The triblock composites (25 wt.% HA) exhibited an 8-fold increase in tensile storage modulus and $\approx 0^\circ$ water contact angle compared to $>100^\circ$ for $P_{DL}LA$:HA composites. Surface grafting L-lactide to HA particles and improving the hydrophilic properties of $P_{DL}LA$ through utilisation of a $P_{DL}LA$-PEG-$P_{DL}LA$ triblock copolymer has demonstrated improved integration of HA particles within scaffolds [283]. Investigation of these methods in $scCO_2$ foamed scaffolds and utilisation of a $P_{DL}LA$:PEG blend rather than a triblock copolymer are viable future directions for this work.

In this work the compressive testing of the scaffolds was potentially flawed because moulded cylindrical foams were tested rather than the polymer and HA composites as a material. The cylinders formed by $scCO_2$ foaming are known to have an outer skin that is less porous. This skin was not removed and the compression of the cylinders may have

been dominated by the compressive strength of this less porous outer skin surrounding a more porous inner core; the strength of the outer skin may not vary significantly with incorporation with HA particles at the concentrations used. This is likely given the lack of statistically significant variations in compressive strength of the scaffolds tested.

The $scCO_2$ foamed scaffolds were milled using a bone mill to produce chips of porous scaffold onto which primary human MSCs were seeded. These seeded chips were impacted and cultured for 2 weeks in osteogenic medium in standard cell culture conditions (37 °C, 5% CO_2). Cell viability on milled $scCO_2$ foamed $P_{DL}LA$, $P_{DL}LA$ + 10% microparticles, $P_{DL}LA$ + 1% HA NRs, $P_{DL}LA$ + 10% NRs, $P_{DL}LA$ + 1% NPs, and $P_{DL}LA$ + 10% NPs was assessed using WST-1 assays (Figure 5.12). The assay results indicated a significantly higher metabolic activity for MSCs cultured on $P_{DL}LA$ scaffolds containing nanoparticles compared to MSCs cultured on $scCO_2$ foamed $P_{DL}LA$ + 10% microparticles ($P<0.05$ for $P_{DL}LA$ + 1% NRs and 1% NPs, $P<0.001$ for $P_{DL}LA$ + 10% NRs and NPs). This suggested a higher number of cells was present on scaffolds containing nanoparticles than scaffolds containing microparticles. There was no significant difference in the metabolic activity of MSCs cultured on scaffolds that contained 1% nanoparticles (NRs and NPs) to MSCs cultured on $P_{DL}LA$ scaffolds containing no HA. However, MSCs cultured on scaffolds that contained 10% HA nanoparticles exhibited significantly greater metabolic activity than MSCs cultured on $P_{DL}LA$ only controls. This suggested a larger cell population on $scCO_2$ foamed $P_{DL}LA$ + 10% nanoparticles (either NRs or NPs) to all other scaffolds after incubation for 2 weeks.

Alkaline phosphatase assays were carried out to assess osteoblastic differentiation (Figure 5.13). These assays were carried out following culture for 2 weeks in osteogenic medium, of MSCs seeded onto milled $P_{DL}LA$ scaffolds containing HA particles. There were no statistically significant differences between the mean values of ALP specific activity results for MSCs cultured on each of the different scaffolds. The results for MSCs cultured on $P_{DL}LA$ + 10% NPs were inconclusive, with both the highest and lowest readings for ALP specific activity. The HA NPs occupied a large volume of the PTFE mould prior to $scCO_2$ foaming which affected the foamed structure formed by the PLA. Additionally, a homogeneous distribution of NPs throughout the scaffolds was not achieved by mixing HA NPs and $P_{DL}LA$ powder within the PTFE moulds then $scCO_2$ foaming. This was observed by inspection of the scaffolds and SEM (Figure 5.9). The heterogeneous distribution of HA NPs and the limited foaming of $P_{DL}LA$ scaffolds with 10% NPs may have resulted in large differences (morphological and HA concentration) in the scaffolds that the MSCs were seeded onto.

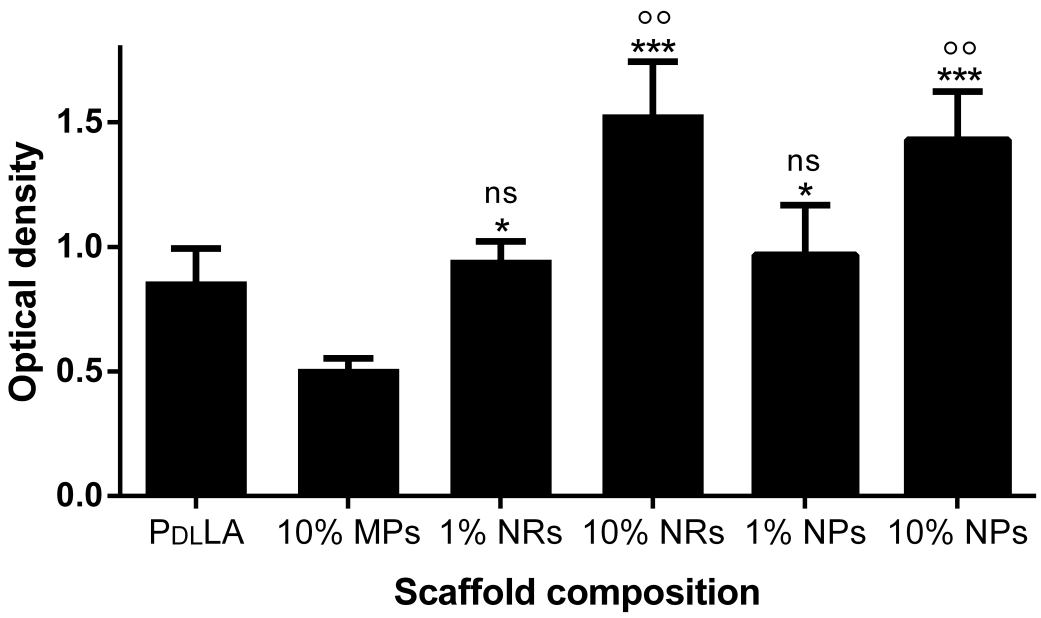

Figure 5.12: WST-1 assay results showing increase in optical density over 4 hr for MSCs cultured on different $scCO_2$ foamed $P_{DL}LA$:HA composition scaffolds for two weeks. SD error bars (n=4). Two-way ANOVA was carried out and presented where * signifies statistical significance compared to $scCO_2$ foamed $P_{DL}LA$ controls and ° signifies statistical significance compared to $scCO_2$ foamed $P_{DL}LA$:10% HA MPs ($^{*}P<0.05$, $^{**}P<0.01$, $^{***}P<0.001$).

This would account for the varied results in ALP specific activity. Disregarding the inconclusive results for MSCs on $P_{DL}LA$ + 10% HA NPs, the lowest ALP specific activity results were for MSCs cultured on $P_{DL}LA$ scaffolds with no HA (0.76 nmol pNPP hr^{-1} ng DNA $^{-1}$) and $P_{DL}LA$ + 10% NRs (0.89 0.758 nmol pNPP hr^{-1} ng DNA $^{-1}$). Higher ALP specific activities were observed for MSCs seeded on $P_{DL}LA$ + 10% HA microparticles, $P_{DL}LA$ + 1% NRs, and $P_{DL}LA$ + 10% NRs scaffolds with slightly higher results for cells cultured scaffolds containing nanoparticles.

While the ALP results in this study were not statistically significant at the P<0.05 level, the trends observed between MSCs cultured on $scCO_2$ foamed $P_{DL}LA$ and $scCO_2$ foamed $P_{DL}LA$ + 10% HA microparticles match the trends reported in Chapter 3; MSCs cultured on $scCO_2$ foamed and milled $P_{DL}LA$ + 10% HA microparticles had a higher ALP specific activity than MSCs cultured on $scCO_2$ foamed and milled $P_{DL}LA$ (Figure 3.12). In the study within this chapter, cells cultured on scaffolds containing 1 wt.% nanoparticles had slightly higher ALP specific activity levels than cells cultured on $P_{DL}LA$ + 10% HA microparticles (not significant at P<0.05 level). The scaffolds containing 1% nanoparticles had a poor distribution of HA, for both NRs and NPs. A homogeneous distribution of HA nanoparticles may improve the osteoinductive properties of the scaffolds with MSCs cultured on such scaffolds potentially demonstrating improved osteogenic differentiation compared to $P_{DL}LA$ + 10% HA microparticles scaffolds. The greater metabolic activity and similar ALP specific activities observed for MSCs cultured on $P_{DL}LA$ + 1% HA nanoparticle scaffolds suggest a minor improvement based on cellular compatibility compared to $P_{DL}LA$ + 10% HA microparticles scaffolds.

Following 2 weeks *in vitro* incubation in osteogenic medium, samples were immunohistochemically stained for osteoblastic differentiation markers (collagen-1, col-1; osteocalcin, OC; and bone sialoprotein BSP). The confocal microscopy images (Figure 5.14 indicated the presence of col-1, OC, and BSP (green) on $P_{DL}LA$ + 1% NRs scaffolds. There was limited evidence of expression of all three markers on $P_{DL}LA$ + 1% NPs scaffolds but BSP stained strongly positive on $P_{DL}LA$ + 10% HA microparticles scaffolds. Limited staining of col-1 on $P_{DL}LA$ + 10% HA microparticles scaffolds contrasts strong staining after 2 weeks incubation in osteogenic medium that was observed in previous studies in Chapter 3. Some expression of all three osteoblastic markers was evident on $P_{DL}LA$ + 10% nanoparticles scaffolds (both NRs and NPs).

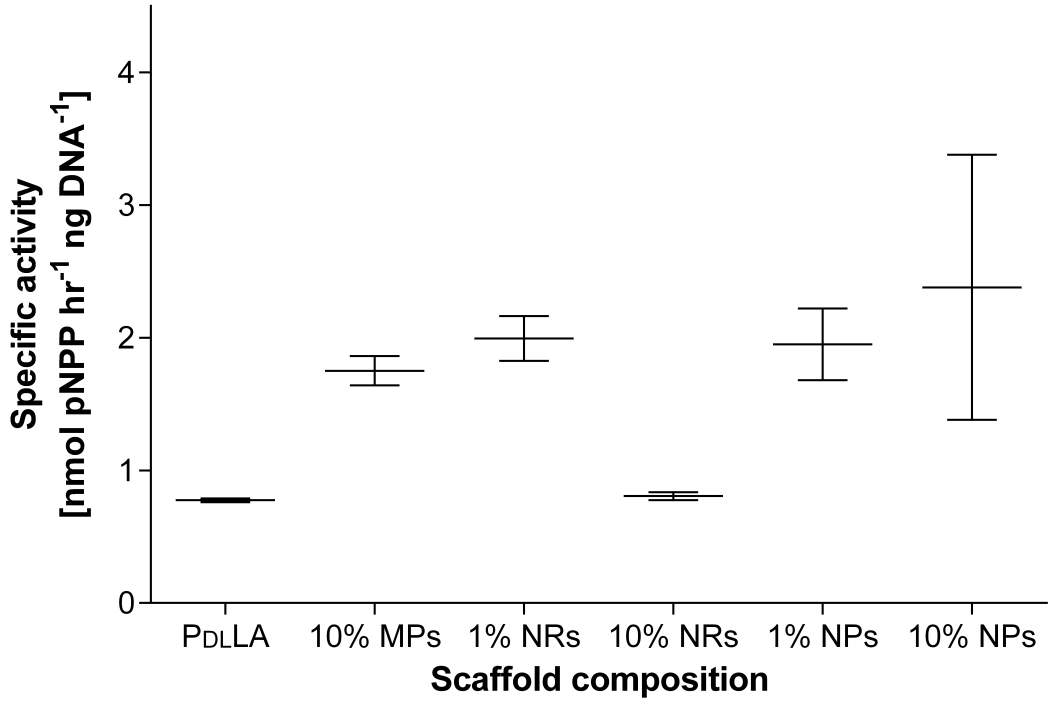

Figure 5.13: Mean specific ALP activity of MSCs cultured on different $scCO_2$ foamed $P_{DL}LA$:HA composition scaffolds for two weeks. SD error bars (n=4). No statistical significance at $P<0.05$ level.

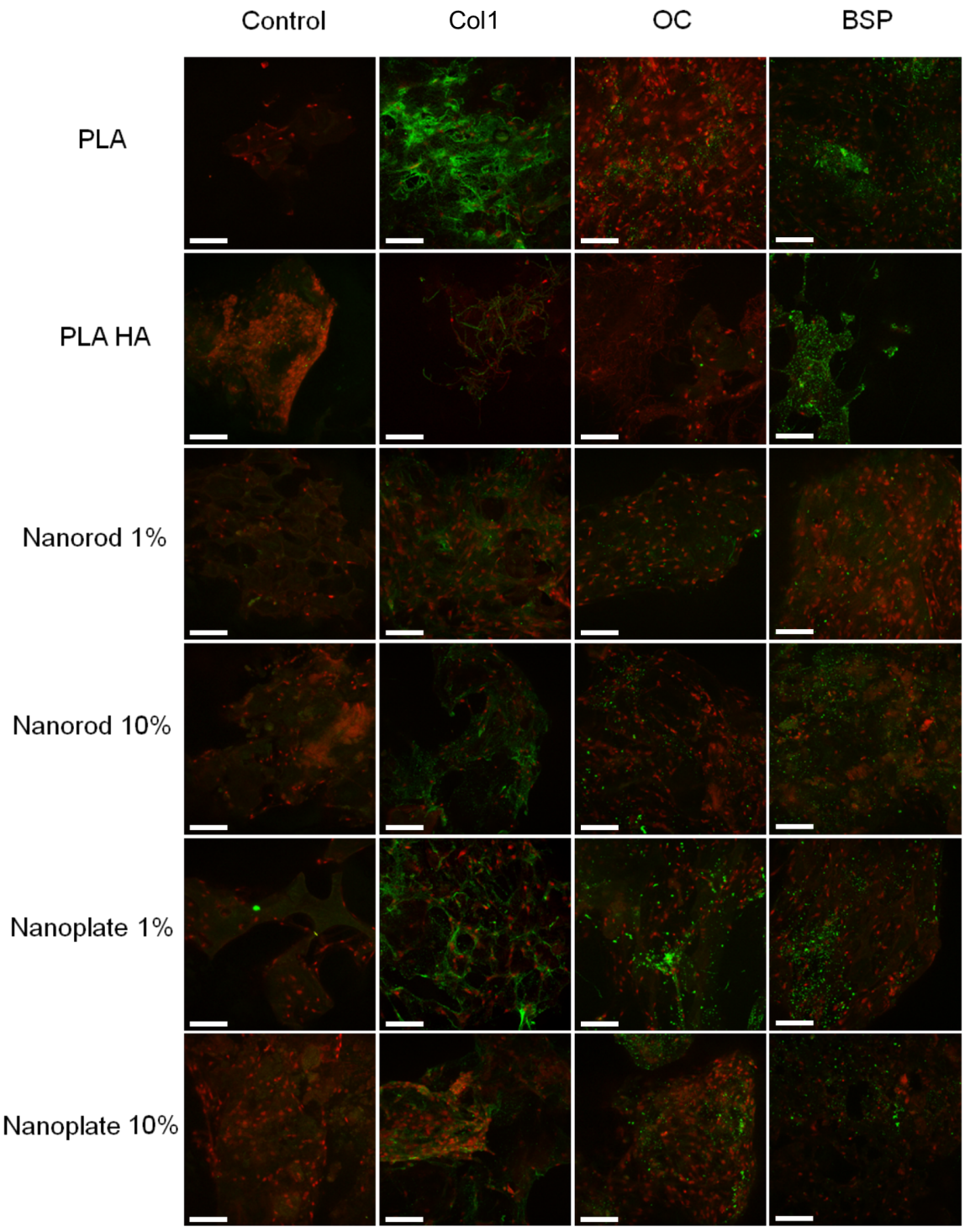

Figure 5.14: Collagen-1, Osteocalcin, and Bone sialoprotein immunostains (green) with DAPI nuclear counterstain (red) for different scCO$_2$ foamed P$_{DL}$LA:HA composition scaffolds following two week incubation with MSCs viewed under confocal microscopy. Scale bars = 100 μm.

The combination of cellular assays and immunohistochemical staining suggested that $P_{DL}LA$ + 1% NPs scaffolds may be more favourable than $P_{DL}LA$ + 10% HA microparticles. However, the differences observed were minor and the use of nanoparticles in $scCO_2$ foamed $P_{DL}LA$ scaffolds needs further investigation for application as allograft alternatives. Specifically, the study period should be extended to 4 weeks (the time for full osteoblastic differentiation), and mechanical shear testing is required. Additionally, focus should be placed on producing homogeneous distributions of particles within the scaffolds, and avoiding particle agglomeration to improve the mechanical strength and provide a greater surface area of osteoinductive HA.

Compressive dynamic mechanical analysis (DMA) tests were performed on $scCO_2$ foamed $P_{DL}LA$:HA composite scaffolds (10 wt.% HA microparticles, 1 wt.%, and 10 wt.% HA NRs and NPs). However, the results between identical samples varied widely with large standard deviations and for this reason the results were not included. The variation was attributed to heterogeneous distributions of HA particles within the scaffolds. Further DMA tests (dual cantilever bending) were conducted on $P_{DL}LA$:HA composite bars (results not included). The $P_{DL}LA$:HA composites were created by dispersing HA particles (through sonication and mixing) in a $P_{DL}LA$ solution in 1,4-dioxane, followed by venting then lyophilization. Thermogravimetric analysis of the composites confirmed presence of solvent within the $P_{DL}LA$:HA composite bars tested and it was for this reason the results were not included. These tests should be repeated and a $scCO_2$ solvent extraction step added prior to forming the $P_{DL}LA$:HA composites into uniform bars for mechanical characterisation.

5.4 Conclusion

Results presented in Chapter 3 demonstrated that the osteogenic differentiation of MSCs differed between cells cultured on $P_{DL}LA$ and $P_{DL}LGA$ scaffolds, a novel result. The work presented in this chapter was undertaken to investigate this. Polymer films were used rather than foamed scaffolds to remove any morphological differences that were present in the foamed scaffolds in Chapter 3. It was demonstrated that there were no significant quantitative differences in hMSCs cultured *in vitro* on $P_{DL}LA$ and $P_{DL}LGA$ films. Proliferation and osteogenic differentiation were assessed with WST-1 and ALP assays, respectively, at one week and two week time-points.

Qualitative immunohistochemical stains were also used to visualise any differences.

Collagen-1 immunohistochemical stains after 2 weeks demonstrated absence of collagen-1 in flat areas of P_{DL}LGA films; the same was not observed on P_{DL}LA and P_{DL}LA:P_{DL}LGA (50:50) films. The presence of col-1 was confirmed on ridged areas of all films, which demonstrated osteoblastic differentiation of cells on both polymers. Morphology, surface roughness, degradation rates, and polymer stiffness may all affect osteoblastic differentiation of cells cultured on these polymers. The wettability of the films was characterised, and there was no significant difference between P_{DL}LA and P_{DL}LGA films. Both polymers were matched for M_W and inherent viscosity according to manufacturerâĂŹs specification sheets.

Throughout the culture period the polymer films pulled away from the glass substrate and ridges were formed which affected the results. Spincoated films were used initially, followed by dipcoated films used in an attempt to avoid the formation of ridges. Clamping edges of the films to prevent changes to polymer film topology throughout culture is advised for a repeat experiment. Experiments should be extended to four weeks to allow for completion of osteogenic differentiation protocol and compare differences in MSC differentiation on P_{DL}LA and P_{DL}LGA scaffolds over this time period.

Within the literature and in Chapter 3 the importance of HA particles in scaffolds for bone regeneration is established. In Chapter 3 scaffolds incorporating HA microparticles demonstrated improved performance *in vivo*, which stimulated further studies. In this chapter human MSCs were seeded on milled $scCO_2$ foamed P_{DL}LA scaffolds containing either HA NRs or NPs at 1 wt.% and 10 wt.% concentrations, or microparticles at 10 wt.% concentration with milled $scCO_2$ foamed pure P_{DL}LA scaffolds as controls. The seeded milled scaffolds were impacted to mimic IBG and cultured for two weeks in osteogenic medium. There was evidence of improved MSC proliferation on scaffolds containing HA nanoparticles compared to HA microparticles. No significant differences in the yield stresses of all scaffold compositions tested were observed.

The osteoblastic differentiation of MSCs appeared enhanced on scaffolds containing 10 wt.% microparticles or 1 wt.% HA nanoparticles (for both rods or plates) compared to P_{DL}LA control scaffolds. Osteoblastic differentiation of MSCs was comparable between cells cultured on P_{DL}LA and P_{DL}LA + 10 wt.% NRs scaffolds. The results were inconclusive for P_{DL}LA + 10 wt.% HA NPs scaffolds. Scaffolds containing 10 wt.% HA nanoparticles morphologically differed from pure P_{DL}LA and P_{DL}LA + HA (10 wt.% MPs and 1 wt.% HA nanoparticles) scaffolds due to the high relative volume of HA nanoparticles, which affected

$scCO_2$ foaming, and the poor dispersion of particles within the scaffolds; morphological differences will have affected results observed and limit conclusions that can be drawn.

$P_{DL}LA$ + 1 wt.% HA nanoparticles provided equivalent compressive strength to other scaffolds and demonstrated improved MSC proliferation and differentiation with no quantiative differences between scaffolds containing NRs or NPs. Qualitatively, immunohistochemical stains demonstrated greater evidence of osteocalcin on $P_{DL}LA$ + 1 wt.% NRs.

The use of $scCO_2$ foamed $P_{DL}LA$ scaffolds containing 1% HA nanoparticles appeared the most promising scaffold formulation, of those tested, for MSC culture on the scaffolds when used for IBG. The volume of 1 wt.% HA NPs is roughly equivalent to that of 10 wt.% HA microparticles (as loosely packed powders). Greater proliferation and osteoblastic differentiation of MSCs was observed for cells cultured on $scCO_2$ foamed $P_{DL}LA$ containing 1 wt.% HA NPs than on $scCO_2$ foamed $P_{DL}LA$ foamed controls and those containing 10 wt.% HA microparticles.

Further work is required to improve the dispersion of nanoparticles within the scaffolds, characterise the mechanical properties of nanocomposites, optimise HA concentration, and characterise porosity and pore size. Organic solvents (chloroform or 1,4-dioxane) are utilised within the literature to create HA nanoparticle dispersions. The use of organic solvents in these scaffolds is undesirable, however $scCO_2$ may be investigated as an extraction process should nanoparticle containing scaffolds continue to offer improved results.

CHAPTER 6

Final conclusions

The current material used in impaction bone grafting to rebuild bone stock within the femur, allograft bone, is not ideal; inspite of this it remains the clinical "gold standard". The increasing number of revision hip arthroplasty procedures, which commonly require impaction bone grafting, and limited allograft supply, place increasing demand for an alternative. The risk of transmission of infectious agents is, however small, a present and real risk with the utilisation of allograft bone, and indeed all allogeneic tissue grafting. Allograft bone, unlike autograft bone, has no osteogenic properties, which can be introduced into an alternative by utilising stem cell populations, specifically MSCs.

The growth of the regenerative medicine field and the investigation of porous polymeric scaffolds introduced the possibility for alternative materials for bone repair. The properties of bone vary with location and function and the desired qualities in synthetic scaffolds for bone repair also change with the desired function. For revision hip arthroplasty a common prosthesis failure mechanism is femoral stem subsidence, where the implant sinks further into the femur than was desired with subsequent impairment to joint functionality; a resistance to the shear forces experienced within the femur is therefore desirable in graft materials. Material, such as allograft bone, is impacted into the femur and must also resist these impaction forces. Additionally, when cell populations are impacted with the graft material, it must be able to protect the cells from the forces to ensure that a viable cell population survives the implantation procedure.

The work presented within this thesis describes the performance of supercritical CO_2 foamed polymer scaffolds in experiments designed to determine the suitability of these scaffolds for impaction bone grafting. Allograft bone is milled in a bone mill to create small chips of bone for impaction bone grafting and $scCO_2$ foamed scaffolds were milled in this way for both *in vitro* and *in vivo* experiments contained within this thesis. In Chapter 3, mechanical shear experiments demonstrated the superiority of $scCO_2$ foamed scaffolds ($P_{DL}LA$ and $P_{DL}LGA$) over non-foamed scaffolds of the pure polymers and allograft bone. Cellular studies within the same chapter determined superiority in terms of proliferation and differentiation of MSCs on $scCO_2$ foamed scaffolds over non-foamed scaffolds and higher levels of osteoblastic differentiation after two weeks of MSCs on $P_{DL}LA$ scaffolds over $P_{DL}LGA$. The inclusion of 10 wt.% HA microparticles demonstrated no significant differences in shear resistance of milled $scCO_2$ foamed scaffolds of both polymers, and higher levels of osteoblastic differentiation of MSCs. These experiments also demonstrated survival of MSCs seeded on $scCO_2$ foamed scaffolds through a simulated impaction procedure.

The most promising formulation at this stage was $scCO_2$ foamed $P_{DL}LA$ scaffolds containing 10 wt.% HA microparticles. This was established through *in vitro* cellular experiments and a subcutaneous murine model. For the small-scale murine *in vivo* model $scCO_2$ foamed scaffolds were milled, sterilised, seeded with MSCs, and then impacted into open ended pots which were implanted for 5 weeks. Controls without MSCs were also used. The presence of bony matrix was detected within the implanted pots using μCT and significantly higher levels were observed within the pots containing $scCO_2$ foamed $P_{DL}LA$ scaffolds with 10 wt.% HA microparticles. Scaffolds containing HA implanted without MSCs showed significantly higher levels of new bony matrix than $P_{DL}LA$ scaffolds without HA implanted with MSCs. This demonstrated a high level of osteoinduction for $P_{DL}LA$ scaffolds containing HA.

In Chapter 4 $scCO_2$ foamed $P_{DL}LA$ scaffolds containing 10 wt.% HA microparticles were investigated in a large animal *in vivo* model. Autologous ovine MSCs were seeded on the scaffolds prior to implantation and controls without cells were also used. Histological staining and μCT analysis demonstrated the formation of new bone within the condyle defects. This was far more pronounced within condyles filled with milled $scCO_2$ foamed scaffolds without MSCs. This result was unexpected as results reported within literature demonstrate improved bone regeneration when MSCs are utilised. Parallel *in vitro* studies suggested limited osteoblastic differentiation of the MSCs and the ovine cells likely required different differentiation media to human cells which were used in the investigations prior to the ovine *in vivo* study. *In vivo* incubation of $scCO_2$ foamed $P_{DL}LA$ + 10 wt.% HA microparticles for 12 weeks within an ovine condyle defect demonstrated formation of new bone and indicated over time full healing of the defect site may be anticipated. There is potential for further improvement of the scaffolds through inclusion of osteoinductive factors such as BMP-2 that can be incorporated within the scaffolds through the $scCO_2$ foaming process. Additionally, further *in vivo* studies that utilise an optimised ovine osteoblastic differentiation procedure for MSCs of the appropriate animal (e.g. sheep) are likely to demonstrate greater healing and improvement in line with findings reported within the literature.

Chapter 4 also contained studies that demonstrated the potential scale-up of manufacturing $scCO_2$ foamed scaffolds. The potential to produce one hundred and eighty $scCO_2$ foamed scaffolds (54 g) within a single vessel in a single batch was shown in a 1000 ml vessel. This represents a scale-up of 3000% compared to the six scaffolds per batch (1.8 g) capable in the 60 ml lab-scale autoclave used to produce the scaffolds utilised in the *in vivo* and *in vitro*

studies within this thesis. The scaffolds produced in the 1000 ml vessel had little variation in porosity and mean pore size based on their location within the vessel when foamed. While the porosities of scaffolds produced in the larger vessel matched those produced in the 60 ml autoclave their internal structures differed; optimisation of the $scCO_2$ foaming protocol to match scaffolds produced in the larger vessel to those produced in the smaller vessel is required. Furthermore, a repeat of experiments performed with scaffolds produced in the 60 ml autoclave with scaffolds produced in the 1000 ml vessel would further confirm the potential scale-up of $scCO_2$ foamed scaffolds. The evidence presented here provides proof-of-concept of the potential to scale-up the $scCO_2$ foaming process. This scale-up potential is necessary for $scCO_2$ foamed scaffolds to be a viable synthetic alternative to allograft bone.

The work in Chapter 5 investigated differences observed in MSC osteoblastic differentiation when cultured on $P_{DL}LA$ scaffolds to $P_{DL}LGA$ scaffolds. Utilisation of polymer films rather than foamed scaffolds removed morphological differences in the scaffolds that were present in the foamed scaffolds. These experiments were inconclusive due to the polymer films lifting away from the glass substrates and becoming crumpled. There was evidence of collagen-1 on both $P_{DL}LA$ and $P_{DL}LGA$ films in crumpled regions, demonstrating osteoblastic differentiation on both films. The collagen-1 expression observed on $P_{DL}LA$ films in flat regions was not observed on $P_{DL}LGA$ films. Differences in the osteoblastic differentiation may be due to several variables that include morphology, surface roughness, degradation rates, polymer stiffness. The wettability of the films was characterised, and there was no significant difference, while the polymer M_Ws and inherent viscosities were matched for $P_{DL}LA$ and $P_{DL}LGA$ for these studies.

The importance of HA particles demonstrated in Chapter 3 through superior performance *in vivo* of $scCO_2$ scaffolds $P_{DL}LA$ scaffolds + 10 wt.% HA microparticles stimulated further studies. The incorporation of HA nanoparticles was investigated in $scCO_2$ foamed $P_{DL}LA$ scaffolds. While aggregation of nanoparticles was a problem, MSCs cultured on scaffolds containing 1 wt.% HA nanoparticles, a similar volume to 10 wt.% HA microparticles (of loosely packed powder), demonstrated greater proliferation and osteoblastic differentiation to MSCs cultured on $scCO_2$ foamed $P_{DL}LA$ containing 10 wt.% HA and no HA. To overcome aggregation of nanoparticles and create homogeneous dispersions of nanoparticles within $scCO_2$ foamed scaffolds methods in the literature utilise organic solvents such as chloroform or 1,4-dioxane. This is not desirable, however, and the $scCO_2$ foaming process may also be investigated in the future as an extraction process, should nanoparticle containing scaffolds

continue to offer improved results over microparticles.

Overall, the work presented in this thesis has demonstrated that $scCO_2$ foaming has the potential to create polymeric scaffolds suitable for impaction bone grafting and production on an industrial scale would be possible. Optimisation of specific formulations to be utilised remains to be performed. From the studies presented here $P_{DL}LA$ ($M_W \approx 110$ kDa) scaffolds containing HA microparticles (10 wt.%) have the potential to regenerate bone *in vivo* both with and without MSCs.

References

[1] PURCELL, M., M HOWDLE, S., M SHAKESHEFF, K. and J WHITE, L. (2013) Supercritical Fluid Processing of Materials for Regenerative Medicine. *Recent Patents on Regenerative Medicine* 3, 3, 237–248

[2] TANG, M., PURCELL, M., STEELE, J.A., LEE, K.Y., MCCULLEN, S., SHAKESHEFF, K.M., BISMARCK, A., STEVENS, M.M., HOWDLE, S.M. and WILLIAMS, C.K. (2013) Porous Copolymers of ϵ-Caprolactone as Scaffolds for Tissue Engineering. *Macromolecules* 46, 20, 8136–8143

[3] TAYTON, E.R., SMITH, J.O., EVANS, N., DICKINSON, A., AARVOLD, A., KALRA, S., PURCELL, M., HOWDLE, S., DUNLOP, D.G. and OREFFO, R.O. (2013) Effects of Setting Bone Cement on Tissue-Engineered Bone Graft: a Potential Barrier to Clinical Translation? *The Journal of Bone & Joint Surgery* 95, 8, 736–743

[4] TAYTON, E., FAHMY, S., PURCELL, M., AARVOLD, A., SMITH, J.O., KALRA, S., BRISCOE, A., LANHAM, S., HOWDLE, S., SHAKESHEFF, K., DUNLOP, D.G. and OREFFO, R.O.C. (2012) An analysis of polymer type and chain length for use as a biological composite graft extender in impaction bone grafting: A mechanical and biocompatibility study. *Journal of Biomedical Materials Research Part A* 100A, 12, 3211–3219

[5] TAYTON, E., PURCELL, M., AARVOLD, A., SMITH, J., KALRA, S., BRISCOE, A., SHAKESHEFF, K., HOWDLE, S., DUNLOP, D. and OREFFO, R. (2012) Supercritical CO_2 fluid-foaming of polymers to increase porosity: A method to improve the mechanical and biocompatibility characteristics for use as a potential alternative to allografts in impaction bone grafting? *Acta biomaterialia* 8, 5, 1918–1927

[6] MASON, C. and DUNNILL, P. (2008) A brief definition of regenerative medicine. *Regenerative medicine* 3, 1, 1–5

[7] HASELTINE, W.A. (2001) The emergence of regenerative medicine: a new field and a new society. *e-biomed: the journal of regenerative medicine* 2, 4, 17–23

[8] MIRONOV, V., VISCONTI, R. and MARKWALD, R. (2004) What is regenerative

medicine? Emergence of applied stem cell and developmental biology. *Expert opinion on biological therapy* 4, 6, 773–781

[9] GREENWOOD, H.L., THORSTEINSDÓTTIR, H., PERRY, G., RENIHAN, J., SINGER, P. and DAAR, A. (2006) Regenerative medicine: new opportunities for developing countries. *International journal of biotechnology* 8, 1, 60–77

[10] VACANTI, C.A. (2006) History of tissue engineering and a glimpse into its future. *Tissue Engineering* 12, 5, 1137–1142

[11] LANGER, R. and VACANTI, J.P. (1993) Tissue engineering. *Science* 260, 5110, 920–6

[12] VACANTI, J.P. (1988) Beyond TransplantationThird Annual Samuel Jason Mixter Lecture. *Archives of Surgery* 123, 5, 545–549

[13] VACANTI, C. and VACANTI, J. (1991) Functional organ replacement: the new technology of tissue engineering. *Surgical Technology International* , 43–49

[14] DEPARTMENT OF HEALTH & HUMAN SERVICES, U.S., 2020: A New Vision–A Future for Regenerative Medicine.

[15] TRUST, B.L. (2009), British Liver Trust analysis of Office for National Statistics mortality statistics covering all deaths related to liver dysfunction covering ICD K70-76 and other codes including C22-24 (liver cancer), and B15-B19 (viral hepatitis)

[16] HOYERT, D. and XU, J. (2012), Deaths: preliminary data for 2011. National Vital Statistics Reports

[17] HUTMACHER, D.W. (2000) Scaffolds in tissue engineering bone and cartilage. *Biomaterials* 21, 24, 2529 – 2543, orthopaedic Polymeric Biomaterials: Applications of Biodegradables

[18] PARK, J.B. (1984) *Biomaterials science and engineering*, volume 4. Plenum Press New York

[19] AGRAWAL, C.M. (1998) Reconstructing the human body using biomaterials. *JOM* 50, 1, 31–35

[20] LEE, C.H., SINGLA, A. and LEE, Y. (2001) Biomedical applications of collagen. *International journal of pharmaceutics* 221, 1, 1–22

[21] ZHANG, Y., CHENG, X., WANG, J., WANG, Y., SHI, B., HUANG, C., YANG, X. and LIU, T. (2006) Novel chitosan/collagen scaffold containing transforming growth factor-β1 DNA for periodontal tissue engineering. *Biochemical and biophysical research communications* 344, 1, 362–369

[22] MA, L., GAO, C., MAO, Z., ZHOU, J., SHEN, J., HU, X. and HAN, C. (2003) Collagen/chitosan porous scaffolds with improved biostability for skin tissue engineering. *Biomaterials* 24, 26, 4833–4841

[23] LEE, C., GRODZINSKY, A. and SPECTOR, M. (2001) The effects of cross-linking of collagen-glycosaminoglycan scaffolds on compressive stiffness, chondrocyte-mediated contraction, proliferation and biosynthesis. *Biomaterials* 22, 23, 3145–3154

[24] PARK, S.N., PARK, J.C., KIM, H.O., SONG, M.J. and SUH, H. (2002) Characterization of porous collagen/hyaluronic acid scaffold modified by 1-ethyl-3-(3-dimethylaminopropyl) carbodiimide cross-linking. *Biomaterials* 23, 4, 1205–1212

[25] YANNAS, I.V. (1990) Biologically active analogues of the extracellular matrix: artificial skin and nerves. *Angewandte Chemie International Edition in English* 29, 1, 20–35

[26] BOYCE, S.T., CHRISTIANSON, D.J. and HANSBROUGH, J.F. (1988) Structure of a collagen-GAG dermal skin substitute optimized for cultured human epidermal keratinocytes. *Journal of biomedical materials research* 22, 10, 939–957

[27] YAMADA, N., UCHINUMA, E. and KUROYANAGI, Y. (1999) Clinical evaluation of an allogeneic cultured dermal substitute composed of fibroblasts within a spongy collagen matrix. *Scandinavian journal of plastic and reconstructive surgery and hand surgery* 33, 2, 147–154

[28] MURATA, M., HUANG, B.Z., SHIBATA, T., IMAI, S., NAGAL, N. and ARISUE, M. (1999) Bone augmentation by recombinant human BMP-2 and collagen on adult rat parietal bone. *International journal of oral and maxillofacial surgery* 28, 3, 232–237

[29] REDDI, A.H. (2000) Morphogenesis and tissue engineering of bone and cartilage: inductive signals, stem cells, and biomimetic biomaterials. *Tissue Engineering* 6, 4, 351–359

[30] MORONI, A., CAJA, V., EGGER, E., TRINCHESE, L. and CHAO, E. (1994) Histomorphometry of hydroxyapatite coated and uncoated porous titanium bone implants. *Biomaterials* 15, 11, 926–930

[31] GEESINK, R., DE GROOT, K. and KLEIN, C. (1988) Bonding of bone to apatite-coated implants. *Journal of Bone & Joint Surgery, British Volume* 70, 1, 17–22

[32] YEN, S., GUO, M. and ZAN, H. (2001) Characterization of electrolytic ZrO_2 coating on Co–Cr–Mo implant alloys of hip prosthesis. *Biomaterials* 22, 2, 125–133

[33] VAN HAAREN, E., SMIT, T., PHIPPS, K., WUISMAN, P., BLUNN, G. and HEYLIGERS, I. (2005) Tricalcium-phosphate and hydroxyapatite bone-graft extender for use in impaction grafting revision surgery AN IN VITRO STUDY ON HUMAN FEMORA. *Journal of Bone & Joint Surgery, British Volume* 87, 2, 267–271

[34] BERRY, D.J., HARMSEN, W.S., CABANELA, M.E. and MORREY, B.F. (2002) Twenty-five-Year Survivorship of Two Thousand Consecutive Primary Charnley Total Hip Replacements Factors Affecting Survivorship of Acetabular and Femoral Components. *The Journal of Bone & Joint Surgery* 84, 2, 171–177

[35] BIRRELL, F., JOHNELL, O. and SILMAN, A. (1999) Projecting the need for hip replacement over the next three decades: influence of changing demography and threshold for surgery. *Annals of the rheumatic diseases* 58, 9, 569–572

[36] REGISTRY, N.J. (2012), National Joint Registry for England and Wales 9^{th} Annual Report 2012

[37] ORNSTEIN, E. (2002) Hip revisions with impacted morselized allograft bone and cement. *Acta Orthopaedica* 73, s306, 1–66

[38] SCHMALZRIED, T.P., KWONG, L.M., JASTY, M., SEDLACEK, R.C., HAIRE, T.C., O'CONNOR, D.O., BRAGDON, C.R., KABO, J.M., MALCOLM, A.J. and HARRIS, W.H. (1992) The mechanism of loosening of cemented acetabular components in total hip arthroplasty: analysis of specimens retrieved at autopsy. *Clinical orthopaedics and related research* 274, 60–78

[39] WIRTH, M.A., AGRAWAL, C.M., MABREY, J.D., DEAN, D.D., BLANCHARD, C.R., MILLER, M.A. and ROCKWOOD, C.A. (1999) Isolation and Char-

acterization of Polyethylene Wear Debris Associated with Osteolysis Following Total Shoulder Arthroplasty*. *The Journal of Bone & Joint Surgery* 81, 1, 29–37

[40] SCHMALZRIED, T., JASTY, M. and HARRIS, W. (1992) Periprosthetic bone loss in total hip arthroplasty. Polyethylene wear debris and the concept of the effective joint space. *The Journal of bone and joint surgery. American volume* 74, 6, 849–863

[41] MABREY, J.D., AFSAR-KESHMIRI, A., ENGH, G.A., SYCHTERZ, C.J., WIRTH, M.A., ROCKWOOD, C.A. and AGRAWAL, C. (2002) Standardized analysis of UHMWPE wear particles from failed total joint arthroplasties. *Journal of biomedical materials research* 63, 5, 475–483

[42] ABU-AMER, Y., DARWECH, I. and CLOHISY, J.C. (2007) Aseptic loosening of total joint replacements: mechanisms underlying osteolysis and potential therapies. *Arthritis Research and Therapy* 9, 1, S6

[43] GREEN, T.R., FISHER, J., MATTHEWS, J.B., STONE, M.H. and INGHAM, E. (2000) Effect of size and dose on bone resorption activity of macrophages by in vitro clinically relevant ultra high molecular weight polyethylene particles. *Journal of biomedical materials research* 53, 5, 490–497

[44] CLOHISY, J.C., CALVERT, G., TULL, F., MCDONALD, D. and MALONEY, W.J. (2004) Reasons for revision hip surgery: a retrospective review. *Clinical orthopaedics and related research* 429, 188–192

[45] SLOOFF, T., SCHIMMEL, J. and BUMA, P. (1993) Cemented fixation with bone grafts. *The Orthopedic clinics of North America* 24, 4, 667

[46] GIE, G., LINDER, L., LING, R., SIMON, J.P., SLOOFF, T., TIMPERLEY, A. *et al.* (1993) Contained morselized allograft in revision total hip arthroplasty. Surgical technique. *The Orthopedic clinics of North America* 24, 4, 717

[47] CUE, G., LING, R. and LINDER, L. (1993) Impacted cancellous allografts and cement for revision total hip arthroplasty. *Journal of Bone and Joint Surgery* 21

[48] PEKKARINEN, J., ALHO, A., LEPISTÖ, J., YLIKOSKI, M., YLINEN, P. and PAAVILAINEN, T. (2000) Impaction bone grafting in revision hip surgery A HIGH INCIDENCE OF COMPLICATIONS. *Journal of Bone & Joint Surgery, British Volume* 82, 1, 103–107

[49] DAWSON, J.I. and OREFFO, R.O. (2008) Bridging the regeneration gap: Stem cells, biomaterials and clinical translation in bone tissue engineering. *Archives of Biochemistry and Biophysics* 473, 2, 124 – 131

[50] ILAN, D.I. and LADD, A.L. (2002) Bone graft substitutes. *Operative Techniques in Plastic and Reconstructive Surgery* 9, 4, 151–160

[51] GIANNOUDIS, P.V., DINOPOULOS, H. and TSIRIDIS, E. (2005) Bone substitutes: an update. *Injury* 36, 3, S20–S27

[52] HIDAKA, C., CUNNINGHAM, M.E., RODEO, S.A., MAHER, S.A. and ZHU, W. (2006) Modern biologics used in orthopaedic surgery. *Current opinion in rheumatology* 18, 1, 74–79

[53] BOYCE, T., EDWARDS, J. and SCARBOROUGH, N. (1999) Allograft bone: the influence of processing on safety and performance. *Orthopedic Clinics of North America* 30, 4, 571–581

[54] BOLLAND, B.J., PARTRIDGE, K., TILLEY, S., NEW, A.M., DUNLOP, D.G. and OREFFO, R.O. (2006) Biological and mechanical enhancement of impacted allograft seeded with human bone marrow stromal cells: potential clinical role in impaction bone grafting. *Regenerative medicine* 1, 4, 457–467

[55] JONES, A., FOONG, T., NEW, A., BOLLAND, B., POUND, J., DUNLOP, D. and OREFFO, R. (2009) The effect of skeletal stem cells, hydroxyapatite coated stem cells and collagen coated allograft on the biomechanical properties of impacted bone graft. *Eur Cell Mater* 18, 26

[56] TILLEY, S., BOLLAND, B.J., PARTRIDGE, K., NEW, A.M., LATHAM, J.M., DUNLOP, D.G. and OREFFO, R.O. (2006) Taking tissue-engineering principles into theater: augmentation of impacted allograft with human bone marrow stromal cells. *Regenerative medicine* 1, 5, 685–692

[57] SIMONDS, R., HOLMBERG, S.D., HURWITZ, R.L., COLEMAN, T.R., BOTTENFIELD, S., CONLEY, L.J., KOHLENBERG, S.H., CASTRO, K.G., DAHAN, B.A., SCHABLE, C.A. *et al.* (1992) Transmission of human immunodeficiency virus type 1 from a seronegative organ and tissue donor. *New England Journal of Medicine* 326, 11, 726–732

[58] GREENWALD, A.S., BODEN, S.D., GOLDBERG, V.M., KHAN, Y., LAURENCIN, C.T. and ROSIER, R.N. (2001) Bone-graft substitutes: facts, fictions, and applications. *The Journal of Bone & Joint Surgery* 83, S98–103

[59] GALEA, G., KOPMAN, D. and GRAHAM, B. (1998) Supply and demand of bone allograft for revision hip surgery in Scotland. *Journal of Bone & Joint Surgery, British Volume* 80, 4, 595–599

[60] HUO, M.H., FRIEDLAENDER, G.E. and SALVATI, E.A. (1992) Bone graft and total hip arthroplasty: a review. *The Journal of arthroplasty* 7, 2, 109–120

[61] ALBREKTSSON, T. and JOHANSSON, C. (2001) Osteoinduction, osteoconduction and osseointegration. *European Spine Journal* 10, 2, S96–S101

[62] VERT, M., LI, S., SPENLEHAUER, G. and GUERIN, P. (1992) Bioresorbability and biocompatibility of aliphatic polyesters. *Journal of Materials Science: Materials in Medicine* 3, 6, 432–446

[63] BAYLISS, L., MAHONEY, D.J. and MONK, P. (2012) Normal bone physiology, remodelling and its hormonal regulation. *Surgery (Oxford)* 30, 2, 47–53

[64] WILLIAMS, P.L. *et al.* (1995) *Gray's anatomy*, volume 58. Churchill livingstone New York

[65] PRICE, J., OYAJOBI, B. and RUSSELL, R. (1994) The cell biology of bone growth. *European journal of clinical nutrition* 48, S131

[66] BARON, R. (1989) Molecular mechanisms of bone resorption by the osteoclast. *The Anatomical Record* 224, 2, 317–324

[67] SAFTIG, P., HUNZIKER, E., WEHMEYER, O., JONES, S., BOYDE, A., ROMMERSKIRCH, W., MORITZ, J.D., SCHU, P. and VON FIGURA, K. (1998) Impaired osteoclastic bone resorption leads to osteopetrosis in cathepsin-K-deficient mice. *Proceedings of the National Academy of Sciences* 95, 23, 13453–13458

[68] STREET, J., BAO, M., BUNTING, S., PEALE, F.V., FERRARA, N., STEINMETZ, H., HOEFFEL, J., CLELAND, J.L., DAUGHERTY, A., VAN BRUGGEN, N. *et al.* (2002) Vascular endothelial growth factor stimulates bone repair by promoting angiogenesis and bone turnover. *Proceedings of the National Academy of Sciences* 99, 15, 9656–9661

[69] LEE, S.H. and SHIN, H. (2007) Matrices and scaffolds for delivery of bioactive molecules in bone and cartilage tissue engineering. *Advanced drug delivery reviews* 59, 4, 339–359

[70] CHEN, F.M., ZHAO, Y.M., WU, H., DENG, Z.H., WANG, Q.T., ZHOU, W., LIU, Q., DONG, G.Y., LI, K., WU, Z.F. *et al.* (2006) Enhancement of periodontal tissue regeneration by locally controlled delivery of insulin-like growth factor-I from dextran–co-gelatin microspheres. *Journal of controlled release* 114, 2, 209–222

[71] KAWAGUCHI, H., KUROKAWA, T., HANADA, K., HIYAMA, Y., TAMURA, M., OGATA, E. and MATSUMOTO, T. (1994) Stimulation of fracture repair by recombinant human basic fibroblast growth factor in normal and streptozotocin-diabetic rats. *Endocrinology* 135, 2, 774–781

[72] KATO, T., KAWAGUCHI, H., HANADA, K., AOYAMA, I., HIYAMA, Y., NAKAMURA, T., KUZUTANI, K., TAMURA, M., KUROKAWA, T. and NAKAMURA, K. (1998) Single local injection of recombinant fibroblast growth factor-2 stimulates healing of segmental bone defects in rabbits. *Journal of orthopaedic research* 16, 6, 654–659

[73] QUARTO, N. and LONGAKER, M.T. (2006) FGF-2 inhibits osteogenesis in mouse adipose tissue-derived stromal cells and sustains their proliferative and osteogenic potential state. *Tissue engineering* 12, 6, 1405–1418

[74] FERRARA, N., GERBER, H.P. and LECOUTER, J. (2003) The biology of VEGF and its receptors. *Nature medicine* 9, 6, 669–676

[75] STANGENBERG, L., SCHAEFER, D.J., BUETTNER, O., OHNOLZ, J., MÖBEST, D., HORCH, R.E., STARK, G.B. and KNESER, U. (2005) Differentiation of osteoblasts in three-dimensional culture in processed cancellous bone matrix: quantitative analysis of gene expression based on real-time reverse transcription-polymerase chain reaction. *Tissue engineering* 11, 5-6, 855–864

[76] VACANTI, C.A., BONASSAR, L.J., VACANTI, M.P. and SHUFFLEBARGER, J. (2001) Replacement of an avulsed phalanx with tissue-engineered bone. *New England Journal of Medicine* 344, 20, 1511–1514

[77] DROSSE, I., VOLKMER, E., CAPANNA, R., BIASE, P.D., MUTSCHLER, W. and SCHIEKER, M. (2008) Tissue engineering for bone defect healing: an update on a multi-component approach. *Injury* 39, S9–S20

[78] HENCH, L.L. (2006) The story of Bioglass®. *Journal of Materials Science: Materials in Medicine* 17, 11, 967–978

[79] SEEBACH, C., SCHULTHEISS, J., WILHELM, K., FRANK, J. and HENRICH, D. (2010) Comparison of six bone-graft substitutes regarding to cell seeding efficiency, metabolism and growth behaviour of human mesenchymal stem cells (MSC) *in vitro*. *Injury* 41, 7, 731–738

[80] TRACY, B.M. and DOREMUS, R. (1984) Direct electron microscopy studies of the boneâĂŤhydroxylapatite interface. *Journal of biomedical materials research* 18, 7, 719–726

[81] MALAFAYA, P.B., SILVA, G.A. and REIS, R.L. (2007) Natural–origin polymers as carriers and scaffolds for biomolecules and cell delivery in tissue engineering applications. *Advanced drug delivery reviews* 59, 4, 207–233

[82] REZWAN, K., CHEN, Q., BLAKER, J. and BOCCACCINI, A.R. (2006) Biodegradable and bioactive porous polymer/inorganic composite scaffolds for bone tissue engineering. *Biomaterials* 27, 18, 3413 – 3431

[83] RADANO, C.P., BAKER, G.L. and SMITH, M.R. (2000) Stereoselective polymerization of a racemic monomer with a racemic catalyst: direct preparation of the polylactic acid stereocomplex from racemic lactide. *Journal of the American Chemical Society* 122, 7, 1552–1553

[84] IANNACE, S., MAFFEZZOLI, A., LEO, G. and NICOLAIS, L. (2001) Influence of crystal and amorphous phase morphology on hydrolytic degradation of PLLA subjected to different processing conditions. *Polymer* 42, 8, 3799–3807

[85] GILDING, D. and REED, A. (1979) Biodegradable polymers for use in surgery—polyglycolic/poly (actic acid) homo-and copolymers: 1. *Polymer* 20, 12, 1459–1464

[86] ENGELBERG, I. and KOHN, J. (1991) Physico-mechanical properties of degradable polymers used in medical applications: a comparative study. *Biomaterials* 12, 3, 292–304

[87] SÖDERGÅRD, A. and STOLT, M. (2002) Properties of lactic acid based polymers and their correlation with composition. *Progress in Polymer Science* 27, 6, 1123–1163

[88] SHEN, Z.R., ZHU, J.H. and MA, Z. (1993) Synthesis and characterization of poly (DL-lactic acid/glycolic acid). *Die Makromolekulare Chemie, Rapid Communications* 14, 7, 457–460

[89] PUPPI, D., CHIELLINI, F., PIRAS, A. and CHIELLINI, E. (2010) Polymeric materials for bone and cartilage repair. *Progress in Polymer Science* 35, 4, 403–440

[90] SIPARSKY, G.L., VOORHEES, K.J. and MIAO, F. (1998) Hydrolysis of polylactic acid (PLA) and polycaprolactone (PCL) in aqueous acetonitrile solutions: autocatalysis. *Journal of environmental polymer degradation* 6, 1, 31–41

[91] GRIZZI, I., GARREAU, H., LI, S. and VERT, M. (1995) Hydrolytic degradation of devices based on poly (DL-lactic acid) size-dependence. *Biomaterials* 16, 4, 305–311

[92] LIAO, C.J., CHEN, C.F., CHEN, J.H., CHIANG, S.F., LIN, Y.J. and CHANG, K.Y. (2002) Fabrication of porous biodegradable polymer scaffolds using a solvent merging/particulate leaching method. *Journal of biomedical materials research* 59, 4, 676–681

[93] MIKOS, A.G. and TEMENOFF, J.S. (2000) Formation of highly porous biodegradable scaffolds for tissue engineering. *Electronic Journal of Biotechnology* 3, 2, 23–24

[94] SCHUGENS, C., MAQUET, V., GRANDFILS, C., JÉRÔME, R. and TEYSSIE, P. (1996) Polylactide macroporous biodegradable implants for cell transplantation. II. Preparation of polylactide foams by liquid-liquid phase separation. *Journal of Biomedical Materials Research* 30, 4, 449–461

[95] AVERILL, B. and ELDREDGE, P. *Principles of General Chemistry (v. 1.0)*. unknown

[96] CAGNIARD DE LA TOUR, C. (1822) Exposé de quelques resultats obtenus par l'action combinée de la chaleur et de la compression sur certaines liquides, tels que l'eau, l'éther sulfurique et l'essence de pétrole rectifié [Report on some results obtained by the combined action of heat and pressure on certain liquids, such as water, alcohol, sulfuric ether and petroleum distillate]. *Ann. Chim. et Phys.*

[97] TAI, H., MATHER, M.L., HOWARD, D., WANG, W., WHITE, L.J., CROWE, J.A., MORGAN, S.P., CHANDRA, A., WILLIAMS, D.J., HOWDLE, S.M. *et al.* (2007) Control of pore size and structure of tissue engineering scaffolds produced by supercritical fluid processing. *Eur Cell Mater* 14, 64–77

[98] DAVIES, O.R., LEWIS, A.L., WHITAKER, M.J., TAI, H., SHAKESHEFF, K.M. and HOWDLE, S.M. (2008) Applications of supercritical CO2 in the fabrication of polymer systems for drug delivery and tissue engineering. *Advanced drug delivery reviews* 60, 3, 373–387

[99] DE PONTI, R., TORRICELLI, C., MARTINI, A. and LARDINI, E. (1991), Use of supercritical fluids to obtain porous sponges of biodegradable polymers

[100] MARTINI-VEDENSKY, J.E., SUH, N.P. and WALDMAN, F.A. (1982), Microcellular closed cell foams and their method of manufacture

[101] HARDENBROOK, S.B., HARASTA JR., L.P., FAULKENBERRY, S.T. and BOMBA, R.D. (1987), Method for producing microcellular foamed plastic material with smooth integral skin

[102] CHA, S.W., SUH, N.P., BALDWIN, D.F. and PARK, C.B. (1991), Microcellular thermoplastic foamed with supercritical fluid

[103] GOEL, S.K. and BECKMAN, E.J. (1992) Modelling the swelling of crosslinked elastomers by supercritical fluids. *Polymer* 33, 23, 5032–5039

[104] GOEL, S.K. and BECKMAN, E.J. (1993) Plasticization of poly(methyl methacrylate) (PMMA) networks by supercritical carbon dioxide. *Polymer* 34, 7, 1410–1417

[105] GOEL, S.K. and BECKMAN, E.J. (1994) Generation of microcellular polymeric foams using supercritical carbon dioxide. I: Effect of pressure and temperature on nucleation. *Polymer Engineering & Science* 34, 14, 1137–1147

[106] GOEL, S.K. and BECKMAN, E.J. (1994) Generation of microcellular polymeric foams using supercritical carbon dioxide. II: Cell growth and skin formation. *Polymer Engineering & Science* 34, 14, 1148–1156

[107] MOONEY, D.J., BALDWIN, D.F., SUH, N.P., VACANTI, J.P. and LANGER, R. (1996) Novel approach to fabricate porous sponges of poly(d,l-lactic-co-glycolic acid) without the use of organic solvents. *Biomaterials* 17, 14, 1417–1422

[108] HILE, D.D., AMIRPOUR, M.L., AKGERMAN, A. and PISHKO, M.V. (2000) Active growth factor delivery from poly(d,l-lactide-co-glycolide) foams prepared in supercritical {CO2}. *Journal of Controlled Release* 66, 2Ãćâ Ćňâ ĂIJ3, 177 – 185

[109] RICHARDSON, T.P., PETERS, M.C., ENNETT, A.B. and MOONEY, D.J. (2001) Polymeric system for dual growth factor delivery. *Nat Biotech* 19, 11, 1029–1034

[110] SHERIDAN, M.H., SHEA, L.D., PETERS, M.C. and MOONEY, D.J. (2000) Bioabsorbable polymer scaffolds for tissue engineering capable of sustained growth factor delivery. *Journal of Controlled Release* 64, 1Ãćâ Ćňâ ĂIJ3, 91–102

[111] HOWDLE, S.M., WATSON, M.S., WHITAKER, M.J., POPOV, V.K., DAVIES, M.C., MANDEL, F.S., WANG, J.D. and SHAKESHEFF, K.M. (2001) Supercritical fluid mixing: preparation of thermally sensitive polymer composites containing bioactive materials. *Chemical Communications* , 1, 109–110

[112] YEO, S.D., LIM, G.B., DEBENDETTI, P.G. and BERNSTEIN, H. (1993) Formation of microparticulate protein powder using a supercritical fluid antisolvent. *Biotechnology and Bioengineering* 41, 3, 341–346

[113] SUBRAMANIAM, B., RAJEWSKI, R.A. and SNAVELY, K. (1997) Pharmaceutical processing with supercritical carbon dioxide. *Journal of Pharmaceutical Sciences* 86, 8, 885–890

[114] PILZ, V. and RUPP, R. (1981), Process for rendering solids sterile

[115] FISCHER, W. and MULLER, B.W. (1991), Method and apparatus for the manufacture of a product having a substance embedded in a carrier

[116] HOWDLE, S.M. and POPOV, V. (1998), Biofunctional polymers prepared in supercritical fluid

[117] SAND, M.L. (1986), Method for impregnating a thermoplastic polymer

[118] RICHARD, R.E. (2002), Using supercritical fluids to infuse therapeutic on a medical device

[119] MCHUGH, M., SHEN, Z., GEE, D., KARLES, G., NEPOMUCENO, J. and HUVARD, G. (2005), Method of producing fibers by electrospinning at high pressures

[120] LEVIT, N. and TEPPER, G. (2004) Supercritical CO_2-assisted electrospinning. *The Journal of Supercritical Fluids* 31, 3, 329–333

[121] DILLOW, A.K., LANGER, R.S., FOSTER, N. and HRKACH, J.S. (1999), Supercritical fluid sterilization method

[122] HOWDLE, S.M., SHAKESHEFF, K.M., WHITAKER, M.J. and ROSE, F.R.A.J. (2005), Polymer composition loaded with cells

[123] GINTY, P.J., HOWARD, D., UPTON, C.E., BARRY, J.J.A., ROSE, F., SHAKESHEFF, K.M. and HOWDLE, S.M. (2008) A supercritical CO_2 injection system for the production of polymer/mammalian cell composites. *Journal of Supercritical Fluids* 43, 3, 535–541

[124] REVERCHON, E. and CARDEA, S. (2012) Supercritical fluids in 3-D tissue engineering. *The Journal of Supercritical Fluids* 69, 0, 97–107

[125] REIGNIER, J. and HUNEAULT, M.A. (2006) Preparation of interconnected poly(ϵ-caprolactone) porous scaffolds by a combination of polymer and salt particulate leaching. *Polymer* 47, 13, 4703–4717

[126] TABOAS, J.M., MADDOX, R.D., KREBSBACH, P.H. and HOLLISTER, S.J. (2003) Indirect solid free form fabrication of local and global porous, biomimetic and composite 3D polymer-ceramic scaffolds. *Biomaterials* 24, 1, 181–194

[127] TURNG, L.S. and KRAMSCHUSTER, A.J. (2011), Method of fabricating a tissue engineering scaffold

[128] CHATTOPADHYAY, P., SHEKUNOV, B.Y. and SEITZINGER, J.S. (2011), Production of porous materials by supercritical fluid processing

[129] HOLLISTER, S.J. (2005) Porous scaffold design for tissue engineering. *Nature Materials* 4, 7, 518–524

[130] TSUJI, H. (2005) Poly(lactide) Stereocomplexes: Formation, Structure, Properties, Degradation, and Applications. *Macromolecular Bioscience* 5, 7, 569–597

[131] KIM, S.H., JUNG, Y.M., KIM, S.H. and PURBA, P. (2011), Method for preparing biodegradable polymer stereocomplexes using a supercritical fluid-organic solvent system and stereocomplexes prepared by the same

[132] ARMENTANO, I., DOTTORI, M., FORTUNATI, E., MATTIOLI, S. and KENNY, J.M. (2010) Biodegradable polymer matrix nanocomposites for tissue engineering: A review. *Polymer Degradation and Stability* 95, 11, 2126–2146

[133] KANNAN, R.M., BAKER, K.C., BELLAIR, R., MANITIU, M. and HERKOWITZ, H. (2011), Supercritical carbon-dioxide processed biodegradable polymer nanocomposites

[134] GEIGER, M., LI, R.H. and FRIESS, W. (2003) Collagen sponges for bone regeneration with rhBMP-2. *Advanced Drug Delivery Reviews* 55, 12, 1613–1629

[135] KEMPEN, D.H.R., LU, L., KIM, C., ZHU, X., DHERT, W.J.A., CURRIER, B.L. and YASZEMSKI, M.J. (2006) Controlled drug release from a novel injectable biodegradable microsphere/scaffold composite based on poly(propylene fumarate). *Journal of Biomedical Materials Research Part A* 77A, 1, 103–111

[136] DUARTE, A.R.C., MANO, J.F. and REIS, R.L. (2009) Preparation of chitosan scaffolds loaded with dexamethasone for tissue engineering applications using supercritical fluid technology. *European Polymer Journal* 45, 1, 141–148

[137] KOLTZENBURG, S., KOLTER, K., SANDLER, J.K.W., DJURIC, D. and BELLIN, I. (2011), Preparations of biologically active substances with enlarged surface based on amphiphilic copolymers

[138] HOWDLE, S.M. and POPOV, V. (2010), Biofunctional polymers prepared in supercritical fluid

[139] CHATZINIKO-LAIDOU, M. (2010), Method for producing a product having a polymer matrix, implants made thereof and use thereof

[140] SANDLER, J.K.W., BELLIN, I., DJURIC, D., KOLTER, K. and RUCKDSCHEL, H. (2011), Nanoporous foamed active compound-containing preparations based on pharmaceutically acceptable thermoplastically workable polymers

[141] CHANG, C.F. and CHANG, K.K. (2012), Degradable hemostatic sponge andÂăextrusion system and method for manufacturing the same

[142] RAHMAN, C.V., KUHN, G., WHITE, L.J., KIRBY, G.T., VARGHESE, O.P., MCLAREN, J.S., COX, H.C., ROSE, F.R., MÜLLER, R., HILBORN, J. *et al.* (2013) PLGA/PEG-hydrogel composite scaffolds with controllable mechanical properties. *Journal of Biomedical Materials Research Part B: Applied Biomaterials*

[143] KIRBY, G.T., WHITE, L.J., RAHMAN, C.V., COX, H.C., QUTACHI, O., ROSE, F.R., HUTMACHER, D.W., SHAKESHEFF, K.M. and WOODRUFF, M.A. (2011) PLGA-based microparticles for the sustained release of BMP-2. *Polymers* 3, 1, 571–586

[144] JUNG, J. and PERRUT, M. (2001) Particle design using supercritical fluids: Literature and patent survey. *The Journal of Supercritical Fluids* 20, 3, 179–219

[145] KNEZ, Z. and WEIDNER, E. (2003) Particles formation and particle design using supercritical fluids. *Current Opinion in Solid State and Materials Science* 7, 353–361

[146] YEO, S.D. and KIRAN, E. (2005) Formation of polymer particles with supercritical fluids: A review. *The Journal of Supercritical Fluids* 34, 3, 287–308

[147] OLIVEIRA, M.B. and MANO, J.F. (2011) Polymer-based microparticles in tissue engineering and regenerative medicine. *Biotechnology Progress* 27, 4, 897–912

[148] SHETH, P., SANDHU, H., SINGHAL, D., MALICK, W., SHAH, N. and KISLALIOGLU, M.S. (2012) Nanoparticles in the pharmaceutical industry and the use of supercritical fluid technologies for nanoparticle production. *Current Drug Delivery* 9, 3, 269–284

[149] FULTON, J.L., DEVERMAN, G.S., MATSON, D.W., YONKER, C.R., TAYLOR, C.D., MCCLAIN, J.B. and CROWLEY, J.M. (2011), System and method for enhanced electrostatic deposition and surface coatings

[150] FULTON, J.L., DEVERMAN, G.S., YONKER, C.R., GRATE, J.W., YOUNG, J.D. and MCCLAIN, J.B. (2003) Thin fluoropolymer films and nanoparticle coatings from the rapid expansion of supercritical carbon dioxide solutions with electrostatic collection. *Polymer* 44, 13, 3627–3632

[151] SUN, Y.P. (2010), Aqueous suspension of nanoscale drug particles from supercritical fluid processing

[152] MOHSEN, N.M. and ARMER, T.A. (2011), Method to generate water soluble or nonwater soluble in nanoparticulates directly in suspension of dispersion media

[153] RAVICHANDRAN, R. (2009) Nanotechnology-Based Drug Delivery Systems. *NanoBioTechnology* 5, 1, 17–33

[154] SUBRAMANIAM, B., SAID, S., RAJEWSKI, R.A. and STELLA, V. (2011), Methods and apparatus for particle precipitation and coating using near-critical and supercritical antisolvents

[155] SUNDHOLM, G.E., DEMIRBUKER, M. and MOSHASHAEE, S. (2010), Process

[156] SHEKUNOV, B.Y., CHATTOPADHYAY, R. and SEITZINGER, J.S. (2010), Nanoparticles from supercritical fluid antisolvent process using particle growth and agglomeration retardants

[157] CHATTOPADHYAY, P., SHEKUNOV, B.Y. and SEITZINGER, J.S. (2012), Method and apparatus for supercritical fluid assisted particle production

[158] DESCHAMPS, F., JUNG, J. and LEBOEUF, F. (2012), Method for preparing pharmaceutical compositions comprising fine particles of active substance

[159] OSADA, F., FUKUZAWA, S. and NAGAI, K. (2011), Method of atomization

[160] TSUNG, M., EASSON, D., D., MEHR, E. and BOURHIS, ALAIN, L. (2010), Methods of processing microparticles

[161] CASTOR, T.P. (2010), Polymer microspheres/nanospheres and encapsulating therapeutic proteins therein

[162] KAISO, K., ABE, M. and SUGIMOTO, T. (2011), Polyamide particles and process for producing same

[163] DAY, R.M. and BLAKER, J. (2010), Microspheres

[164] BROWN, L., MCGEEHAN, J.K., RASHBA-STEP, J. and SCOTT, T.L. (2011), Methods for fabrication, uses and compositions of small spherical particles prepared by controlled phase separation

[165] BREWSTER, N.T., GILLESPIE, W.J., HOWIE, C.R., MADABHUSHI, S.P., USMANI, A.S. and FAIRBAIRN, D.R. (1999) Mechanical considerations in impaction bone grafting 81, 118–24–

[166] BERRIDGE, M.V., HERST, P.M. and TAN, A.S. (2005) Tetrazolium dyes as tools in cell biology: new insights into their cellular reduction. *Biotechnology annual review* 11, 127–152

[167] DEANS, R.J. and MOSELEY, A.B. (2000) Mesenchymal stem cells: Biology and potential clinical uses. *Experimental Hematology* 28, 8, 875 – 884

[168] OLIVARES-NAVARRETE, R., HYZY, S.L., HUTTON, D.L., ERDMAN, C.P., WIELAND, M., BOYAN, B.D. and SCHWARTZ, Z. (2010) Direct and indirect effects of microstructured titanium substrates on the induction of mesenchymal stem cell differentiation towards the osteoblast lineage. *Biomaterials* 31, 10, 2728 – 2735

[169] STEIN, G.S., LIAN, J.B. and OWEN, T.A. (1990) Relationship of cell growth to the regulation of tissue-specific gene expression during osteoblast differentiation. *The FASEB Journal* 4, 13, 3111–23

[170] HERFORD, A.S. and CICCIÃŹ, M. (2010) Recombinant Human Bone Morphogenetic Protein Type 2 Jaw Reconstruction in Patients Affected by Giant Cell Tumor. *Journal of Craniofacial Surgery* 21, 6

[171] KRUYT, M., VAN GAALEN, S., ONER, F., VERBOUT, A., DE BRUIJN, J. and DHERT, W. (2004) Bone tissue engineering and spinal fusion: the potential of hybrid constructs by combining osteoprogenitor cells and scaffolds. *Biomaterials* 25, 9, 1463 – 1473, <ce:title>Animal Models for Tissue Engineering Applications</ce:title>

[172] KARAGEORGIOU, V. and KAPLAN, D. (2005) Porosity of 3D biomaterial scaffolds and osteogenesis. *Biomaterials* 26, 27, 5474 – 5491

[173] KUBOKI, Y., TAKITA, H., KOBAYASHI, D., TSURUGA, E., INOUE, M., MURATA, M., NAGAI, N., DOHI, Y. and OHGUSHI, H. (1998) BMP-Induced osteogenesis on the surface of hydroxyapatite with geometrically feasible and nonfeasible structures: Topology of osteogenesis. *Journal of Biomedical Materials Research* 39, 2, 190–199

[174] FUJIBAYASHI, S., NEO, M., KIM, H.M., KOKUBO, T. and NAKAMURA, T. (2004) Osteoinduction of porous bioactive titanium metal. *Biomaterials* 25, 3, 443 – 450

[175] YUAN, H., KURASHINA, K., DE BRUIJN, J.D., LI, Y., DE GROOT, K. and ZHANG, X. (1999) A preliminary study on osteoinduction of two kinds of calcium phosphate ceramics. *Biomaterials* 20, 19, 1799 – 1806

[176] PEK, Y., GAO, S., ARSHAD, M.M., LECK, K.J. and YING, J.Y. (2008) Porous

collagen-apatite nanocomposite foams as bone regeneration scaffolds. *Biomaterials* 29, 32, 4300 – 4305

[177] RAUCCI, M., DÃĆÂĆÑÂĎĆANTÃČÂš, V., GUARINO, V., SARDELLA, E., ZEPPETELLI, S., FAVIA, P. and AMBROSIO, L. (2010) Biomineralized porous composite scaffolds prepared by chemical synthesis for bone tissue regeneration. *Acta Biomaterialia* 6, 10, 4090 – 4099

[178] LIU, X., RAHAMAN, M.N. and FU, Q. (2013) Bone regeneration in strong porous bioactive glass (13-93) scaffolds with an oriented microstructure implanted in rat calvarial defects. *Acta Biomaterialia* 9, 1, 4889 – 4898

[179] HULBERT, S.F., YOUNG, F.A., MATHEWS, R.S., KLAWITTER, J.J., TALBERT, C.D. and STELLING, F.H. (1970) Potential of ceramic materials as permanently implantable skeletal prostheses. *Journal of Biomedical Materials Research* 4, 3, 433–456

[180] KUBOKI, Y., JIN, Q. and TAKITA, H. (2001) Geometry of carriers controlling phenotypic expression in BMP-induced osteogenesis and chondrogenesis. *Journal of Bone and Joint Surgery-American Volume* 83-A Suppl 1, Pt 2, S105–15

[181] TSURUGA, E., TAKITA, H., ITOH, H., WAKISAKA, Y. and KUBOKI, Y. (1997) Pore Size of Porous Hydroxyapatite as the Cell-Substratum Controls BMP-Induced Osteogenesis. *Journal of Biochemistry* 121, 2, 317–324

[182] SIMSKE, S., AYERS, R. and BATEMAN, T. (1997) Porous materials for bone engineering. In *Materials Science Forum*, volume 250, Trans Tech Publ, 151–182

[183] KIENAPFEL, H., SPREY, C., WILKE, A. and GRISS, P. (1999) Implant fixation by bone ingrowth. *The Journal of Arthroplasty* 14, 3, 355 – 368

[184] RYAN, G., PANDIT, A. and APATSIDIS, D.P. (2006) Fabrication methods of porous metals for use in orthopaedic applications. *Biomaterials* 27, 13, 2651 – 2670

[185] WALSCHOT, L.H., SCHREURS, B.W., VERDONSCHOT, N. and BUMA, P. (2011) The effect of impaction and a bioceramic coating on bone ingrowth in porous titanium particles. *Acta Orthopaedica* 82, 3, 372–377, pMID: 21504310

[186] MONTJOVENT, M.O., MATHIEU, L., SCHMOEKEL, H., MARK, S., BOURBAN, P.E., ZAMBELLI, P.Y., LAURENT-APPLEGATE, L.A. and PIOLETTI, D.P. (2007) Repair of critical size defects in the rat cranium using ceramic-reinforced PLA scaffolds obtained by supercritical gas foaming. *Journal of Biomedical Materials Research Part A* 83A, 1, 41–51

[187] JI, C., ANNABI, N., HOSSEINKHANI, M., SIVALOGANATHAN, S. and DEHGHANI, F. (2012) Fabrication of poly-DL-lactide/polyethylene glycol scaffolds using the gas foaming technique. *Acta Biomaterialia* 8, 2, 570 – 578

[188] WATSON, M., WHITAKER, M., HOWDLE, S. and SHAKESHEFF, K. (2002) Incorporation of Proteins into Polymer Materials by a Novel Supercritical Fluid Processing Method. *Advanced Materials* 14, 24, 1802–1804

[189] YANG, X.B., WHITAKER, M.J., SEBALD, W., CLARKE, N., HOWDLE, S.M., SHAKESHEFF, K.M. and OREFFO, R.O. (2004) Human osteoprogenitor bone formation using encapsulated bone morphogenetic protein 2 in porous polymer scaffolds 10, 1037–45–

[190] DUNLOP, D.G., BREWSTER, N.T., MADABHUSHI, S.P., USMANI, A.S., PANKAJ, P. and HOWIE, C.R. (2003) Techniques to improve the shear strength of impacted bone graft: the effect of particle size and washing of the graft. *The Journal of Bone & Joint Surgery* 85, 4, 639–646

[191] BOLLAND, B., KANCZLER, J., DUNLOP, D. and OREFFO, R. (2008) Development of textitin vivo μCT evaluation of neovascularisation in tissue engineered bone constructs. *Bone* 43, 1, 195–202

[192] MIAO, D. and SCUTT, A. (2002) Histochemical localization of alkaline phosphatase activity in decalcified bone and cartilage. *Journal of Histochemistry & Cytochemistry* 50, 3, 333–340

[193] PAN, Z. and DING, J. (2012) Poly(lactide-co-glycolide) porous scaffolds for tissue engineering and regenerative medicine. *Interface Focus* 2, 3, 366–377

[194] BOLLAND, B.J., KANCZLER, J.M., GINTY, P.J., HOWDLE, S.M., SHAKESHEFF, K.M., DUNLOP, D.G. and OREFFO, R.O. (2008) The application of human

bone marrow stromal cells and poly(dl-lactic acid) as a biological bone graft extender in impaction bone grafting. *Biomaterials* 29, 22, 3221 – 3227

[195] O'BRIEN, F., HARLEY, B., YANNAS, I. and GIBSON, L. (2005) The effect of pore size on cell adhesion in collagen-GAG scaffolds. *Biomaterials* 26, 4, 433 – 441

[196] KORDA, M., SHARPE, J., RUST, P., HUA, J., PHIPPS, K., DI SILVIO, L., COATHUP, M., GOODSHIP, A. and BLUNN, G. (2006) The effect of impaction forces on viability of mesenchymal stem cells in revision total hip replacements. *Journal of Bone & Joint Surgery, British Volume* 88-B, SUPP III, 364

[197] KORDA, M., BLUNN, G., PHIPPS, K., RUST, P., DI SILVIO, L., COATHUP, M., GOODSHIP, A. and HUA, J. (2006) Can mesenchymal stem cells survive under normal impaction force in revision total hip replacements? *Tissue Engineering* 12, 3, 625–30, korda, Michelle Blunn, Gordon Phipps, Kirsty Rust, Philippa Di Silvio, Lucy Coathup, Melanie Goodship, Allen Hua, Jia United States Tissue Eng. 2006 Mar;12(3):625-30.

[198] KIM, S.S., PARK, M.S., JEON, O., CHOI, C.Y. and KIM, B.S. (2006) Poly(lactide-co-glycolide)/hydroxyapatite composite scaffolds for bone tissue engineering. *Biomaterials* 27, 8, 1399 – 1409

[199] LIU, Y., WANG, G., CAI, Y., JI, H., ZHOU, G., ZHAO, X., TANG, R. and ZHANG, M. (2009) In vitro effects of nanophase hydroxyapatite particles on proliferation and osteogenic differentiation of bone marrow-derived mesenchymal stem cells. *Journal of Biomedical Materials Research Part A* 90A, 4, 1083–1091

[200] RAJAGOPALAN, S., YASZEMSKI, M.J. and ROBB, R.A. (2004) Evaluation of thresholding techniques for segmenting scaffold images in tissue engineering , 1456–1465

[201] KIM, C.H., ZHANG, H., MIKHAIL, G., VON STECHOW, D., MULLER, R., KIM, H.S. and GUO, X.E. (2007) Effects of thresholding techniques on microCT-based finite element models of trabecular bone. *J Biomech Eng* 129, 4, 481–6, kim, Chi Hyun Zhang, Henry Mikhail, George von Stechow, Dietrich Muller, Ralph Kim, Han Sung Guo, X Edward United States J Biomech Eng. 2007 Aug;129(4):481-6.

[202] LEMON, G., REINWALD, Y., WHITE, L.J., HOWDLE, S.M., SHAKESHEFF, K.M. and KING, J.R. (2012) Interconnectivity analysis of supercritical CO2-foamed scaffolds. *Computer Methods and Programs in Biomedicine* 106, 3, 139 – 149

[203] KAMITAKAHARA, M., OHTSUKI, C. and MIYAZAKI, T. (2008) Review Paper: Behavior of Ceramic Biomaterials Derived from Tricalcium Phosphate in Physiological Condition. *Journal of Biomaterials Applications* 23, 3, 197–212

[204] RENOOIJ, W., HOOGENDOORN, H.A., VISSER, W.J., LENTFERINK, R.H.F., SCHMITZ, M.G.J., IEPEREN, H.V., OLDENBURG, S.J., JANSSEN, W.M., AKKERMANS, L.M.A. and WITTEBOL, P. (1985) Bioresorption of Ceramic Strontium-85-Labeled Calcium Phosphate Implants in Dog Femora: A Pilot Study to Quantitate Bioresorption of Ceramic Implants of Hydroxyapatite and Tricalcium Orthophosphate In Vivo. *Clinical Orthopaedics and Related Research* 197, 272–285

[205] HEUGHEBAERT, M., LEGEROS, R.Z., GINESTE, M., GUILHEM, A. and BONEL, G. (1988) Physicochemical characterization of deposits associated with HA ceramics implanted in nonosseous sites. *J Biomed Mater Res* 22, 3 Suppl, 257–68, heughebaert, M LeGeros, R Z Gineste, M Guilhem, A Bonel, G DE 04123/DE/NIDCR NIH HHS/United States Research Support, Non-U.S. Gov't Research Support, U.S. Gov't, P.H.S. UNITED STATES J Biomed Mater Res. 1988 Dec;22(3 Suppl):257-68.

[206] RIPAMONTI, U. (1996) Osteoinduction in porous hydroxyapatite implanted in heterotopic sites of different animal models. *Biomaterials* 17, 1, 31 – 35

[207] HOWARD, D., PARTRIDGE, K., YANG, X., CLARKE, N.M., OKUBO, Y., BESSHO, K., HOWDLE, S.M., SHAKESHEFF, K.M. and OREFFO, R.O. (2002) Immunoselection and adenoviral genetic modulation of human osteoprogenitors: in vivo bone formation on {PLA} scaffold. *Biochemical and Biophysical Research Communications* 299, 2, 208 – 215

[208] WANG, H., LI, Y., ZUO, Y., LI, J., MA, S. and CHENG, L. (2007) Biocompatibility and osteogenesis of biomimetic nano-hydroxyapatite/polyamide composite scaffolds for bone tissue engineering. *Biomaterials* 28, 22, 3338 – 3348

[209] NEWMAN, E., TURNER, A. and WARK, J. (1995) The potential of sheep for the study of osteopenia: Current status and comparison with other animal models. *Bone* 16, 4, Supplement, S277 – S284

[210] BERGMANN, G., SIRAKY, J., ROHLMANN, A. and KOELBEL, R. (1984) A comparison of hip joint forces in sheep, dog and man. *Journal of Biomechanics* 17, 12, 907 – 921

[211] REICHERT, J.C., EPARI, D.R., WULLSCHLEGER, M.E., SAIFZADEH, S., STECK, R., LIENAU, J., SOMMERVILLE, S., DICKINSON, I.C., SCHÜTZ, M.A., DUDA, G.N. *et al.* (2010) Establishment of a preclinical ovine model for tibial segmental bone defect repair by applying bone tissue engineering strategies. *Tissue Engineering Part B: Reviews* 16, 1, 93–104

[212] TAYLOR, W.R., EHRIG, R.M., HELLER, M.O., SCHELL, H., SEEBECK, P. and DUDA, G.N. (2006) Tibio-femoral joint contact forces in sheep. *Journal of Biomechanics* 39, 5, 791–798

[213] PEARCE, A., RICHARDS, R., MILZ, S., SCHNEIDER, E., PEARCE, S. *et al.* (2007) Animal models for implant biomaterial research in bone: a review. *European Cells and Materials* 13, 1–10

[214] FONSECA, J. (2012) Bone biology: from macrostructure to gene expression. *Medicographia* 34, 142–148

[215] SIMS, N.A. and GOOI, J.H. (2008) Bone remodeling: Multiple cellular interactions required for coupling of bone formation and resorption. In *Seminars in Cell & Developmental B iology*, volume 19, Elsevier, 444–451

[216] NAFEI, A., DANIELSEN, C., LINDE, F. and HVID, I. (2000) Properties of growing trabecular ovine bone Part I: mechanical and physical properties. *Journal of Bone & Joint Surgery, British Volume* 82, 6, 910–920

[217] LIEBSCHNER, M.A. (2004) Biomechanical considerations of animal models used in tissue engineering of bone. *Biomaterials* 25, 9, 1697–1714

[218] RAVAGLIOLI, A., KRAJEWSKI, A., CELOTTI, G., PIANCASTELLI, A., BACCHINI, B., MONTANARI, L., ZAMA, G. and PIOMBI, L. (1996) Mineral evolution of bone. *Biomaterials* 17, 6, 617–622

[219] MARTIN, R., BURR, D. and SHARKEY, N. (1998) *Skeletal Tissue Mechanics*. Springer

[220] DEN BOER, F.C., PATKA, P., BAKKER, F.C., WIPPERMANN, B.W., VAN LINGEN, A., VINK, G.Q., BOSHUIZEN, K. and HAARMAN, H.J.T.M. (1999) New segmental long bone defect model in sheep: Quantitative analysis of healing with dual energy X-ray absorptiometry. *Journal of Orthopaedic Research* 17, 5, 654–660

[221] WILLIE, B.M., BLOEBAUM, R.D., BIRELEY, W.R., BACHUS, K.N. and HOFMANN, A.A. (2004) Determining relevance of a weight-bearing ovine model for bone ingrowth assessment. *Journal of Biomedical Materials Research Part A* 69, 3, 567–576

[222] NUSS, K.M., AUER, J.A., BOOS, A. and VON RECHENBERG, B. (2006) An animal model in sheep for biocompatibility testing of biomaterials in cancellous bones. *BMC Musculoskeletal Disorders* 7, 1, 67

[223] ANDERSON, M.L., DHERT, W.J., DE BRUIJN, J.D., DALMEIJER, R.A., LEENDERS, H., VAN BLITTERSWIJK, C.A. and VERBOUT, A.J. (1999) Critical size defect in the goat's os ilium: A model to evaluate bone grafts and substitutes. *Clinical Orthopaedics and Related Researche* 364, 231–239

[224] SCHMITZ, J.P. and HOLLINGER, J.O. (1986) The critical size defect as an experimental model for craniomandibulofacial nonunions. *Clinical Orthopaedics and Related Research* 205, 299–308

[225] HOLLINGER, J.O. and KLEINSCHMIDT, J.C. (1990) The critical size defect as an experimental model to test bone repair materials. *Journal of Craniofacial Surgery* 1, 1, 60–68

[226] BURKS, R.T., GREIS, P.E., ARNOCZKY, S.P. and SCHER, C. (2006) The Use of a Single Osteochondral Autograft Plug in the Treatment of a Large Osteochondral Lesion in the Femoral Condyle: An Experimental Study in Sheep. *The American Journal of Sports Medicine* 34, 2, 247–255

[227] PATEL, N., BROOKS, R., CLARKE, M., LEE, P., RUSHTON, N., GIBSON, I., BEST, S. and BONFIELD, W. (2005) In vivo assessment of hydroxyapatite and silicate-substituted hydroxyapatite granules using an ovine defect model. *Journal of Materials Science: Materials in Medicine* 16, 5, 429–440

[228] WORTH, A., MUCALO, M., HORNE, G., BRUCE, W. and BURBIDGE, H.

(2005) The evaluation of processed cancellous bovine bone as a bone graft substitute. *Clinical Oral Implants Research* 16, 3, 379–386

[229] SCHAGEMANN, J.C., ERGGELET, C., CHUNG, H.W., LAHM, A., KURZ, H. and MROSEK, E.H. (2008) Cell-laden and cell-free biopolymer hydrogel for the treatment of osteochondral defects in a sheep model. *Tissue Engineering Part A* 15, 1, 75–82

[230] VAN DER POL, U., MATHIEU, L., ZEITER, S., BOURBAN, P.E., ZAMBELLI, P.Y., PEARCE, S.G., BOURE, L. and PIOLETTI, D.P. (2010) Augmentation of bone defect healing using a new biocomposite scaffold: an in vivo study in sheep. *Acta Biomaterialia* 6, 9, 3755–3762

[231] FLAUTRE, B., DELECOURT, C., BLARY, M.C., VAN LANDUYT, P., LEMAIÌĆTRE, J. and HARDOUIN, P. (1999) Volume effect on biological properties of a calcium phosphate hydraulic cement: experimental study in sheep. *Bone* 25, 2, 35S–39S

[232] EITEL, F., KLAPP, F., JACOBSON, W. and SCHWEIBERER, L. (1981) Bone regeneration in animals and in man. *Archives of Orthopaedic and Traumatic Surgery* 99, 1, 59–64

[233] HOLLISTER, S.J. (2009) Scaffold engineering: a bridge to where? *Biofabrication* 1, 1, 012001

[234] BEHRENS, J., WALKER, P. and SHOJI, H. (1974) Variations in strength and structure of cancellous bone at the knee. *Journal of Biomechanics* 7, 3, 201–207

[235] ARMSTRONG, S.J., READ, R.A. and PRICE, R. (1995) Topographical variation within the articular cartilage and subchondral bone of the normal ovine knee joint: a histological approach. *Osteoarthritis and Cartilage* 3, 1, 25–33

[236] ZIOUPOS, P., COOK, R.B. and HUTCHINSON, J.R. (2008) Some basic relationships between density values in cancellous and cortical bone. *Journal of Biomechanics* 41, 9, 1961 – 1968

[237] SUMNER, D., WILLKE, T., BERZINS, A. and TURNER, T. (1994) Distribution of Young's modulus in the cancellous bone of the proximal canine tibia. *Journal of Biomechanics* 27, 8, 1095–1099

[238] ANDERSON, J.M. and SHIVE, M.S. (1997) Biodegradation and biocompatibility of PLA and PLGA microspheres. *Advanced Drug Delivery Reviews* 28, 1, 5 – 24, biodegradable Microspheres/Therapeutic Peptide Delivery

[239] FANKHAUSER, F., PASSLER, J.M., SCHIPPINGER, G., BOLDIN, C. and SCARPATETTI, M. (2004) Tendon-to-bone healing of a quadrupled hamstring tendon graft fixed with biodegradable screws in an immature athlete: A radiologic, arthroscopic, histologic, and electromicroscopic investigation. *Arthroscopy: The Journal of Arthroscopic & Related Surgery* 20, 9, 992 – 997

[240] JONG, W.H.D., BERGSMA, J.E., ROBINSON, J.E. and BOS, R.R. (2005) Tissue response to partially in vitro predegraded poly-L-lactide implants. *Biomaterials* 26, 14, 1781 – 1791

[241] VAVKEN, P., PROFFEN, B., PETERSON, C., FLEMING, B.C., MACHAN, J.T. and MURRAY, M.M. (2013) Effects of Suture Choice on Biomechanics and Physeal Status After Bioenhanced Anterior Cruciate Ligament Repair in Skeletally Immature Patients: A Large-Animal Study. *Arthroscopy: The Journal of Arthroscopic & Related Surgery* 29, 1, 122 – 132

[242] GORDON, J.A., TYE, C.E., SAMPAIO, A.V., UNDERHILL, T.M., HUNTER, G.K. and GOLDBERG, H.A. (2007) Bone sialoprotein expression enhances osteoblast differentiation and matrix mineralization *in vitro*. *Bone* 41, 3, 462–473

[243] GANSS, B., KIM, R.H. and SODEK, J. (1999) Bone sialoprotein. *Critical Reviews in Oral Biology & Medicine* 10, 1, 79–98

[244] FISHER, L.W., WHITSON, S., AVIOLI, L. and TERMINE, J. (1983) Matrix sialoprotein of developing bone. *Journal of Biological Chemistry* 258, 20, 12723–12727

[245] BIANCO, P., FISHER, L.W., YOUNG, M.F., TERMINE, J.D. and ROBEY, P.G. (1991) Expression of bone sialoprotein (BSP) in developing human tissues. *Calcified Tissue International* 49, 6, 421–426

[246] WALTREGNY, D., BELLAHCÈNE, A., DE LEVAL, X., FLORKIN, B., WEIDLE, U. and CASTRONOVO, V. (2000) Increased expression of bone sialoprotein in bone metastases compared with visceral metastases in human breast and prostate cancers. *Journal of Bone and Mineral Research* 15, 5, 834–843

[247] DUCY, P., ZHANG, R., GEOFFROY, V., RIDALL, A.L. and KARSENTY, G. (1997) Osf2/Cbfa1: a transcriptional activator of osteoblast differentiation. *Cell* 89, 5, 747–754

[248] DUCY, P. and KARSENTY, G. (1995) Two distinct osteoblast-specific cis-acting elements control expression of a mouse osteocalcin gene. *Molecular and Cellular Biology* 15, 4, 1858–1869

[249] GRONTHOS, S., GRAVES, S., OHTA, S. and SIMMONS, P. (1994) The STRO-1+ fraction of adult human bone marrow contains the osteogenic precursors. *Blood* 84, 12, 4164–4173

[250] MCCARTY, R.C., GRONTHOS, S., ZANNETTINO, A.C., FOSTER, B.K. and XIAN, C.J. (2009) Characterisation and developmental potential of ovine bone marrow derived mesenchymal stem cells. *Journal of Cellular Physiology* 219, 2, 324–333

[251] NIEMEYER, P., FECHNER, K., MILZ, S., RICHTER, W., SUEDKAMP, N.P., MEHLHORN, A.T., PEARCE, S. and KASTEN, P. (2010) Comparison of mesenchymal stem cells from bone marrow and adipose tissue for bone regeneration in a critical size defect of the sheep tibia and the influence of platelet-rich plasma. *Biomaterials* 31, 13, 3572 – 3579

[252] CAO, L., LIU, G., GAN, Y., FAN, Q., YANG, F., ZHANG, X., TANG, T. and DAI, K. (2012) The use of autologous enriched bone marrow MSCs to enhance osteoporotic bone defect repair in long-term estrogen deficient goats. *Biomaterials* 33, 20, 5076–5084

[253] STRAUSS, W.C. (2005) *Saturation and foaming of thermoplastic nanocomposites using supercritical CO_2*. Master's thesis, University of North Texas

[254] LIAO, S., CUI, F., ZHANG, W. and FENG, Q. (2004) Hierarchically biomimetic bone scaffold materials: Nano-HA/collagen/PLA composite. *Journal of Biomedical Materials Research Part B: Applied Biomaterials* 69, 2, 158–165

[255] ZHANG, R. and MA, P.X. (1999) Poly (α-hydroxyl acids)/hydroxyapatite porous composites for bone-tissue engineering. I. Preparation and morphology

[256] ZHANG, L.F., SUN, R., XU, L., DU, J., XIONG, Z.C., CHEN, H.C. and XIONG, C.D. (2008) Hydrophilic poly (ethylene glycol) coating on PDLLA/BCP

bone scaffold for drug delivery and cell culture. *Materials Science and Engineering: C* 28, 1, 141 – 149

[257] MOU, Z.L., ZHAO, L.J., ZHANG, Q.A., ZHANG, J. and ZHANG, Z.Q. (2011) Preparation of porous PLGA/HA/collagen scaffolds with supercritical CO2 and application in osteoblast cell culture. *The Journal of Supercritical Fluids* 58, 3, 398 – 406

[258] EL-AMIN, S., LU, H., KHAN, Y., BUREMS, J., MITCHELL, J., TUAN, R. and LAURENCIN, C. (2003) Extracellular matrix production by human osteoblasts cultured on biodegradable polymers applicable for tissue engineering. *Biomaterials* 24, 7, 1213–1221

[259] DALBY, M.J., GADEGAARD, N., TARE, R., ANDAR, A., RIEHLE, M.O., HERZYK, P., WILKINSON, C.D. and OREFFO, R.O. (2007) The control of human mesenchymal cell differentiation using nanoscale symmetry and disorder. *Nature materials* 6, 12, 997–1003

[260] ENGEL, E., MARTÍNEZ, E., MILLS, C.A., FUNES, M., PLANELL, J.A. and SAMITIER, J. (2009) Mesenchymal stem cell differentiation on microstructured poly (methyl methacrylate) substrates. *Annals of Anatomy-Anatomischer Anzeiger* 191, 1, 136–144

[261] BURDICK, J.A. and VUNJAK-NOVAKOVIC, G. (2008) Engineered microenvironments for controlled stem cell differentiation. *Tissue Engineering Part A* 15, 2, 205–219

[262] GUVENDIREN, M. and BURDICK, J.A. (2010) The control of stem cell morphology and differentiation by hydrogel surface wrinkles. *Biomaterials* 31, 25, 6511–6518

[263] BRAMMER, K.S., OH, S., FRANDSEN, C.J. and JIN, S. (2010) TiO_2 nanotube structures for enhanced cell and biological functionality. *Jom* 62, 4, 50–55

[264] YANG, Y., KUSANO, K., FREI, H., ROSSI, F., BRUNETTE, D. and PUTNINS, E. (2010) Microtopographical regulation of adult bone marrow progenitor cells chondrogenic and osteogenic gene and protein expressions. *Journal of Biomedical Materials Research Part A* 95, 1, 294–304

[265] KAUR, G., VALARMATHI, M.T., POTTS, J.D., JABBARI, E., SABO-ATTWOOD, T. and WANG, Q. (2010) Regulation of osteogenic differentiation of rat bone marrow stromal cells on 2D nanorod substrates. *Biomaterials* 31, 7, 1732–1741

[266] YOU, M.H., KWAK, M.K., KIM, D.H., KIM, K., LEVCHENKO, A., KIM, D.Y. and SUH, K.Y. (2010) Synergistically enhanced osteogenic differentiation of human mesenchymal stem cells by culture on nanostructured surfaces with induction media. *Biomacromolecules* 11, 7, 1856–1862

[267] REILLY, G.C. and ENGLER, A.J. (2010) Intrinsic extracellular matrix properties regulate stem cell differentiation. *Journal of biomechanics* 43, 1, 55–62

[268] RUIZ, S.A. and CHEN, C.S. (2008) Emergence of patterned stem cell differentiation within multicellular structures. *Stem cells* 26, 11, 2921–2927

[269] BRETT, P. (2013) The control of mesenchymal stromal cell osteogenic differentiation through modified surfaces. *Stem Cells International* , 361637, 2013

[270] ZHAO, G., SCHWARTZ, Z., WIELAND, M., RUPP, F., GEIS-GERSTORFER, J., COCHRAN, D. and BOYAN, B. (2005) High surface energy enhances cell response to titanium substrate microstructure. *Journal of Biomedical Materials Research Part A* 74, 1, 49–58

[271] OH, S., BRAMMER, K.S., LI, Y.J., TENG, D., ENGLER, A.J., CHIEN, S. and JIN, S. (2009) Stem cell fate dictated solely by altered nanotube dimension. *Proceedings of the National Academy of Sciences* 106, 7, 2130–2135

[272] WEI, G. and MA, P.X. (2004) Structure and properties of nano-hydroxyapatite/polymer composite scaffolds for bone tissue engineering. *Biomaterials* 25, 19, 4749–4757

[273] HONG, Z., ZHANG, P., HE, C., QIU, X., LIU, A., CHEN, L., CHEN, X. and JING, X. (2005) Nano-composite of poly (L-lactide) and surface grafted hydroxyapatite: mechanical properties and biocompatibility. *Biomaterials* 26, 32, 6296–6304

[274] KOTHAPALLI, C.R., SHAW, M.T. and WEI, M. (2005) Biodegradable HA-PLA 3-D porous scaffolds: Effect of nano-sized filler content on scaffold properties. *Acta Biomaterialia* 1, 6, 653–662

[275] ZHOU, D., ZHAO, K., LI, Y., CUI, F. and LEE, I. (2006) Repair of segmental defects with nano-hydroxyapatite/collagen/PLA composite combined with mesenchymal stem cells. *Journal of Bioactive and Compatible Polymers* 21, 5, 373–384

[276] NEJATI, E., MIRZADEH, H. and ZANDI, M. (2008) Synthesis and characterization of nano-hydroxyapatite rods/poly (l-lactide acid) composite scaffolds for bone tissue engineering. *Composites Part A: Applied Science and Manufacturing* 39, 10, 1589–1596

[277] CUI, Y., LIU, Y., CUI, Y., JING, X., ZHANG, P. and CHEN, X. (2009) The nanocomposite scaffold of poly (lactide-co-glycolide) and hydroxyapatite surface-grafted with L-lactic acid oligomer for bone repair. *Acta biomaterialia* 5, 7, 2680–2692

[278] NEJATI, E., FIROUZDOR, V., ESLAMINEJAD, M. and BAGHERI, F. (2009) Needle-like nano hydroxyapatite/poly (l-lactide acid) composite scaffold for bone tissue engineering application. *Materials Science and Engineering: C* 29, 3, 942–949

[279] NGIAM, M., LIAO, S., PATIL, A.J., CHENG, Z., CHAN, C.K. and RAMAKRISHNA, S. (2009) The fabrication of nano-hydroxyapatite on PLGA and PLGA/collagen nanofibrous composite scaffolds and their effects in osteoblastic behavior for bone tissue engineering. *Bone* 45, 1, 4–16

[280] ZHANG, P., HONG, Z., YU, T., CHEN, X. and JING, X. (2009) *In vivo* mineralization and osteogenesis of nanocomposite scaffold of poly (lactide-*co*-glycolide) and hydroxyapatite surface-grafted with poly(l-lactide). *Biomaterials* 30, 1, 58–70

[281] ESLAMINEJAD, M.B., BAGHERI, F., ZANDI, M., NEJATI, E., ZOMORODIAN, E. and MIVEHCHI, H. (2010) Comparison of proliferation and osteoblast differentiation of marrow-derived mesenchymal stem cells on nano-and micro-hydroxyapatite contained composite scaffolds. *Iranian Journal of Biotechnology (IJB)* 8, 4

[282] DIAO, H., SI, Y., ZHU, A., JI, L. and SHI, H. (2012) Surface modified nano-hydroxyapatite/poly (lactide acid) composite and its osteocyte compatibility. *Materials Science and Engineering: C* 32, 7, 1796–1801

[283] KUTIKOV, A.B. and SONG, J. (2013) An amphiphilic degradable polymer/hydroxyapatite composite with enhanced handling characteristics promotes osteogenic gene expression in bone marrow stromal cells. *Acta Biomaterialia*

[284] DOWLING, D.P., MILLER, I.S., ARDHAOUI, M. and GALLAGHER, W.M.

(2011) Effect of Surface Wettability and Topography on the Adhesion of Osteosarcoma Cells on Plasma-modified Polystyrene. *Journal of Biomaterials Applications* 26, 3, 327–347

[285] LAMPIN, M., WAROCQUIER-CLÃČÂL'ROUT, R., LEGRIS, C., DEGRANGE, M. and SIGOT-LUIZARD, M.F. (1997) Correlation between substratum roughness and wettability, cell adhesion, and cell migration. *Journal of Biomedical Materials Research* 36, 1, 99–108

[286] VAN WACHEM, P., BEUGELING, T., FEIJEN, J., BANTJES, A., DETMERS, J. and VAN AKEN, W. (1985) Interaction of cultured human endothelial cells with polymeric surfaces of different wettabilities. *Biomaterials* 6, 6, 403 – 408

[287] CAI, K., YAO, K., CUI, Y., YANG, Z., LI, X., XIE, H., QING, T. and GAO, L. (2002) Influence of different surface modification treatments on poly(d,l-lactic acid) with silk fibroin and their effects on the culture of osteoblast in vitro. *Biomaterials* 23, 7, 1603 – 1611

[288] HONG, Z., QIU, X., SUN, J., DENG, M., CHEN, X. and JING, X. (2004) Grafting polymerization of L-lactide on the surface of hydroxyapatite nano-crystals. *Polymer* 45, 19, 6699–6706

Appendix 1

Supercritical CO_2 foaming standard operating procedure

The standard operating procedure of the high pressure foaming rig is detailed as follows:

Please refer to Figure 2.1 for equipment layout. The inlet valve is valve 1 and the outlet valve is valve 2.

Preparations

- Ensure the external thermocouple is attached to the band heater.
- Ensure the rig is at atmospheric pressure by checking valve 1 is closed, valve 2 is open, and the safety key is unscrewed.
- Switch on the power supply of the pressure indicator, back pressure regulator, and temperature controller.
- Select the temperature for the pressure vessel at the temperature controller. The temperature may overheat during the initial 5 minutes of heating.
- Wait for a stable temperature to be obtained.
- Place the prepared and closed foaming mould into the pressure vessel. Close the vessel, tighten the clamp, and screw in the security key.
- Open outlet valve (valve 2).

Starting the procedure

- Start the program FlowDDE. Select "open communication" in menu " communication". Wait for response "server is active and ready for any client".
- If temperature recording is desired start PLW Recorder. Click "new file", select directory and filename and click "save". Click "start recording" to start temperature log.

- Start the program FlowPlot. Click "setpointscript" in menu "extra". Click "load" and open filename (e.g. 20 60 30 program HY.txt) (switch "files of type" to "all files".
- Close menu "setpointscript". Click "script" buttion (NOT "start" button). Three lines will be displayed: red indicates the pressure setpoint, green indicates the measured pressure, yellow indicated the BPR opening in %.
- Wait for the pressure set-point (red) to reach the value 5. Carefully open the inlet valve (valve 1). The Pickel pump will begin pumping.
- Ensure with the Pickel pump operating there is no blocking between the inlet valve and the BPR through obersvation of an increase in the internal pressure (green line).
- Keep the valve opening line (yellow) between 25–35% by regulating inlet valve (valve 1). During the vent phase valve 1 may be almost closed.

Shutting down

- If the program has finished completely close the inlet valve (valve 1). If desires save a screen shot of the flow plot window.
- Switch off temperature controller.
- Click "stop recording" on PLW Recorder. Select "close communication" in men "communication" of FlowDDE. Exit all programs.
- Ensure the pressure has reached atmospheric pressure (pressure indicator). Unscrew safety key and open pressure vessel. Remove the sample.
- Switch off pressure indicator and back pressure regulator.